JUSTUS-LIEBIG-UNIVERSITÄT GIESSEN

# cGMP Signalling in Smooth Muscle Cells of the Vasculature and the Male Reproductive Tract

INAUGURAL DISSERTATION

As part of the binational joint award PhD program of
the Justus-Liebig-University Giessen and the Monash University Melbourne
submitted to the Faculty of Biology in partial fulfillment of the requirements for the
Dr.rer.nat degree of the Faculty of Biology of the Justus-Liebig-University Giessen

Submitted by

**Christine Angelika Rager**

From Sigmaringen, Germany

Giessen, 2025

Institute of Anatomy and Cell Biology

Signalling Transduction Group

Faculty of Medicine

Justus-Liebig-University,

Giessen, Germany

Main Supervisor: **Prof. Dr. Ralf Middendorff**

◊

Internal Supervisor and Committee Member/ Reviewer: **Prof. Dr. Ivan Manzini**

External Supervisor and Committee Member/ Reviewer: **Prof. Dr. Ralf Middendorff**

Committee Member/ Reviewer/Chair: **PD Dr. Ellen Kauschke**

Committee Member/ Reviewer: **Prof. Dr. Florian Wagenlehner**

Date of Disputation: 24th of November 2025

With Permission of the Faculty of Biology and Chemistry (FB 08)

Of the Justus-Liebig-University, Giessen, Germany

Dean: **Prof. Dr. Holger Zorn**

# cGMP Signalling in Smooth Muscle Cells of the Vasculature and the Male Reproductive Tract

**Christine Angelika Rager**

(MSc in Biology, BSc in Biology)

A thesis submitted for the degree (joint award) of Doctor of Philosophy at the Monash University, Australia and Justus Liebig University Giessen, Germany in November 2025

Faculty of Medicine, Nursing and Health Sciences

School of Molecular and Translational Sciences

Monash University

Clayton, VIC, Australia

Main Supervisor: **Dr. Betty Exintaris**

Supporting Supervisor: **Dr. Michael Raymond Whittaker**

from the Monash Institute of Pharmaceutical Sciences

Parkville, VIC, Australia

Melbourne, 2025

# Table of Contents

*“If you cannot explain it simply, you do not understand it well enough.”*

*- A. Einstein*

*This work is dedicated to all present and future PhD candidates. Hang in there!*

# Thesis Structure & Authorship Disclaimer

The results section of this thesis comprises two comprehensive results chapters (**4.1** and **4.2**). Chapter **4.1** summarizes the results obtained from experiments with vascular smooth muscle cells and most paragraphs and illustrations (**Figures 27 -35**, Table 15) for this chapter have previously been published as part of the following research articles:

**1) "Reference Gene U2 Enables Direct Comparison between Relative Gene Expression Levels of Vascular Smooth Muscle Cells in Tissue and Culture Using Real-Time Quantitative PCR."**

C. Rager, T. Klöpper, U. Pfeil, S. Tasch, M. R. Whittaker, B. Exintaris, A. Mietens & R. Middendorff *Cells* (2023), 12(17), 2135. https://www.mdpi.com/2073-4409/12/17/2135



**2) "The Influence of Cell Isolation and Culturing on Natriuretic Peptide Receptors in Aortic Vascular Smooth Muscle Cells."**

C. Rager, T. Klöpper, S. Tasch, M. R. Whittaker, B. Exintaris, A. Mietens & R. Middendorff

*Cells* (2025), 14, 51. https://doi.org/10.3390/ cells14010051



Chapter **4.2** summarizes all results obtained from experiments with testicular tissue. These results are unpublished and part of a publication in progress with the preliminary title "Novel FIJI-based live imaging analysis reveals dependence of spontaneous contractions pattern on spermatogenic stages in rats."

Both chapters (**4.1** and **4.2**) focus on the cGMP signalling system in smooth muscle cells and share the introduction, materials and methods and discussion.

# List of Publications, Posters, and Prizes

## Publications

First authors are underlined.

Published:

1) "Reference Gene U2 Enables Direct Comparison between Relative Gene Expression Levels of Vascular Smooth Muscle Cells in Tissue and Culture Using Real-Time Quantitative PCR." - **C. Rager**, T. Klöpper, U. Pfeil, S. Tasch, M. R. Whittaker, B. Exintaris, A. Mietens & R. Middendorff (2023). *Cells*, *12*(17), 2135. https://www.mdpi.com/2073-4409/12/17/2135
2) "The Influence of Cell Isolation and Culturing on Natriuretic Peptide Receptors in Aortic Vascular Smooth Muscle Cells."- **C. Rager**, T. Klöpper, S. Tasch, M. R. Whittaker, B. Exintaris, A. Mietens & R. Middendorff (2025). *Cells*,14(1), 51; https://doi.org/10.3390/cells14010051

In progress:

3) "Novel FIJI-based live imaging analysis reveals dependence of spontaneous contractions pattern on spermatogenic stages in rats."- **C. Rager**, A. Mietens, C. Nowell, S. Tasch, M. R. Whittaker, B. Exintaris & R. Middendorff

## Posters

Presenter is highlighted in **bold**.

1) "A novel approach to visualize superficial wall movements in seminiferous tubules" – **C. Rager**, A. Mietens, A. Ernst, S. Tasch, C. Nowell, T. Saikiraglou, R. Middendorff (*14th GGL Annual Conference 2021*)
2) "Character and relevance of superficial wall movements in seminiferous tubules" - A. Mietens, **C. Rager**, S. Tasch, B. Stadler, C. Nowell, R. Middendorff (*European Testis Workshop 2021-digital*)
3) "Die drei Fragezeichen und Tubuli seminiferi, ihre schnellen spontanen Kontraktionen, sowie deren Reduktion durch NO" - **C. Rager**, A. Mietens, S. Tasch, C. Nowell, R. Middendorff (*9th DVR Congress 2021-digital*)
4) "The Natriuretic Peptide Receptors in vascular Smooth Muscle Cells: Cell culture the approach of choice?" - **C. Rager**, T. Klöpper, M. A. Kuchta, A. Mietens, D. Müller, R. Middendorff (*10th International Conference on cGMP 2022*)

5) "The influence of NPs on vascular SMCs: Is cell culture the approach of choice?" - **C. Rager**, T. Klöpper, D. Müller, B. Exintaris & R. Middendorff (*Biomed Link Conference 2022*)
6) "Relevance of Epididymal Duct Contractions before Puberty" - **C. Rager**, D. Weiser, D. Pössl, D. Ježek, S. Tasch, R. Middendorff (*Von Behring-Röntgen-Symposium 2022 -The Epididymis*)
7) "The influence of natriuretic peptides on vascular SMCs: Is cell culture the approach of choice?" - **C. Rager**, T. Klöpper, D. Müller, B. Exintaris & R. Middendorff (*APSA-ASCEPT Annual Meeting 2022*)
8) "Search for reference gene to enable direct comparison between relative expression levels of vascular smooth muscle cells in tissue and culture using RT- qPCR" – **C. Rager**, T. Klöpper, U. Pfeil, S. Tasch, M. R. Whittaker, B. Exintaris, A. Mietens, R. Middendorff (*World Congress of Basic & Clinical Pharmacology 2023*)
9) "The influence of cell culture on the expression and function of natriuretic peptide receptors in smooth muscle cells" – **C. Rager**, T. Klöpper, S. Tasch, M. R. Whittaker, B. Exintaris, D. Müller, A. Mietens, R. Middendorff1 (*16th GGL Annual Conference 2023*)
10) "The influence of cell culture on the expression and function of natriuretic peptide receptors in aortic smooth muscle cells" – **C. Rager**, T. Klöpper, S. Tasch, M. R. Whittaker, B. Exintaris, A. Mietens, R. Middendorff (*ASCEPT Annual Meeting 2023*)
11) "The Influence of Cell Isolation and Culturing on Natriuretic Peptide Receptors in Aortic Vascular Smooth Muscle Cells" - **C. Rager**, T. Klöpper, S. Tasch, M. R. Whittaker, B. Exintaris, A. Mietens, R. Middendorff (*11th International Conference on cGMP 2024*)

## Prizes

1) MIPS most enthusiastic Teaching Associate for Pharmacy 1st Year 2024
2) Monash MNHS Faculty Travel Grant 2023
3) ASCEPT Uro-Gut Symposium Best Presentation 2022
4) Monash Graduate Scholarship (MGS) & Faculty International Tuition Scholarship (FITS) 2021

# List of Abbreviations

| | |
|---|---|
| Actb | Beta Actin |
| ADP | Adenosine Diphosphate |
| ANP | Atrial Natriuretic Peptide |
| ANS | Autonomic Nervous System |
| AR | Adrenergic Receptor |
| ATP | Adenosine Triphosphate |
| BNP | B-Type Natriuretic Peptide |
| $Ca^{2+}$ | Calcium |
| CaM | Calmodulin |
| cAMP | Cyclic Adenosine Monophosphate |
| cGMP | Cyclic Guanosine Monophosphate |
| CNP | C-Type Natriuretic Peptide |
| CNS | Central Nervous System |
| Ct | Cycle threshold, aka. Crossing Point (CP) or Quantification Cycle (Cq) |
| DAG | Diacylglycerol |
| ECM | Extracellular Matrix |
| ELISA | Enzyme-linked Immunosorbent Assay |
| ER | Endoplasmic Reticulum |
| FBS | Fetal Bovine Serum |
| FRET | Fluorescence Resonance Energy Transfer |
| GAPDH | Glyceraldehyde-3-phosphate dehydrogenase |
| GC | Guanylyl Cyclase |
| GC-A | Guanylyl Cyclase A (aka. NPR-A or NPR-1) |
| GC-B | Guanylyl Cyclase B (aka. NPR-B, NPR-2) |
| GDP | Guanosine Diphosphate |
| GE | Germinal Epithelium |
| GEF | Guanine Nucleotide Exchange-Factor |
| GTP | Guanosine Triphosphate |
| GPCR | G Protein Coupled Receptor |
| GOI | Gene of Interest |
| HKG | Housekeeping Gene |
| $IP_3$ | Inositol Triphosphate |
| JLU | Justus-Liebig-University |
| MAPK | Mitogen-activated Protein Kinase |
| MLCK | Myosin Light-Chain Kinase |
| MLCP | Myosin Light-Chain Phosphatase |
| MU | Monash University |
| NA | Noradrenaline (aka. Norepinephrine) |
| NADPH | Nicotinamide adenine dinucleotide phosphate |
| NBS | Non-specific Binding Control |

| | |
|---|---|
| NEP | Neprilysin (aka. MME, CD10, CALLA) |
| NO | Nitric Oxide |
| NONOate | Diethylamine NONOate Sodium Salt Hydrate |
| NOS | Nitric Oxide Synthases<br>endothelial NOS (eNOS), inducible NOS (iNOS), neuronal NOS (nNOS) |
| NP | Natriuretic Peptide |
| NPR | Natriuretic Peptide Receptor |
| NPRC | Natriuretic peptide Clearnce Receptor (aka. NPR-3) |
| ns | Non-significant |
| OD | Optical Density |
| P | Phosphate |
| Pa | Passage (as in Cell Culture Passage) |
| PCR | Polymerase Chain Reaction |
| PDE | Phosphodiesterase |
| Pen/Strep | Penicillin/Streptomycin |
| $PIP_2$ | Phosphatidylinositol 4,5-Bisphosphate |
| PKC | Protein Kinase C |
| PKG I | cGMP Dependent Protein Kinase I (aka. PRKG I, cGKI) |
| PLCβ | Phospholipase C |
| PTC | Peritubular Cell (as in SMCs in seminiferous tubules) |
| qPCR | Quantitative Polymerase Chain Reaction (here synonym to RT -qPCR) |
| RG | Reference Gene, aka. Housekeeping Gene (HKG) |
| RT | Reverse Transcription |
| SD | Standard Deviation |
| sGC | Soluble Guanylyl Cyclase |
| SMA | Smooth Muscle Actin |
| SMC | Smooth Muscle Cell |
| snRNP | Small Nuclear Ribonucleoprotein |
| SR | Sarcoplasmic Reticulum |
| ST | Seminiferous Tubule |
| vWF | von Willebrand Factor |
| WB | Western Blot |

# List of Figures

# List of Supplements

# List of Tables

# Abstract

Smooth muscle cells (SMCs) are found in a variety of tissues (e.g., cardiovascular and male reproductive tissues). Their relaxation is precisely regulated, inter alia by the cyclic guanosine monophosphate (cGMP) signalling system. The intracellular release of cGMP is mediated either through binding of nitric oxide to the soluble guanylyl cyclase or through natriuretic peptides (ANP, BNP and CNP) binding to specific membrane-bound guanylyl cyclases.

cGMP induced SMC relaxation is a promising target that is already addressed in therapies for cardiovascular and male reproductive disorders. However, in both cases the potential the natriuretic peptide cascade possesses is not yet fully exhausted, even though it seems that the relevance of different natriuretic peptides shifts during cardiovascular disease and natriuretic peptides were detected in seminal fluid of different mammals.

The current state of knowledge about vascular SMCs was predominantly generated using *in vitro* setups. More recent studies showed, however, that vascular SMCs in culture quickly adapt to the drastically changing circumstances. The results obtained for the first thesis chapter suggest that numerous pathways, including the cGMP signalling cascade, are affected by these adaptations.

For the first part in Chapter one, U2 was identified as appropriate reference gene for the direct comparison of SMCs in intact aorta and their counterparts in culture. This enables a more precise characterization of the significant modifications that the cGMP system undergoes upon culturing and provides a tool for fellow scientists to verify their *in vitro* data.

In the second part of Chapter one, U2 was applied for the direct comparison of cGMP related receptor expression which showed a significant increase for all receptors upon culturing of SMCs except for the ANP/BNP-receptor that remained unchanged. This shift resulted in an entirely different expression pattern in cultured aortic SMCs in comparison to their intact tissue of origin. cGMP responses to the stimulation with natriuretic peptides confirmed the expression results at the functional level, however, they seemed to show a delayed manifestation of the shift in receptor expression. This was found in aortic SMCs of both sexes suggesting a marginal influence of sex-hormones on the cGMP signalling system, at least in vascular SMCs.

In the male reproductive tract, SMCs are known to be influenced by testosterone and SMC contractions contribute to the capacity to procreate. SMCs are found in a circumferential layer surrounding the germinal epithelium of seminiferous tubules in the testis. Through their precisely

regulated spontaneous contractions of the testicular SMCs the seminal fluid in the tubular lumen is propelled towards the epididymis.

On the basis of an already established live imaging approach, the second thesis Chapter aimed to develop a sophisticated evaluation of spontaneous smooth muscle contractions and their change upon substance treatments in correlation to the spermatogenesis. Therefore, a custom-built Fiji-based code was developed to characterize superficial wall movements of two spermatogenic stages in seminiferous tubules. The data generated with the code confirmed a significant difference between their spontaneous movements regarding the contraction amplitude, frequency and overall movement intensity suggesting that these contractions contribute to the precisely timed sperm release from the germinal epithelium as well as to its transport. Upon treatment of the seminiferous tubules with nitric oxide, the code detected a significant reduction of the spontaneous contractions, independent of the respective spermatogenic stage. Considering that nitric oxide induces SMC relaxation this outcome was expected. When the seminiferous tubules were treated with noradrenaline, which is usually associate with SMC contraction, the analysis also detected a reduction of the spontaneous contractions. The reason for this unexpected outcome remains to be investigated further together with the relaxing capacities of natriuretic peptides. Nevertheless, the newly developed Fiji analysis holds potential as a diagnostic tool and sophisticated method for drug testing.

# 1 Introduction

## 1.1 Smooth Muscle – An Overview

Smooth muscle, in comparison to skeletal or heart muscle, has no visible striations (Sweeney & Hammers, 2018) and contracts involuntarily. SMCs are usually shorter and smaller than those of skeletal muscles (Hafen et al., 2023), which are found in syncytia. SMCs are present in a variety of tissues including the walls of hollow organs (Donadon & Santoro, 2021) like the digestive tract, urinary tract, the lungs (Halayko et al., 1996), in the vasculature (Davis & Hill, 1999; Dinardo et al., 2014), and many other tissues within the human body (e.g., reproductive organs (Exintaris et al., 2006; Robaire & Hinton, 2015; Weiser et al., 2020) or in the eye (Jensen, 2005)). SMCs are generally thought to possess the ability to spontaneously contract and to either hold their cellular tone for an extended period or to adapt it in a phasic manner, depending on their contraction type. These abilities essentially contribute to respective organ functions (Fleck et al., 2021; Stadler et al., 2021; Tykocki et al., 2017). The SMC functions investigated in the present study could be summarized as the transport or propulsion of body fluids (i.e., blood, semen) and its regulation.

*In vivo* SMCs are characterized by a spindle-shaped cell body and a single central cigar-shaped nucleus (**Figure1**). SMCs are either densely packed into groups or arrange themselves into

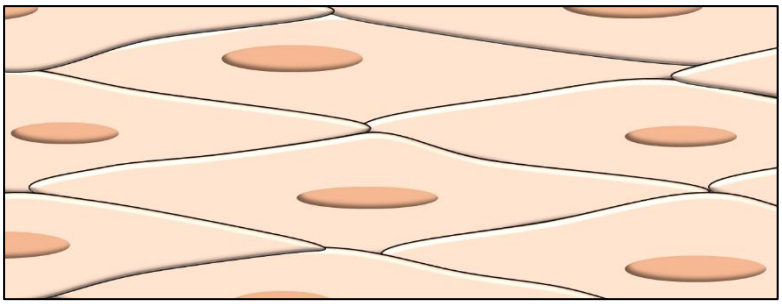

***Figure 1**: Schematic impression of the smooth muscle cell morphology.*

partially branching bundles (Hafen et al., 2023) that follow a unique direction. In culture primary SMCs try to adapt this pattern while growing in a multilayered so-called “hill-and-valley” structure (Chi et al., 2017; Majack, 1987). Under physiological circumstances SMCs display a low turnover (Lutgens et al., 1999). The cells express high levels of SMC-typical cytoskeletal (i.e., Smooth muscle actin (SMA)) and proteins indicative of contractility such as calponin (el-Mezgueldi, 1996; Winder & Walsh, 1993) but show low levels of proliferation and extracellular matrix (ECM) protein expression (Chamley-Campbell et al., 1979; Lehners et al., 2018; Owens, 1995).

However, even though SMCs in different tissues share multiple characteristics and functions several studies postulate that the genetic as well as phenotypic hallmarks of these cells can vary not only between different tissues but even in different areas of the same tissue (e.g., different segments of the aorta) depending on their embryological origin (Donadon & Santoro, 2021). Furthermore, it has been shown that SMCs, especially in vasculature, are characterized by an extraordinary plasticity (Frismantiene et al., 2018) and therefore they adapt into different subtypes of SMCs as a result of pathological alterations such as hypoxia or disruption of cell-cell contacts (Jia et al., 2024; Lehners et al., 2018) like The two most popular hypotheses on SMC differentiation will be discussed in relation to aortic disease in the chapters **1.3.1** and **1.3.2**. In short, however, this means that SMCs seem to be sensitive to changing conditions in their tissue environment and that they quickly adapt accordingly. This mechanism is often referred to as "phenotype switching" (Lincoln et al., 2006) (**Figure 2**).

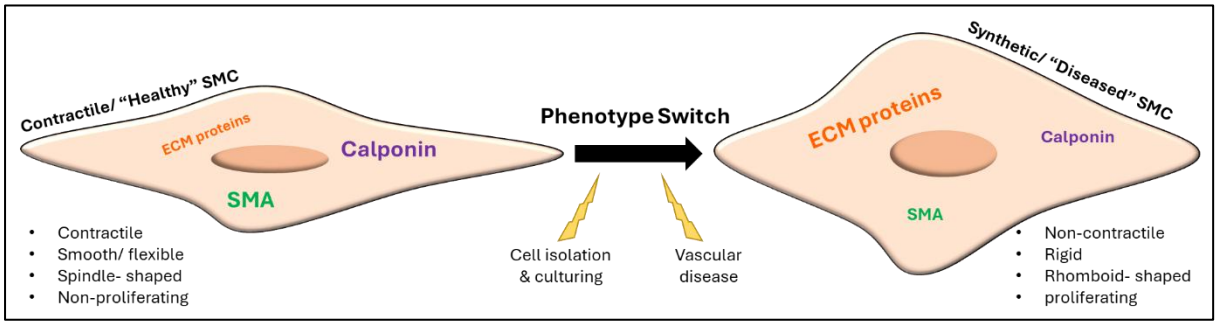


***Figure 2**: Classic dichotomous model of phenotype switching of vascular smooth muscle cells (SMCs).* Extracellular matrix (ECM), Smooth muscle actin (SMA).

Traditionally vascular SMCs were thought to undergo a dichotomous switch between contractile and synthetic phenotypes only (Tian et al., 2017). The recent understanding of the phenotypical transition, especially in the context of vascular disease, cumulated the development of a rather polymorphic switch model where contractile SMCs have the innate potential to differentiate into multiple different subtypes (Jia et al., 2024).

Smooth muscle is classified into two subtypes according to their electrophysiological coupling, single- and multi-unit type. The single-unit or unitary type is the most common smooth muscle type in the human body. In the single-unit type individual SMCs are connected by gap junctions through which a rapid exchange of second messenger molecules or ions is assured. A shift in the ion levels is fundamental to the transmission of action potentials between neighbouring cells (Pape et al., 2018; Pogoda et al., 2019). The arrangement of SMCs in the single-unit type allows them to contract as a unit or syncytium. These syncytia are activated by adjacent pacemaker cells, stimulated by the autonomic nervous system (ANS) (Hafen et al., 2023). The single-unit smooth muscle can be found in the outer wall of almost all hollow organs such as in the

gastrointestinal tract, but it is also found in the uterus, and smaller blood vessels (Pape et al., 2018). Because the single-unit smooth muscle produces slower but steady contractions it helps substances to move through the body (e.g., food through the gut).

The multi-unit type on the other hand, consists of SMCs that are innervated individually by autonomic nerve fibres. They have fewer gap junctions; hence they contract independently of their neighbouring cells. This type of smooth muscle is found in the ciliary muscles and iris of the eye, larger blood vessels, and bronchi, and allows for a more precise coordination of contractions (Hafen & Burns, 2023).

Smooth muscle is an involuntarily acting type of muscle. The ability to contract spontaneously is precisely regulated by the ANS, hormones and neurotransmitters. The molecular events of SMC contraction and relaxation will be explained in more detail in the following section of this chapter **1.2**, while the subsections **1.2.1** and **1.2.2** focus on the noradrenergic pathway and cGMP signalling respectively.

## 1.2 Smooth muscle - Contraction and Relaxation

SMC contractions are initiated by an increasing intracellular concentration of calcium ($Ca^{2+}$). $Ca^{2+}$ influx into the SMC can be triggered in different ways (**Figure 3A**).

Some of the $Ca^{2+}$ inflow is realized by the opening of voltage-gated and stretch-sensitive $Ca^{2+}$ channels in the cell membrane (Thorneloe & Nelson, 2005). In addition, there are G protein coupled receptors (GPCRs) (Weis & Kobilka, 2018) which can be activated by neurotransmitters. The subgroup of the adrenergic receptors (ARs) for instance is activated by noradrenaline (NA) (subsection **1.2.1**). The activated GPCRs in turn stimulate phospholipase C (PLCβ) to cleave phosphatidylinositol 4,5-biphosphate ($PIP_2$) into inositol triphosphate ($IP_3$) and diacylglycerol (DAG). $IP_3$ binds to receptors located on the endoplasmic reticulum (ER) and the release of $Ca^{2+}$ into the cytoplasm is activated (Phelps et al., 2023; Webb, 2003). DAG, together with $Ca^{2+}$, now activates the protein kinase C (PKC). $Ca^{2+}$ binds to calmodulin (CaM) (Means et al., 1991) building the $Ca^{2+}$/CaM complex that activates the myosin light-chain kinase (MLCK). Furthermore, the

$Ca^{2+}$/CaM complex stops the blockage of the ATPase by caldesmon and calponin (Makuch et al., 1991; Winder et al., 1998) (**Figure 3 B**).

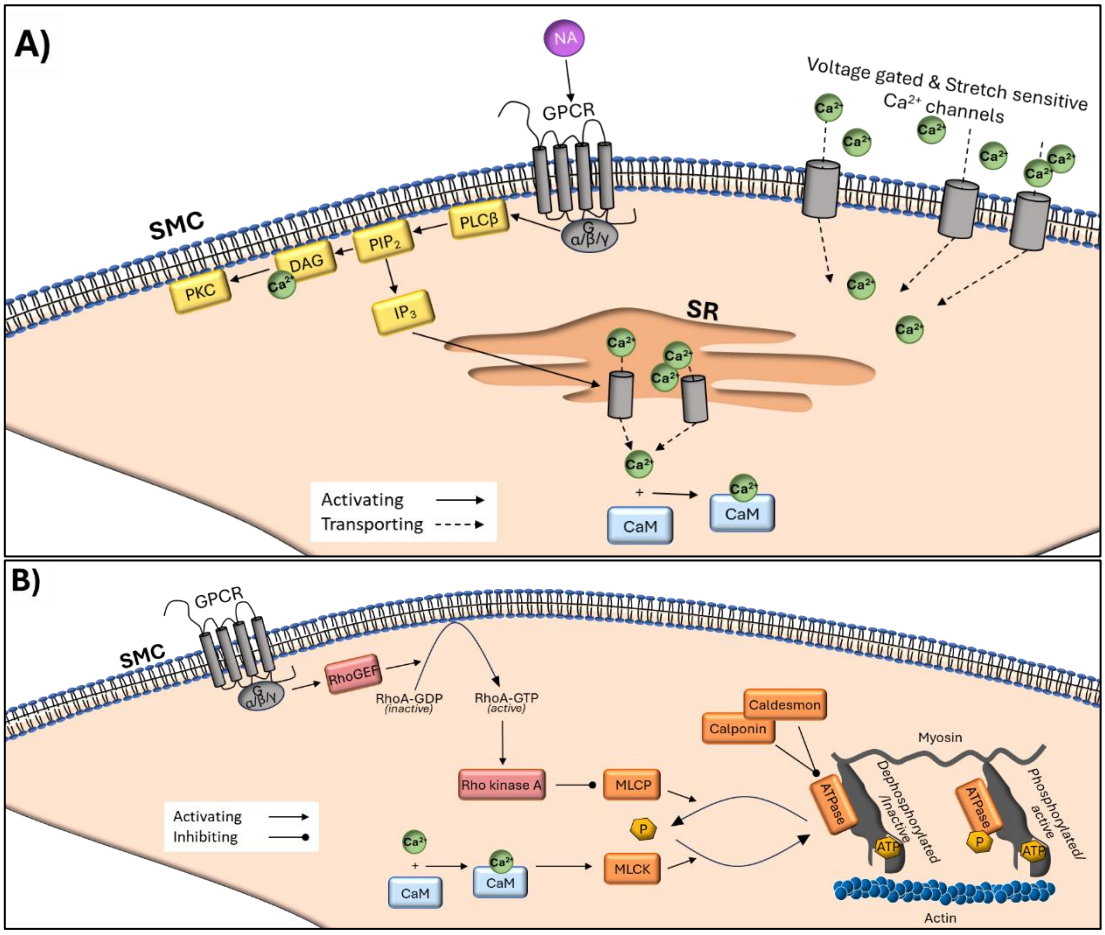


***Figure 3**: Signalling background of smooth muscle cell (SMC) contractility.*
(**A**) Calcium ($Ca^{2+}$) signalling and (**B**) Cross-bridging cycle of actin and myosin are crucial for SMC contraction. Figure adapted from (Webb, 2003). Adenosine triphosphate (ATP); Calmodulin (CaM); Diacylglycerol (DAG); Guanosine diphosphate (GDP); Guanine nucleotide-exchange factor (GEF); G protein (Gα/β/γ); G protein coupled receptor (GPCR); Guanosine triphosphate (GTP); Inositol triphosphate (IP3); Myosin light-chain kinase (MLCK); Myosin light-chain phosphatase (MLCP); Noradrenaline (NA); Phosphate (P); Phosphatidylinositol 4,5-bisphosphate (PIP2); Protein kinase C (PKC); Phospholipase C (PLCβ); Sarcoplasmic Reticulum (SR).

MLCK now phosphorylates the myosin light-chain, and the activated ATPase enables the interaction between myosin and actin (Kraft & Brenner, 2018; Webb, 2003) (**Figure 4**). The myosin light-chain phosphatase (MLCP) dephosphorylates the myosin light chain and therefore prevents the binding of myosin and actin. This causes SMC relaxation while excessive $Ca^{2+}$ is either transported out of the cell or back into the ER. The binding of myosin and actin usually is prolonged through MLCP inhibition by Rho kinase and PKC (Christ & Andersson, 2007; Webb, 2003). The cytoskeleton of SMCs is mainly composed of myofilaments which consist of actin (part of the thin filament asides tropomyosin) and the motor protein myosin (thick filament) (Sweeney & Hammers, 2018). The visible contraction of muscle cells, no matter smooth muscle or else, is the result of multiple shortenings by sliding actin along the myosin filaments under energy consumption.

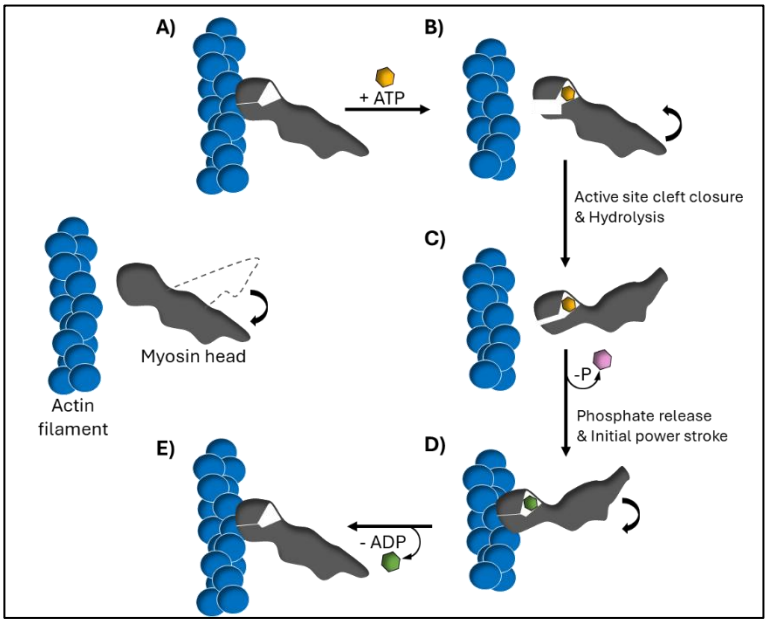


***Figure 4**: Actin and myosin interaction during smooth muscle cell (SMC) contraction.* Adenosine triphosphate (ATP), Adenosine diphosphate (ADP). Figure adapted from (Rayment et al., 1993).

A single myosin filament is connected to several actin filaments in a crossing manner. Bundles of actin filaments are anchored in membrane and attached to cytoplasmic dense bodies (**Figure 5**) (Sweeney & Hammers, 2018).

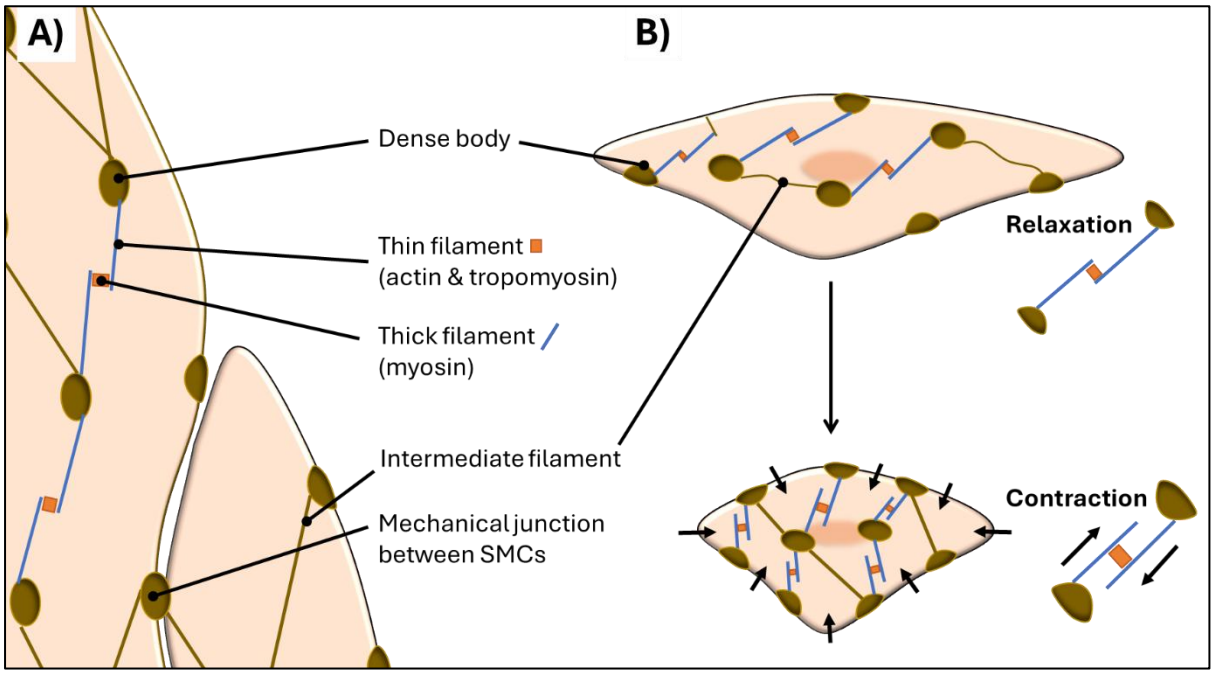


***Figure 5**: Cytoskeletal proteins and their action during a relaxed and contracted stage of smooth muscle cells (SMCs).* (**A**) Overview of SMC proteins involved. (**B**) Cytoskeletal changes due to SMC contraction. Figure adapted from (Sweeney & Hammers, 2018).

The repeated attachment and reorientation of the myosin heads on the actin filament under the consumption of adenosine triphosphate (ATP) allow for the sliding of actin along myosin (**Figure 4**) (Rayment et al., 1993). When the myosin head is charged with ATP it has a low binding affinity

to actin. When the myosin head is phosphorylated, and the ATPase is activated, ATP is split into adenosine diphosphate (ADP) and phosphate (P). The myosin neck now can bend towards and bind actin with high affinity creating a cross-bridge between the two filaments. After ATP dephosphorylation is completed myosin releases ADP and P. Consequently, the myosin is flexing back its head part which in turn is pulling actin to slide along the thick myosin filament. This movement is known as power stroke. The myosin head now recharges with ATP and detaches from the actin (Rayment et al., 1993). When the MLCP is inhibited, the myosin stays phosphorylated, and the cycle can start over.

The repeated attachment and flexion of multiple myosin heads build up to an organized contraction. If the MLCP is activated the P is cleaved from the myosin head which blocks the binding of actin by myosin (Kraft & Brenner, 2018). MLCP is inter alia activated by the cGMP dependent protein kinase (PKG I) (Surks, 2007) which can be stimulated by nitric oxide (NO) or natriuretic peptide (NP) induced cGMP release (subsection **1.2.2**).

### 1.2.1 SMC Contracting Pathways – Noradrenergic Signalling

NA, also known as norepinephrine, was identified in the 1940s. It belongs to the family of catecholamines and can either act as neurotransmitter or as a hormone (Zouhal et al., 2008). As a neurotransmitter NA is released from synapses in the nervous system. NA initiates sympathetic responses in numerous organs (O'Donnell et al., 2012) for example in those of the male reproductive tract where it plays an essential role in the regulation of sexual arousal (Mills et al., 2001) (chapter **1.5.1.4**).

To elicit its effects, NA binds to ARs (Zouhal et al., 2008). The ARs can be classified as α (1 & 2) and β ARs (1-3). They all are GPCRs, but their localization and effects differ (Strosberg, 1993). How GPCR related $Ca^{2+}$ release from the ER is initiated has already been described above (chapter **1.2**; **Figure 3**). Especially in male reproductive tissues, the α1 AR is known to mediate SMC contraction (Caine et al., 1975; Michel, 2007; Traish et al., 2000). In the present study NA was used as a treatment for vitality control for rat reproductive tissue (chapter **1.5**).

### 1.2.2 SMC Relaxing Pathways - cGMP Signalling

SMC relaxation can be mediated by the intracellular second messenger molecule cyclic guanosine 3',5'-monophosphate (cGMP) (Hofmann, 2020; Lucas et al., 2000) (**Figure 6**).

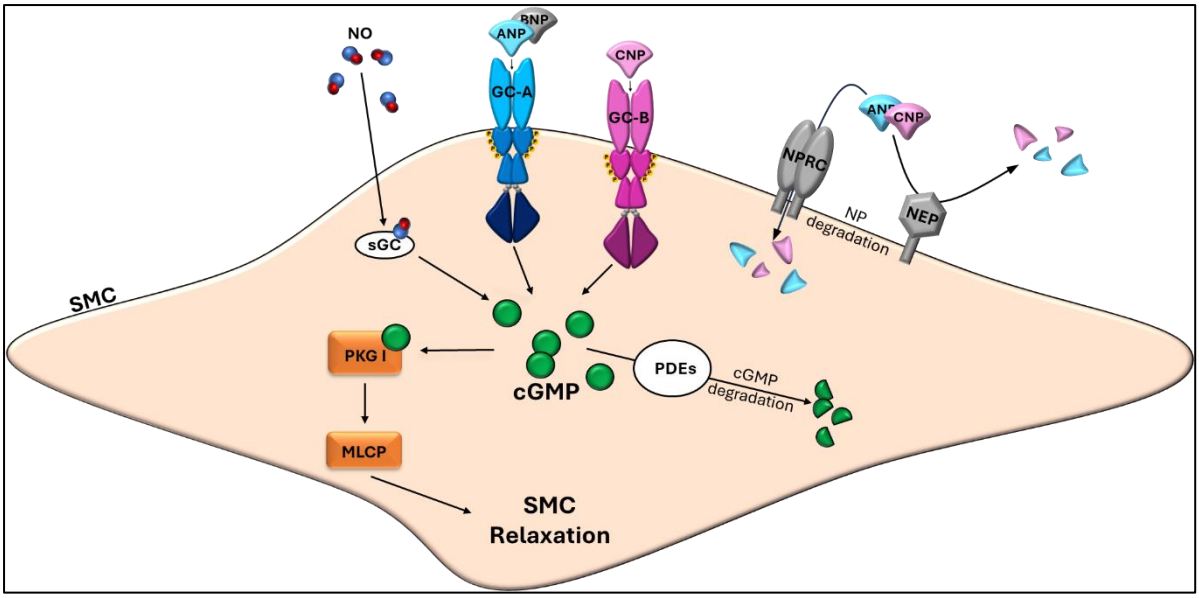


***Figure 6**: cGMP signalling.*
Atrial natriuretic peptide (ANP), B-type natriuretic peptide (BNP), C-type natriuretic peptide (CNP), cyclic guanosine monophosphate (cGMP), Guanylyl cyclase A (GC-A), Guanylyl cyclase B (GC-B), Myosin light chain phosphatase (MLCP), Neprilysin (NEP), Natriuretic peptide clearance receptor (NPRC), Nitric oxide (NO), Phosphodiesterase (PDE), cGMP dependent protein kinase I (PKG I), soluble guanylyl cyclase (sGC), Smooth muscle cell (SMC). Figure in parts adapted from (Potter, 2011a) and (Potter, 2011b).

cGMP is produced through guanosine triphosphate (GTP) reduction (Müller et al., 2006) by guanylyl cyclases (GCs) (Lucas et al., 2000). A common way of cGMP production is via nitric oxide (NO) (Robbins & Grisham, 1997) induced activation of the cytosolic soluble GC (sGC) (Wu et al., 2022). However, cGMP is also produced by particulate GCs with the membrane-bound GC-A and GC-B (Kuhn, 2004; Kuhn, 2016) being the most relevant for the present study. The signalling cascades of cGMP production as well as cGMP degradation will be explained in more detail in the subsequent sections (**1.2.2.1**, **1.2.2.2** & **1.2.2.3**). Once cGMP is released into the cytoplasm it binds to the cGMP dependent protein kinase I (PKG I) which additionally causes a decrease in intracellular [$Ca^{2+}$] (Carvajal et al., 2000). PKG I then binds to MLCP that inhibits the actin and myosin interaction through dephosphorylation of the myosin light chain. As a result, SMC relaxation is induced.

### *1.2.2.1 Nitric oxide and the sGC/cGMP signalling cascade*

The endogenous activator of the cGMP signalling cascade that is studied the most, especially in the cardiovascular field (Yetik-Anacak & Catravas, 2006), is NO. NO was first discovered as a gaseous air pollutant in 1722 (Goshi et al., 2019). Later it was considered to have important regulatory functions in the endothelium which was subsequently proven in a seminal study by Ignarro and colleagues in 1987 (Ignarro et al., 1988) who showed that the major endothelial derived relaxing factor was indeed NO (as cited in Fleming & Busse, 1999; Sandner et al., 2021). NO is known to be produced by NO synthases (NOS) (Goshi et al., 2019; Hong et al., 2009; Potter,

2011a). NOS are heterodimers that exist in three different isoforms named after their site of action and production: endothelial (eNOS), inducible (iNOS), and neuronal NOS (nNOS). eNOS and nNOS act $Ca^{2+}$-dependently while iNOS is $Ca^{2+}$-independent (Luo et al., 2021). NOS use L-arginine as their main substrate, which together with the co-substrate nicotinamide adenine dinucleotide phosphate (NADPH) and oxygen is converted to NO, citrulline, $NADP^+$ and water (Förstermann & Sessa, 2012; Potter, 2011a).

nNOS is constitutively expressed in neuronal tissue where it's NO production is associated with synaptic function in the CNS as in neurogenesis, learning and memory (Huang et al., 1993; Kasamatsu et al., 2022; Nelson et al., 1995). Furthermore, NO synthesis by nNOS plays an essential role in the central regulation of blood pressure and vasodilation by activation through peripheral nerves (Capettini et al., 2010; Togashi et al., 1992). nNOS dysregulation is associated with several diseases such as stroke, Alzheimer's and Parkinson's disease as well as multiple sclerosis (Steinert et al., 2010). Besides neuronal effects, NO synthesized by nNOS affects the relaxation of SMCs in different tissues throughout the body. For instance, in the male reproductive tract nNOS plays a key role for the penile erection by induction of SMC relaxation in the corpus cavernosum (de Souza et al., 2022; Gur et al., 2020; Ignarro et al., 1990). Therefore, NO induced cGMP production became a major therapeutic target for the treatment of erectile dysfunction (Davies, 2015; Gong et al., 2017).

eNOS, besides endothelial cells, was found to be expressed in a series of other cells such as cardiomyocytes, platelets, neurons in the brain and tubular epithelial cells in the kidneys (Förstermann et al., 1994). NO production through eNOS plays a particular role in the cardiovascular system. Here it is mainly responsible for the dilation of all types of blood vessels (Capettini et al., 2010; Förstermann & Sessa, 2012). It has been shown that endogenous NO prevents thrombosis through inhibition of platelet aggregation to the blood vessel wall, but it remains unclear if this NO is actually produced by eNOS (Tymvios et al., 2009). Furthermore, NO produced by eNOS may have anti-inflammatory and anti-atherosclerotic roles as it impairs leukocyte adhesion to the blood vessel wall (Hong et al., 2019) and acts anti-apoptotic (Dimmeler & Zeiher, 1999) in a cGMP-dependent or independent manner (Razavi et al., 2005). Lastly, eNOS and NO have been shown to regulate vascular SMC proliferation as NO inhibits DNA synthesis and mitogenesis (Sarkar et al., 1997). An abnormal activation of eNOS is usually associated with cardiovascular risk factors, e.g., hypertension, diabetes mellitus, and hypercholesterolaemia (Förstermann & Sessa, 2012).

iNOS, in comparison to nNOS and eNOS, is not expressed under normal conditions and is not found in most cells but its expression can be induced by different factors (Förstermann & Sessa,

2012). iNOS expression is activated and maintained in scenarios of inflammation thus a large amount of NO is released during inflammation (Nathan & Hibbs, 1991). In scenarios such as tumorigenesis, bacterial and parasite infections NO diffuses into the tumour or bacterial cells where it interacts with the respective (tumorigenic/pathogenic) DNA causing tumour/bacterial cell death.

This points out an important feature of NO, is that it can easily diffuse through the cell membrane to interact with intracellular components.

Even though many target tissues of NO have been identified, only one real receptor for NO is known. The cytosolic receptor sGC is a heterodimer that consists of α and β subunits of with the β1 subunit being chosen most crucial for sGC activation by NO (Potter, 2011a). Hence, the sequence of which β1 subunit was chosen to investigate the expression of the sGC in this study (chapter **4.1.4**). Most relevant to this thesis sGC appears to be the sole mediator of NO effects on the cardiovascular and reproductive systems (Rajfer et al., 1992).

sGC is highly specific for NO and responds to an elevation of the NO concentration by cGMP generation from GTP (Wu et al., 2022). Since the elevation of cGMP leads to a variety of cellular and physiological events and sGC plays an essential role for NO-induced cGMP increase, it is important to understand the molecular events that govern the function of this system for clinical use. Recently, several NO-independent sGC regulators have been characterized and are already approved for patient treatment in the field of cardiac or vascular disease (Sandner et al., 2021).

#### *1.2.2.2 Natriuretic peptides and the NPR/cGMP signalling cascade*

The family of natriuretic peptides (NPs) comprises three structurally related paracrine factors (Potter et al., 2009). Atrial or A-type NP (ANP) was the first NP to be discovered in 1981(de Bold et al., 1981). A few years later B-type NP (BNP) (Sudoh et al., 1988) and subsequently C-type NP (CNP) (Sudoh et al., 1990) were identified after being extracted from porcine brain. Because of that BNP was initially called brain-NP. ANP as well as BNP are primarily synthesised in the heart (de Bold et al., 1986; Edwards et al., 1988; Nakagawa et al., 2019). In the cardiovascular system they are cardioprotective and induce vasodilation (Kuhn, 2016; Potter, 2005). ANP in addition is found at lower concentrations in other tissues such as the kidneys (Potter et al., 2006).

ANP and BNP are biomarkers for myocardial stretch and used for the diagnosis and prognosis of heart failure (Han et al., 2020). BNP, however, is the preferred clinical marker for heart failure due to its 10-times longer half-life than ANP and CNP (Potter et al., 2006). CNP is the predominant NP in the brain and additionally is built in chondrocytes where it fulfils a crucial role in long bone growth (Chusho et al., 2001). In addition, CNP is found in the endothelium throughout the body, in the heart and in blood plasma (Vollmar et al., 1993). In the cardiovascular context CNP release

is thought to fulfill a modulating role at its site of action (Dickinson et al., 2024), e.g., as a response to a local increase in blood pressure (Chun et al., 1997). Lastly, moderate CNP concentrations could be detected in porcine seminal fluid (Chrisman et al., 1993).

The three NPs share a similar structure, which seems to be highly conserved across different species (Potter et al., 2009). The basic structural component of all NPs is a cysteine- flanked 17-amino acid disulphide-linked ring that is crucial for their biological activity (Misono et al., 1984) (**Figure 7**).

ANP and BNP in addition have two tails, one at the N- and one at the C-terminus, while CNP only

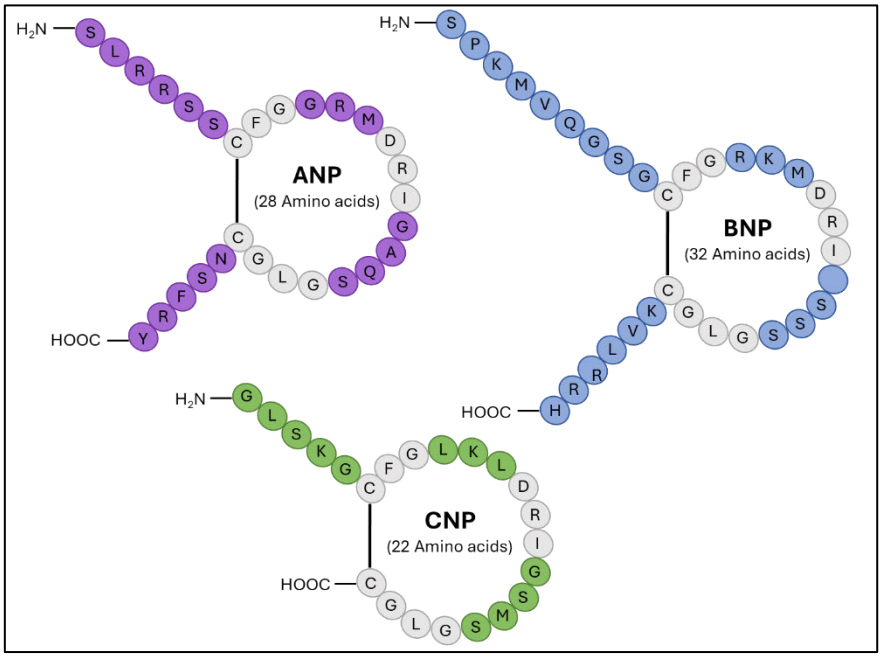


***Figure 7**: Structure of the human natriuretic peptides.*
Atrial natriuretic peptide (ANP), B-type natriuretic peptide (BNP), C-type natriuretic peptide (CNP). Figure adapted from (Potter et al., 2009).

carries a tail at the at the N-terminus. Thus, all NPs have a similar size. The NPs are synthesized as prepropeptides which are then cleaved by enzymes (e.g., corin and furin) to a propeptide, which subsequently is cleaved again by specific enzymes to obtain the biologically active NP (Potter et al., 2009). The mature ANP consists of 28 amino acids, BNP of 32, and CNP is either 53 or 22 amino acids long (Potter et al., 2006). The mature CNP-53 in some tissues is further processed to build CNP-22 by an enzyme yet remaining to be identified (Kuwahara, 2021). Nevertheless, CNP-53 as well as CNP-22 are equally capable of activating the CNP specific receptor (Tawaragi et al., 1991; Yeung et al., 1996).

NPs bind specific membrane-bound receptors to induce intracellular cGMP production and to initiate SMC relaxation. ANP and BNP specifically bind to the particulate receptor GC-A (also known as NP receptor 1 or A; NPR-1/A) and CNP to GC-B (also known as NP receptor 2 or B; NPR-

2/B) (Potter et al., 2009; Suga, Nakao, Mukoyama, et al., 1992). GC-A and -B are characterized by a similar structure that comprises four domains with different features that contribute to the overall function of these receptors (**Figure 8**).

The largest domain is the extracellular ligand binding domain with a short membrane-spanning

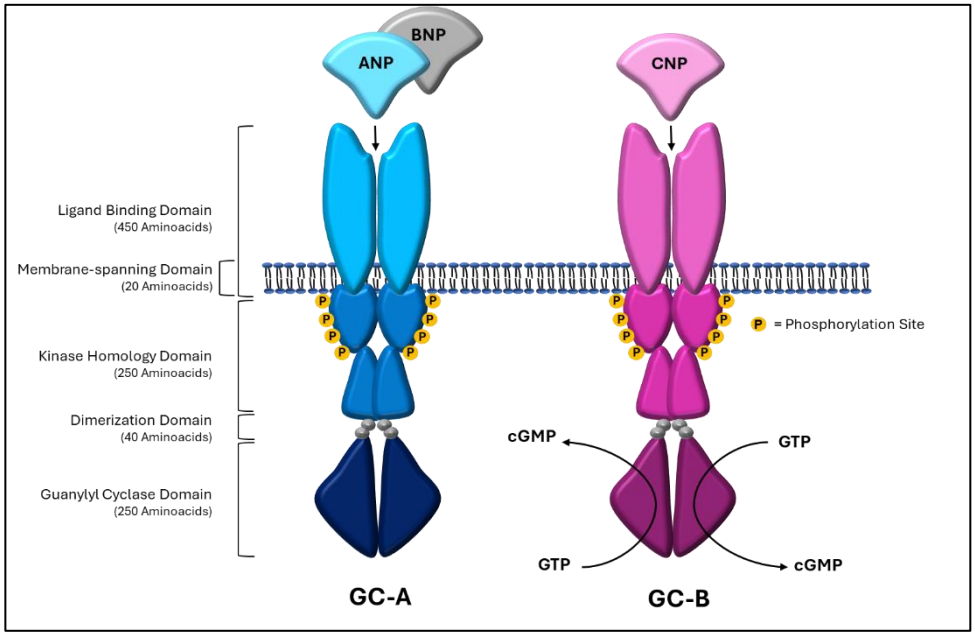


***Figure 8**: Structure of the natriuretic peptide receptors GC-A and GC-B.*
Atrial natriuretic peptide (ANP), B-type natriuretic peptide (BNP), C-type natriuretic peptide (CNP), cyclic guanosine monophosphate (cGMP), Guanylyl cyclase A (GC-A), Guanylyl cyclase B (GC-B), Guanosine triphosphate (GTP). Figure adapted from (Potter, 2011b, Figure 1).

region. At the intracellular side both GC-A and GC-B possess a large kinase homology domain which is followed by a dimerization domain and a carboxyl-terminal guanylyl domain (Potter, 2011a). Like the NO-induced sGC, both GCs generate cGMP from GTP after binding their respective ligands. cGMP then binds to the PKG I and SMC relaxation is triggered through phosphorylation and activation of the MLCP (MacDonald & Walsh, 2018) (chapter **1.2.2**, **Figure 6**).

#### *1.2.2.3 Regulation of the Natriuretic peptide and cGMP levels*

The regulation of the intracellular cGMP level, generated through the NP signalling cascade specifically, is complex. It entails several regulatory mechanisms such as receptor-mediated NP clearance, extracellular proteolysis, intracellular cGMP degradation and receptor (de)sensitization.

Besides the NP receptors GC-A and -B, a third non-GC-coupled receptor the NP clearance receptor NPRC (also known as NPR-3) exists (D. Liu et al., 2023; Rubattu et al., 2010). NP clearance by the NPRC was firstly described during the late 1980s (Maack et al., 1987). NPRC shares structural similarities with GC-A/B (Porter et al., 1990), especially in the ligand binding

domain, and binds all NPs with a comparable affinity. NPRC is a disulfide-linked homodimer receptor that degrades NPs upon receptor-mediated internalization (Matsukawa et al., 1999). Physiological studies suggest that its main function is NP clearance, however, its involvement in other signalling functions has been suggested (Rubattu et al., 2010). It is worth mentioning that the NPRC is the most expressed NPR in endothelial cells (Leitman et al., 1986).

Furthermore, NPs can be degraded through extracellular proteolysis (Potter, 2011b). Neprilysin (NEP) (also known as neutral endopeptidase, enkephalinase, CD10, CALLA) is a zinc-containing, membrane-bound, extracellular protease that cleaves NPs (Thong et al., 2014; Kerr & Kenny, 1974) at specific sites. In comparison to the NPRC, which degrades NPs specifically, NEP is a more general protease (Potter, 2011b). NEP not only degrades NPs but also other peptides that are involved in the regulation of SMC relaxation, such as angiotensin 1 and 2, bradykinin, endothelin, which makes it a promising therapeutic target in the treatment of heart failure (Bozkurt et al., 2023) and arterial hypertension (Salazar et al., 2020).

Lastly, the most important mechanism of intracellular cGMP level reduction is through hydrolysis by cGMP-specific phosphodiesterases (PDEs). Eleven PDEs are present in mammalian cells (Francis et al., 2009). PDE1A and B, PDE5, PDE6 and PD9 hydrolyse cGMP specifically. PDE1C (Zhao et al., 1997) PDE2, PDE3, PDE10 and PDE11 hydrolyse cGMP as well as cyclic adenosine monophosphate (cAMP). By degrading intracellular cGMP, the cGMP specific PDEs disrupt SMC relaxation (Maurice et al., 2014). PDE1 is the predominant PDE in cardiomyocytes (Lukowski et al., 2010), while PDE6 is specifically expressed in photoreceptors. PDE9, being highly specific for cGMP, is primarily expressed in the central nervous system (Kleppisch, 2009). PDE1A, 1B, and 1C, PDE3A and 3B, and PDE5 are the most abundant cGMP-dependent PDEs present in arterial smooth muscle with PDE5 showing highest gene expression amongst PDEs in the aorta (Rybalkin et al., 2003; Cesarini et al., 2019). Thus far, PDE5 is also exploited the most for clinical applications (Cesarini et al., 2019). To date not much is known about the expression of PDE9, the last cGMP-specific PDE, in the aorta. Recent gene expression studies of the Middendorff lab using a purchased human aortic SMC cell line showed a very low to undetectable PDE9 expression. It remains to be seen whether isolation and culturing of these cells contribute to an abnormal PDE9 expression in comparison to intact aortic tissue.

However, not only depending on the tissue but also on the signalling pathway by which the cGMP is produced (either via NO/sGC or NPs/GC-A/B), different PDEs seem to be responsible for most of the cGMP degradation. Using a fluorescence resonance energy transfer (FRET)- based cGMP indicator studying PDEs in primary vascular SMCs, Krawutschke and colleagues found that cGMP signals produced via the NO/sGC cascade were more tightly controlled by PDE5 than PDE3.

However, in contrast the case of NP-produced cGMP, PDE3 and 5 seemed to be of similar relevance. Under their experimental conditions PDE1 did not seem to have any effect on the cGMP level (Krawutschke et al., 2015). Again, not much was mentioned about the contribution to the cGMP degradation regarding PDE9.

It is important to address the involvement of different PDEs in the cGMP degradation in aortic smooth muscle as this could potentially interfere with the cGMP measurements performed for the present study. Cells and tissue were therefore treated with 3-Isobutyl-1-methylxanthine (IBMX) a specific PDE inhibitor that is known to sufficiently antagonize all cGMP-dependent PDEs except for PDE9, of which we can assume no or minor contribution to the cGMP reduction.

PDEs are essential regulators of the cGMP system and are involved in numerous physiological functions, where they previously gained recognition as therapeutic targets for the treatment of various diseases that are somehow related to SMC malfunction, e.g., heart failure, asthma, depression, and erectile dysfunction (Conti et al., 1995; Mehats et al., 2002; Rotella, 2002; Torphy, 1998).

Lastly, there are self-regulatory mechanisms for homologous and heterologous desensitization of GC-A and GC-B (**Figure 9**). Both receptors are desensitized through a prolonged exposure to their specific peptide ligands (homologous desensitization) or other peptide ligands (heterologous desensitization). The desensitization is not only confirmed by a reduced guanylyl activity but also, a decreased sensitivity of the receptors for their ligands (Foster et al., 1999; Kuhn, 2004; Potter et al., 2006). This ligand-dependent decrease in GC activity was found to be

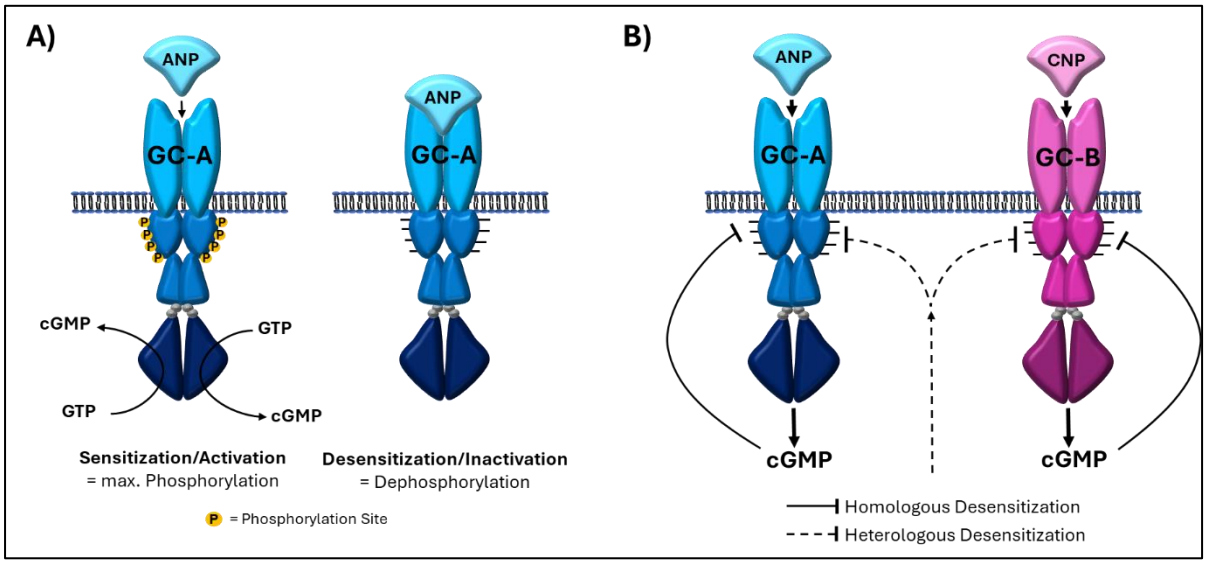


***Figure 9**: Sensitization and Desensitization of GC-A and GC-B.*
Atrial natriuretic peptide (ANP), C-type natriuretic peptide (CNP), cyclic guanosine monophosphate (cGMP), Guanylyl cyclase A (GC-A), Guanylyl cyclase B (GC-B), Guanosine triphosphate (GTP). Figure adapted from (Potter, 2011b, Figure 1).

correlated with the phosphorylation status of intracellular serine threonine residues at the kinase homology domain of these particulate GCs (Potter et al., 2006).

## 1.3 Vasculature

In the early 17th century physiologist William Harvey, as cited in Ribatti's publication 2009, first described the circulation in larger blood vessels (Ribatti, 2009) of the peripheral vascular system. The peripheral vascular system encompasses all blood vessels outside the heart and could therefore be defined as the aorta and its branches (**Figure 10**). These branches then can be further classified in arteries and arterioles, veins and venules, and capillaries (Tucker et al., 2024).

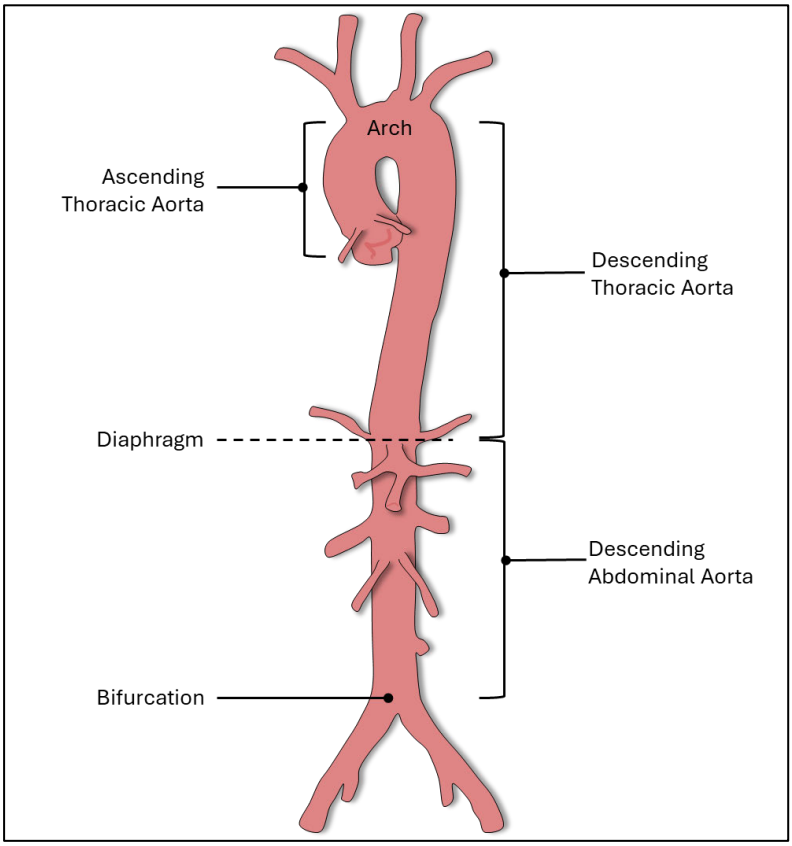


***Figure 10**: Schematic human aorta.*

The main functions of the vascular system are the transport of oxygenated blood to organs and the venous return of deoxygenated blood to the heart. It therefore maintains cellular homeostasis of peripheral tissues and ensures their steady supply with oxygen and nutrients as well as other essential factors (e.g., hormones) (Pugsley & Tabrizchi, 2000). The structure and specific functions of each vessel depend on the region and the tissue it supplies but all blood vessels, apart from capillaries, share the same basic three-layered structure (Tucker et al., 2024) (**Figure 11**).

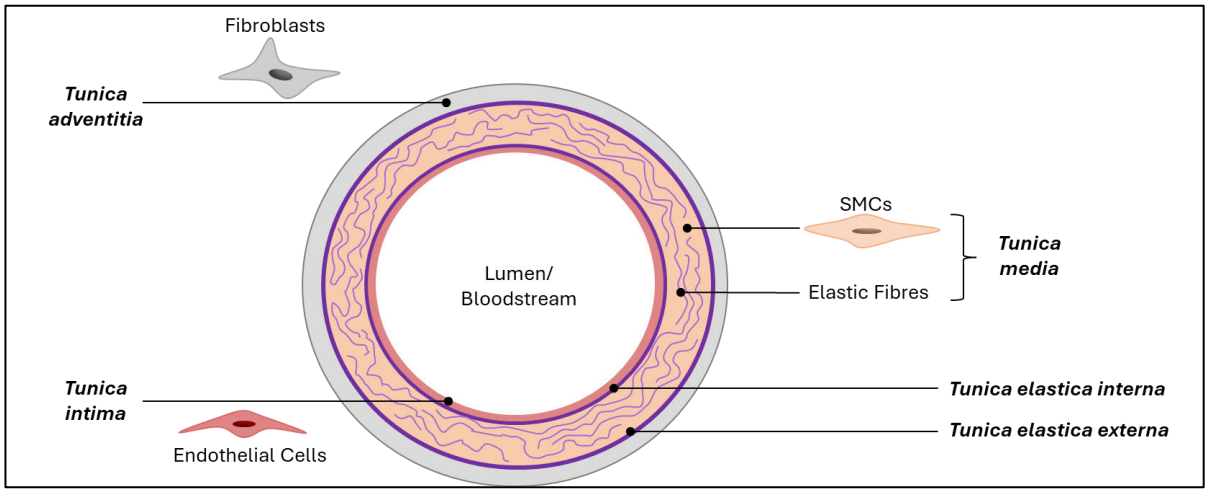


***Figure 11**: Schematic wall structure of elastic arteries.*
Smooth muscle cells (SMCs).

From the lumen towards the outside of the vessel the three layers (tunicae) are the *tunica intima*, the *tunica media,* and the *tunica adventitia* (Borysenko & Beringer, 1984). The amount of muscle and elastic components in each layer varies between the vessel types that perform different functions and is already determined at early developmental stages (Pugsley & Tabrizchi, 2000). These differences are usually considered for histological distinction between the different vessel types.

The *intima* is the inner thin lining of endothelial cells, or highly specialized cell monolayer between the blood and the tissue, which mainly exists to create a frictionless passageway for the blood. The endothelium therefore is the layer exposed to the most shear stress and pressure of the passing blood stream (Pohl et al., 1986).

Endothelial cells are thought to be involved in the maintenance of tissue homeostasis, in the process of thrombolysis and coagulation, and inflammatory and immunological events (Köhler & Hoyer, 2007; Pugsley & Tabrizchi, 2000). Most importantly, the endothelium is thought to regulate the contractility and tone of the vascular smooth muscle (Furchgott & Zawadzki, 1980) and therefore blood pressure (Köhler & Hoyer, 2007) for instance through the release of NO.

The middle layer, or *media*, of larger elastic arteries like the aorta contains mainly SMCs which are interlaced by elastic fibres (Pugsley & Tabrizchi, 2000) (following chapter **1.3.1**). It is the layer that contributes to the diameter changes of the vessel through relaxation and contraction to regulate the blood pressure (Krawutschke et al., 2015). The *media* is consequently the most important layer for this study, and special features of these cells will be further elaborated (chapter **1.3.1**).

The outer layer (*tunica adventitia*) has always been thought to be composed of fibro-elastic connective tissue and to provide structural support and a dense mesh of collagen-rich ECM that

maintains the vessel structure (Pugsley & Tabrizchi, 2000). Further studies investigated the involvement of the *adventitia* in processes such as tissue growth, inflammation and repair in response to vessel disease and hypothesize that this layer possesses features exhibited by stem cell niches (Majesky et al., 2012; Zengin et al. 2006; Hu et al., 2004). The *adventitia* is interlaced by nerval and lymphatic plexus and of the *vasa vasorum*, a microvascular network that provides the thick wall of larger blood vessels, such as the aorta (following chapter **1.3.1**), with oxygen and nutrients (Heistad et al., 1981; Majesky et al., 2012). Interestingly, in rat and mice, this *vasa vasorum* network cannot be found.

Until recently, rats used to be and are still a preferred animal model for instance in studying hypertension (Dornas & Silva, 2011; Lerman et al., 2019). Rats are larger than mice and therefore surgical interventions, serial blood draws and physiological measurements are easier than in mice (Jacob, 2010; Szpirer, 2020). To facilitate the harvest of a large amount of primary aortic SMCs, rat was the model of choice in the present study (chapter **4.1.1**).

### 1.3.1 Arterial Blood Vessels - Aorta

In general, SMCs account for the majority of cells in the arterial vessel wall (Davis & Hill, 1999; Dinardo et al., 2014; Tykocki et al., 2017). However, according to their content and arrangement of elastic components two types of arteries can be distinguished (Pugsley & Tabrizchi, 2000; Tucker et al., 2024). Most importantly it is the *tunica media* that is substantially different in elastic and muscular arteries (Becker & Kuznetsov, 2013).

The elastic arteries (e.g., aorta) or conducting arteries are found in proximity to the heart where they are mainly involved in the accommodation of larger blood volumes (Yu & McEniery, 2020). The high density of elastic fibres within the SMC layer (Lannoy et al., 2014) enables their adaptation to ample changes in the blood volume upon the periodic ejection of stroke volumes from the beating heart. Elastic arteries dampen the pulsatile oscillations to create a homogenous blood flow (Yu & McEniery, 2020).

In muscular or distributing arteries the proportion of SMCs to elastic components is significantly higher than in elastic arteries. Here, the thick SMC layer contains fewer discontinuous elastic fibres. Muscular arteries account for the majority of arteries in the body, and they are responsible for the distribution of blood to all organs, as their SMCs are able to regulate diameter of the vessel (Becker & Kuznetsov, 2013).

Since the beginning of 2024, the aorta has officially been recognized as an independent organ, putting it on the same level with the heart and the lungs (Czerny et al., 2024). This not only impacts

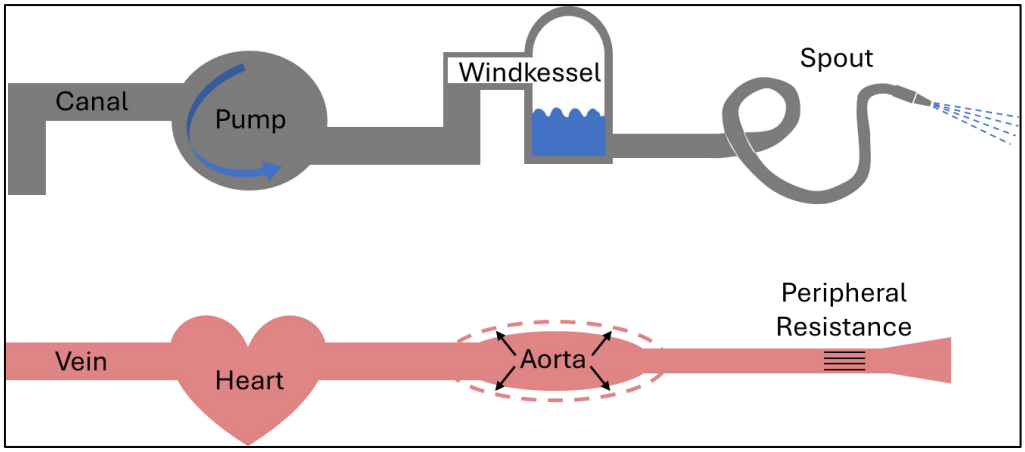


***Figure 12**: Schematic visualization of the concept of the "Windkessel" function of the aorta.*
Figure adapted from (Westerhof et al., 2009).

the clinical and scientific fields but properly acknowledges the essential role of the aorta in distributing blood through the human body.

The aorta could be described as the main "draining tube" for the heart and therefore is exposed to notable forces due to the proximity to the pumping heart and its continuous discharge, especially at the proximal aortic end. Hence, the aorta is equipped with numerous elastic fibres and acts "[... as an elastic buffering chamber behind the heart ...]" (Belz, 1995). The cycle of systolic storage and diastolic forwarding of the stroke blood volume mainly relies on the elasticity/stiffness of the aortic wall and is referred to as the "*Windkessel*" function (according to Frank's *Windkessel* model) (Westerhof et al., 2009) (**Figure 12**).

This function enables the vessel to transform a discontinuous into an almost continuous blood flow and thereby not only regulates the peripheral circulation but also mitigates the afterload and pressure on the left ventricle.

As the elastic capacity of the aorta decreases (or the aortic stiffness increases) with age blood pressure rises and so does the risk for pathological changes (e.g., atherosclerosis) of the aortic wall (Belz, 1995). One cell group directly affected by this are vascular SMCs. Most research groups that investigated the influence of arterial disease on blood vessel SMCs published comparable observations, such as, changes in cell shape and orientation, increased rigidity of the vessel wall and proliferation of the SMCs (Bennett et al., 2016) and decreased expression of proteins associated with contractility, while the presence of ECM proteins increased (Owens et al., 2004). Some groups mentioned an almost "fibroblast- or macrophage -like" character (Andreeva et al., 1997; Rong et al., 2003). Most interestingly, the majority of these atypical features has not only been observed in diseased blood vessels but also in primary vascular SMCs under culturing conditions (Chamley-Campbell et al., 1979; Worth et al., 2001). Until now there are two potential hypotheses circulating that try to explain this phenomenon. The more accepted

theory considers vascular SMCs in general to have the capability to switch their phenotypes upon changing environmental conditions (Chamley-Campbell et al., 1979; Frismantiene et al., 2018; Owens, 1995). The second, less known but equally plausible, hypothesis supports the existence of a vascular SMC subtype with stem cell potential that gives rise to muscle cells with a specific genetic equipment that allows them to adapt quicker to the changing circumstances (Tang et al., 2012). A similar theory was postulated for pericytes (Armulik et al., 2011).

However, it is a fact that these cells are changing in a way that affects their capabilities to contract and relax, e.g. through changes in the NP/cGMP pathway. In the early 1990s a group of researchers focussing on GC-A and GC-B specifically found that the mRNA levels of these receptors significantly changed between intact rat aorta and cultured primary aortic SMCs (Suga, Nakao, Mukoyama, et al., 1992). No structured efforts have been made to unravel the culture-induced differences of the NP/cGMP pathway components in detail. Therefore, it was the aim of the first chapter of this study so examine culture-induced changes of selected cGMP pathway components in primary vascular SMCs, at the level of transcription as well as at the functional level. One of the main reasons the aorta was chosen as the model tissue was the size of the vessel and thickness of the *tunica media*.

### 1.3.2 cGMP Signalling in Vascular Disease

Another reason for choosing the aorta as the model tissue for this study was that vascular SMCs are known to express several components of the cGMP signalling cascade (Kuhn, 2016), i.e., GC-A and GC-B (Nagase et al., 1997; Potter et al., 2006; Steinmetz et al., 2004).

Cardiovascular diseases are frequently correlated with dysfunctional vascular SMCs (Ahmed et al., 2024). In healthy vasculature cGMP plays a pivotal role in blood flow regulation through fine tuning of the SMC contractility and thus tone. Numerous clinical studies identified disruptions in the cGMP signalling cascade in hypertension, myocardial infarction, and coronary artery disease (Leineweber et al., 2017) and it is known that even minimal deviations from the physiological norm influence blood pressure regulation (Ehret et al., 2011; Emdin et al., 2018). Since the role of cGMP and cGMP-producing enzymes is so critical to cardiovascular health, the development of cGMP-based drugs and therapy approaches has recently become one of the most successful areas of drug development (Friebe et al., 2017; Kraehling & Sessa, 2017).

Even though it is commonly accepted that cGMP is cardioprotective, an increase in intracellular cGMP can have varying and even opposing effects in different cell types during the progression of cardiovascular disease (Lehners et al., 2018). This includes for instance the influence of the cGMP cascade on the regulation of the vascular SMC plasticity and therefore the display of their

phenotypic heterogeneity, which is important during e.g., atherosclerotic plaque formation (Wolfsgruber et al., 2003) or during the formation of new blood vessels (Duda et al., 2004).

However, as mentioned already in chapter **1.3.1**, cultured primary vascular SMCs display similar features like their counterparts in diseased blood vessels. Cell culture therefore might offer an excellent opportunity to study pathological changes in cardiovascular disease and even to identify new therapeutic targets.

### 1.3.4 Cardiovascular Sex-dependent differences

Numerous common diseases, especially in cardiovascular health, show significant differences regarding epidemiology, pathophysiology, disease progression and outcomes between sexes. Sex-dependent differences are defined as biological differences between men and women, whereas gender differences are influenced by interaction of each individual with the environment and society (Regitz-Zagrosek & Kararigas, 2017). Until recently the topic of sex and gender did not receive sufficient recognition in society, health, and of course in funding for research which explains why knowledge is still very limited. Besides genetic and epigenetic reasons for sex differences, the influence of sex hormones and their receptors became a hot lead for the identification of future drug targets in personalized care for patients with cardiovascular disease (Regitz-Zagrosek & Kararigas, 2017).

To give an example, male and female patients develop different types of ischemic heart disease. Men usually suffer from cardiac ischemia due to occlusive coronary artery disease caused by wide-spread and severe atherosclerosis. In addition, men develop myocardial infarction an average 10 years earlier in their lives (around the age of 65) than women (around the age of 72) (Benjamin et al., 2018; Ojha & Dhamoon, 2025). As a main reason for this, a higher estrogen level in women before menopause is suggested (Khalil, 2005; Orshal & Khalil, 2004), even though the mechanism of this premenopausal protection from cardiac ischemia and hypertension is not entirely understood. Researchers in the field assume that the postmenopausal estrogen decrease is accompanied by an enhanced cardiac sensitivity to circulating catecholamines (Waqar et al., 2022). In other words, the risk of cardiovascular disease for women increases after menopause.

The influence of sex hormones on SMCs specifically has already been investigated in the late 1990s and early 2000s. Besides the fact that estrogen, progesterone and testosterone receptors were found to be expressed in endothelial cells and vascular SMCs (Mendelsohn, 2002; Thompson & Khalil, 2003) it has been shown *in vitro* and *in vivo* that estrogen and testosterone can have varying effects on vascular SMCs. Even though the hormonal cycle between humans

and rodents shows differences (Regitz-Zagrosek & Kararigas, 2017), however keeping in mind certain advantages of rodents that have been mentioned earlier (beginning of chapter **1.3**), it has been shown in rats that the capacity of aortic SMCs to spontaneously contract is generally lower in females than in males. It has been hypothesized that this sex difference might be due to a different relative abundance of the hormone receptors in arteries of both sexes (Collins et al., 1995). In any case, estrogen, progesterone and testosterone treatments were found to cause SMC relaxation in endothelium-denuded blood vessels pre-constricted with NA, with estrogen having the highest relaxing capacity in both sexes (Crews & Khalil, 1999).

Besides a different abundance of the hormonal receptors in both sexes, another reason could be an estrogen-dependent induction of NO synthesis, since estrogen can enhance the expression of eNOS (Forte et al., 1998). In addition to the influence on the contractility of vascular SMCs, it was found that estrogen and testosterone regulate cellular growth and proliferation of these cells. As shown *in vitro,* estrogen has an antiproliferative effect on human aortic SMCs (Barchiesi et al., 2002) which seems to be facilitated by progesterone (Orshal & Khalil, 2004). This is achieved by activation of the estrogen receptor E2 which then inhibits the mitogen-activated protein kinase (MAPK) pathway and therefore proliferation is reduced (Dubey et al., 1999). Testosterone on the other hand seems to influence proliferation in a dose-dependent manner, with inhibition at higher concentrations (Somjen et al., 1998).

More recent research highlights the involvement of sex hormones in the process of the phenotypic conversion of vascular SMCs during cardiovascular disease. For a while researchers believed that estrogen has beneficial effects for the contractile SMC phenotype, while testosterone was thought to promote the conversion towards a synthetic cell character. Latest research discovered that both, estrogen as well as testosterone, seem to have dual effects on the phenotypic switching of vascular SMCs under different circumstances (Jia et al., 2024).

Given that the biological sex is such an important factor regarding cardiovascular health, it was decided to include a male and a female study cohort for the first chapter of this thesis.

## 1.4 Aortic SMCs – Gene Expression Analysis

Before diving into the specifics of the gene expression studies for the vascular thesis chapter, it is important to mention that knowledge on the signalling transduction within vascular smooth muscle until recently was generated almost exclusively in *in vitro* cell culture. Since it appears that isolation and short cultivation periods already cause drastic changes in the gene expression profile of vascular SMCs, it is all the more important to aim for a precise characterization of these changes, especially, in the age of single-cell transcriptomics and RNAseq.

### 1.4.1 Reference Gene U2 Enables Direct Comparison between Relative Gene Expression Levels of Vascular Smooth Muscle Cells in Tissue and Culture Using Real-Time Quantitative PCR (1st Publication)

#### *1.4.1.1 Relevance of this Study*

Cell culture models are an irreplaceable part of *in vitro* research, especially in the diagnostic field. Even though researchers today are more than ever aware that isolation and prolonged culturing periods have dramatic impacts on the cells, the issue remains to what extent cultured cells reflect those within their physiological tissue environment (Al-Lamki et al., 2017). Vascular SMCs are no exception of this, thus a direct comparison of SMCs within intact blood vessels to their equivalents *in vitro* is an essential step to a better evaluation of functional results (Qiu et al., 2014; Worth et al., 2001). The analysis of the transcriptome may provide the most comprehensive view of changes due to cell isolation and culturing, both in a spatial and temporal resolution (Pedroza et al., 2020). In this study quantitative polymerase chain reaction (qPCR, RT-qPCR in this case) was used to monitor differences in gene expression in cultured vascular SMCs versus the intact media of rat aorta (Rameshrad et al., 2016) (**Figure 13**).

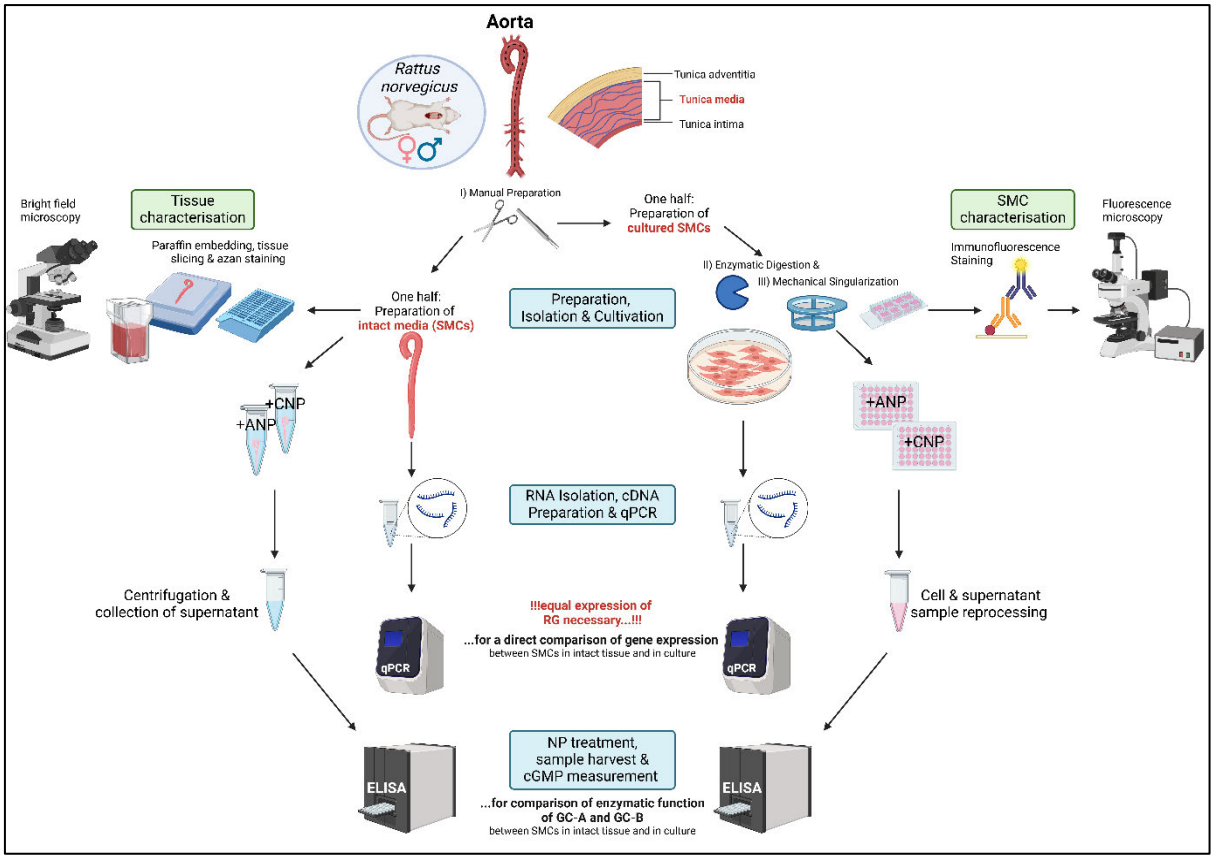


***Figure 13**: Workflow and experimental design for the expressional and functional examination of NPRs in smooth muscle cells (SMCs).*
Atrial natriuretic peptide (ANP), C-type natriuretic peptide (CNP), cyclic guanosine monophosphate (cGMP), Guanylyl cyclase A (GC-A), Guanylyl cyclase B (GC-B), complementary DNA (DNA), Enzyme-linked immunosorbent assay (ELISA), Smooth muscle cell (SMC), Natriuretic peptide (NP), reference gene (RG), quantitative polymerase chain reaction (qPCR). Figure was created with **BioRender.com**.

There are two ways to quantify the mRNA level for a gene of interest (GOI) measured by qPCR (Livak & Schmittgen, 2001). Besides the absolute quantification method, which requires serial dilutions of a cDNA sample and extensive calculations for a calibration curve (Morrison et al., 1998), the relative quantification by normalisation to a reference gene (RG) is preferred by most researchers (Pfaffl, 2001). The quality of qPCR depends on the RNA and cDNA preparation, the chosen primers (Li & Brownley, 2010) and reaction conditions, as well as on the selection of an appropriate RG for the normalisation (Kozera & Rapacz, 2013).

Therefore, the aim of the first publication for this thesis was to determine an RG that is equally expressed in vascular SMCs within the intact aortic media and in the corresponding cells in culture, thus enabling their direct comparison at the level of gene expression.

#### *1.4.1.2 Quantitative Polymerase Chain Reaction*

Since its introduction by Mullis and colleagues in 1983 (Mullis et al., 1986), polymerase chain reaction (PCR) has been under constant development. PCR is valued for its reliability and

sensitivity (Pfaffl, 2001) and nowadays belongs to the standard repertoire of an average scientific laboratory. In general, PCR relies on the logarithmic amplification of a genetic sequence that is defined by the applied template and the respective primers binding to it. The reaction comprises three consecutive steps (denaturation, primer hybridisation, and elongation), each carried out at a specific temperature. The product size is then usually validated through visualization of the molecular size in electrophoresis (Wittmeier & Hummel, 2022). Additionally, qPCR allows for the quantification of the amplification of a sample sequence while following the reaction in real-time. In fluorescence-based qPCR, this is realised by the application of fluorescent reporter molecules (Bustin et al., 2005; Morrison et al., 1998).

The key value necessary for quantification is the cycle threshold (Ct). The Ct, also known as the quantification cycle (Cq) or crossing point (CP), is the number of PCR cycles necessary to reach a defined fluorescence level or rather to exceed a fluorescence threshold level above background level (Bustin et al., 2005). In case of a PCR reaction with maximum efficiency (100%), the amount of target copies at the beginning of the reaction, along with the intensity of the fluorescent signal, is duplicated in each PCR cycle. The higher the GOI is expressed, the faster the cycle threshold is reached, thus yielding a smaller Ct value.

#### *1.4.1.3 Reference Genes and their Requirements for Relative Gene Expression Quantification*

The major advantage of relative gene expression quantification is the correction of variations in the levels of the detected gene expression of different samples. The variations are usually due to tissue or matrix effects, inconsistent RNA harvest (Fleige & Pfaffl, 2006), or an insufficient cDNA synthesis by reverse transcription (RT) (Bustin et al., 2005).

The term RG is often used synonymously with housekeeping gene (HKG). While RG could in general be referred to as internal control gene with a sequence different to the GOI, HKGs are thought to be essential for the maintenance of basic cell functions and are expressed at a constant level; therefore, they are often considered promising RG candidates (Kozera & Rapacz, 2013). Routinely used examples are ubiquitin, ribosomal or histone subunits, beta actin (Actb), and glyceraldehyde-3-phosphate dehydrogenase (Gapdh) (Marten et al., 1994).

A reliable quantification requires specific properties of the RG. Most importantly, it requires a constant expression regardless of the experimental conditions. Furthermore, the RG should ideally be expressed within a similar expression range (similar range of Ct value) as the GOI (Kozera & Rapacz, 2013). Lastly, the variance of the RG expression should not exceed the variance of the expression of the GOIs one would like to compare.

#### *1.4.1.4 Aortic SMCs and Cell Culture*

The aorta, being the largest blood vessel in the body (chapter **1.3.1**), is usually the main source of extraction for cell culture experiments with vascular SMCs (Sampilvanjil et al., 2020; Torres et al., 2001). Their singularisation for cell culture requires the destruction of the original vessel by mechanical dissection, enzymatic digestion and subsequent straining of the cell solution (Huber & Badylak, 2012) (**Figure 13**). Once cells become detached from their physiological environment, their survival depends on a quick adaptation to the circumstances *in vitro*. In the case of vascular SMCs, this for instance includes the loss of physiological contact and exchange with neighbouring cells (Al-Lamki et al., 2017; Hortells et al., 2015; Méndez-Barbero et al., 2021; Qiu et al., 2014), the lack of a constant supply with essential oxygen and nutrients through the bloodstream, the missing exposure to oscillating pressure changes (systole and diastole of the heart), and hence, the necessity to constantly adapt their cellular tone. Thus, extracting cells from their original tissue and bringing them into culture has a tremendous impact and could mimic pathological conditions, such as blood vessel injury and disease, rather than a healthy tissue environment (Allahverdian et al., 2018; Jensen et al., 2021; Owens et al., 2004; Shi et al., 2020). Finding an RG expressed stably enough throughout the entire experimental procedure from the intact media to cultured and singularised vascular SMCs thus literally constitutes the search for a needle in the haystack.

A group of genes that seemed promising to provide an adequate RG for the direct comparison is the group of the small nuclear RNAs. They encode for the small nuclear ribonucleoproteins (snRNPs). snRNPs in combination with other proteins, such as fibrillarin (Zhang et al., 2024), build the subunits of the spliceosome. This protein complex is essential for the excision of introns of the pre-mRNA right before the translation to protein-encoding DNA, a process also known as splicing (Krämer et al., 1990). The snRNP U2 in particular, together with U1, is responsible for intron marking (Wilkinson et al. 2020).

### 1.4.2 Effects of Cell Isolation and Culture on the Expression and Function of cGMP pathway components in rat aortic SMCs (2nd Publication)

#### *1.4.2.1 Relevance of this Study*

Based on the previous publication, the second part of the vascular studies for this thesis aimed to investigate isolation and culturing effects on the expression of the NP receptors GC-A, GC-B, NPRC and the NO receptor sGC. Again, intact *tunica media* and primary SMCs derived from the same rat aortae were compared (**Figure 13**). GC activity was assessed by NP-induced cGMP production using a competitive enzyme-linked immunosorbent assay (ELISA).

Vascular SMCs have been and are still intensively studied in cell culture and a substantial amount of common knowledge on NPRs stems from *in vitro* experiments, even though it is largely accepted that most *in vitro* experiments reflect physiological circumstances to a limited extent.

Therefore, to rule out misjudgement of the NP signalling pathway, especially for functional studies investigating activation and crosstalk between the different NPRs, direct comparisons between *in vivo* and *in vitro* essentially contribute to the common knowledge around vascular cell culture.

#### *1.4.2.2 Experimental Preliminary Work*

In the previous study (Rager et al., 2023), the suitability of popular HKGs was validated for the comparison between intact aortic *media* and derived primary aortic SMCs by RT-qPCR. Besides the identification of U2 as a valid HKG we found that most HKGs, especially classic examples such as Actb, did not fulfil the requirements for this comparison and showed a significantly different expression between the cells and the tissue.

#### *1.4.2.3 Sex-dependent Differences*

The interest in the development of sex-specific medicine is increasing (Seeland & Regitz-Zagrosek, 2012). This inevitably requires researchers to include the biological sex as a limiting factor for their studies. Since it has been shown that sex hormones can have a substantial impact on the cardiovascular physiology (Asunción-Alvarez et al., 2024; Dehaini et al., 2018; Karbasion et al., 2024), a male and a female study cohort were included to rule out sex-related differences in the cGMP signalling cascade.

## 1.5 Male Reproductive Tract – Seminiferous Tubules

### 1.5.1 Male Reproductive Tract and Seminiferous Tubules

The mammalian male reproductive tract encompasses the paired testes, their closely attached epididymis and vas deferens for sperm maturation and transport, as well as the accessory sex glands and the penis (**Figure 14**) (Stadler et al., 2020).

SMCs are located in the testis (Müller et al., 2004), the epididymis (Robaire & Hinton, 2015), and the prostate (Exintaris et al., 2006). In most, if not all male reproductive tissues, SMCs fulfil an essential role for the individual organ function and thus for male fertility and reproduction. In fact, there are urogenital diseases attributable to SMC dysfunction and dysregulation, such as benign prostatic hyperplasia that is often associated with lower urinary tract symptoms (Madersbacher et al., 2019; Mónica & De Nucci, 2019), or disorders which are treated by interference with SMC-related signalling cascades such as the cGMP pathway, as in the treatment of erectile

dysfunction (Rotella, 2002). The focus of the present thesis, however, is the testicular SMCs often referred to as peritubular cells (PTCs).

#### *1.5.1.1 Testis and Seminiferous Tubules in Humans and Rodents*

In humans the seminiferous tubules (STs) are surrounded by multiple layers of SMCs whilst in rodents only a monolayer of PTCs is found. Knowledge about the relevant differences between humans and the chosen animal model is crucial. They can impact the generation of results and their interpretation, especially when translating the outcome of animal studies into human circumstances. Nevertheless, it should be emphasized that this does not only challenge the justification of research, but occasionally comes with major advantages for researchers. Why rodents and rats specifically are an excellent research model to investigate SMC contraction in relation to spermatogenesis in STs will be explained in the next subsection **1.5.1.2**.

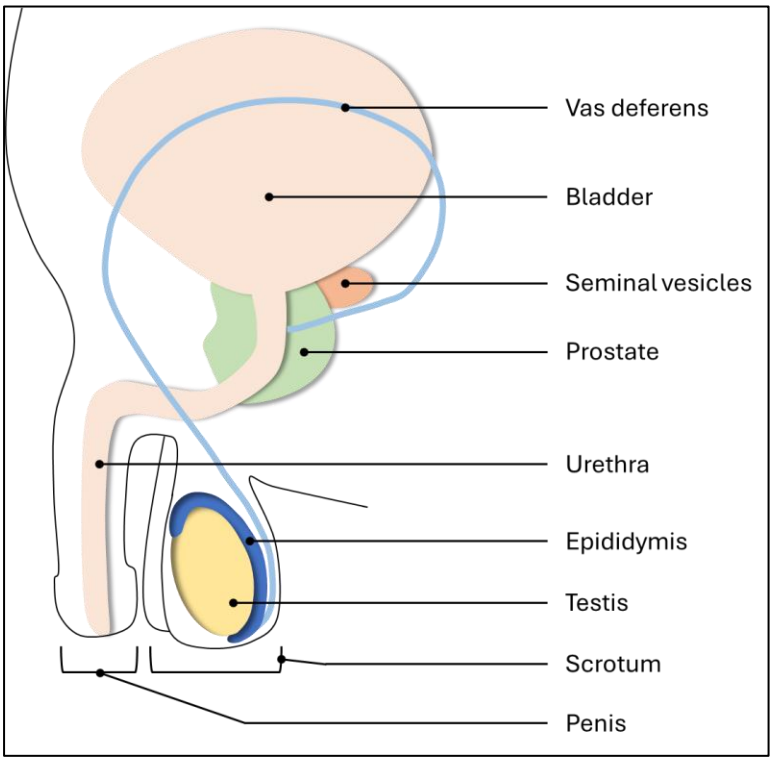


***Figure 14**: Overview of the male urogenital tract.*
Figure adapted from (Stadler et al., 2020).

In the testis the male germ cells develop within the germinal epithelium (GE), which is lining the inside of the STs (**Figure 15**). The STs are densely coiled and encapsulated inside the testicular *tunica albuginea* where they are separated into lobules by septa (Robaire &Hinton, 2015). The STs eventually merge into efferent ducts, which exit the testis at the rete testis area (Figueiredo et al., 2021) as a highly coiled larger epididymal duct (the epididymis) adjacent to the testis. During their passage through the epididymis (Elfgen et al., 2018) the yet immotile and infertile spermatozoa

acquire their fertilizing capability; this process is also known as capacitation (Balbach et al., 2023; Zaneveld et al., 1991).

During the early 1950s Roosen-Runge was the first to describe undulating ST wall movements in rat (as cited in Sasagawa et al., 1995; Suvanto & Kormano, 1970). He suggested that the Sertoli cells are responsible for these contractions. It is, however, the contractile SMCs on site which contract spontaneously and thereby propel the sperm cells, once released from the GE into the tubular lumen, towards the epididymal duct. The SMCs surround the GE as the outer layer of the STs (**Figure 15 B**) and are also referred to as peritubular cells (PTCs).

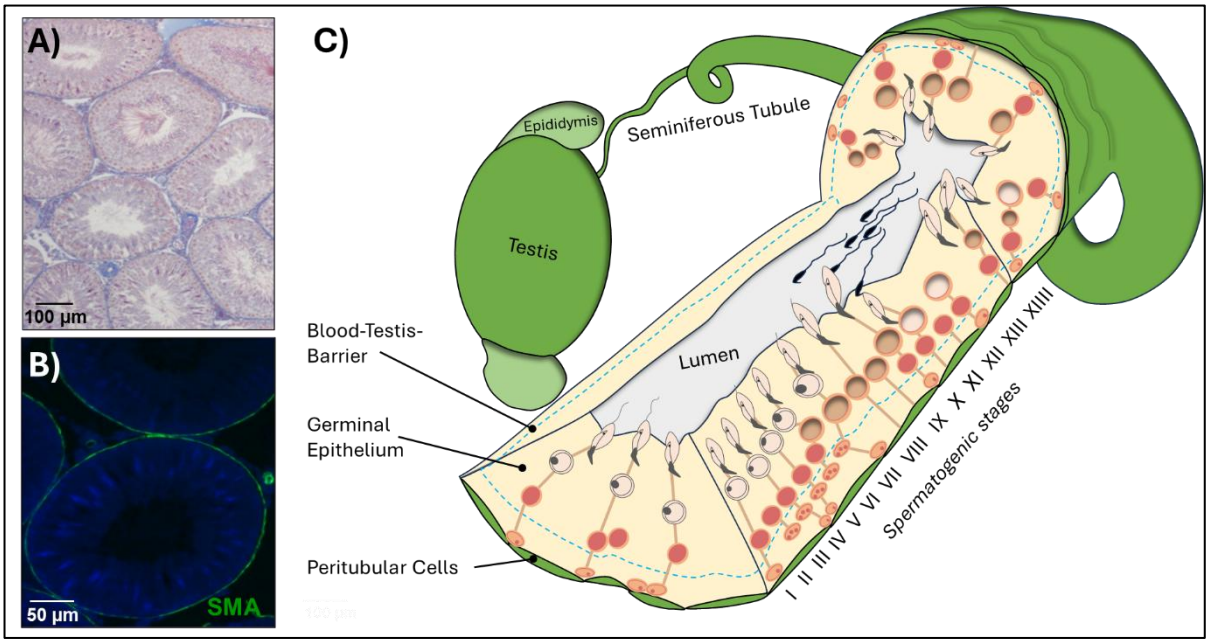


***Figure 15**: Rat seminiferous tubule structure and localization of the peritubular cells.*
(**A**) Azan histology staining of cross-sectioned rat testis**,** smooth muscle actin (SMA). (**B**) Immunofluorescent staining for smooth muscle actin (SMA) of cross-sectioned rat testis. Both stainings performed by Sabine Tasch of the Middendorff Lab. (**C**) Figure adapted from (Fleck et al., 2021).

### *1.5.1.2 Spermatogenesis and Spermatogenic Stages*

Spermatogenesis is the process during which haploid male germ cells (spermatids) develop from diploid spermatogenic stem cells into infertile spermatozoa. Spermatogenesis takes place in the testicular GE (**Figure 16**) within the STs, starts right after puberty and is under tight hormonal control (Ramaswamy & Weinbauer, 2014; Russell et al., 1987). Within the GE of the testicular STs the germ cells are arranged in concentric layers. These layers are interrupted by tree-like shaped somatic cells, discovered in 1865 by Enrico Sertoli (França et al., 2016). The Sertoli cells nurture the germ cells and provide a mesh to maintain the cell associations during spermatogenesis (Hess & Renato de Franca, 2008).

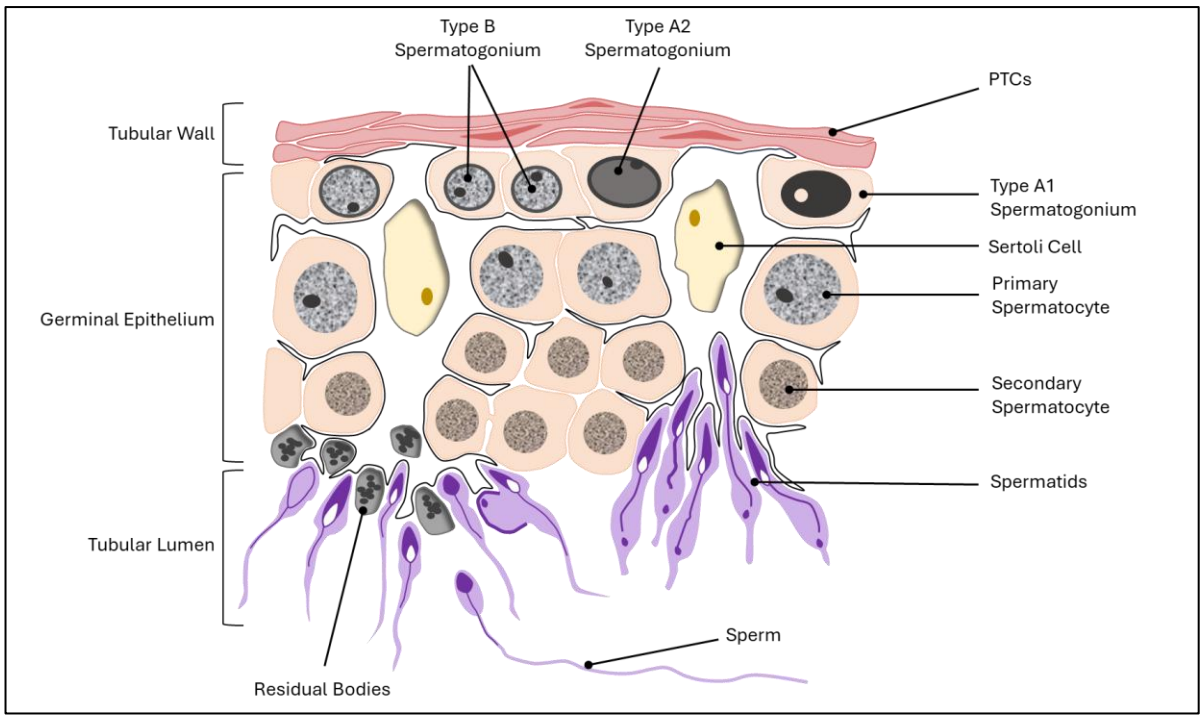


***Figure 16**: Structure of the male germinal epithelium (GE) in the seminiferous tubules (STs).* Peritubular cells (PTCs). Figure adapted from (Gilbert, 2000) Figure 19.17.

Spermatogenesis can be distinguished into different phases (mitosis, meiosis, spermatogenesis) and spermatogenic stages according to characteristic morphological features of the GE. These stages are species-specific and progress through precisely timed repetitive cycles to ensure continuous sperm production (Hess & Renato de Franca, 2008). Leblond and Clermont were the first to distinguish between different spermatogenic stages with regard to the observed cell associations in ST cross sections (**Figure 15 A**) of the rat (Leblond & Clermont, 1952). The stages used to be visualized by periodic acid-Schiff's reaction (PAS staining), which revealed 12 different stages in the mouse, mainly focusing on the Golgi region of the spermatids that eventually forms the acrosomal head part of the sperm (Hess & Renato de Franca, 2008). In the rat initially 14 stages were defined (Leblond & Clermont, 1952). Within the layer of the testicular GE the developing germ cells then surpass all the stages of spermatogenesis (from spermatogonia to spermatozoa) until they are shed from the GE into the lumen of the ST in the final spermatogenic stage (**Figure 17 A**).

In rats and mice, the spermatogenic stages occur in a repetitive order one after another along the length of the tubule. This phenomenon is also described as the "spermatogenic wave" (Parvinen & Vanha-Perttula, 1972) and explains why only one spermatogenic stage is visible per ST cross section (**Figure 15 A**). In male humans, multiple stages occur simultaneously in the same ST section (Luetjens et al., 2005). It is hypothesized that the spermatogenic stages are arranged in a

corkscrew-like manner along the tubule (**Figure 17 B**), hence multiple spermatogenic stages can be found per ST cross section (Chaturvedi & Johnson, 1993).

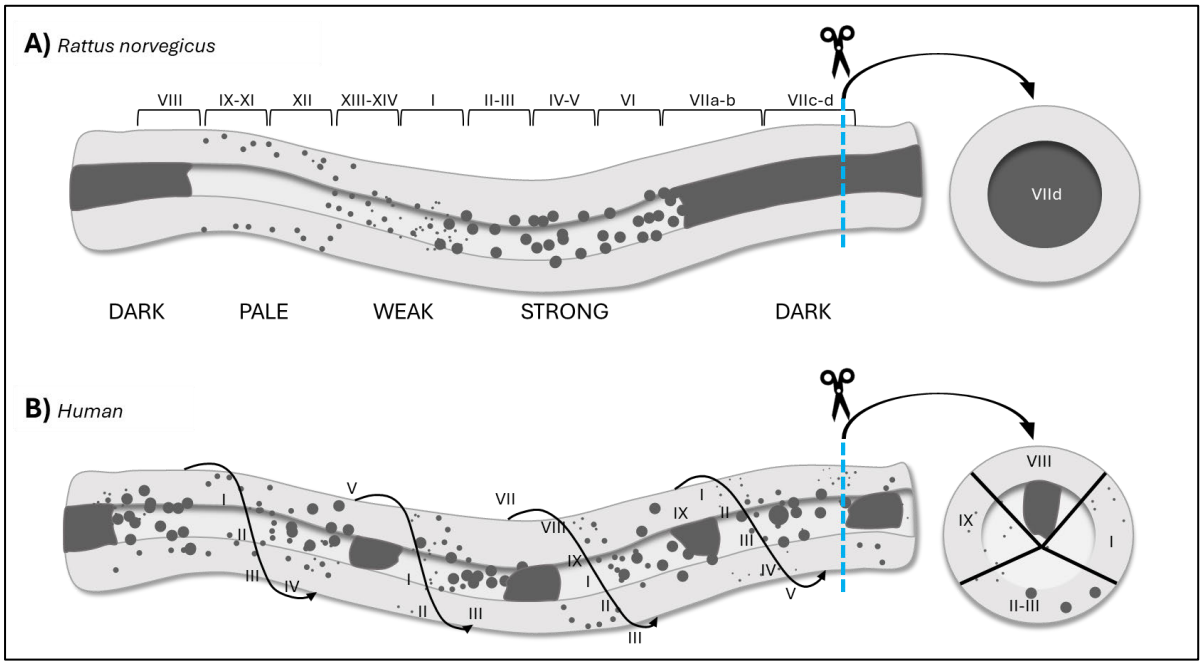


***Figure 17:*** *Arrangement of spermatogenic stages in the seminiferous tubules.*
(**A**) Sectional arrangement in rat and (**B**) spiral arrangement in human seminiferous tubules.

This highlights a major advantage of the rat as an animal model when it comes to stage-specific investigations in the male testis, because the spermatogenic stages are a lot easier to distinguish and experiments can be performed in a stage-dependent manner. Given that transillumination allows us to distinguish four groups (weak, strong, dark and pale tubules) of spermatogenic stages, dissection can be performed according to appearance and without the need to perform exact histological identification of the spermatogenic stage (Kangasniemi et al., 1990). Each of the groups covering four to five of the spermatogenic stages is defined by Leblond and Clermont (Leblond & Clermont, 1952). Dark (before spermiation) and pale (after spermiation) are the stages chosen for the live imaging experiments in this thesis, because they are the easiest to distinguish between one another.

#### *1.5.1.3 SMCs and SMC contractility in the Seminiferous Tubules*

As mentioned before, in the testis SMCs surround the GE of the STs in a circumferential manner. Their ability to spontaneously contract as well as to hold their muscle tone for an extended period of time is precisely tailored to the continuous cycle of spermatogenesis. Hence, it is assumed that the contraction pattern of the tubular wall is synchronized with the spermatogenic stage of the GE (Suvanto & Kormano, 1970). It is conceivable that the SMC contractions support the developing germ cells to move from the outermost layer of the GE towards the tubular lumen, or that during the process of spermiation (the release of sperm cells into the lumen) (O'Donnell et

al., 2011) the contractions assist to shed the spermatozoa from the GE and to propel them towards the epididymis (Clermont, 1958; Ellis et al., 1981).

The contractions of the tubular wall in the rat STs continuously occur with a fixed pattern. Until now it is, however, unclear how these contractions are initiated from an electrophysiological standpoint and how the electrophysiological impulses are propagated and transferred in the testicular SMCs. It remains to be researched whether testicular SMCs show electrophysiological coupling according to the multiunit type of smooth muscle (like in the aorta) or whether they are connected in patches, and the electrical impulses are initiated by pacemaker cells and transferred to neighbouring cells (chapter **1.1**). One way to investigate that could be by identifying pacemaker cells in STs through the localization of reliable marker genes, which unfortunately are still unknown.

Another factor that should be taken into consideration when comparing vascular and testicular SMCs is that they most likely do not arise from the same embryonic origin (Donadon & Santoro, 2021). In fact, it has been shown by lineage tracing and fate mapping experiments (Jiang et al., 2000) that even the vascular SMCs of different parts of the aorta are of different heritage. Nevertheless, even though SMCs of different tissues may be equipped differently, they share a large set of smooth muscle specific markers and are known to express proteins that are relevant for contracting and relaxing cascades, such as the cGMP signalling pathway.

#### *1.5.1.4 SMC relaxing and contracting pathways in the Male Reproductive Tract*

Previous studies by the research groups of Middendorff and others confirmed the abundance of cGMP related proteins and the relevance of cGMP in several tissues of the male reproductive tract (Middendorff et al., 2000; Müller et al., 2011; Sarzani et al., 1996). Components of the CNP/GC-B axis for instance, with CNP being detected in the seminal fluid (Chrisman et al., 1993; Nielsen et al., 2008; Nielsen et al., 2009).

As in the vasculature, however, in male reproductive tissue mainly NO-induced cGMP effects have been studied (chapter **1.2.2.1**). Due to its general abundance and importance for male fertility (Dutta & Sengupta, 2022), NO-targeted treatment options are still a hot topic of current research (Pozzi et al., 2021). NO is known to affect spermatogenesis, sperm maturation and motility, as well as capacitation in the testis and epididymis (Banihani & Shatnawi, 2020; Herrero et al., 2003). NOS expression was confirmed in the acrosome and tail of human and rodent spermatids and sperm motility was affected by NO in a dose-dependent manner (Staicu et al., 2019; Wang et al., 2014). NOS expression was also found in Leydig cells; hence it is not surprising that NO contributes to the regulation of testosterone secretion (Luo et al., 2021). As part of an enhancing positive feedback loop, testosterone affects cGMP release and degradation and is

able to trigger NO release in Leydig cells (Morelli et al., 2005). In addition to the Leydig cells, NOS expression was also confirmed in Sertoli cells. In other words, NO production was found in interstitial and other somatic cell of the testis, aside from blood vessel cells (O'Bryan et al., 2000). Since NO is a gaseous messenger molecule that can diffuse through cell membranes it is likely that the GE within STs and the (surrounding) PTCs are affected by NO produced by Sertoli or Leydig cells but little is known whether the effect of NO depends on the spermatogenic stages of the ST. In this study, no difference in the magnitude of the NO-effect before and after spermiation could be detected and potential reasons will be discussed in chapter 5.2.5.

Lastly, NO, in addition to playing a role in spermatogenesis, capacitation and sperm motility, is known to play a key role in penile erection (Burnett & Musicki, 2005).

The process of male sexual arousal and the regulation of penile erection and ejaculation is complex and involves multiple neurotransmitters, receptors and signalling components (Alwaal et al., 2015; McMahon et al., 2004). All male reproductive organs that are involved in the ejaculatory process are known to be innervated through the autonomic nervous system (Miyake, Yamamoto, & Mitsuya, 1986). During the emission phase of the ejaculatory process the sympathetic branch of the autonomic nervous system induces strong contractions in the epididymis (Elfgen et al., 2018), the vas deferens, prostate and accessory sex glands. These contractions are known to be induced by NA through activation of adrenergic receptors (Mewe et al., 2007; Michel, 2007; Sanbe et al., 2007). Ejaculatory disorders are often associated with an interruption of the noradrenergic signalling (chapter **1.2.1**), as is the case in spinal cord damage (Ibrahim et al., 2016) or when patients are treated with adrenergic receptor blockers for hypertension treatment (Wong et al., 2015) or benign prostatic hyperplasia (Carbone & Hodges, 2003; Narayan & Lepor, 2001). However, most importantly it has been shown in early studies that the transport of spermatozoa through the STs rely on the activation of α1-ARs by NA (Miyake, Yamamoto, & Mitsuya, 1986; Miyake, Yamamoto, Narita, et al., 1986; Sasagawa et al., 1995).

While the roles of NO and NA in the context of male reproduction have been thoroughly investigated, further scientific clarification on the interplay between both signalling pathways is required and promises future opportunities in drug development (Rossi et al., 2018).

## 1.6 Live Imaging Analysis of Seminiferous Tubules Contractions

This section summarizes the evolution of a sophisticated imaging analysis, that has recently been developed for the evaluation of contractions of the epididymal duct (Stadler et al., 2021) and prostatic tissue, to study the movement patterns of rat STs and their substance-induced changes with regard to the spermatogenic stage. This technique entails an *ex vivo* live imaging procedure

(Mietens et al., 2014), described in detail in chapter **3.2.4.2**, and a FIJI-based semi-automated analysis codes (chapter **3.2.4.3**). The later evolved from the "Wiggle Index" code which initially was developed to investigate the movement behaviour of nematodes as an indicator for their vitality (Denecke et al., 2015; Preston et al., 2015; Preston et al., 2016).

### 1.6.1 Early approaches of contraction analysis in rat STs

An early approach to analyse the superficial wall movements of rat STs (**Figure 18 A**) was based on the readout of kymographs (**Figure 18 B**). Kymographs display the contractions at a static spot within the captured image by following a virtual slice section over the time (Mietens et al., 2014; Weiser et al., 2020). The contractions are displayed as a peak profile of the captured image sequence. The number of peaks over a defined period can then be used to calculate the frequency of the contractions. This method is suitable to gain a first impression on the superficial wall movements, but the information generated is limited because it is reduced to the frequency at a single spot within the tissue. Furthermore, the definition of a peak is not standardised, and the peak selection can vary due to subjectivity.

A second approach is Fourier analysis, in which the movements of the ST walls are transferred into sinus curves that display not only the frequency but also the intensity (amplitude) of the wall contractions at predefined spots of the observed tissue (**Figure 18 C**). Interestingly, Fourier analysis is widely used for the evaluation of blood pressure curves (Staessen et al., 1993) and echocardiograms (Chu & Raeside, 1978). Fourier seems to be a very precise option to analyse ST contractions. However, analysis according to Fourier requires a high level of mathematical skill, is therefore harder to grasp and difficult to translate for a broader scientific audience. In addition, Fourier analysis focuses on randomly selected spots in the tissue, rather than capturing the entire tissue section.

The FIJI-based imaging analysis introduced by Bester and Nowell (Stadler et al., 2021) converts the detected changes in the contrast of the entire tissue section in a pixel precise manner into a movement score. The movement score is then displayed according to a cumulative frequency distribution. The recorded movement scores for the entire tissue section filmed are then displayed as a colour-coded heat map (**Figure 18 D**) and can be followed in the corresponding heat map movies.

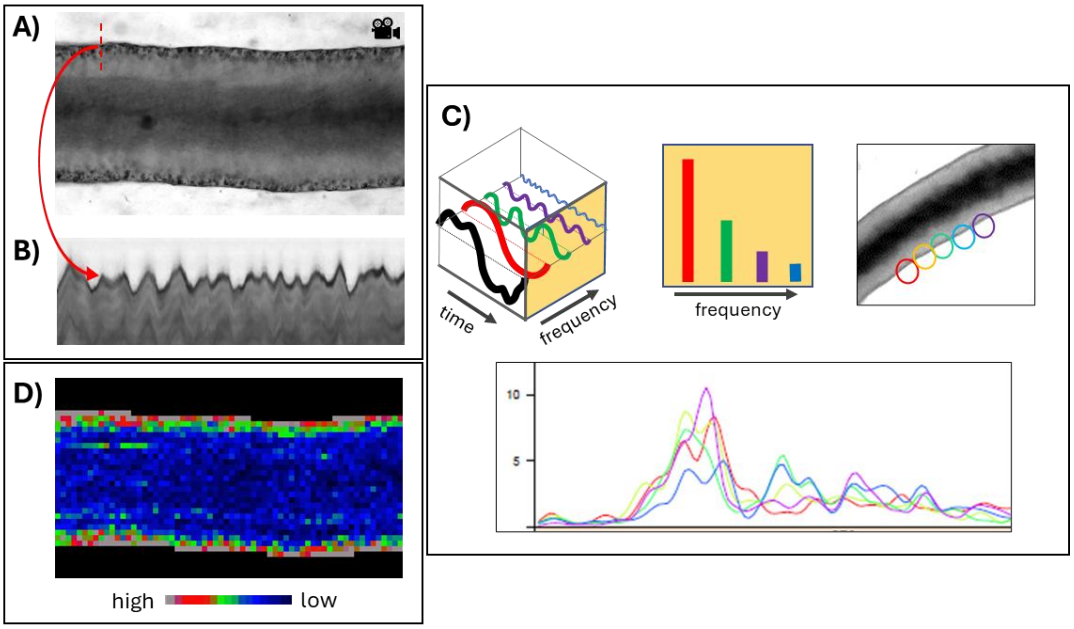


***Figure 18**: Previous live imaging analysis of contractions of rat seminiferous tubules.*
(**A**) Exemplary live image of a pale rat seminiferous tubules in bright field microscopy, (**B**) kymograph generated from a static reslice at a certain position of the tubular wall, (**C**) schematic steps of the Fourier analysis, (**D**) heat map and according to intensity scale generated using a previously described FIJI based code for movement analysis (Stadler et al., 2021).

### 1.6.2 Selection of Spermatogenic Stages and Substances for Live imaging of Seminiferous Tubules

The selection of the spermatogenic sections of the rat STs are based on their morphology (Kangasniemi et al., 1990), physiology and contractile behaviour. The pale and dark sections can be characterized by their unique appearance in transillumination, which facilitates their distinction under the microscope (**Figure 18 A**). The dark tubule is characterized by a darker contrast in the lumen. At this stage within the spermatogenic cycle (during spermiation) (O'Donnell et al., 2011) most of the spermatozoa are released from the GE into the tubular lumen, where they are densely packed and await their propulsion towards the epididymis (Ellis et al., 1981). The GE seems thinner than in other stages and the outermost boundary appears as a thin dark line. This could be due to the filling level in the lumen and therefore the pressure luminal fluid exerts on the tubular wall. The latter could be the reason why at first sight the contractions of the wall in dark STs are barely noticeable. The wall twitches quickly and steadily with a small amplitude.

In the pale section right after spermiation, however, the lumen is mostly freed from spermatozoa and appears a lot brighter than in the dark section. The GE in total seems thicker and few distinct spermatogonia at the outer edge of the tubule give the impression of a patchy pattern of the GE.

The PTC layer seems brighter and slightly more expanded than in the dark tubule. Since the lumen is empty it can be speculated that the pressure on the wall drops in comparison to the dark stage before spermiation. Thus far, however, pressures in the STs have not been properly addressed in research. Preliminary observations capture a more vigorous movement pattern of the pale tubules. The walls seem to contract steadily, more vigorously with a higher amplitude and onset of contractions. Potential reasons for the change in movement patterns of different spermatogenic stages will be discussed thoroughly at the end of the thesis (chapter **5.2**).

An advantage of the tissue preparation and *ex vivo* setup for the live imaging (chapter **3.2.4.2**), besides the capability to keep the tissue alive for an extended period of time, is that the effect of substance administration can be monitored (Mietens et al., 2014). When studying tissue contractility, the drug treatment can either amplify the contractions or cause a relaxation. Therefore, the resulting FIJI-based analysis code at the end of this study should be able to detect deceleration and acceleration of the contraction frequency and extension and reduction of the amplitude of the contractions. Referring to relaxing and contracting signalling pathways in the testis (chapter **1.5.1.4**), the effects of NA (**Figure 19 A**) and NO were investigated respectively. The synthetic NO donor diethylamine sodium salt hydrate (NONOate) (**Figure 19 B**) was chosen to study the relaxing capacity of NO in rat seminiferous tubules (STs) (chapter **4.2.5**).

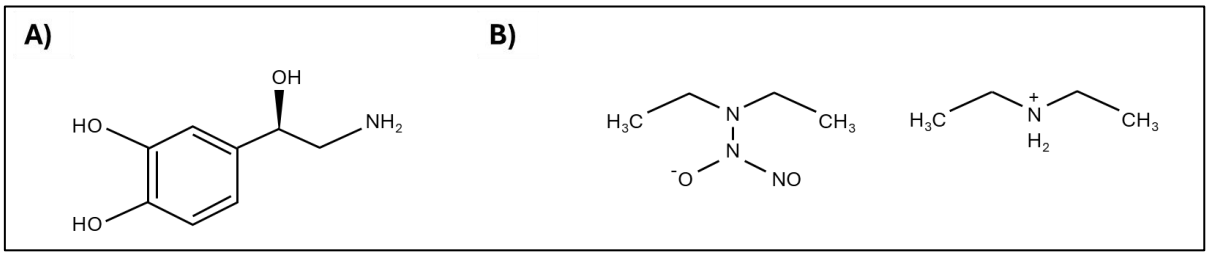


***Figure 19**: Chemical structures of noradrenaline and NONOate.*
(**A**) Noradrenaline identifies as a catecholamine with a characteristic benzene ring carrying two hydroxyl groups which is bound to an amine group. (**B**) NONOate is built by three sequential nitrogen atoms which belong to a central amine group that carries two alkyl groups and bridges a nitric oxide group and a terminal nitrosyl group. NONOate releases nitric oxide upon contact with watery solutions and has a half-life of 2 min in 37 °C and pH 7.4.

# 2 Aims

The aims of this thesis are grouped under two main themes (vascular and male reproductive smooth muscle) as such the aims of each chapter are outlined below.

## 2.1 Vasculature

The aims of the first thesis chapter were:

A) To develop a procedure to extract SMCs from rat aortic media and SMC characterisation
B) To test the reference gene for gene expression comparison of SMCs and intact media of male and female rat aorta
C) To evaluate changes in gene expression of Gc-a, Gc-b, Nprc, sGC due to isolation and culturing of rat aortic SMCs
D) To determine sex-dependent differences in the gene expression of Gc-a, Gc-b, Nprc, sGC in rat aortic SMCs
E) To evaluate changes in enzyme function of Gc-a and Gc-b due to isolation and culturing of rat aortic SMCs

## 2.2 Male Reproduction Tissue

The aims of the second thesis chapter were:

A) To develop a semi-automated imaging analysis technique for the superficial wall contractions of rat STs
B) To evaluate spontaneous wall contractions in rat STs and comparison of dark and pale tubules
C) To evaluate NO- & NA-induced changes of the spontaneous contraction patterns in ‘dark’ (before spermiation) and ‘pale’ tubules (after spermiation)

# 3 Materials and Methods

## 3.1 Materials

### 3.1.1 Animals and Animal Procedures

Aortic tissue was obtained from 2 to 3 months old male and female Wistar rats (*Rattus norvegicus*) housed in the animal facility of the Veterinary Faculty at Justus-Liebig-University (JLU) Giessen, Germany. All procedures were conducted according to the guidelines of the German Animal Welfare Act and approved by the Committee for Laboratory Animals of the JLU, case number JLU Nr. 577_M (approved from 01/2020 until 12/2022 for the laboratory of Martin Diener). Rats were anaesthetized with $CO_2$ and sacrificed by cervical dislocation.

Reproductive tissue was obtained from 3 to 4 months old male Wistar rats (*Rattus norvegicus*) purchased from Janvier (strain: Rj:WI (SPF) Han). All procedures were conducted according to the guidelines of the German Animal Welfare Act and approved by the Committee for Laboratory Animals of the JLU, case numbers JLU Nr. 617_M (approved from 09/2016 until 08/2021 for the laboratory of Andreas Boening). Rats were anaesthetized with isoflurane and sacrificed by cervical dislocation.

### 3.1.2 Chemicals and Substances

Below are lists of chemicals, consumables, devices and software used in this thesis.

*Table 1: List of Chemicals*

| Chemical | Manufacturer |
|---|---|
| 3,3',5,5'-Tetramethylbenzidin (TMB) | Carl Roth, Karlsruhe, Germany |
| 3-isobutyl-1-methylxanthine (IBMX) | Sigma, St. Louis, USA |
| 4-(2-hydroxyethyl)-1-piperazineethanesulfonic acid (HEPES) | Sigma, St. Louis, USA |
| Acetic acid | Merck, Darmstadt, Germany |
| Aniline | VWR, Radnor, USA |
| Aniline blue | Merck, Darmstadt, Germany |
| ANP | Bachem, Bubendorf, CH |
| Azocarmine G | Merck, Darmstadt, Germany |
| BSA | Merck, Darmstadt, Germany |
| CNP | Bachem, Bubendorf, CH |
| cGMP standard | Biolog, Hayward, USA |
| Collagenase Type II, Cls II, >125units/mg solid | Sigma, St. Louis, USA |
| DAPI (Cat.no. 10236276001) | Roche, Karlsruhe, Germany |
| DEANONOate (ALX-430-034) | Enzo Life Sciences, Long Island, USA |

| | |
|---|---|
| DMEM/F12 | Gibco, Thermo Fisher Scientific, Waltham, USA |
| Dimethyl sulfoxide (DMSO) | Carl Roth, Karlsruhe, Germany |
| dNTPs | Invitrogen, Waltham, USA |
| DPBS | Gibco, Thermo Fisher Scientific, Waltham, USA |
| Ethanol | Carl Roth, Karlsruhe, Germany |
| Ethidium bromide solution 1% (v/v) | Carl Roth, Karlsruhe, Germany |
| Ethylenediaminetetraacetic acid (EDTA) | Merck, Darmstadt, Germany |
| Eukit | Sigma, St. Louis, USA |
| Formaldehyde | Carl Roth, Karlsruhe, Germany |
| Glacial acetic acid | Merck, Darmstadt, Germany |
| Glycerol | Merck, Darmstadt, Germany |
| Hydrochloride acid | Merck, Darmstadt, Germany |
| Hydrogen peroxide | Carl Roth, Karlsruhe, Germany |
| iQ™ SYBR® Green Supermix | Bio Rad, Hercules, USA |
| Low-Melt Agarose | Bio Rad, Hercules, USA |
| Methanol | Sigma, St. Louis, USA |
| Noradrenaline bitartrate salt | Sigma, St. Louis, USA |
| Normal Goat serum (Cat.no. G9023) | Roche, Basel, Switzerland |
| Oligio(dT)$_{12-18}$ | Invitrogen, Carlsbad, USA |
| Orange G | Merck, Darmstadt, Germany |
| Paraformaldehyde (PFA) | Carl Roth, Karlsruhe, Germany |
| Paraffin | Merck, Darmstadt, Germany |
| Phosphotungstic acid | Carl Roth, Karlsruhe, Germany |
| Picric acid | neofroxx, Einhausen, Germany |
| RNase, DNase free water | Invitrogen, Carlsbad, USA |
| Sodium acetate | Merck, Darmstadt, Germany |
| Sodium bicarbonate | Merck, Darmstadt, Germany |
| Sodium chloride | Merck, Darmstadt, Germany |
| Sodium dihydrogen phosphate monohydrate | Merck, Darmstadt, Germany |
| Sodium hydroxide | Carl Roth, Karlsruhe, Germany |
| Sodium triphosphate | Carl Roth, Karlsruhe, Germany |
| Streptavidin | Vector Laboratories, San Francisco, USA |
| Sulfuric acid ($H_2SO_4$) | Merck, Darmstadt, Germany |
| Thimerosal | AppliChem, Darmstadt, Germany |
| TRIS | Carl Roth, Karlsruhe, Germany |
| Triton X-100 | Sigma, St. Louis, USA |
| TWEEN® 20 | Carl Roth, Karlsruhe, Germany |
| Xylol | Carl Roth, Karlsruhe, Germany |
| β-Mercaptoethanol | Carl Roth, Karlsruhe, Germany |

### 3.1.3 Consumables

*Table 2: List of Consumables*

| **Consumable** | **Manufacturer** |
|---|---|
| Aluminium foil | Carl Roth, Karlsruhe, Germany |
| 8 Well Chamber Slide | Sarstedt AG & Co. KG, Nuembrecht, Germany |

| | |
|---|---|
| Cell culture flasks T25 (cell growth area 25 $cm^2$) | Thermo Fisher Scientific, Waltham, USA |
| Delta T dishes | Bioptechs Inc., Buttler, USA |
| Greiner Tubes (15 mL and 50 mL) | Greiner Bio-One International GmbH, Frickenhausen, Germany |
| Cell strainers (grid size 40 µm) for 50 mL falcons | BD Biosciences, Bedford, USA |
| Immuno 96 Well plates | Thermo Fisher Scientific, Waltham, USA |
| Pipette tips | StarLab, Hamburg, Germany |
| Reaction tube (1, 2.5 and 5 mL) | Sarstedt AG & Co. KG, Nuembrecht, Germany |
| Reaction tube for qPCR & stripes | Greiner Bio-One International GmbH, Frickenhausen, Germany |
| RNase free water | B. Braun, Melsungen, Germany |
| Serological pipettes | BD GmbH, Heidelberg, Germany |
| Well plates (48 well) | Greiner Bio-One International GmbH, Frickenhausen, Germany |

### 3.1.4 Antibodies

*Table 3: List of Primary Antibodies for Immunofluorescence*

| Target Antigen | Host | Cat.no. | Clonality | Manufacturer | Dilution for cells | Dilution for tissue |
|---|---|---|---|---|---|---|
| anti-Calponin | rabbit | ab46794 | Mono | Abcam, Cambridge, UK | 1:500 | 1:500 |
| anti-SMA | mouse | A5228 | Mono | Sigma-Aldrich, St. Louis, USA | 1:1000 | 1:1000 |
| anti-vWF | rabbit | AB7356 | Poly | Sigma-Aldrich, St. Louis, USA | 1:500 | 1:1000 |
| anti-eNOS | mouse | 610297 | Mono | BDTrans, Franklin Lakes, NJ, USA | 1:500 | 1:200 |
| anti-Nestin | mouse | MAB353 | Mono | Chemicon International, London, UK | 1:75 | - |
| anti-Ki67 | rabbit | NCL-Ki67p | Poly | Novocastra Laboratories, Newcastle upon Tyne, UK | 1:1000 | - |

*Table 4: List of Secondary Antibodies for Immunofluorescence*

| Target Antigen | Host | Cat.no. | Clonality | Manufacturer | Dilution for cells | Dilution for tissue |
|---|---|---|---|---|---|---|
| anti-rabbit Alexa488 | goat | A-11034 | Poly | Invitrogen, Waltham, MA, USA | 1:250 | 1:500 |
| anti-rabbit Cy3 | | 111-166-045 | Poly | Jackson Immuno Research, Cambridgeshire, UK | | |
| anti-mouse Alexa488 | | A-11001 | Poly | Invitrogen, Waltham, MA, USA | | |
| anti-mouse Cy3 | | 115-165-003 | Poly | Jackson Immuno Research, Cambridgeshire, UK | | |

*Table 5: Antibody for cGMP ELISA Plate Coating*

| Target Antigen | Host | Cat.no. | Clonality | Manufacturer | Concentration for ELISA |
|---|---|---|---|---|---|
| anti-rabbit-IgG (H+L) | goat | REF: 31210 | Poly | Invitrogen, Waltham, MA, USA | 6,7 µg/mL |

### 3.1.5 Oligonucleotides

*Table 6: List of Oligonucleotides*

| Gen | Sense (5'-3') | Antisense (5'-3') | Product size (bp) | Source/ BLAST NM |
|---|---|---|---|---|
| Actb | ATCTGATACGTCCTCTATCC | GTGGACGGAGCAAGCTCCTA | 232 | NM_031144.3 |
| Gapdh | CTTGTGCAGTGCCAGCCTC | ACCAGCTTCCCATTCTCAGC | 230 | NM_017008.4 |
| U2 | ATCTGATACGTCCTCTATCC | GTGGACGGAGCAAGCTCCTA | 83 | (Taki et al., 2014) |
| Gc-a | GACCTACTGCCCTGCTGTTC | GAGAGGTGGAAGCTGGACAC | 77 | (Wunder et al., 2013) |
| Gc-b | TGGCTCTTAGGAGAGCGAAA | GCCCATCCAAGTACCAACAG | 84 | (Wunder et al., 2013) |
| Nprc | CTCCTTGCAAATCATGTGGCCT | TCTTGGTGATTTCGCCTCTCA | 142 | NM_012868.1 |
| sGCβ1 | GCGGACACCATGTACGGTT | GCAGCCACCAAGTCATAGGT | 170 | NM_012769.2 |

### 3.1.6 Standard Systems and Commercial Kits

*Table 7: List of Standard Systems and Commercial Kits*

| Name | Manufacturer |
|---|---|
| RNase-Free DNase Set | Qiagen, Hilden, Germany |
| RNeasy Mini Kit ® | Qiagen, Hilden, Germany |
| SuperScript™ II Reverse Transcriptase | Invitrogen, Carlsbad, USA |

### 3.1.7 Buffer and Solutions

*Table 8: List of Buffers and Solutions*

| Buffer | Composition |
|---|---|
| Aniline blue – Orange G Solution | 0.5 g Aniline blue<br>2 g Orange G<br>8 mL Glacial acetic acid<br>100 mL Aqua dest. |
| Aniline-alcohol | 0.1 mL Aniline<br>100 mL 90 % Ethanol |
| Azocarmine Solution | 0.1 g Azocarmine<br>100 mL Aqua dest.<br>Heat until the solution boils, then add 1 mL Glacial Acetic Acid / 100 mL of filtered solution |
| Biotin-cGMP-Tracer Solution | IHF Hamburg, Germany provided by Matthias Schuhmacher (Müller et al., 2011) |
| Bouin Solution | 30 mL saturated Picric Acid<br>10 mL Glacial Acetic Acid<br>2 mL 37 % Formaldehyde |
| cGMP-Antiserum Solution | IHF Hamburg, Germany provided by Matthias Schuhmacher (Müller et al., 2011) |
| DMEM Utility Solution | 10 mL Aqua dest.<br>1.28 g Dulbecco's Modified Eagle Medium/Nutrient Mixture F-12 (DMEM/F12) |
| Dilution Buffer for Immunofluorescence | 0.2 % BSA<br>0.1 % $NaN_3$ |

| | |
|---|---|
| | In PBS |
| ELISA Blocking Buffer | 0.1 M $NaH_2PO_4$ x $H_2O$<br>0.066 M NaOH<br>0.15 M NaCl<br>0.8 % BSA<br>1 nM EDTA<br>0.08 % Tween 20<br>0.0025 % Thimerosal |
| ELISA Coating Buffer | 50 mM $NaHCO_3$ pH 9.6<br>6.7 µg/mL Goat-anti-rabbit IgG |
| ELISA Washing Buffer | 0.5 % NaCl<br>0.02 % Tween 20 |
| ELISA-PBS Buffer (E-PBS) | 0.1 M $Na_3PO_4$ x 12 $H_2O$<br>0.15 M NaCl<br>0.005 M EDTA<br>0.2 % BSA<br>0.01 % Thimerosal<br>pH 7.0 (adjust with HCl) |
| HEPES Utility Solution | 5.6 mM KCl<br>136.4 mM NaCl<br>1 mM MgCl 2x6 $H_2O$<br>2.2 mM CaCl 2x2 $H_2O$<br>11 mM Glucose<br>10 mM HEPES<br>Adjusted to pH 7.4 using 1M NaOH |
| HPR Streptavidin Solution | 0.152 µg/mL E-PBS |
| HPR Substrate Solution | 0.01 M Sodium acetate<br>0.45 mM Citric Acid<br>0.00038 % $H_2O_2$<br>0.0001 % TMB (in DMSO) |
| Orange G Utility Solution | 25 ml 1x TAE Buffer<br>25ml Glycerol<br>Spatula tip Orange G |
| PBS Buffer | 0.136 M NaCl<br>0.05 M $Na_2HPO_4$ x 2 $H_2O$<br>pH 7.4 (adjust with 1 N HCl) |
| TAE (10X) Buffer | 40 mM Tris<br>20 mM Acetic Acid<br>1 mM EDTA |

### 3.1.8 Cell Culture Media, Supplements and Substances

*Table 9: List of Cell Culture Media and Substances*

| Cell culture media/supplement | Manufacturer |
|---|---|
| DMEM/F12 medium | Gibco, Thermo Fisher Scientific, Waltham, USA |
| Dulbecco's Phosphate-Buffered Saline (DPBS) | Gibco, Thermo Fisher Scientific, Waltham, USA |
| Foetal Bovine Serum (FBS) | Gibco, Thermo Fisher Scientific, Waltham, USA |
| MEM 1X medium | Gibco, Thermo Fisher Scientific, Waltham, USA |
| Penicillin/Streptomycin [10,000 U/mL] (Pen/Strep) | Gibco, Thermo Fisher Scientific, Waltham, USA |

| | |
|---|---|
| Trypsin 0.5% (v/v) - EDTA 0.2% (v/v) solution | Sigma, St. Louis, USA |

## .1.9 DNA Ladder

*Table 10: List of DNA Ladder*

| Ladder | Grade | Manufacturer |
|---|---|---|
| Ultra Low Range DNA Ladder | 25 bp | Invitrogen, Thermo Fisher Scientific, Waltham |
| Gene Ruler 100 bp Ladder | 100 bp | Thermo Fisher Scientific, Waltham, USA |

## 3.1.10 Devices

*Table 11: List of Devices*

| Device | Company |
|---|---|
| Biological Safety Cabinet | Nuaire, Plymouth, USA |
| Centrifuge 5804 R | Eppendorf, Hamburg, Germany |
| Concentrator 5301 | Eppendorf, Hamburg, Germany |
| DH Autoflow $CO_2$ Air-Jacketed Incubator | Nuaire, Plymouth, USA |
| DIAS Microplate reader | Dynatech, Denkendorf, Germany |
| Digital Camera C-400 200 M | Olympus, Hamburg, Germany |
| Electrophoresis Power Supply 300 V - 500 mA E835 | Consort, Turnhout, Belgium |
| Electrophoresis chamber | PeqLab, VWR, Pennsylvania, USA |
| Fluorescence microscope, Axioskop 2 plus | Zeiss, Muinch, Germany |
| Heating Immersion Circulator ED Water Bath | Julabo, Seelbach, Germany |
| Heating/Cooling Dry Block CH-100 | Biosan, Riga, Latvia |
| iCycler 5 IQ™ Real-time PCR detection system | Bio Rad, Hercules, USA |
| Mastercycler gradient 5331 | Eppendorf, Hamburg, Germany |
| Mikro 20 Centrifuge | Hettich Zentrifugen, Tuttlingen, Germany |
| Mikrotom Leica RM 2255 | Leica, Wetzlar, Germany |
| Mixer Mill MM400 | Retsch, Haan, Germany |
| Mortar and pestle (ceramic) | Haldenwanger, Fisher Scientific GmbH, Schwerte, Germany |
| Motic binocular light microscope SMZ-171 | Motic, Wetzar, Germany |
| Moticam 3 digital camera (3.0 MP) | Motic, Wetzar, Germany |
| MultiImage Light Cabinet Alpha DigiDoc™ | Biozym Scientific, Hessisch Oldendorf, Germany |
| Multi-8 channel pipet | Eppendorf, Hamburg, Germany |
| Nanodrop 2000 Spectrometer | Thermo Scientific, Waltham, USA |
| Neubauer Cell Counting Chamber | Marienfeld-Superior, Lauda-Königshofen, Germany |
| Olympus BX25WI microscope | Olympus, Tokio, Japan |
| Separation System B1 | Owl Separations Systems Inc., Portsmouth, USA |
| Table centrifuge with vortex | NeoLab, Heidelberg, Germany |
| UV Chamber – Gel Jet Imager | Intas Science, Göttingen, Germany |

### 3.1.11 Software

*Table 12: List of Software*

| Software | Version | Company |
|---|---|---|
| Axiovision | Rel 4.8 | Zeiss, Munich, Germany |
| BioRad CFX Maestro | 2.3 | Bio Rad, Hercules, USA |
| BioRender | *na* | Toronto, Ontario, Canada |
| GraphPad Prism | 9.5.1 (733); 10.4.0 (627) | GraphPad Software, San Diego, USA |
| Fiji Image J | *na* | https://www.fiji.sc |
| Intas GDS Touch 2 | *na* | Intas Science, Göttingen, Germany |
| Motic Images Plus | 2.0 ML | Motic, Wetzar, Germany |
| Revelation | 2.0 | Dynatech, Denkendorf, Germany |

## 3.2 Methods

### 3.2.1 Organ Harvest and Tissue Preparation

#### *3.2.1.1 Organ Harvest and Preparation of Aorta*

Immediately after the rat was sacrificed, aortic tissue was prepared. Aortae were dissected from the heart until the abdominal bifurcation, transferred into MEM 1X medium, supplemented with 1% (v/v) Penicillin/Streptomycin (Pen/Strep), and stored on ice. The aortic SMC layer (*tunica media*) was prepared in cold MEM 1X + Pen/Strep under a Motic® dissection microscope using light from below the object. After removing the surrounding fat layer, branching vessels were cut, and the aortic media was bisected longitudinally. One half of the same animal was used for primary SMC extraction (chapter **3.2.2.1**), and the second half was prepared as follows.

Starting from the proximal end, the surrounding connective tissue (*tunica adventitia*) was manually removed using curved tweezers. The inner endothelial layer (*tunica intima*) was carefully removed.

#### *3.2.1.2 Treatment of Aortic Tissue for cGMP ELISA*

Longitudinal halves of one aorta, prepared as mentioned above, were weighed and equilibrated in 200 µL of prewarmed MEM 1X + Pen/Strep for 10 min at 37°C. For treatment, tissue was incubated in 200 µL MEM 1X + Pen/Strep containing IBMX (0.25 nM) and ANP or CNP, each at a concentration of 100 nM for 30 min at 37°C. One longitudinal half was treated with ANP, and the other half of the same vessel was treated with CNP. After short centrifugation the supernatant was frozen immediately in liquid nitrogen and stored at -80°C until measurement (chapter **3.2.3.2**).

#### *3.2.1.3 Organ Harvest and Preparation of Rat Seminiferous Tubules*

Testicular tissue was removed from the rat situs immediately after sacrifice by grabbing the testicular fat and pulling the testicles out of the scrotum. Tissue was further prepared in ice cold MEM 1X + Pen/Strep. The adjacent fat and epididymis, as well as the capsule (*tunica albuginea*) were removed under a Motic® dissection microscope using the light from below the tissue. The seminiferous tubules were pulled apart and singularized using sterile cannulas. The different spermatogenic stages (dark and pale) were characterized according to their appearance (pattern and darkness) of the tubular lumen in transillumination. The relevant tubule sections (between 1-2 cm in length) were dissected using sterile scissors. STs were then either frozen immediately in liquid nitrogen for RNA isolation (chapter **3.2.3.1**) or embedded in rat collagen for live imaging (chapter **3.2.4.1**).

### 3.2.2 Cell Biological Methods

#### *3.2.2.1 Primary Cell Extraction and Culture*

The SMC extraction from the aortic media required a two-step enzymatic digestion with collagenase (Collagenase Type II). A longitudinal aortic half was prepared as described in chapter **3.2.1.1** and first digested with 10% (w/v) collagenase in MEM 1X + Pen/Strep at 37 °C for 15 min. After being transferred into fresh MEM 1X + Pen/Strep the tunica media was manually separated from the adventitia starting at the proximal end. The thin intimal layer was scratched off using curved tweezers. The remaining media was cut into small pieces (ideally 1 mm x 1mm) using sterile scissors. The media pieces were transferred into fresh MEM1X + Pen/Strep with 10% (w/v) collagenase and incubated for 30 min at 37 °C. Afterwards, digestion was stopped by dilution with approximately 5 mL prewarmed cell culture medium DMEM/F-12 + Pen/Strep containing 10% (v/v) foetal bovine serum (FBS). The suspension was strained through a cell strainer (40 µm grid size) under sterile conditions, and the flow-through (containing the singularised SMCs) was centrifuged for 10 min at 1,000 rpm at room temperature. The pellet was resuspended in 5 mL fresh pre-warmed DMEM/F-12 + FBS + Pen/Strep and transferred into a T25 sterile culture flasks. SMCs were cultured at 37°C, 5 % (v/v) $CO_2$ and culturing media was changed every 2 - 3 days. The extraction passage (Pa) was cultured for 6 days before SMCs were once rinsed with sterile DPBS and then detached with 1mL Trypsin-EDTA solution for 5 min at 37°C and transferred into fresh culture flasks. SMCs (Pa1 till Pa 3 after extraction) were seeded as shown in the following table.

*Table 13: Cultured Cell Number for Molecular Biological Experiments*

| Purpose | Cell number | Dish | Volume |
|---|---|---|---|
| RNA Isolation for RT-qPCR | 4 - 5x$10^5$ | T25 | 5 mL |
| NP treatment for cGMP ELISA | 4x$10^4$ | 48-well plate | 0.5 mL/well |
| Immunofluorescence | 2x$10^4$ | 8-well chamber slide | 0.25 mL/well |

Cell number was determined in 10 µL cell suspension using the Neubauer Counting Chamber according to the equation:

$$cell\ number\ (cells/ml) = average\ cell\ number\ per\ large\ square \times dilution\ factor \times 10^4 \times ml^{-1}$$

#### *3.2.2.2 Treatment of Primary Cells for cGMP ELISA*

For the determination of cGMP production by ELISA, SMCs were seeded in 48 well plates as mentioned above. SMCs were cultured until approximately 80 % of each well bottom was covered with cells. The old DMEM/F12 media was exchanged with FBS-free MEM 1X + Pen-Strep for at least 4 h of equilibration. 200 µL of prewarmed MEM 1X + Pen/Strep containing IBMX [0.25 nM], a PDE inhibitor dissolved in DMSO, and the NPs [100 nM] were added per well. The same medium with IBXM only served as a negative solvent control. The 30 min long treatment in the incubator (37°C and 5 % (v/v) $CO_2$) was stopped by addition of 800 µL ice cold 100 % (v/v) ethanol per well and immediate freeze down of the entire plate at -20°C for at least 1 h. Cells and supernatant were detached using a 1 mL serological pipet with extra-long pipet tips, transferred in fresh sterile 1.5 mL Eppendorf Tubes and centrifuged for 30 min at 4°C and 20,000 g. The clear supernatant was transferred into a fresh tube and lyophilized for at least 1.5-2h in a vacuum concentrator at 60°C until a dry pellet remained at the tube bottom. The pellet was resuspended in 140 µL E-PBS and vortexed thoroughly. The samples were either immediately used for the ELISA measurement (chapter **3.2.3.2**) or kept frozen at -80°C.

### 3.2.3 Molecular Biological methods

#### *3.2.3.1 Determination of mRNA Abundance*

##### Isolation of total RNA from Tissue

Before the RNA isolation the tissue samples were generally freed from remaining moisture, weighed, and immediately frozen in liquid nitrogen. RNA isolation was performed using the RNeasy® Mini Kit (spin technology) according to the manufacturer's instructions with on-column DNase digestion. The tissue was pulverized under liquid nitrogen using a pre-cooled ceramic mortar and pestle. In cases of very tough tissue consistency, the frozen sample was wrapped in

aluminium foil and pulverized with a hammer. RLT buffer containing 1% (v/v) β-Mercaptoethanol was added according to the tissue weight (in general below 20 mg, hence 350 µL). A sterile metal bead was added, and sample was processed for 2 min in a mixer mill at 30 Hz. The lysate was centrifuged for 5 min at full speed (24,500 g) and the supernatant was transferred into a fresh reaction tube and gently mixed with the equal volume of 70 % (v/v) ethanol, where streak formation usually indicated the presence of nucleic acids. The subsequent washing steps were performed according to the manufacturer's instructions. RNA was finally eluted with 30 µL RNase-free water and stored at -80°C. To determine RNA concentration and purity, RNA was thawed at 65°C for 5 min, briefly vortexed, and then cooled on ice for 5 min to break the tertiary structures. Before the RNA concentration was measured, the sample was briefly vortexed again and then the concentration was determined in 1 µL using the NanoDrop® 2000 spectrometer.

### Isolation of total RNA from Cells

For the isolation of total RNA 4-5x$10^4$ cells were seeded into a T25 flask and cultured until 90 % of the flask bottom was covered. Cells were harvested and cell samples were processed according to the instructions of the RNeasy® Mini Kit with on-column DNase digestion. RNA was finally eluted in 30 µL RNase-free water and stored at -80°C. To determine RNA concentration and purity, RNA was thawed at 65°C for 5 min, briefly vortexed, and then cooled on ice for 5 min. Before the RNA concentration was measured in 1 µL of the sample using the NanoDrop 2000® spectrometer, the RNA was vortexed briefly.

### Reverse Transcription for cDNA synthesis

2 µg of extracted RNA served as template for the cDNA synthesis. SuperScript™ II Reverse Transcriptase and the Oligo$(dT)_{20}$ primer were applied according to the manufacturer's instructions using a thermal cycler. Consistency of the RT was verified by measurement of the cDNA concentration using the NanoDrop 2000® spectrometer. In case of notable differences, cDNAs were adjusted to the same concentration for the subsequent qPCR measurement.

### Primer Design and Efficiency Test

Primer pairs for the genes of interest spanning an exon/exon junction were selected using Primer Blast (https://www.ncbi.nlm.nih.gov/tools/primer-blast/). In cases when primer sequences were used from other publications, BLAST was used to check the primer properties and product size. Custom DNA-Oligos (0.01 µM, salt-free, lyophilised, MALDI-TOF MS quality analysis) were purchased from Eurofins, Hamburg, Germany. For details of final primer selection, see (chapter **3.1.5**, Table 6).

The efficiency (**E**) of each primer pair was calculated based on a cDNA dilution series with three steps (undiluted, 1:2 and 1:4). Every dilution sample was measured as triplet in usual RT-qPCR run according to the qPCR steps given in Table 14 below. The resulting Ct mean values of each dilution level were plotted against the concentration of the diluted sample (log10 scale) and used to create a descending slope (**m**) by linear regression.

Primer efficiency calculation:

$$E = 10^{[-1/m]} - 1$$

An **m** of exactly -3.32 is necessary to achieve an efficiency of 100%. In theory the matrix material is duplicated in each reaction cycle, and with it the fluorescence signal when an efficiency of 100% is assumed. Only primer sets that achieved an efficiency between 90-120% were used.

### Reference Gene Search for Expression comparison between intact aortic tissue and cultured aortic SMCs

The selection of potential RG candidates was based on literature research. Only qPCR studies on rat were considered. If indicated, the primer sequences for the RGs as described in these publications was used. If only the name of the RG was given, Primer BLAST was used for the respective primer design as described above. For every gene tested the absolute Ct values of intact aortic media and the corresponding cultured SMCs were determined of four randomly chosen samples of each, male and female rats. To minimize the influence of pipetting inaccuracies, the expression of each sample was measured as triplets. The absolute value of the difference between the Ct values of intact tissue and the cultured SMCs (|Ct intact media-Ct cultured SMCs|) served as preliminary indicator for gene expression stability of the RGs.

Further information on the procedure and results of the establishment of a suitable RG can be retrieved from the research article “Reference gene U2 enables direct comparison between relative gene expression levels of vascular smooth muscle cells in tissue and culture using real-time quantitative PCR.” (Rager et al., 2023).

### Real- Time quantitative Polymerase Chain Reaction (RT-qPCR)

RT-qPCR was performed using the iCycler IQ PCR system and the iQ™ SYBR® Green Supermix using the cycler steps listed in Table 14 below:

*Table 14: Cycler Steps for RT-qPCR*

| | Step | Cycles | Duration | Temperature |
|---|---|---|---|---|
| 1 | Polymerase activation | 1× | 3 min | 95 °C |
| 2 | Denaturation | 35× | 20 s | 95 °C |
| 3 | Primer hybridisation | | 20 s | 60 °C |
| 4 | Elongation | | 20 s | 72 °C |
| 5 | Melt curve analysis | / | | 55 °C–95 °C |

Visualization of PCR products

Depending on their length, the double-stranded PCR products were visualized on a 2-3% (w/v) agarose gel with ethidium bromide (1.5 µL in 100 mL TAE 1x buffer). Agarose gel electrophoresis was executed to check for the size of the PCR products, for off-target products and for an excessive amount of primer or primer dimers. Before electrophoresis was started 2.5 µL of Orange G utility solution were added to each PCR product sample. The final amount of 12.5 µL of the PCR samples were applied to the gel pockets while in case of the DNA ladders 8 µL were sufficient according to the manufacturer's suggestion. Electrophoresis settings were as follows: 45 min, 100 V and 500 mA. After the gel run bands were visualized and captured in a UV chamber.

### *3.2.3.2 Determination of cGMP Production by ELISA*

cGMP levels after NP treatments were determined by ELISA (Institute for Hormone and Fertility Research [IHF], Hamburg, Germany) based on a previously described assay (Müller et al., 2006; Müller et al., 2004) following the principles of a competitive ELISA (**Figure 20**).

Plate Coating for cGMP ELISA

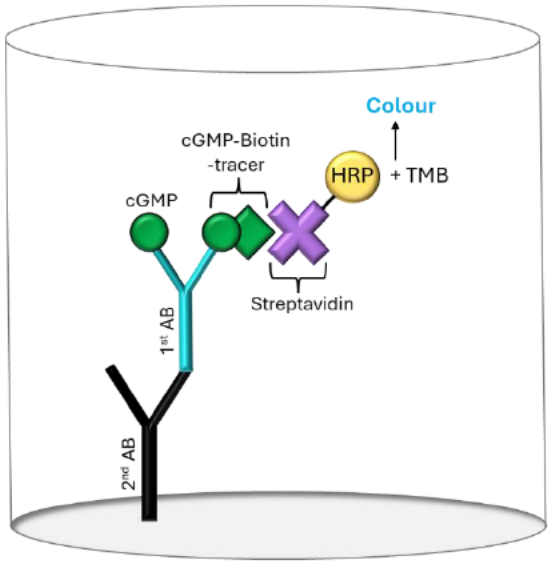


***Figure 20**: Principal mechanism of competitive cGMP ELISA.*
Antibody (AB), cyclic guanosine monophosphate (cGMP), Horseradish peroxidase (HRP), 3,3',5,5'-Tetramethylbenzidin (TMB).

Therefore, pre-coating of Immuno 96-well plates with secondary antibody was necessary. For the plate coating a multi-8 channel pipet was used. 150 µL of coating buffer with 6,7 µg/mL of Goat-anti-rabbit IgG (H+L) was added to each well (chapter **3.1.4**, Table 5). The coated plates were incubated overnight at room temperature in darkness. The following day, 240 µL of blocking buffer was added per well and again the plates were incubated overnight at room temperature in darkness. The following day the plates were drained, and the remaining liquid was removed by tapping. The wells were then washed with 350 µL/well washing buffer

for 3 consecutive steps and again the liquid was removed thoroughly. After that, the coated plates were sealed airtight and stored at -20°C.

### cGMP ELISA

First, the coated Immuno 96-well plate had to be activated by addition of 375 µL EPBS per well for 2 min. In the meantime, the cGMP standard dilution series (0.14; 0.42; 1.26; 3.78; 11.34 and 34.02 pM in EBPS) was prepared. The samples and standards (50 µL per well) were loaded in horizontal duplicates on the antibody-coated 96 well plate together with 100 µL cGMP-antiserum [1:80,000] and 50 µL biotin-cGMP-tracer [170 fM in Aqua dest.]. For the non-specific binding control (NSB), no standard or sample and no cGMP antibody serum was added to the first 2 wells. The plate was covered with a lid and incubated for at least 18 h in a wet chamber at 4°C in darkness. Afterwards, the plate was aspirated and 200 µL of HPR-Streptavidin solution were added per well. The plate was covered with a lid and incubated for 30 min in a wet chamber at 4°C in darkness. The plate was then washed for 3 times for 1 min with washing buffer, and afterwards 250 µL HPR-substrate solution were added per well. After an incubation for 40 min in a wet chamber at room temperature in darkness, 50 µL $H_2SO_4$ [2M] were added per well. Emission intensity detection was performed immediately as described in the following paragraph.

### Calculation of cGMP quantity

The optical intensity (OD) was detected photometrically at 450 nm using the DIAS microplate reader running the software Revelation 2.0, which automatically calculated the cGMP concentration for each sample. In detail, the software performs a background correction for the NSB values with both the standard and the sample values. The cGMP standard curve is created using the average ODs of the standard duplicate values and the specified percentage values. The average cGMP concentration of each sample duplicate is derived from the standard curve pmol/mL. For cGMP measurements of tissue samples, the final concentration was normalized to the tissue weight.

Equation for background correction is the following:

$$B/Bo\ (\%) = \frac{OD_{Standard/Probe} - OD_{NSB}}{OD_{Bo} - OD_{NSB}}\ x\ 100$$

(B= binding factor of sample; Bo= binding factor of zero standard positive control with max. colour development; B/Bo= percentage of sample binding relative to maximum binding, OD= Optical Density/ Emission Intensity at 450 nm; NSB= non-specific binding control/blank)

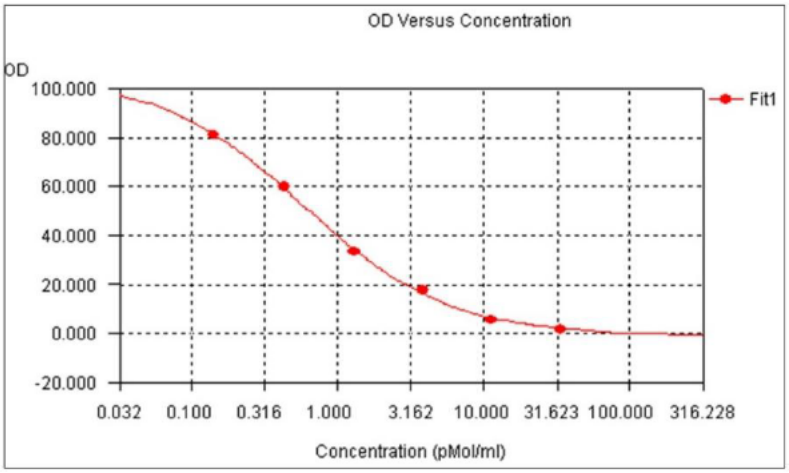


***Figure 21**: Exemplary standard curve of cGMP ELISA measurement.*
Dilution series of the cGMP standard sample results in sigmoidal standard curve reaching a maximum optical density (OD) value at 100 and a minimum value at 0.

## 3.2.4 Imaging Methods

### *3.2.4.1 Preparation of Collagen for Tissue Embedding*

Collagen fibres were extracted from rat tails after removing the skin. The thin collagen fibres were washed and incubated for 15 – 20 min in 70 % (v/v) ethanol. The ethanol was drained, and the collagen fibres left to air-dry overnight. The now dry and crispy fibres were slowly dissolved in 250 mL of 0.1 % (v/v) glacial acetic acid while continuously stirring at 4°C for 48 h. To keep the solution fluid, glacial acetic acid was added as required. The remaining collagen fibres were removed, and the solution cleared by centrifuging at 24.000g at 4°C for 30 min once the desired quantity and viscosity was achieved. Just before tissue embedding for each live imaging experiment 1 g of the prepared rat collagen solution was combined with DMEM utility solution, HEPES [1 M], NaOH [0.5 M]. The proportions of the components can vary depending on the batch of rat collagen produced and require testing beforehand. The proportions for the collagen utility mixture were roughly as follows: 1 g rat collagen, 150 µL DMEM utility solution, 52 µL NaOH [0.5 M] and 50 µL HEPES utility solution (Mietens et al., 2014).

### *3.2.4.2 Live Imaging of Rat Seminiferous Tubules*

Rat seminiferous tubules were prepared (chapter **3.2.1.3**) and kept in fresh MEM 1X solution with 5 % (v/v) Pen/Strep to maintain tissue vitality. 200 µL of the freshly prepared rat collagen utility

mixture were added to a delta T-dish and distributed evenly. The singularized tubules were carefully placed into the dish under visual control to ensure that the tissue lay flat in the dish and was fully covered by rat collagen utility solution. The dish was then placed for 30 min into an incubator (37° and 5% (v/v) $CO_2$) to ensure polymerization of the collagen and thereby fixing the delicate tissue in a steady position. In the meantime, fresh MEM1X medium with 5 % (v/v) Pen/Strep was prewarmed to 37°C and bubbled with $CO_2$. The polymerized collagen in the dish was then covered with 1 mL prewarmed and bubbled MEM1X medium with 5 % (v/v) Pen/Strep and tissue was ready for recording. Image stacks were captured at 1 frame per second using the live imaging set-up as shown below (**Figure 22**).

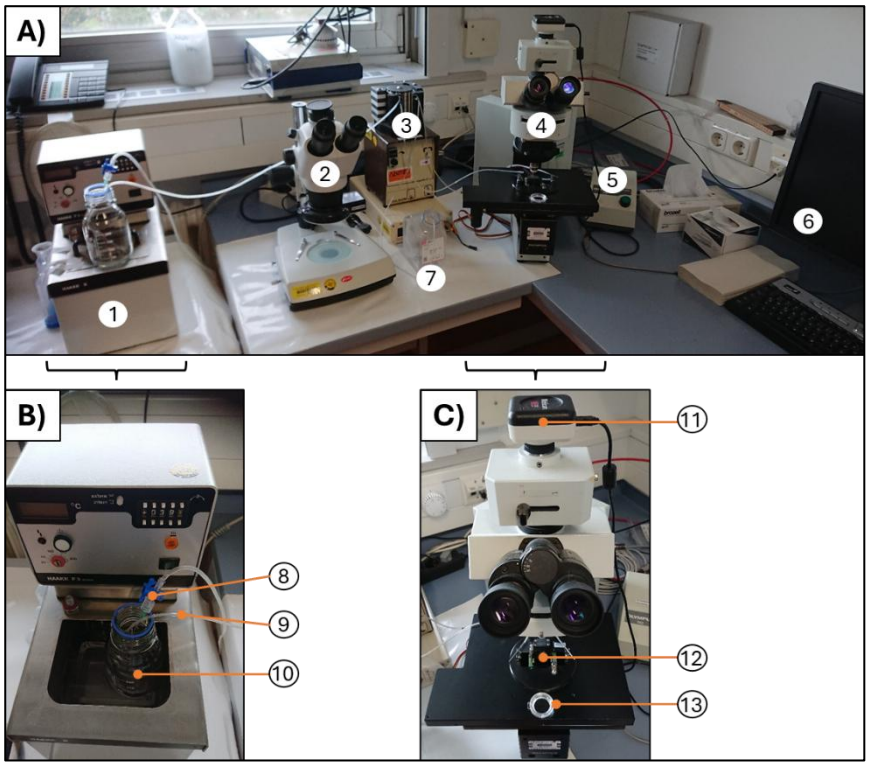


***Figure 22**: Experimental setup for live imaging at the Middendorff laboratory at the JLU Giessen.*
(**A**) Overall setup: 1) Water bath, 2) Bright field microscope for tissue preparation, 3) Media pump, 4) Live imaging microscope, 5) Brightness adjustment, 6) Computer running Leica imaging software, 7) Liquid waste container collecting the drainage of used media; (**B**) Prewarmed media supply: 8) Oxygen supply, 9) Tube supplying tissue with fresh media, 10) glass bottle containing fresh MEM 1x bubbled with oxygen at ~37°C; (**C**) Imaging setup: 11) Leica MoticCam 3.0 (3.0 MP), 12) Heating panel keeps tissue at ~37°C during live imaging, 13) T-Dish containing the tissue in rat collagen matrix.

Stock solutions for NA and NONOate) were prepared at a concentration of 10 mM. Stock solutions were then prediluted in prewarmed, oxygenated MEM1X with 5 % (v/v) Pen/Strep and a certain volume added to reach a 10 µM final concentration for the treatment of the tissue in the dish. Throughout the entire imaging process (length of the films varied from 30 to 40 mins), the tissue was kept at roughly 35°C and flushed with fresh prewarmed and bubbled MEM1X with 5 %

(v/v) Pen/Strep using the culture dish temperature control system and the media pump with the fixed speed setting 250 (this equals 250 µL/min).

#### *3.2.4.3 Evaluation of Live Imaging Movies with FIJI Image J*

For evaluation of tissue contractions, the open access software FIJI (ImageJ) was used (Schindelin et al., 2012) while the statistical analysis was performed with GraphPad Prism (Table 12). The FIJI scripts used for movement and frequency analysis of the live imaging recordings were developed and improved by Cameron Nowell (Head of the Imaging Core Facility at the Monash Institute for Pharmacy and Pharmaceutical Research). The latest scripts of the movement analysis (Nowell, 2021) [doi.org/10.26180/13653614] and the merged amp/freq/mov analysis [doi applicable upon publication] can be retrieved from the Monash Bridges data repository website(https://bridges.monash.edu). The subsequent paragraphs additionally will provide a brief overview of the code development.

##### Original movement score evaluation and cumulative distribution graphs

To analyse multidirectional contractions in epididymal tissue, Beatrix Bester together with Cameron Nowell developed a FIJI script (Stadler et al., 2021) based on a previous manual referred to as the "Wiggle Index". This script was originally developed to investigate the movement patterns of nematodes (Denecke et al., 2015; Preston et al., 2015; Preston et al., 2016; Stadler et al., 2021)). Like the Wiggle index, the new adaptation compared how the sum of movements (extracted from standard deviation scores of the contrast fluctuation per pixel) of a defined region of interest (ROI) in the field of view evolved over the length of the recording. In addition, the code allowed us to measure of the fold change relative to the contraction baseline (spontaneous contractions without stimulations) and to certain treatments (in the case of this thesis, NA and NO). The data then was expressed as a population distribution allowing the detection of even subtle differences in movement intensity. The fold-change for each data point then was exported into GraphPad Prism for further statistical evaluation. First the frequency distribution of the pixel/roi precise fold-change read-out of the intensity fluctuation (change in contrast of the pixel/roi over time) was determined, followed by running a non-linear regression (curve fit) using exponential one phase association testing for the original movement score analysis or a sigmoidal association testing with an indefinite number of peaks in case of the frequency only curves. This test was performed in GraphPad Prism and evaluated if one specific curve shape fits all data sets. The data sets compared were deemed to be significantly different if performing a non-linear regression (curve fit) using the respective association testing, resulted in one curve not adequately fitting both data sets.

In addition, the average movement score over the time of each experiment was visualized as heat maps in which pixels with a high intensity of the movement were shown in red/grey colour, while pixels with a low movement intensity were visualized in blue (**Figure 23**).

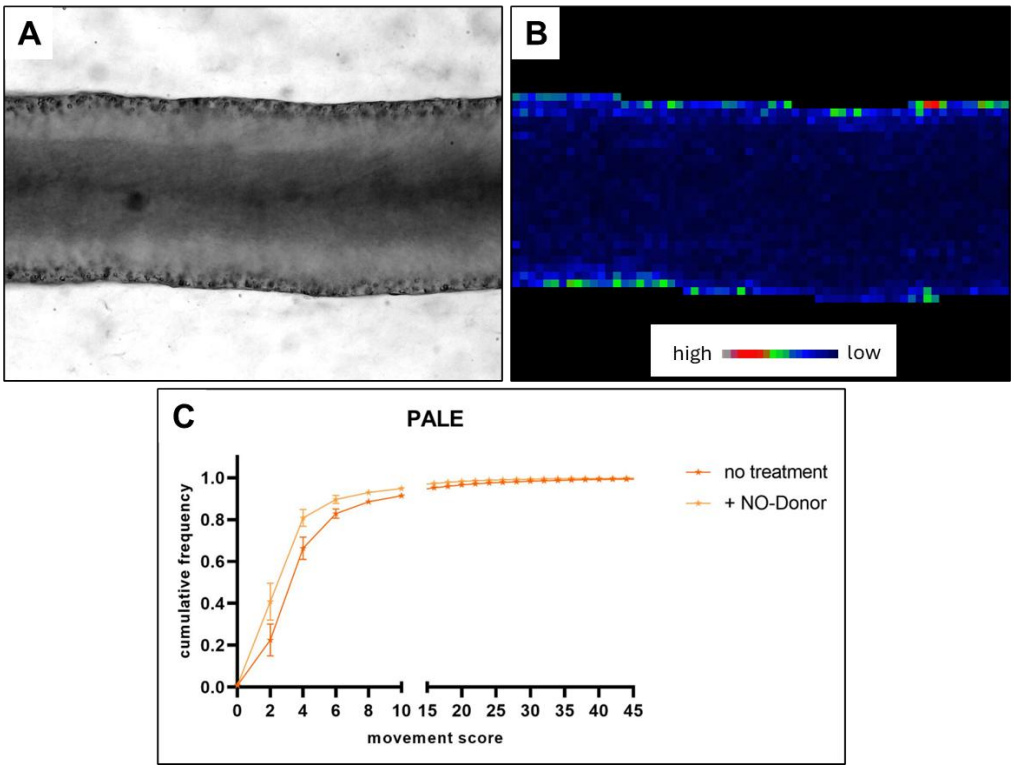


***Figure 23:*** *Imaging analysis according to the previously developed movement score evaluation with FIJI.*
**A)** Exemplary live image of a rat seminiferous tubule (ST) in the pale spermatogenic stage (after spermiation) in bright field microscopy. **B)** Visualization of the tissue movement as pixel-precise heat map. The scale indicates the colour coding of the movement intensity. The region of interest (ROI) in this case is the entire tissue section within the recorded visual range. **C)** Cumulative frequency distribution graphs sort the pixels according to their movement score and the frequency with which these movement scores occur. In GraphPad Prism therefore, a non-linear regression model with exponential one phase association technique was applied. The lower the graph is positioned the higher the movement was, meaning that in the case of the given example the spontaneous contractions of this particular ST are dampened by nitric oxide (NO) donor (NONOate) treatment.

### Intermediate frequency only evaluation and cumulative distribution graphs

The original movement score evaluation already indicated stage-dependent differences in the spontaneous contractions pattern of dark and pale rat STs (summarized in results chapter **4.2.1**). Nevertheless, it is crucial to consider the character of the tissue movement the code initially was developed for (Stadler et al., 2021). The most distal epididymal segment 19 showed a very different spontaneous contraction pattern than the steady wave-like twitching of the ST walls and upon stimulation performed a more cramp-like shrinking of a wide tissue area. That is why the previous analysis focussed on the movement score (the pixel intensity fluctuation that indirectly considered the amplitude of the tissue shrinking) and omitted the analysis of the frequency entirely.

In contrast, the STs spontaneously contracted consistently with a certain rhythm and amplitude. From a physiological point of view this is relevant to maintain a steady output of sperm. Hence, it is hypothesized that the frequency and amplitude of the tubular SMC contractions are regulated according to the spermatogenic stages of the tubular GE. An intermediate analysis step to explore the fine tuning of the spontaneous contractions of the STs in a more detailed manner was to perform a separate stage-dependent frequency-only analysis. The script therefore considered a ROI selection along the wall, the adjacent epithelium and the tubular lumen, rather than the entire tissue section in focus (**Figure 24**). The idea behind this was not only to reduce excess analysis of oversaturated (dark/black) pixel regions, but mainly to visualize a hypothetical transfer of the wall contractions on the adjacent epithelium to promote luminal flow. The data again was displayed as a heatmap but in a ROI-precise manner along the wall, the epithelium and the luminal section.

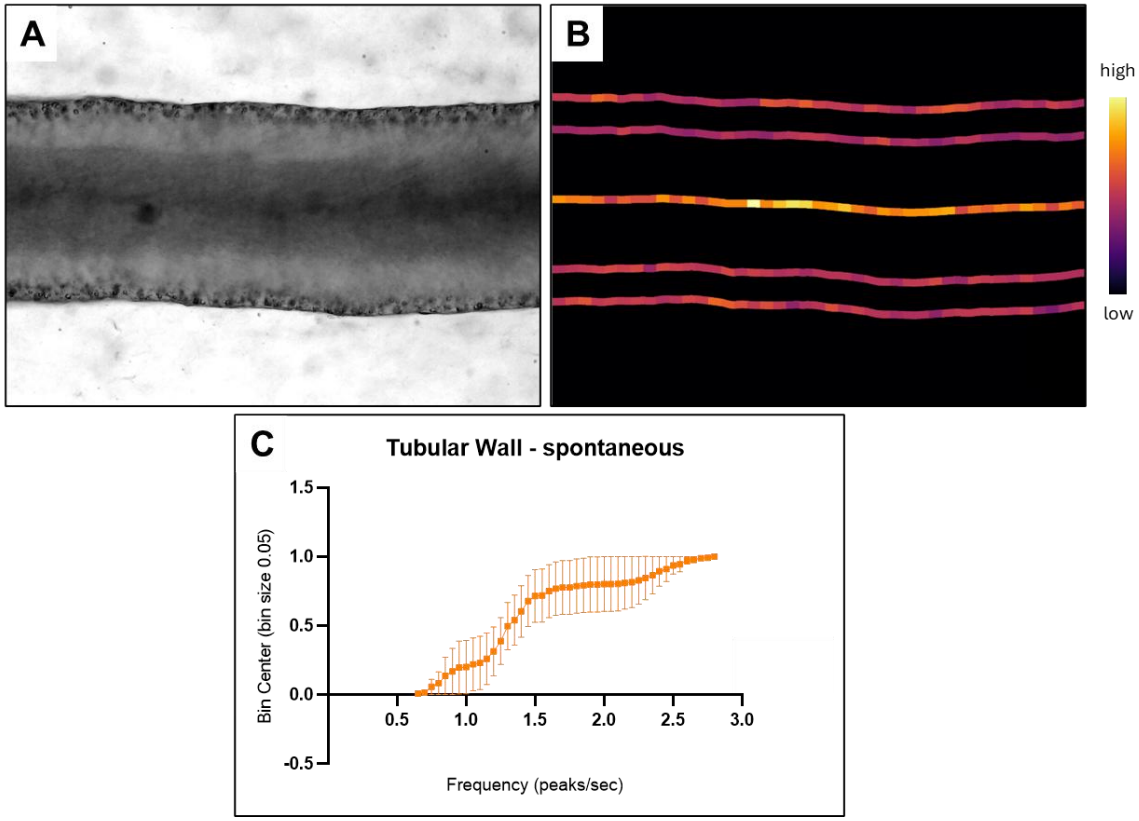


***Figure 24:*** *Imaging analysis according to the frequency evaluation along the wall, the adjacent epithelium and the lumen of the seminiferous tubule using FIJI.*
**A)** Exemplary live image of a rat seminiferous tubule (ST) in the pale spermatogenic stage (after spermiation) in bright field microscopy. **B)** Visualization of the contraction frequency as pixel-precise heat map. The scale indicates the colour coding of the frequency. The regions of interest (ROIs) in this case are automatically arranged by FIJI in stripes with a predefined height along the tubular wall, the adjacent germinal epithelium (GE) and the inner lumen of the rat ST. The scale indicates the coding for the frequency intensity. **C)** Cumulative frequency distribution graphs sort the pixels according to their frequency and the frequency with which these frequency scores occur. In GraphPad Prism therefore, a non-linear regression model with sigmoidal curve shape of a variable slope was applied. The separation of wall, GE and lumen allows the tracking of the propagation of contraction from the wall until the middle of the tubule.

### Merged frequency, amplitude, movement score evaluation and bubble plots

The intermediate frequency analysis used the same statistical evaluation and visualization of the results as cumulative distribution graphs. This revealed that the ultimately intended unified analysis of the amplitude, the movement score and the frequency would require a more sophisticated three-dimensional way to display the results.

The resulting unified code now is tailored specifically to the contractile behaviour of the rat STs and therefore, targets the question of the physiological relevance of the stage-dependent regulation of ST contractions. The merged script now analysed the frequency (contraction peaks per min), the movement score (the pixel intensity fluctuation according to the Wiggle Index calculation) and the amplitude ratio (this ratio is calculated to normalize for contrast fluctuations that might influence the readout of the amplitude in different live recordings, thus enabling the comparison between different movies) of the ROIs that are set along the tubular wall, the adjacent GE and the tubular lumen (**Figure 25 B**). For the final unified analysis, the FIJI script was applied with the following presetting: 1 frame/sec, ROI width 50, ROI height 20, distance from edge 125, rolling window size 20. The obtained data is finally visualized as Bubble Plots in EXCEL (**Figure 25 D**).

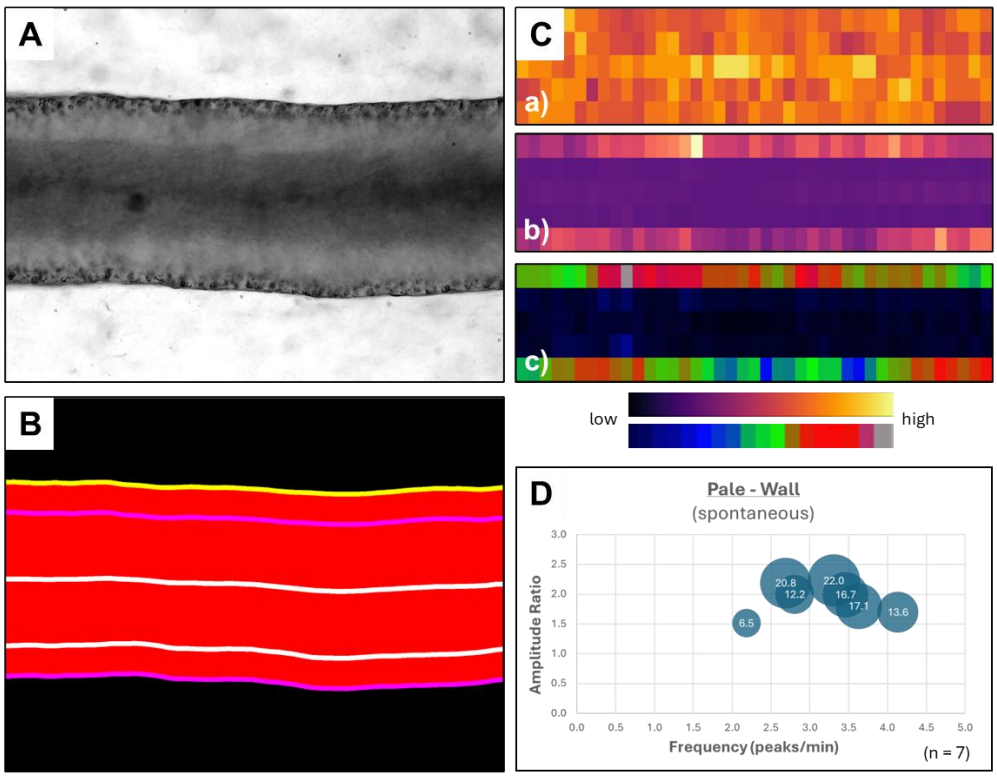


*Figure 25 continues following page.*

***Figure 25:*** *Imaging analysis according to the newly developed unified evaluation of movement score, frequency and amplitude ratio using FIJI.*
**A)** Exemplary live image of a rat seminiferous tubule (ST) in the pale spermatogenic stage (after spermiation) in bright field microscopy. **B)** The regions of interest (ROIs) of a predefined height and width in this case are automatically arranged by FIJI in stripes along the tubular wall, the adjacent germinal epithelium (GE) and the inner lumen of the rat ST. **C)** The readout of the unified analysis is visualized by stacking the five ROI stripe heat maps following their order from upper to lower edge of the tissue in focus on top of one another. The according scales indicate the intensity of a) frequency, b) amplitude ratio and c) movement score. **D)** The results are depicted as two-dimensional bubble plots in EXCEL. The graphs plot the frequency against the amplitude ratio. The bubble size visualizes the movement score. In the given example (pale cohort) the number of bubbles is the number of animals (n). Each bubble originates from the average frequency, amplitude ratio and movement score of each sample by calculation the mean value of the ROIs of the respective stripes along the wall, the GE and lumen.

## 3.2.5 Histological Methods

### *3.2.5.1 Paraffin Embedding and Tissue Slicing*

Rat tissue samples were prepared and fixed in Bouin's solution for 24 h. Tissue was kept in 70 % ethanol until the embedding and ethanol was exchanged frequently. Before manual embedding in paraffin, the tissue was dehydrated in an ascending ethanol series (70 %, 80 %, 90 %, 100 % (v/v)) and finally cleared in xylol. Tissue was transferred into grids (placed into metal molds) and was equilibrated in liquid paraffin at 65°C overnight before the paraffin was left at room temperature to cool down and harden. Tissue blocks were cut into 5 µm thick sections with a microtome. Sections were transferred onto glass slides in a warm tissue float bath and dried at 40°C on a slide warmer. After 24h at 40°C in an incubator, the slides were ready for long-term storage or staining.

### *3.2.5.2 AZAN Trichrome Staining according to Heidenhain*

For a general overview the tissue sections were stained according to Heidenhain's protocol for Azan staining. In this staining the nuclei are stained red and collagen fibres in blue. Therefore, the tissue slides were deparaffinized in xylol (3 x 5 min) and rehydrated in a descending alcohol series (100 %, 96 %, 70 % (v/v) 5 min each step). After briefly washing with Aqua dest. the slides were submerged for 5 min in the aniline-alcohol utility solution. Tissue was then dyed for 10-15 min using the azocarmine utility solution which was preheated to 56°C accounting for the red staining. Following a quick wash with Aqua dest., the tissue was then differentiated with the aniline-alcohol utility solution under visual control. After another quick wash with Aqua dets. the tissue was mordanted for 2 h with 5 % (w/v) phosphotungstic acid. This step was necessary to fix the dye to the tissue. After another quick wash with Aqua dest., the slides were kept for 1-2 h in the aniline-orange utility solution accounting for the blue staining. After a last quick wash in Aqua dest. the tissue was differentiated and dehydrated in isopropanol and 96 % (v/v) ethanol under visual control in a brightfield microscope, followed by clearing the slides in xylol (3x5 min each step). Finally, the slides were conserved under a cover slip using the quick hardening mounting medium Eukitt® and left to dry at room temperature in an air flow chamber.

#### *3.2.5.3 Immunofluorescence*

##### Immunofluorescence with Paraffin Tissue Sections

Deparaffinized and rehydrated tissue sections (chapter **3.2.5.1**) were incubated for 1 h at room temperature in 2% (v/v) normal goat serum in PBS solution (pH 7,4) to prevent non-specific binding of the primary antibodies. Indirect immunostaining was performed by a two-step approach. Primary antibodies (Table 3) were adjusted to the respective concentrations in dilution buffer and tissue sections were incubated at 4°C overnight. For negative controls the primary antibodies were omitted. Following two washing steps with PBS (10 min each step), the sections were incubated with the secondary antibodies (Table 4) diluted to the respective concentrations in PBS for 1 h at room temperature in darkness. Nuclear staining was performed using DAPI at a dilution of 1:1250 in PBS together with the secondary antibodies. Stained tissue sections were rinsed twice with PBS and fixated using 4% (w/v) PFA at a pH 7,2-7,4. After two final washing steps with PBS (10 min each step) the stained tissue sections were covered with glycerol and a cover slip and stored at 4°C in darkness till the images were captured. Fluorescence was observed and captured using a fluorescence microscope Axioskop 2 plus with the Axiovision LE software.

##### Immunofluorescence with Cells

Cultured SMCs (Pa1, after extraction) were fixated for 10 min with 4% (w/v) PFA and washed 3 x 10 min with PBS while gently shaking. PBS was also used for the storage of fixated cells at 4°C in the dark until staining. Cells were permeabilised with 0.1% (v/v) Triton in PBS for 10 min. Indirect immunostaining was performed by a two-step approach. To avoid non-specific binding of the antibodies, permeabilised SMCs were blocked for 1 h at room temperature with 2% (v/v) normal goat serum in PBS. Primary antibodies (Table 3) in dilution buffer were applied overnight at 4°C in darkness. For negative controls the primary antibodies were omitted. After washing twice for 10 min with PBS, the secondary antibodies (Table 4) carrying the fluorescent tags Cy3 (excitation peak at 555nm, dark orange in the visible spectrum) and Alexa 488 (excitation peak at 488 nm, green in the visible spectrum) diluted in PBS were applied for 1 h at room temperature in darkness. Nuclear staining was performed together with the secondary antibodies using DAPI at a dilution of 1:1250 in PBS. The slides were washed twice with PBS (10 min each step) and fixated with 4% PFA for 10 min at room temperature and two subsequent PBS washing steps before preservation in glycerol and covering with a cover slip. Slides were stored at 4°C in the dark until image capture. Fluorescence was observed and captured using a fluorescence microscope Axioskop 2 plus with the Axiovision LE software.

### 3.2.6 Statistics

For the statistics of the first part of this thesis (vasculature), GraphPad Prism versions 9.5.1 (733), 10.2.2 (397) and 10.4.0 (627) for Windows (GraphPad Software, La Jolla, CA, USA, www.graphpad.com) were used for data analysis and display. All vascular data was pre-checked for normal distribution and analysed according to non-normal distribution methods.

For the statistics of the second part of this thesis (seminiferous tubules), GraphPad Prism versions 9.5.1 (733) and 10.4.0 (627), as well as the latest version of Excel® for Microsoft 365 MSO (Version 2501 Build 16.0.18429.20132) were used for data analysis and display.

A detailed description of all relevant analysis is given in the respective figure legends. The n-number, either indicated in each figure or corresponding figure legend, always refers to the number of biological replicates (number of animals). Significances (p-values) are either indicated as asterisks and described in the respective legends or indicated as numeric values in the figures themselves, while ns indicates non-significant p-values. Apart from the cumulative frequency distribution of the ST contraction analysis, which displays the standard deviation as standard error of the mean (SEM), all the other results display standard deviations as classic SD.

# 4 Results

## 4.1 Aortic smooth muscle cells

It is commonly accepted that cultured vascular SMCs do not reproduce the physiological circumstances of SMCs within the intact blood vessel wall (Chamley-Campbell et al., 1979; Frismantiene et al., 2018; Huber & Badylak, 2012; Worth et al., 2001). However, research still often requires *in vitro* SMC culture, e.g. in cases of drug testing (Karbassi et al., 2020; Rameshrad et al., 2016). The main goal of Chapter 1, focussing on vasculature, was therefore to provide the direct comparison of vascular SMCs in intact aortic tissue and in primary cell culture to estimate the change in expression of genes that are essentially involved in cGMP regulation. The identification of an appropriate reference gene (RG) (Kozera & Rapacz, 2013) was the crucial first hurdle. The following chapters summarize the results of the undertaken RG verification process the outcome of the subsequent comparison of GC-A, GC-B, NPRC, and sGC in intact aorta versus cultured aortic SMCs at the gene expression and of GC-A and GC-B at the functional level.

### 4.1.1 Characterization of cultured aortic smooth muscle cells

#### *4.1.1.1 Manual preparation of tunica media and verification by Azan staining*

The thick SMC-containing *tunica media* accounts for the majority of cellular components in the aortic wall (see **Figure 11**) (Davis & Hill, 1999; Dinardo et al., 2014; Tykocki et al., 2017). However, because the SMCs are tightly wrapped in a multidimensional net of elastic fibres (Lannoy et al., 2014) the extraction and singularization of these cells makes the mechanical as well as enzymatic digestion of the physiological cell association necessary (Chi et al., 2017; Sun et al., 2021). In efforts to isolate the aortic SMCs exclusively the outer connective tissue layer, accommodating mainly fibroblasts, was removed mechanically after an initial incubation with collagenase. Azan staining was performed before (**Figure 26 A**) and after (**Figure 26 B**) the initial enzymatic digestion to check for remaining connective tissue. The staining confirmed the accuracy of the manual preparation by the absence of the *tunica adventitia* (**Figure 26 B**). The thin *tunica intima*, which is basically a monolayer of endothelial cells in rats (Kobayashi et al., 1992), was removed by gently brushing over the inner surface of the longitudinally opened aortic tube using sterile tweezers.

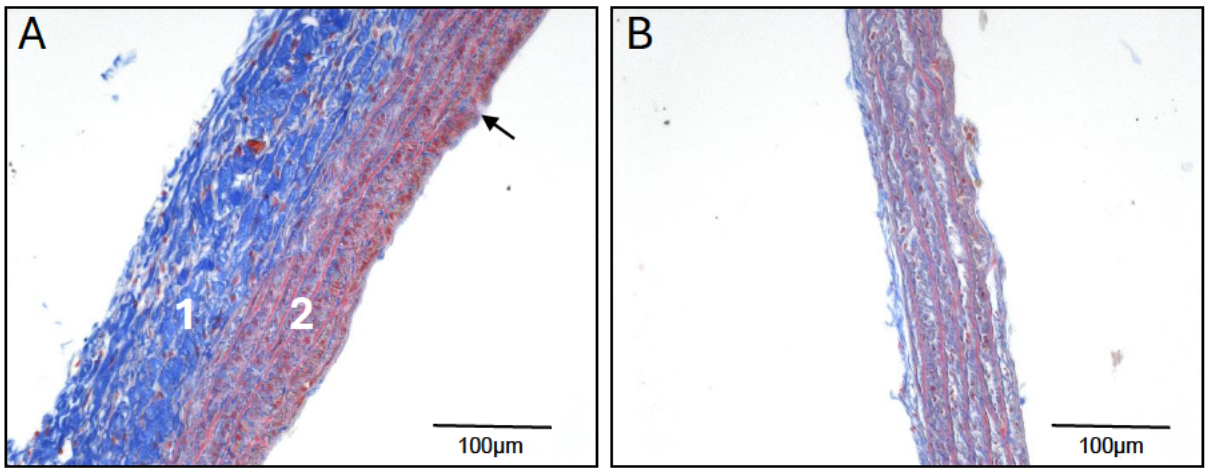


**Figure 26:** Azan staining of paraffin-embedded cross sections of rat aorta.
(**A**) before collagenase digestion with an intact *tunica adventitia* (**1**) and *tunica media* (**2**) and remaining endothelial cells (**arrow**), and (**B**) after manual removal of the adventitia and intima following the 15 min digestion with collagenase.

#### *4.1.1.2 Confirmation of SMC character of isolated and cultured primary rat cells by immunostainings*

After the subsequent steps for extraction and cultivation to obtain an aortic SMC culture (see chapter **3.2.2.1**) the homogeneity of the cell population was investigated by immunostainings for relevant SMC, endothelial and fibroblast markers (**Figure 27**). The *tunica media* of the intact aorta showed a homogeneous positive staining for classic SMC markers SMA (**Figure 27 A**) and calponin (**Figure 27 B**). The *vasa vasorum* in the *tunica adventitia* served as an internal positive control for the SMC markers and were found to express SMA (**Figure 27 A**). The smooth muscle character of the extracted primary cells was confirmed by the expression of SMA and calponin (**Figure 27 D**). Even though the majority of cells were found to be positive for both markers, a few cells seemed to lack calponin expression (el-Mezgueldi, 1996; Winder & Walsh, 1993). This suggests a less contractile stage of these SMCs as perhaps the result of a shift towards a more synthetic phenotype (briefly touched on in chapter **1.1**). The presence of an intact *tunica intima* was confirmed by a positive staining for eNOS in IF (**Figure 27 B**) and DAB staining (**Figure 27 C**) alike. Again, the *vasa vasorum* served as an internal positive control for the primary antibody staining (**Figure 27 A**). The absence of endothelial cells was confirmed by negative staining for the endothelial markers von Willebrand Factor (vWF) (**Figure 27 F**) and eNOS (**Figure 27 I**). Even though the absence of the connective tissue layer *tunica adventitia* was confirmed by azan staining (**Figure 26 B**) numerous cultured cells were found to express vimentin (**Figure 27 E, G**), a marker routinely used for (myo-)fibroblast identification (Ostrowska-Podhorodecka & McCulloch, 2021).

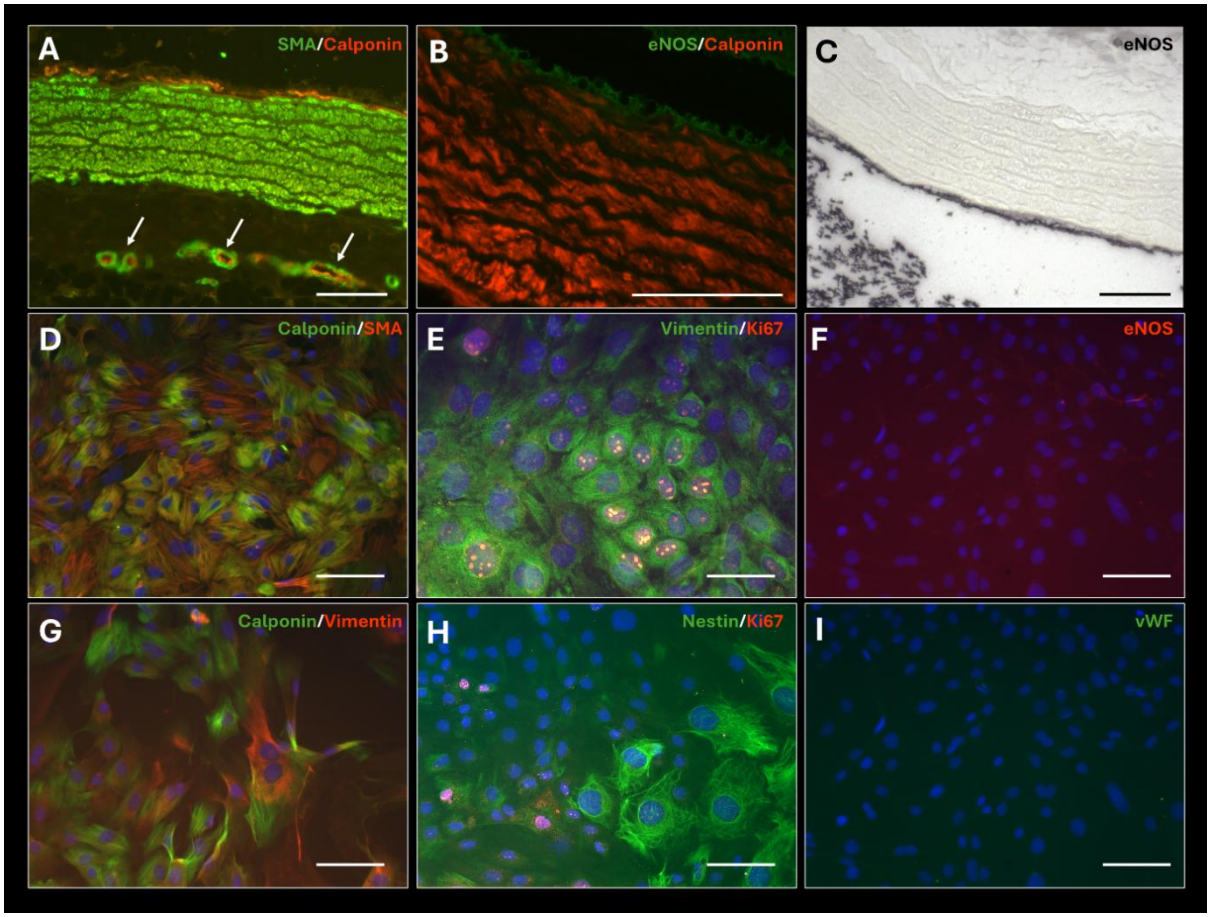


***Figure 27:*** *Immunostaining of intact rat aorta and primary rat aortic smooth muscle cells.*
Immunofluorescence (**A**, **B**) and 3,3-diaminobenzidine (DAB) staining (**C**) of cross sectioned paraffin-embedded rat aorta reveal a smooth muscle actin (SMA) (**A**, in green) and calponin (**B**, in red) positive *tunica media*. The intact *tunica intima* was found positive for endothelial nitric oxide synthase (eNOS) expression (**A**, in red; **B**, in green; **C**, in black). The *vasa vasorum* within the *tunica adventitia* (**arrows**) were found SMA (**A**, in green) and eNOS (**A**, in red) positive. Immunofluorescence staining of primary rat aortic cells (passages 2-3 after extraction) (**D-I**) revealed positive staining for smooth muscle cell markers SMA (**D**, in red) and calponin (**D** & **G**, in green). Most cells were positive for vimentin (**G**, in red; **E**, in green), but only a few cells were positive for the stem cell marker nestin (H, in green) or Ki67 (**E** & **H**, in red) a nuclear marker for proliferation. Nuclei of the cells were stained with DAPI in blue. The scale bar equals 100 µm.

Some cells showed a nuclear staining for Ki67 (**Figure 27 E, H**) suggesting proliferative activity (Tang et al., 2012). Additionally, a few cells showed a positive staining of the neuronal stem cell marker nestin (Saboor et al., 2016; Tang et al., 2012) (**Figure 27 H**). However, it seemed like the expression of nestin and Ki67 did not overlap in most cells.

### 4.1.2 Identification of U2 as suitable reference gene for direct comparison of gene expression of rat smooth muscle cells in intact aortic *tunica media* and in culture

#### *4.1.2.1 Expression of routinely used reference genes showed significant difference in expression due to SMC isolation and culture*

As initial step to identify a reliable RG for the direct comparison of cultured aortic SMCs and their tissue of origin, the expression of the routinely used RGs Actb and Gapdh was measured (**Figure 28**). The stability of their expression throughout the extraction process was estimated by a pairwise comparison between the mRNA levels of the intact *tunica media* and the corresponding primary SMCs derived from the exact same vessel. The reason for choosing Actb and Gapdh was that they are both considered as classical housekeeping genes. The term housekeeping gene (HKG) was formerly used to distinguish a specific subgroup of RGs that stood out by constitutively stable expression in all cell types and therefore their expression was assumed to be essential for cell survival (Kozera & Rapacz, 2013). However, nowadays the designation HKG and RG are almost used interchangeably, although the term RG seems to be preferred by researchers performing expression analysis. Most likely this is due to the fact that all universal RGs are regulated to a certain extent and none of them are expressed ubiquitously (Bustin et al., 2005).

RT-qPCR was performed for the intact media and the corresponding cultured cells of 28 rats. The Ct values obtained, which inversely correlate to the level of gene expression (Bustin et al., 2005) of the intact *tunica media* significantly exceeded the Ct values of the cultured SMCs for both Actb (**Figure 28 A**) and Gapdh (**Figure 28 B**) by a factor of 10. The initial amount of the cDNA template is ideally duplicated with each PCR cycle hence the final amount of gene copies supposes to be $2^{10}$ (more than 1000) times higher in cultured SMCs. In addition to the significant difference between cultured cells and tissue, an impressive variance of the RG expression levels between the tissue samples only, was notable. In contrast to that, the expression of the cultured cells of different rats was found to be extremely stable. Nevertheless, both Actb and Gapdh, depending on the question of an expression study may be suitable for the comparison of tissue or cell samples from different animals, but most likely unsuitable for their direct comparison.

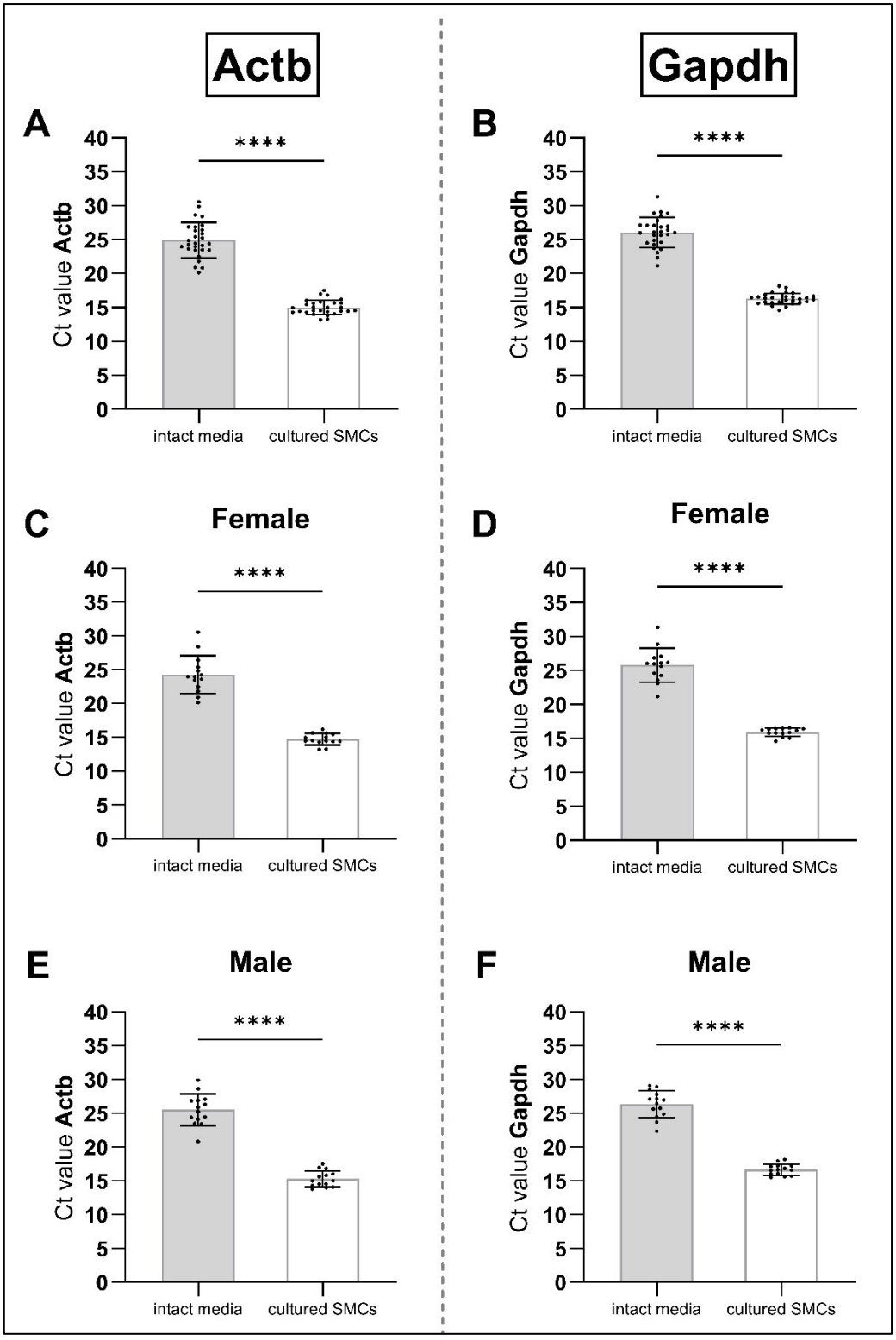


***Figure 28:*** *Comparison of classical reference gene expression in intact media and corresponding cultured smooth muscle cells of rat aorta*.
Comparison of the cycle threshold (Ct) values of beta-actin (Actb, left column) and glyceraldehyde-3-phosphate-dehydrogenase (Gapdh, right column) in intact aortic *tunica media* (grey bars) and corresponding cultured smooth muscle cells (SMCs, white bars). Ct values of the total cohort (male and female combined) of both, (**A**) Actb and (**B**) Gapdh were significantly higher ($p < 0.0001$, indicated by ****), in intact media compared to cultured SMCs (paired two-tailed Student's t-test; n = 28). The same result was found when comparing the expression of (**C**, **E**) Actb and (**D**, **F**) Gapdh in (**C**, **D**) female and (**E**, **F**) male rats separately (each n = 14). The whiskers indicate ± SD.

#### *4.1.2.2 SMC extraction and cultivation affect expression of classical housekeeping genes independently of the sex*

Biological sex has not been considered as a relevant variable in research studies for too long. The concern that variable hormonal changes, especially in females (due to different stages in their hormone cycle) may induce a broader variance of study results is a common argument of scientists not to involve females in their studies. The study cohort contained an equal number of both sexes because it was an intention to not only enable the direct comparison between aortic cells and tissue but also between male and female subjects for future expression analysis (chapter **4.1.5**). When analysing the gene expression of Actb and Gapdh for female (**Figure 28 C, D**) and male rats (**Figure 28 E, F**) separately the difference between intact tissue and cultured cells remained significant with a range similar to the total study cohort (**Figure 28 A, B**). Hence, the increase in RG expression in cultured aortic SMCs was found to be independent of the sex.

#### *4.1.2.3 Literature review reveals preliminary selection of potential reference gene candidates*

Despite an increase in research output on gene expression analyses and RG definition, hardly any of these studies (e.g., Benak et al., 2019; Taki et al., 2014 from Table 15 below) attempt the search for RGs to enable the direct comparison of cultured cells and their tissue of origin. Databases like RefFinder (Xie et al., 2023) provide a comprehensive overview of relevant RGs for different species and therefore can be a powerful tool during the search for suitable RGs. A disadvantage of these databases is, however, that in most cases the gene expression is listed for a specific organ/tissue whether the Ct values were captured *in vivo*, *ex vivo* or *in vitro* for intact tissues or cultured cells is usually not recorded. At the same time, this is also evidence that the direct comparison of gene expression of cultured cells and their original tissue is scarcely addressed by researchers. In total 15 RGs were selected (**Table 15**) based on literature research according to predetermined criteria. Gene expression studies were considered when rat was the chosen animal model, and expression was compared in either tissue or cells before and after drug administration and/or any kind of surgical intervention (Benak et al., 2019; El Mourabit et al., 2016; Faibish et al., 2016; Kloss et al., 2003). For all 15 RGs chosen the Ct values were determined for the aortic tissue and corresponding cells of 4 male and 4 female rats. In some cases, multiple primer sets for the same gene were tested. The absolute value of the difference between the average Ct for tissue and corresponding cells served as a preliminary measure of the stability of gene expression. A smaller difference indicated higher stability over the course of cell isolation and culturing, which was a prerequisite for an RG. The average Ct difference between tissue and cells of all genes tested was approximately 4.5. Two third of the genes tested showed a difference of at least 4.

***Table 15:*** *Preselection of 15 potential reference genes.*
The difference of the cycle threshold (Ct) values (intact aortic media - corresponding cultured smooth muscle cells (SMCs)) served as indicator for reference gene (RG) stability. 8 animals were analysed (male and female, each n=4) per gene. The heat scale ranks the difference values from higher (dark red) to lower (dark green) cycle threshold (Ct) value difference (Benak et al., 2019; Taki et al., 2014).

| Gene | Gene group | Primer | $\lvert Ct_{\text{intact media}} - Ct_{\text{cultured SMCs}} \rvert$ | | |
|---|---|---|---|---|---|
| | | | Total | Male | Female |
| Hypoxanthine phosphoribosyl transferase 1 | nucleotide synthesis | Hprt1_4 | 6.45 | 4.51 | 8.40 |
| | | Hprt1_B | 5.16 | 4.48 | 5.84 |
| Nucleoporin like 2 | protein export from nucleus | Nupl2_B | 6.29 | 7.48 | 5.48 |
| Tankyrase | protein stability and interaction | Tnks_T | 7.42 | 7.30 | 7.55 |
| | | Tnks_1 | 6.37 | 5.81 | 6.92 |
| TATA box binding protein | transcription | Tbp_T | 6.19 | 6.17 | 6.20 |
| Ribosomal protein L30 | protein synthesis | Rpl30_3 | 6.51 | 6.35 | 6.67 |
| | | Rpl30_1 | 5.55 | 5.78 | 5.83 |
| Ribosomal protein L32 | | Rpl32_4 | 4.77 | 4.69 | 4.84 |
| | | Rpl32_1 | 3.78 | 2.56 | 5.00 |
| Actin alpha 2, smooth muscle | cell structure and motility | Acta2_2 | 4.53 | 4.43 | 4.64 |
| | | Acta2_3 | 3.66 | 2.90 | 4.41 |
| Beta-2-microglobulin | serum protein | B2m_9 | 4.28 | 4.19 | 4.37 |
| | | B2m_T | 3.75 | 3.40 | 4.10 |
| Eukaryotic translation elongation factor 1 alpha 1 | translation | Eef1a1_T | 4.25 | 4.08 | 4.42 |
| Eukaryotic translation elongation factor 2 | | Eef2_1 | 4.60 | 4.04 | 5.16 |
| | | Eef2_2 | 4.58 | 4.39 | 4.76 |
| DNA topoisomerase 1 | DNA topology during transcription | Top1_B | 5.42 | 5.45 | 5.79 |
| | | Top1_1 | 3.66 | 3.49 | 3.84 |
| small nucleolar RNA, C/D box 87 | methylation of pre-ribosomal RNA precursors | Snord87_T | 2.92 | 3.22 | 2.66 |
| 5S ribosomal RNA | ribosomal RNAs | 5SrRNA_T | 2.37 | 2.07 | 2.33 |
| Small nuclear RNA U5A | splicing | U5A_T | 0.99 | 0.58 | 1.11 |
| Small nuclear RNA U2 | | U2_T | 0.31 | 0.39 | 0.23 |

#### *4.1.2.4 U2 expression is unaffected by SMC isolation and culture in males and females*

According to the initial evaluation the group of small nuclear ribonucleoproteins (snRNPs aka., "snurps") were found to show the most stable gene expression. The snRNPs are found in the splicing speckles and Cajal bodies of the eukaryotic nucleus, where they contribute to the processing of pre-mRNAs (van der Feltz & Hoskins, 2019; Will & Lührmann, 2011). The representative U5A and U2 were both found to have the smallest absolute difference between the Cts of the tissue and corresponding cells (around 0.5 Ct) in both male and female rats (**Table 15**). It can therefore be assumed that snRNPs are of similar importance in vascular SMCs in culture and intact aortic media, which, as mentioned earlier, is a crucial prerequisite for our RG. To confirm this observation more reliably, the absolute Ct values of U5A and U2 were determined again for a larger group of rats (n=14, **Figure 29**).

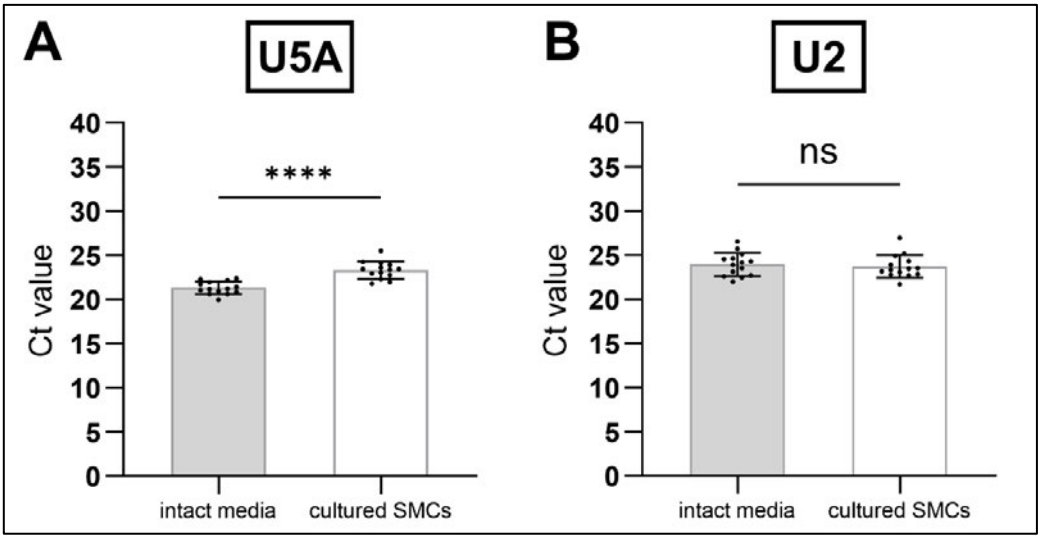


***Figure 29:*** *Comparison of small nuclear ribonucleoproteins expression in intact media and corresponding cultured smooth muscle cells of rat aorta.*
Comparison of the absolute cycle threshold (Ct) values of (**A**) U5A and (**B**) U2 in intact aortic media (grey bars, n = 14) and the corresponding cultured smooth muscle cells (SMCs, white bars, n = 14). The comparison was performed by paired two-tailed Student's t-test. Differences were considered significant when $p < 0.0001$, indicated by **** and non-significant (ns) when $p > 0.05$. The whiskers indicate ±SD.

In contrast to the initial results (**Table 15**) the direct comparison between the Ct values of tissue and cells for the U5A expression of the entire cohort was found to be significant (**Figure 29 A**) with a difference of approximately 2 Ct. For the second snRNP candidate U2, however, the statistical analysis of the larger sample size (n=14) did not reveal a significant difference between tissue and cells of the same aortae (**Figure 29 B**). U2 therefore, was classified as a suitable RG for the direct comparison of intact aortic *tunica media* versus the isolated and cultured SMCs.

When taking the second parameter, the biological sex, into account no significant difference in gene expression neither in intact tissue nor in cells between male and female rats (n=7, each) was detected for U5A and U2 (**Figure 30**). This suggests that both are eligible to serve as RGs for the comparison between male and female samples of either intact media or of cultured aortic SMCs. When comparing male and female rats regarding the expression of U5A (**Figure 30 C**) and U2 (**Figure 30 D**) in samples from intact tissue versus the corresponding cultured aortic SMCs, U5A was expressed significantly higher in the intact tissue (indicated by a lower Ct mean value) than in cells. U2 expression showed no significant difference. This was found for both sexes and confirmed the earlier observations for the entire study cohort (**Figure 26**).

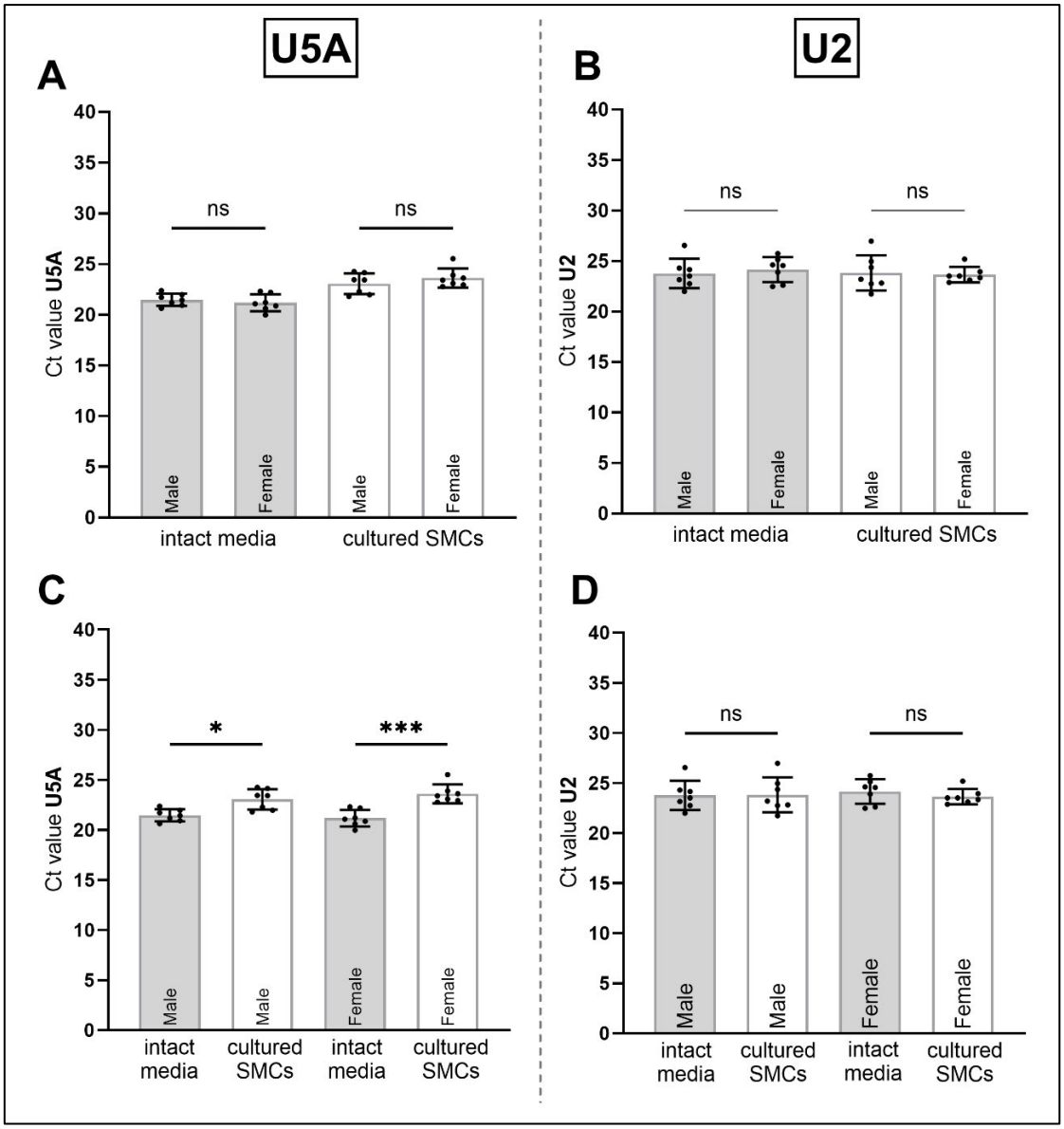


***Figure 30:*** *Sex-dependent comparison of small nuclear ribonucleoproteins expression in intact media and corresponding cultured smooth muscle cells.*
(**A**), (**C**) Comparison of absolute cycle threshold (Ct) values of U5A and (**B**), (**D**) U2 in the intact aortic media (grey bars) and the corresponding cultured smooth muscle cells (SMCs, white bars) of male (n = 7) and female (n = 7) rats (Tukey's multiple comparisons test). Only relevant comparisons are displayed. Significant differences are indicated as $p \leq 0.05$ *, $p < 0.001$ ***, or ns. The whiskers indicate ±SD.

### 4.1.3 Revelation of significant changes in gene expression of the NP and NO receptors in aortic smooth muscle cells upon isolation and culturing

Even though it is known that cultured vascular SMCs reflect physiological circumstances to a limited extent (Chamley-Campbell et al., 1979), cell culture remains one of the first experimental steps for investigating intracellular signalling or for preclinical studies (Malorni et al., 2008).

While the importance of vascular SMCs for the regulation of the blood flow in resistance arteries is widely accepted their relevance in elastic arteries, like the aorta, remains underestimated (Carvajal et al., 2000; Jaminon et al., 2019). The cGMP signalling system is one of the most relevant smooth muscle relaxing pathways (Hofmann, 2020; Krawutschke et al., 2015). Earlier studies by Suga and colleagues (Suga, Nakao, Kishimoto, et al., 1992; Suga, Nakao, Mukoyama, et al., 1992) indicated that the NP/cGMP signalling pathway in aortic SMCs is affected by isolation and culturing of these cells due to phenotypic transitions (Huber & Badylak, 2012; Lehners et al., 2018; Lincoln et al., 2006). However, their methodological approach did not allow them to make an exact quantitative evaluation of the transcription level. Using the previously verified RG U2 for the direct comparison of the mRNA level in SMCs of intact aortic media and cultured aortic SMCs (Rager et al., 2023), the second part of the vascular chapter of this thesis aims to provide a detailed overview of transcriptional and functional alterations of key receptors of the cGMP system induced by mere SMC isolation and culturing (Rager et al., 2025).

#### *4.1.3.1 Culturing aortic SMCs dramatically changes Gc-b, sGC, and Nprc expression but not of Gc-a expression in comparison to the intact tunica media*

For this study the expression level of the cGMP -generating Gc-a and Gc-b, as well as the NP clearing receptor Nprc was measured in intact aortic media and cultured SMCs from the same rat aortae. As an additional prominent source of cGMP, the intracellular NO receptor sGC was included in these RT-qPCR investigations. Gc-a expression was found to significantly exceed Gc-b and Nprc which both showed the lowest expression in intact media (**Figure 31 A**).

sGC was significantly higher expressed than Gc-b and Nprc and appeared to show a slightly lower expression compared to Gc-a although no significant difference was detectable (**Figure 31 A**).

In the isolated and cultured aortic SMCs of the exact same animals (**Figure 31 B**), Gc-a showed the lowest of all the receptor expressions, whilst in contrast Nprc showed the highest. Nprc even significantly exceeded Gc-b at mRNA level. The sGC expression also increased significantly and was now higher than Gc-a and in an expression range comparable to Gc-b and Nprc.

One of Suga's earlier findings suggested that Gc-a is barely expressed in cultured aortic SMCs in comparison to intact rat aortic tissue (Suga, Nakao, Mukoyama, et al., 1992). When performing

the direct comparison between the expression in tissue and cells (**Figure 31 C-F**), enabled by the previously identified RG U2, Gc-a expression was found to be nearly unchanged (**Figure 31 B**). In contrast, the expression of Gc-b and Nprc (**Figure 31 D, E**), respectively, showed a drastic increase under culturing conditions.

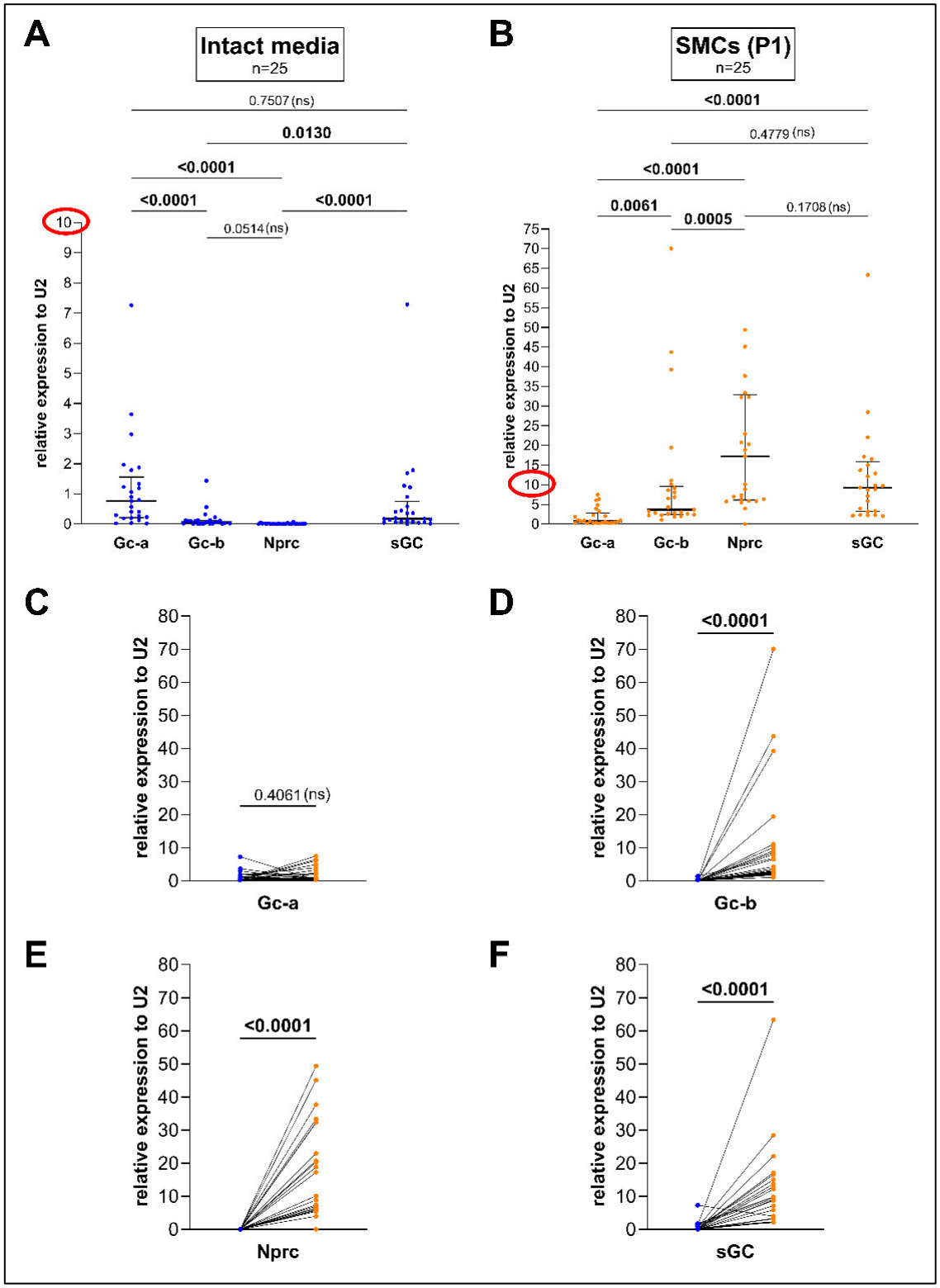


*Figure 31 continues following page.*

***Figure 31:*** *Relative gene expression analyses of the natriuretic peptide (NP)/cyclic guanosine monophosphate (cGMP) pathway components in the intact media and corresponding cultured smooth muscle cells (SMCs) of the rat aortae.* The gene expression levels of guanylyl cyclase A (Gc-a) and -B (Gc-b), natriuretic peptide clearance receptor (Nprc), and soluble guanylyl cyclase (sGC) in the (**A**) intact media (blue dots) and (**B**) corresponding cultured aortic SMCs of the first culture passage after extraction (P1) (orange dots). Please note the different scales of the y-axis in both graphs highlighted by the red circles. Differences in (**A**, **B**) were analysed by non-parametric Friedman test with Dunn's correction for multiple comparisons of paired measurements. Individual values are depicted for each gene. The median is indicated by a thick line while whiskers indicate the interquartile range. Direct comparisons between intact media (blue dots) and corresponding cells (orange dots) of each individuum are visualized by connecting lines (**C**–**F**). Individual data points visualize the dispersion and the slope of each line and the amount of change in gene expression for each individual gene. Differences were analysed using a non-parametric Wilcoxon matched-pairs signed rank test. All data were normalized to small nuclear ribonucleoprotein U2 according to the ΔCt method for relative expression analysis. The total cohort (n = 25) consists of male (n = 13) and female (n = 12) rats. Numeric p-values are given for each comparison, while significant differences are highlighted in bold and non-significant values are indicated with (ns).

The same was the case for sGC (**Figure 31 F**). Besides the drastic increase (depicted by the slope of the connecting line between each data pair), the spread between the Gc-b, Nprc, and sGC expression of the analysed cells should be highlighted. Regarding the ANP and CNP receptor, it is worth emphasizing the outcome of the direct comparison between intact media and retrieved primary cells, that the physiological ratio between Gc-a and Gc-b, at least at the transcriptional level seems to be reversed in cell culture.

#### *4.1.3.2 Comparison between Gc-a, Gc-b, Nprc, and sGC expression reveals differences in males and in females separately but no differences could be detected between both sexes*

In the previous section (chapter **4.1.3.1, Figure 31**), the RT-qPCR results were described without taking the biological sex into account. This study, however, contained an equal number of male and female rats to compare both sexes. The reduction of the n-number of the total mixed cohort in the male and female subgroups resulted in a reduction in statistical power causing a lack of significance of differences in expression, which were found to be significant beforehand in the total cohort. Hence, the sex-specific results are described in an explorative manner to generate new hypotheses.

When separating the male and female animals (**Figures 32 A-D**), both cohorts mirrored the gene expression profile of the total cohort (**Figure 31 A & B**). While a significant difference between the expression of Gc-b and sGC could be detected in intact media of the total cohort (**Figure 31 A**), this difference was abolished when analysing the male (**Figure 32 A**) and female (**Figure 32 B**) tissue separately. As mentioned earlier, however, it cannot be excluded that the difference between the sexes escaped detection due to a reduced n-number of the male (n = 13) and female (n = 12) animals.

In the corresponding isolated and cultured aortic SMCs, the difference between the expression of Gc-b and Nprc was found to be significant for the cells extracted from female aortae (**Figure 32 D**) but not for the cells from male aortae (**Figure 32 C**). It is most likely the spread of the female

expression values that accounts for a higher average value of the Nprc expression in cells of the total cohort and therefore produces a significant difference between Nprc and sGC expression of the total group (**Figure 31 B**).

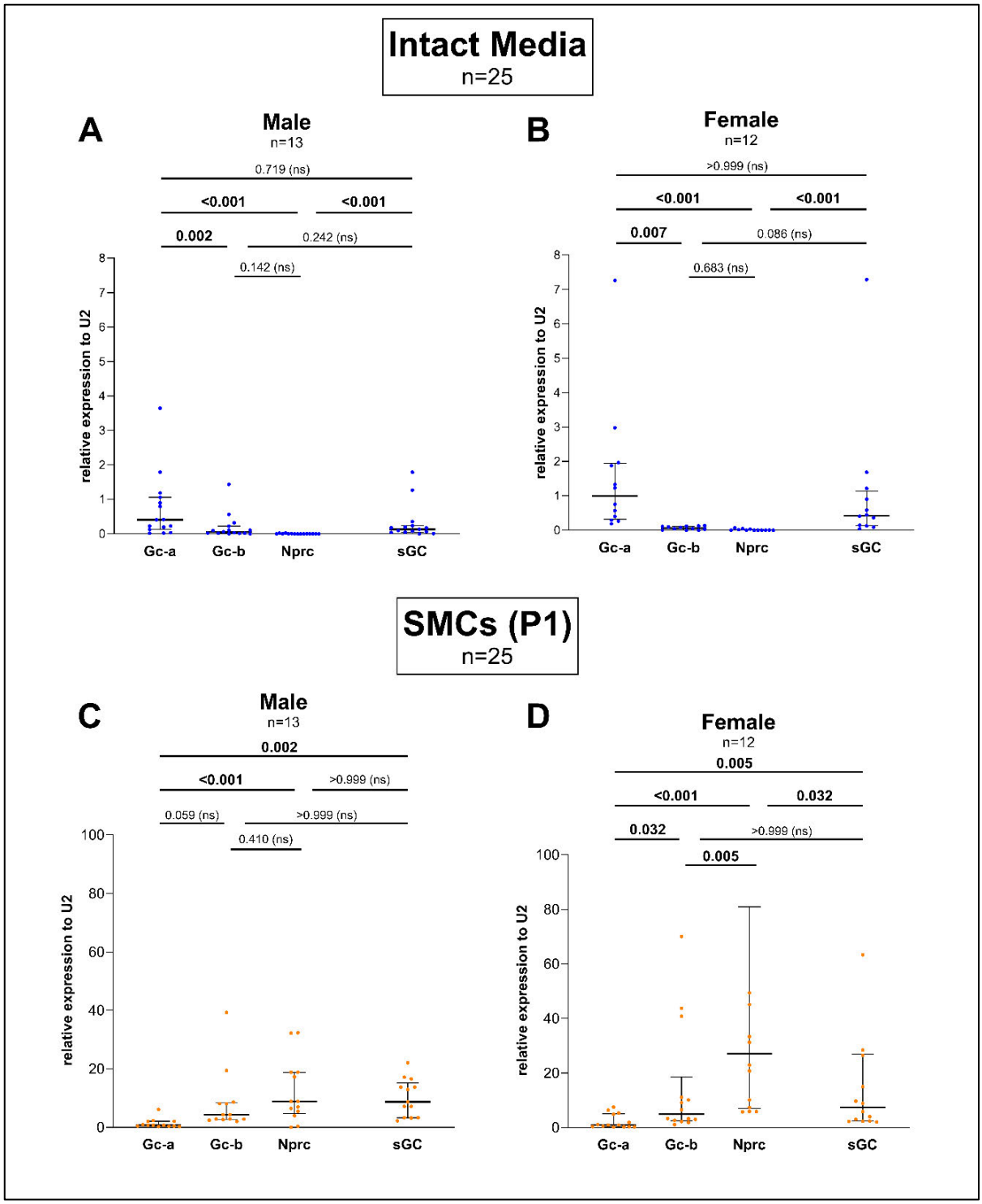


*Figure 32 continues the following page.*

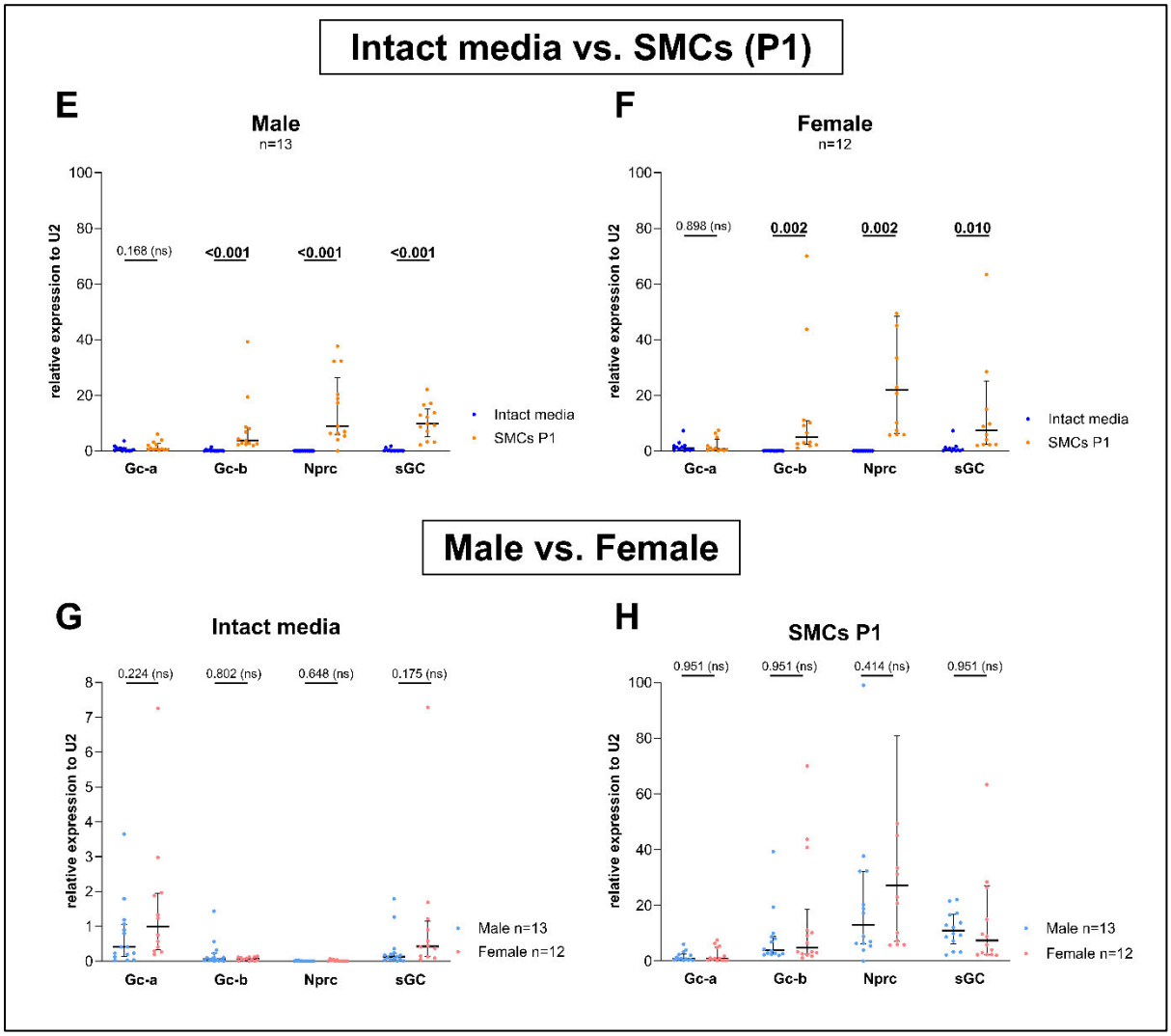


***Figure 32:*** *Sex-dependent gene expression analyses of the natriuretic peptide (NP)/cyclic guanosine monophosphate (cGMP) pathway components in the intact media and corresponding cultured smooth muscle cells (SMCs) of the rat aortae.*
The expression levels of guanylyl cyclase A (Gc-a) and -B (Gc-b), natriuretic peptide clearance receptor (Nprc), and soluble guanylyl cyclase (sGC) in the intact media (blue dots) and corresponding cultured aortic SMCs (orange dots) of the first culture passage after extraction (P1) were normalized to small nuclear ribonucleoprotein U2 according to the ΔCt method for relative gene expression analysis. Differences in the expression of the genes studied in the intact media of (**A**) male (n = 13) and (**B**) female (n = 12) rats and the corresponding SMCs of the same (**C**) male and (**D**) female rats were analysed by non-parametric Friedman test with Dunn's correction for multiple comparisons of paired values. Pairwise comparison of the relative gene expression levels between the intact media and corresponding cultured SMCs of (**E**) male and (**F**) female rat aortae was performed by non-parametric Wilcoxon's t-test with Holm–Sidak correction for multiple comparisons of paired measurements. The comparison of expression levels in the (**G**) intact media and (**H**) cultured SMCs between the male (light blue dots) and female rats (pink dots) was performed by a non-parametric Mann–Whitney test with Holm–Sidak correction for multiple comparisons of unpaired measurements. Individual values are depicted for each gene. The median is indicated by a thick line while whiskers indicate the interquartile range. Numeric p-values are given for each comparison while significant differences are highlighted in bold and non-significant values are indicated with (ns).

When comparing the intact media with the corresponding cultured SMCs for both sexes separately, significant differences were found for the expression of Gc-b, sGC and Nprc, but not for Gc-a (**Figure 32 E, F**). Thus, not only the expression profile of the male and female group was

similar to the expression profile of the total cohort (**Figure 32 A, B**) but also the detected differences between the genes under investigation remained the same.

When directly comparing the gene expression levels between both sexes the statistical analysis did not reveal any significant differences neither in the intact media (**Figure 32 G**) nor in the cultured SMCs (**Figure 32 H**).

### 4.1.4 cGMP production by the GC-A ligand ANP and by the GC-B ligand CNP in cultured SMCs differed in higher passages in comparison to the intact media but not within early passages

The focus of this thesis remained the NP-regulated axis of the cGMP signalling system and its alteration in vascular SMCs induced by their isolation and culturing. Since the changes in the transcriptional status were thoroughly investigated by RT-qPCR the second part of this specific study aimed to characterize changes at functional level of GC-A and GC-B.

The chosen method to evaluate changes in protein activity due to cell culture was a competitive ELISA (chapter **3.2.3.2**). This ELISA allows a very precise measurement of the cGMP level released upon NP-treatment of the aortic tissue and extracted cells. Hence, the readout of the ELISA indirectly confirms the presence of GC-A and GC-B and, in addition, allows an estimation of their enzyme activity (chapter **1.2.2.3, Figure 9**).

In the intact media the cGMP levels released in response to ANP and CNP significantly differed in the total cohort (**Figure 33 A**) and in the male group (**Figure 33 B**). In both cases ANP had a significantly higher effect than CNP, yielded a significantly higher cGMP release from the tissue. In female tissue, however, no significant difference was found in the cGMP production upon ANP and CNP treatment (**Figure 33 C**). When comparing the $Delta_{cGMP}$(ANP-CNP) between males and females (**Figure 33 D**), no significant difference could be detected either.

When comparing male and female rats with regards to their ANP- (**Figure 33 E**) and CNP-induced (**Figure 33 F**) cGMP release, however, no significant difference was found in the intact *tunica media*.

The results of the ELISA measurement for intact tissue align with the gene expression levels of GC-A and GC-B in intact tunica media (**Figure 32 G**).

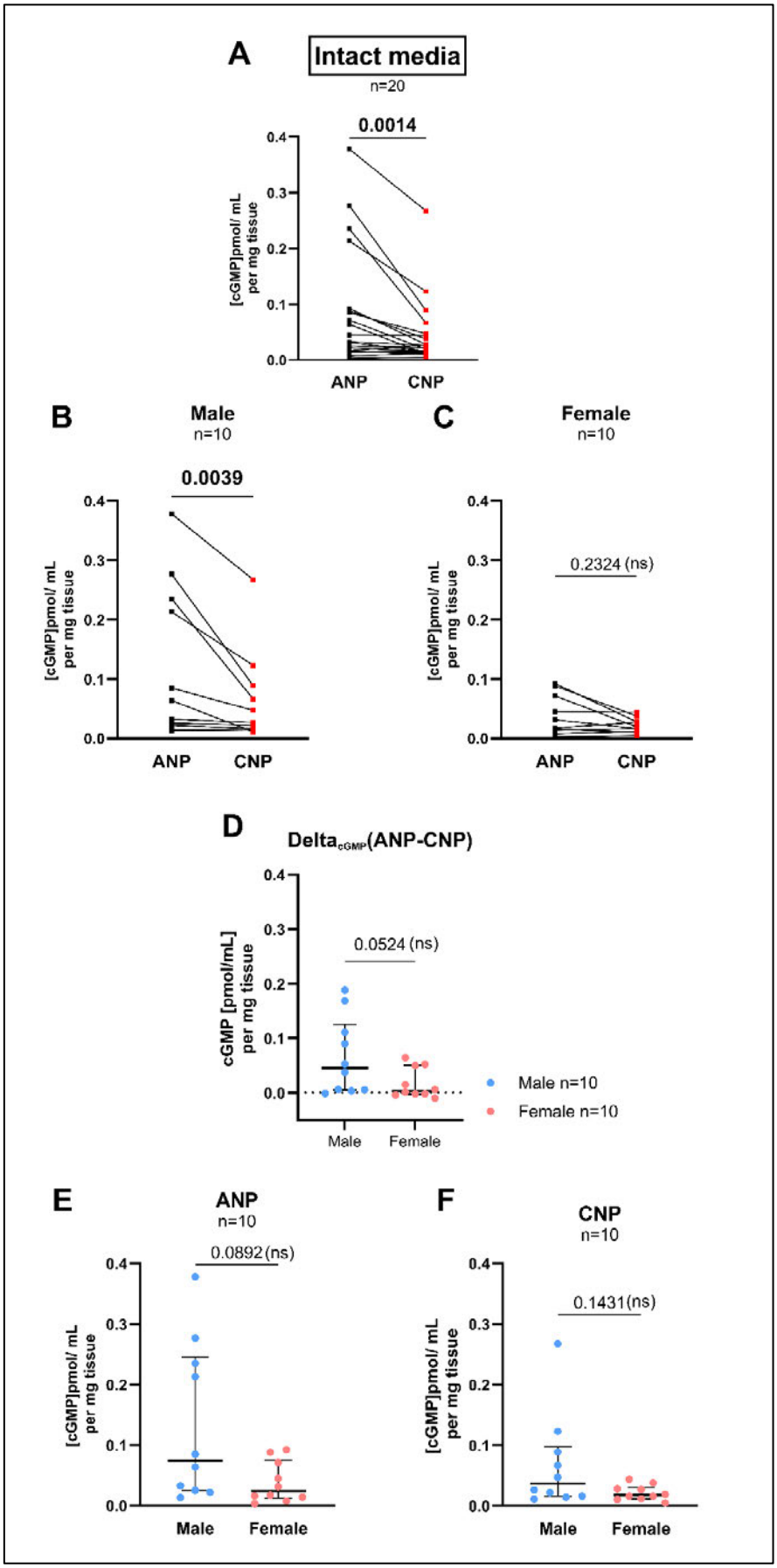


*Figure 33 continues following page.*

***Figure 33:*** *Measurement of cyclic guanosine monophosphate (cGMP) release by the intact media after the natriuretic peptide (NP) treatment.*
The cGMP concentrations of the sample supernatants, given in pmol/mL, were normalized to the weight (mg) of the aortic tissue samples. cGMP measurement followed a 30 min incubation time with either atrial natriuretic peptide (ANP) or C-type natriuretic peptide (CNP) at a concentration of 100 nm each. The basic cGMP level of the IBMX (phosphodiesterase inhibitor) control treatment was on average 0.51 pmol/mL per mg tissue. (**A**–**C**) Lines connect the single values for the ANP- (black) and CNP- (red) stimulated cGMP of the same individuum. Differences in the ANP- and CNP-induced cGMP release in (**A**) the total study cohort (n = 20), and (**B**) in the male (n = 10) and (**C**) female rats (n = 10) only were calculated by two-tailed non-parametric Wilcoxon's matched-pairs signed rank test. (**D**) To explore the influence of sex on the cGMP release, the difference between the ANP- and CNP-induced cGMP release was calculated as $Delta_{cGMP}$(ANP-CNP) and compared between the male (light blue dots) and female (pink dots) individuals by non-parametric Mann–Whitney test of unpaired measurements. Additionally, the (**E**) ANP- and (**F**) CNP-induced cGMP release between the male and female rats (n = 10 each) was calculated by the non-parametric Mann–Whitney test of unpaired measurements. Individual values are depicted for each gene. Median is indicated by a thick line while whiskers indicate the interquartile range. Numeric p-values are given for each comparison while significant differences are highlighted in bold and non-significant values are indicated with (ns). Due to the reduced n-number in the male and female groups compared to the total cohort, the resulting p-values should be interpreted in an explorative manner.

In addition, in the cultured SMCs (first passage after extraction), ANP-induced cGMP production was significantly higher than the cGMP levels after the CNP treatment (**Figure 34 A**). This was unexpected when recalling the inverse expression levels for Gc-a and Gc-b of exactly the same cells (Gc-a < Gc-b, see **Figure 31 B**). Surprisingly, this time, even the female cohort (**Figure 34 C**) showed a significantly higher cGMP production after the ANP treatment, and not only the total (**Figure 34 A**) and male groups (**Figure 34 B**), in contrast to the findings in intact media (see **Figure 33 A–C**). Again, no sex differences could be detected neither for the ANP-nor CNP-induced cGMP production (**Figure 33 D–F**).

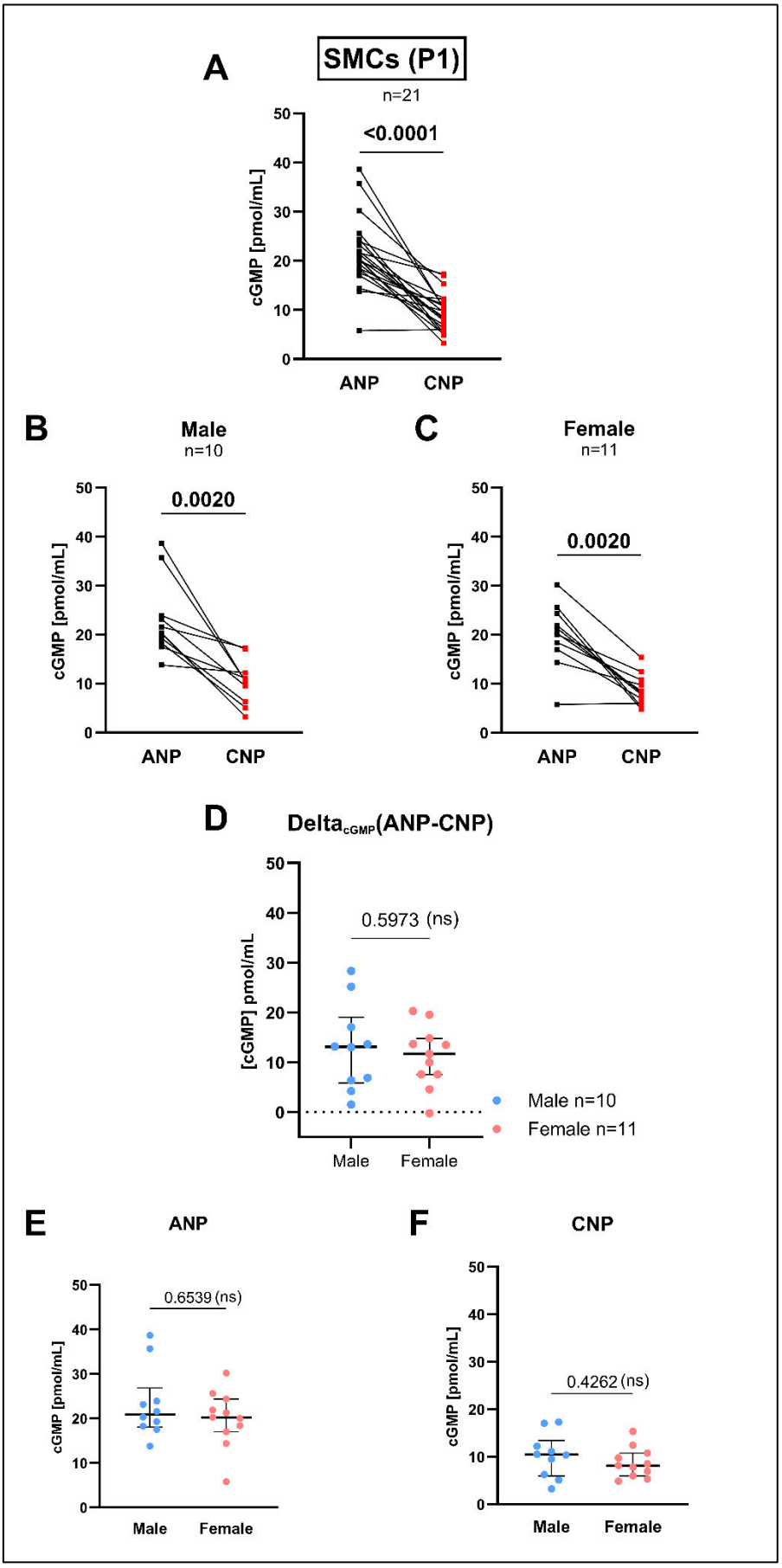


*Figure 34 continues following page.*

***Figure 34:*** *Measurement of cyclic guanosine monophosphate (cGMP) release after the natriuretic peptide (NP) treatment of the cultured aortic smooth muscle cells (SMCs) of the first passage after extraction (P1).*
The cGMP concentrations of the sample supernatants, given in pmol/mL. cGMP measurement, followed a 30 min incubation time with either atrial natriuretic peptide (ANP) or C-type natriuretic peptide (CNP) at a concentration of 100 nm each. The basic cGMP level of the IBMX (phosphodiesterase inhibitor) control treatment was on average 0.48 pmol/mL. (**A**–**C**) Lines connect the single values for the ANP- (black) and CNP- (red) stimulated cGMP of the cells extracted from the same individuum. Differences in the ANP- and CNP-induced cGMP release in (**A**) the total study cohort (n = 21), and (**B**) in the male (n = 10) and (**C**) female rats (n = 11) only were calculated by two-tailed non-parametric Wilcoxon's matched-pairs signed rank test. (**D**) To explore the influence of sex on the cGMP release, the difference between the ANP- and CNP-induced cGMP release was calculated as $Delta_{cGMP}$(ANP-CNP) and compared between the male (light blue dots) and female (pink dots) individuals by non-parametric Mann–Whitney test of unpaired measurements. Additionally, the (**E**) ANP- and (**F**) CNP-induced cGMP release between the male (n = 10) and female rats (n = 11) was calculated by non-parametric Mann–Whitney test of unpaired measurements. Individual values are depicted for each gene. The median is indicated by a thick line while whiskers indicate the interquartile range. Numeric p-values are given for each comparison while significant differences are highlighted in bold and non-significant differences are indicated with (ns). Due to the reduced n-number in the male and female groups compared to the total cohort, the resulting p-values should be interpreted in an explorative manner.

No significant difference in cGMP release in response to ANP or CNP could be detected in SMCs of the second passage after extraction (P2) (**Figure 35 A**). This was in contrast to the SMCs of the first passage after extraction (P1) where ANP induced a higher cGMP release (see **Figure 34 A**). However, the $Delta_{cGMP}$(ANP-CNP) was found to be significantly different when comparing P1 with P2 (**Figure 35 B**).

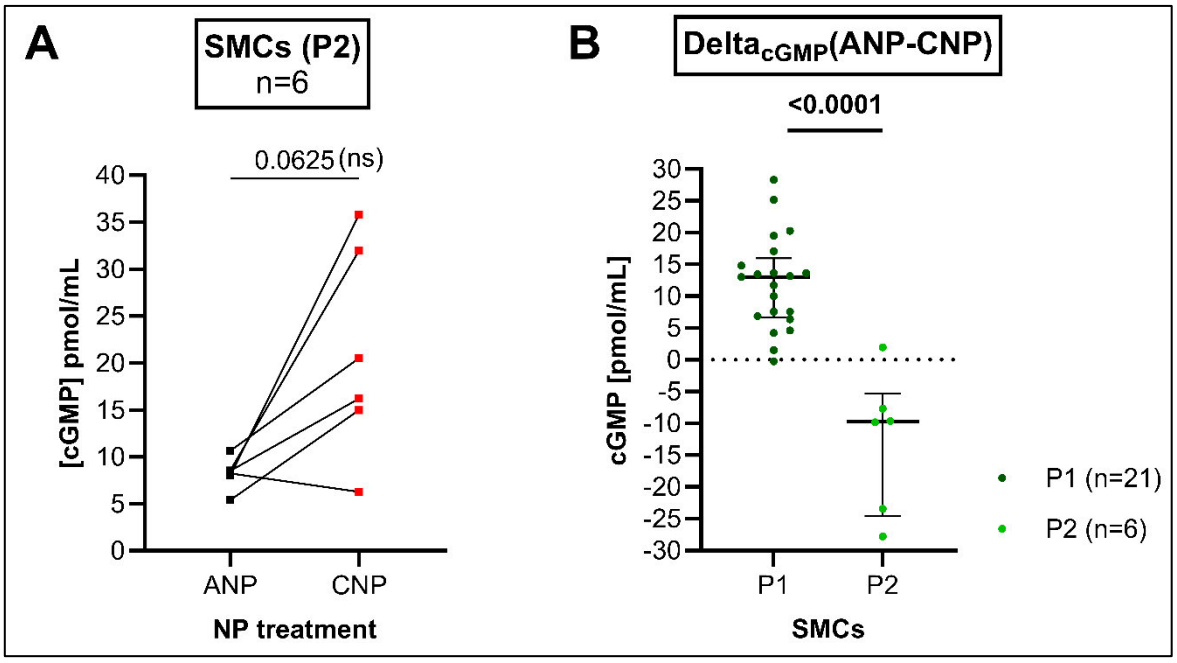


***Figure 35:*** *Measurement of cGMP release after the natriuretic peptide (NP) treatment of the cultured aortic smooth muscle cells (SMCs) of passage 2 (P2).*
The cGMP concentrations of the sample supernatants given in pmol/mL. (**A**) The cGMP measurement followed a 30 min incubation time with either ANP or CNP at a concentration of 100 nm each. The basic cGMP level of the IBMX (phosphodiesterase inhibitor) control treatment was on average 0.09 pmol/mL. Lines connect the single values for atrial natriuretic peptide (ANP)- (black) and C-type natriuretic peptide (CNP)- (red) stimulated cGMP of the cells extracted from the same individuum. Differences between the ANP- and CNP-induced cGMP release in the total study cohort (n = 6) were analysed by two-tailed non-parametric Wilcoxon's matched-pairs signed rank test. The numeric p-value was found to be not significant (ns). (**B**) Comparison of $Delta_{cGMP}$(ANP-CNP) between the cells of the first (P1, n = 21) and second passage (P2, n = 6) by unpaired non-parametric Mann–Whitney test. Due to the reduced n-number of the P2 cohort, the resulting p-value should be interpreted in an explorative manner.

## 4.2 Testicular (peritubular) smooth muscle cells

The following chapter summarizes the main results regarding the movement analysis of rat STs live imaging recordings using a custom-built FIJI script. This chapter distinguishs between the spontaneous movements (naturally occurring movements without any treatment) of STs in two different spermatogenic stages, dark (before spermiation) and pale (after spermiation), and treatment induced effects on these spontaneous contractions. The order in which the results are described follows the consecutive stages of the development of the script that was tailored specifically to the shape and movement characteristics of rat STs (described in more detail in the methods section, chapter **3.2.4.3**).

### 4.2.1 Seminiferous tubules show more vigorous superficial wall movements after than before spermiation according to their movement score

The initial movement score analysis, similar to the original Wiggle index script (Denecke et al., 2015), assesses the movement intensity of the entire tissue section within focus, while evaluating the contrast fluctuations in a pixel-precise manner. The movement score analysis detected a significant difference between the spontaneous contractions of dark and pale tubules (**Figure 36**).

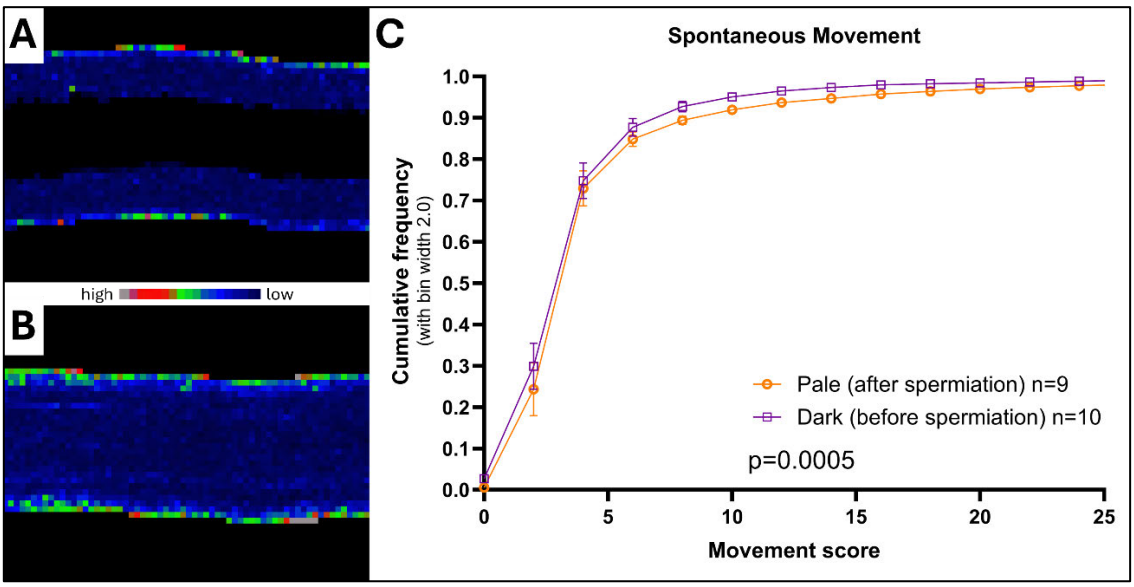


***Figure 36**: Intensity of the spontaneous superficial wall movements of rat seminiferous tubules depends on the spermatogenic stage according to the initial movement score analysis.*
Exemplary heat-maps of **A)** dark and **B)** pale seminiferous tubules (STs) reveal that the most intense movement occurs along the tubular wall. **C)** Spontaneous contractions of pale (orange line) and dark (purple line) STs of 10 male rats were live recorded as image stacks capturing one frame per sec for a recording period of 5 min. All pixels within the selected region of interest (ROI) were sorted according to a frequency distribution with regard to their movement score. The resulting distribution data is depicted as a cumulative frequency curve using a non-linear regression with sigmoidal curve fit in GraphPad Prism. For the comparison of the spontaneous contractions the similarity of the curve shapes was assessed. The bin width (2.0) for the pixel sorting was determined automatically by the software. The error bars of each bin center indicate ± SEM.

The cumulative frequency distribution of the pixel movement scores revealed a significantly more vigorous spontaneous contraction pattern for the pale tubules (orange line, **Figure 36 C**). This matches the corresponding heat-maps (**Figure 36 A, B**) but also the mere observations of the live recordings. In the cumulative frequency plots the positioning of the graphs indirectly relates to the movement intensity (**Figure 36 C**). The closer to the graph is positioned to the x-axis, the higher the movement of the respective live recording and vice versa.

### 4.2.2 Movement score analysis suggest a similar relaxing capacity of nitric oxide in seminiferous tubules before and after spermiation

The sophisticated *ex vivo* setup (chapter **3.2.4.2**) enables the treatment of the tissue while the recording is in progress. The flow settings of the media pump provide a fluid circulation at a specific speed, and this ensures that reagents that have been added to the fresh media supply are washed out of the dish after a certain amount of time.

Live imaging recordings of both ST stages under NO treatment, as expected revealed a decrease in contractility (for iteration of the relaxing pathway see **Figure 6**). When having a look at the previous approach assessing the kymographs (**Figure 37 A, B** below the respective heat map), which are static optical slices observed over the entire length of the recording, a notable relaxation could be appreciated by a reduction of the number of recorded contraction peaks. It was interesting to see, however, that the relaxing effect of the applied NO-donor seems to be non-permanent and that the speed with which consecutive contractions appeared eventually picked up again. This observation was supported by the according heat-maps that resulted from the movement score analysis (**Figure 37 A, B**). The NO treatment caused a reduction of pixels at the high movement score spectrum along the tubular wall and resulted in a significant difference between the spontaneous and NO-frequency curves for both dark (**Figure 37 C**) and pale (**Figure 37 D**) STs. When comparing the relative reduction of the movement score between the spontaneous recoding segment and the consecutive NO-segment, no significant difference between tubules before and after the sperm release could be detected (**Figure 37 E**), even though it seemed as if the relaxation lasted longer in the case of dark tubules.

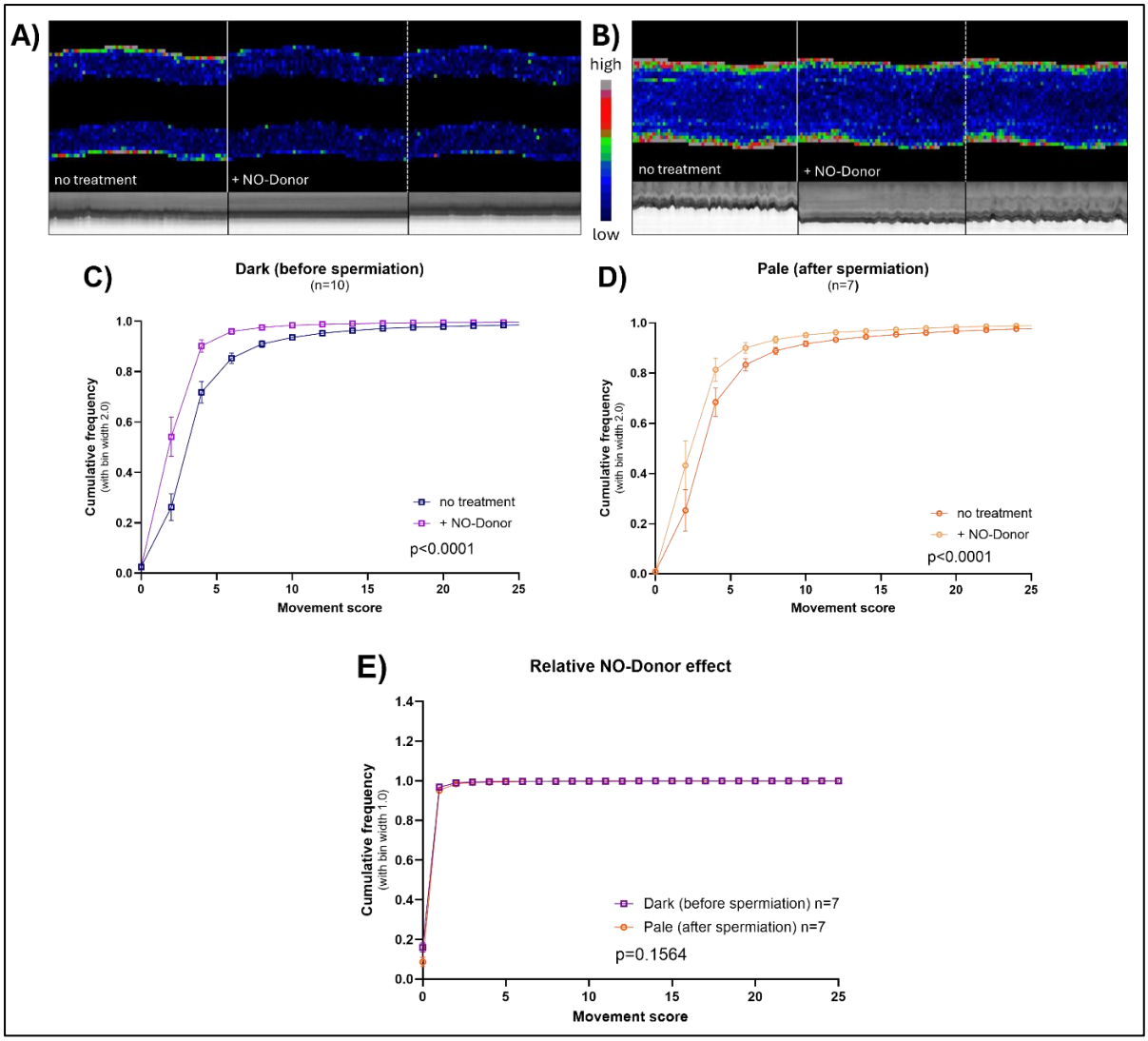


***Figure 37**: Nitric oxide induces a significant reduction of spontaneous superficial wall movements and shows equipotent relaxing effect in seminiferous tubules before and after spermiation.*
Exemplary heat-maps and kymographs of **A)** dark and **B)** pale seminiferous tubules (STs) visualize a significant reduction in their spontaneous tissue movement (no treatment) upon nitric oxide (NO) treatment (NONOate [10µM]). The spontaneous contractions and the contractions following an NO administration of **C**) dark (n=10) and **D**) pale (n=7) STs were assessed by analysing live imaging recordings (capturing speed at one frame per sec) according to the movement score analysis in Fiji and subsequent cumulative frequency distribution in GraphPad Prism. The comparison between the spontaneous and the NO curve resulted in a significant difference for both spermatogenic stages. The NO curve is localized above the spontaneous baseline, thus identifies a significant reduction in contractility upon NO administration. **E)** When plotting the relative movement score data, reflecting the difference between the live imaging segment without and with treatment, and comparing the resulting cumulative frequency curves between dark and pale STs from the same animals no significant difference was detected. Bin widths for the pixel-precise movement score sorting was determined automatically by GraphPad. The error bars of each bin center indicate ± SEM.

### 4.2.3 Noradrenaline does not increase contractility of seminiferous tubules according to their movement score

When analysing the effect of NA on the spontaneous contractions of STs pre- and post - spermiation, the movement score revealed a small tissue response (**Figure 38**) that was visually difficult to notice. The exemplary heat-maps and corresponding kymographs (**Figure 38 A, B**) both

show a minimal change in pixel intensity and pattern of the peaks after NA treatment that is difficult to assess with human perception. While in the STs after spermiation (pale) NA did not seem to elicit any remarkable change in the spontaneous contractility (**Figure 38 B, D**) it was even more unexpected to see a slight reduction of the wall contractions in STs before spermiation (dark) upon NA treatment (**Figure 38 A, C**).

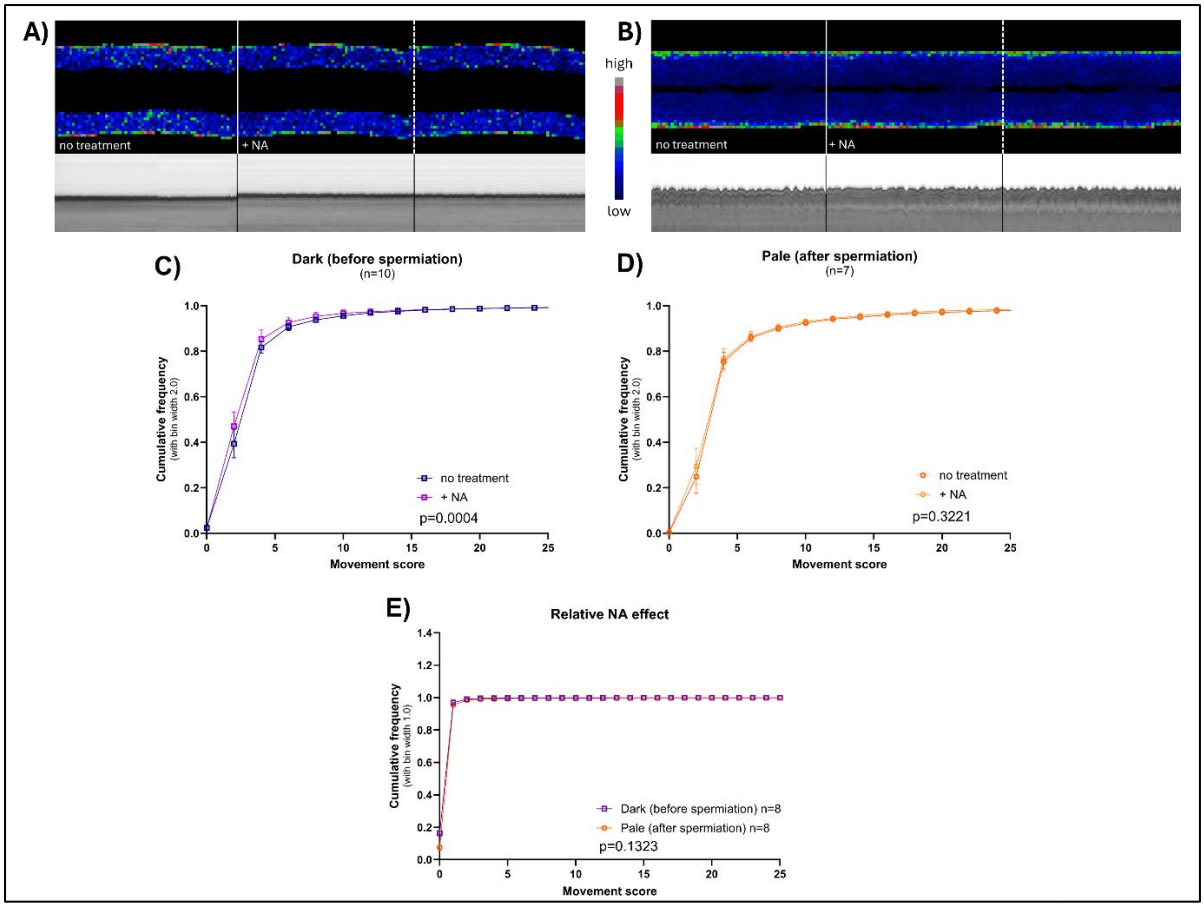


***Figure 38:*** *Noradrenaline unexpectedly shows little to no effect on spontaneous contractions in rat seminiferous tubules according to movement score analysis.*
Exemplary heat-maps and kymographs of **A)** dark and **B)** pale seminiferous tubules (STs) visualize a marginal movement reduction before spermiation but no response after spermiation upon noradrenaline (NA) treatment [10µM]. The spontaneous contractions and the contractions following NA administration of **C**) dark (n=10) and **D**) pale (n=7) STs were assessed by analysing live imaging recordings (capturing speed at one frame per sec) according to the movement score analysis in Fiji and subsequent cumulative frequency distribution in GraphPad Prism. The comparison between the spontaneous and the NA curve revealed a significant difference in dark but not in pale STs. The NA curve is localized above the spontaneous baseline, thus identifies a significant reduction in contractility upon NA administration. **E)** When plotting the relative movement score data, reflecting the difference between the live imaging segment without and with treatment, and comparing the resulting cumulative frequency curves between dark and pale STs from the same animals no significant difference was detected. Bin widths for the pixel-precise movement score sorting was determined automatically by GraphPad. The error bars of each bin center indicate ± SEM.

Even though the comparison of the spontaneous contractions and the contractions influenced by NA yielded a significant difference in dark tubules (**Figure 38 C**), the comparison of the relative change in the movement score values between dark and pale did not result in a difference between both stages (**Figure 38 E**), similar to the NO induced responses (**Figure 37 E**).

### 4.2.4 Tubules before and after spermiation contract with a similar frequency along the wall but not along the adjacent epithelium

The original movement score analysis is a sophisticated tool to assess tissue motility according to pixel intensity fluctuations over the recorded period of time. The movement score FIJI script was initially tailored to the movement of the most distal segments of the epididymal duct (Stadler et al., 2021) and therefore put the emphasis more on the contraction amplitude rather than considering the frequency of the contractions. In the context of the transport of seminal fluid through the testis, however, the frequency may or may not be equally relevant to the amplitude. Furthermore, the previously established code evaluated all pixels of the entire tissue section in focus. The majority of the contractions, however, according to the movement score analysis (**Figure 36 A, B**), occur along the tubular wall and the adjacent GE layer. Thus, most recorded pixels, with regard to the research questions (chapter **2.2**), can be ignored when analysing ST contractions. In addition, and this is especially important for the dark tubules, undersaturated dark pixels cannot be evaluated properly and might therefore add insignificant excess data.

The frequency only script was therefore not only designed to evaluate the frequency only but to automatically set regions of interest (ROIs) along the ST walls and the adjacent GE.

When comparing the frequency of the spontaneous contractions along the tubular wall in dark and pale STs (**Figure 39 A**) not significant difference was detected. Most surprisingly, the frequency evaluation detected a difference between the spontaneous contractions in the GE of the same subset of tubules (**Figure 39 B**). Another observation that is noticeable is that the shapes of the cumulative frequency curves are different to that of the curves resulting from the movement score analysis (**Figure 36 C**). Rather than an exponential shape with a continuously increasing slope in the beginning that eventually reaches a plateau, the frequency only curves seem to have a more arbitrary shape with multiple peaks, suggesting multiple subsets of ROIs of which the frequency occurs with a similar likelihood. Thus, for the frequency analysis a regression model with sigmoidal curve shape of a variable slope was applied for the curves shape comparison in Prism (chapter **3.2.4.3**).

In addition, it should be mentioned that the peaks of the pale and dark curves are not overlapping, especially the section of very high and very low frequencies, which seems to be quite distinct between the dark and pale tubules of the same rats.

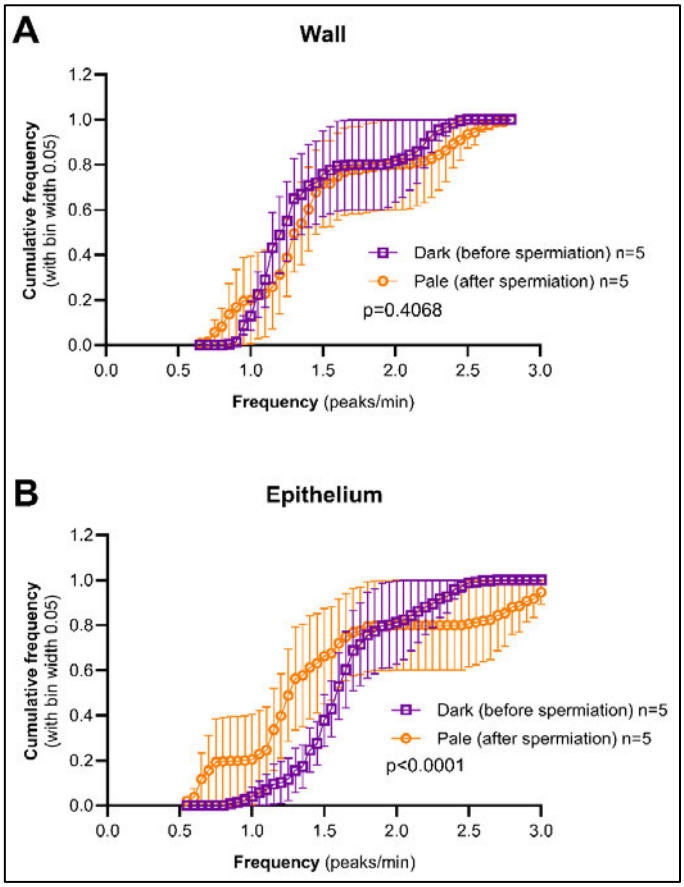


***Figure 39:*** *Frequency of the spontaneous contractions differs in the germinal epithelium but not along the tubular wall of rat seminiferous tubules before and after spermiation.*
Spontaneous contraction frequency (peaks per min) of dark (purple curve) and pale (orange curve) seminiferous tubules (STs) of the same male rats (n=5) was compared **A)** along the tubular wall and **B)** in the adjacent germinal epithelium (GE) using an amended version of the movement score analysis in FIJI. Rat STs were live recorded as image stacks capturing one frame per sec for a recording period of 5 min. All regions of interest (ROI) along the wall or adjacent GE were selected for a height of 20 and width of 50 pixels each and sorted according to a cumulative distribution with regard to their frequency. The resulting distribution data is depicted as a cumulative frequency curve using a non-linear regression with sigmoidal curve shape of variable slope in GraphPad Prism. For the comparison of the spontaneous contractions the similarity of the curve shapes was assessed. The bin width (0.5) for the pixel sorting was determined automatically by the software. The error bars of each bin center indicate ± SEM.

### 4.2.5 Nitric oxide significantly decreases contraction frequency independent of the spermatogenic stage of rat seminiferous tubules

Like the movement score analysis, the frequency adaptation of the FIJI Code detected a significant decrease in the frequency of spontaneous contractions in the wall (**Figure 40 A, C)** and the GE (**Figure 40 B, D**) before and after spermiation. The cumulative frequency curve of the NO treatment segment in both stages was located above the corresponding curve of the no treatment segment, thus visualized a reduction of the spontaneous contraction frequency. The curves of the dark STs (**Figure 40 A, B**) in comparison to the pale equivalents (**Figure 40 C, D**), are located further to the left on the x-axis. Therefore, more ROIs are characterized by a greater

likelihood to show lower frequencies of the contractions along the wall (**Figure 40 A**) and the adjacent epithelium (**Figure 40 B**). In both stages the spontaneous and NO curves show a comparable shape, suggesting a homogeneous propagation of the contraction signal from the wall, where the signal originates, towards the lumen.

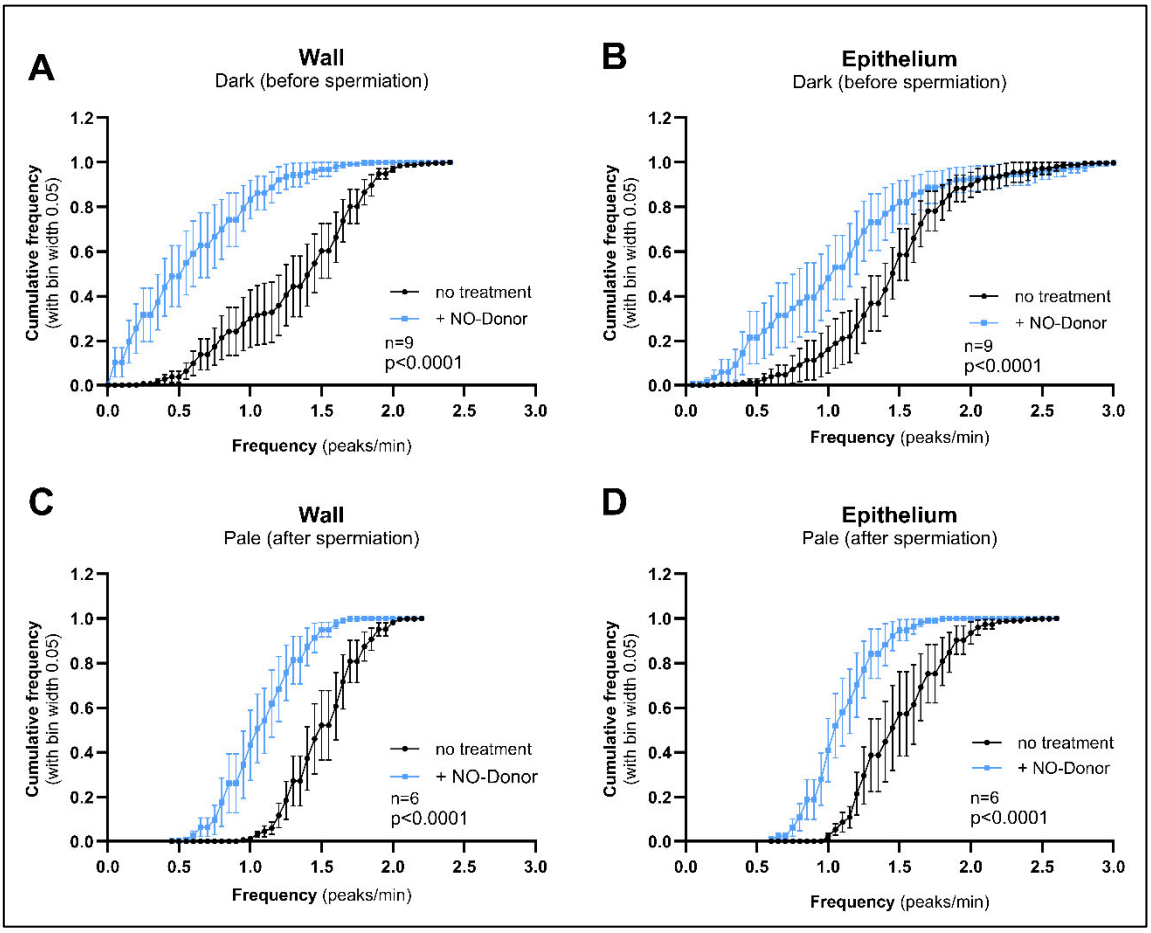


***Figure 40:*** *Nitric oxide significantly reduces the frequency of the spontaneous contractions in rat tubules before and after spermiation.*
The change of the spontaneous contraction frequency (black curves) upon NO-Donor (NONOate, 10 µM) treatment (blue curves) was evaluated in the **A, C)** walls and **B, D)** adjacent germinal epithelium (GE) of **A, B)** dark and **C, D)** pale seminiferous tubules (STs) from male rats (n=9) using the frequency adaptation of the original movement score analysis in FIJI. STs were live recorded as image stacks capturing one frame per sec for a recording period of 5 min. All regions of interest (ROI) along the wall or the adjacent GE were selected for a height of 20 and width of 50 pixels each and sorted according to a cumulative distribution regarding their frequency. The resulting distribution data is depicted as a cumulative frequency curve using a non-linear regression with sigmoidal curve shape of variable slope in GraphPad Prism. For the comparison of the spontaneous and NO-induced contractions the similarity of the curve shapes was assessed. The bin width (0.5) for the pixel sorting was determined automatically by the software. The error bars of each bin center indicate ± SEM.

The size of the gap between the spontaneous and NO curves in both, dark and pale tubules, seems to be greater in the wall (**Figure 40 A, C**) than in the epithelium (**Figure 40 B, D**). The biggest area between curves, however, is in between the spontaneous and NO curve of the wall of dark tubules, suggesting that dark tubules show the biggest effect upon the NO donor treatment. However, the difference between the relative effect when comparing dark and pale was found to be non-significant (data not shown).

### 4.2.6 Noradrenaline decreases spontaneous contraction frequency in dark and pale tubules

NA treatment unexpectedly induced a reduction in the spontaneous contraction frequency regardless of the spermatogenic stage (**Figure 41**). Similar to the observations in the NO treatment recordings (**Figure 40**), the gap between the spontaneous and the NA curves in dark and pale tubules seems greater along the walls (**Figure 41 A, C**) than the adjacent epithelial layer (**Figure 41 B, D**), where the contraction signal originates from. Again, a comparable curve shape was found in the walls and the respective epithelial curves, which may indicate a similar propagation of the SMC contractions from the wall towards the tubular lumen.

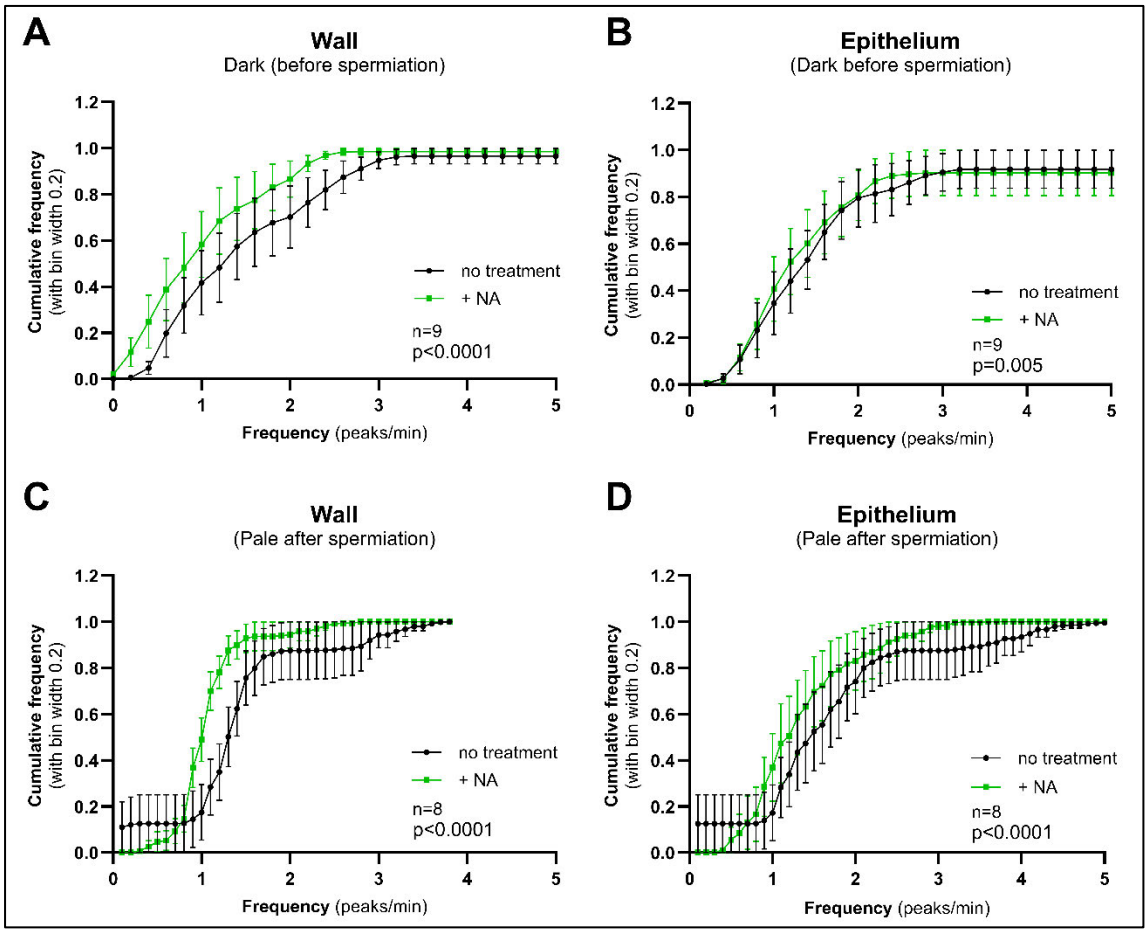


***Figure 41:*** *Noradrenaline reduces the spontaneous contraction frequency in rat tubules before and after spermiation.* The change of the spontaneous contraction frequency (black curves) upon noradrenaline (NA, 10 µM) treatment (green curves) was evaluated in the **A, C)** walls and **B, D)** adjacent germinal epithelium (GE) of **A, B)** dark (n=9) and **C, D)** pale seminiferous tubules (STs) (n=8) from male rats using the frequency adaptation of the original movement score analysis in FIJI. STs were live recorded as image stacks capturing one frame per sec for a recording period of 5 min. All regions of interest (ROI) along the wall or the adjacent GE were selected for a height of 20 and width of 50 pixels each and sorted according to a cumulative distribution regarding their frequency. The resulting distribution data is depicted as a cumulative frequency curve using a non-linear regression with sigmoidal curve shape of variable slope in GraphPad Prism. For the comparison of the spontaneous and NA-induced contractions the similarity of the curve shapes was assessed. The bin width (0.2) for the pixel sorting was determined automatically by the software. The error bars of each bin center indicate ± SEM.

The ROIs selected in the dark cohort show an even distribution of frequencies visualized by a more steadily increasing slope of the frequency curves. In contrast, the frequency pattern of the curves of the corresponding pale tubules shows a steep ascent around a frequency of one peak per minute, which means that the majority of ROIs contract with a similar frequency. Potential explanations for the unexpected results of the NA treatment will be discussed in chapter **5.2.5**.

### 4.2.7 The contribution of the contraction frequency and the amplitude to the tissue movement differs in seminiferous tubules before and after spermiation

Similar to the previous movement score (**Figure 36**) and frequency analysis (**Figure 39**), the newly developed merged code that combines and depicts the evaluation of the frequency, amplitude and movement score at once confirmed that the STs after spermiation in the pale spermatogenic stage move more vigorously than their dark counterparts. Pale tubules show a higher movement score, a value that to some extent includes the frequency but predominantly the amplitude (Denecke et al., 2015). On average the movement score of the pale STs is higher than of the dark STs by roughly 10-fold. This difference can be acknowledged by the larger bubble size of the orange in comparison to the purple cohort and reflects earlier findings of the movement analysis that included the whole tissue section (**Figure 36 C**). The difference between the movement intensity of the spontaneous contractions, however, seems to be more prominent along the tubular wall (**Figure 42 A**) than in the adjacent epithelial layer (**Figure 42 B**). In case of the tubular wall, the gap between the two populations predominantly occurs due to a much larger difference in the amplitude. Therefore, it seems as if the amplitude contributes more to the spontaneous movement score than the frequency in pale tubules in comparison to dark.

In general, the movement score (size of the bubbles) of both cohorts decreases in the epithelium, likely due to a notable reduction in the amplitude of spontaneous contractions in both stages. The frequency in the pale cohort remains constant when comparing the wall and epithelial

recordings of the same tubules. In the dark tubules surprisingly a slight increase in frequency in the epithelial recordings could be detected.

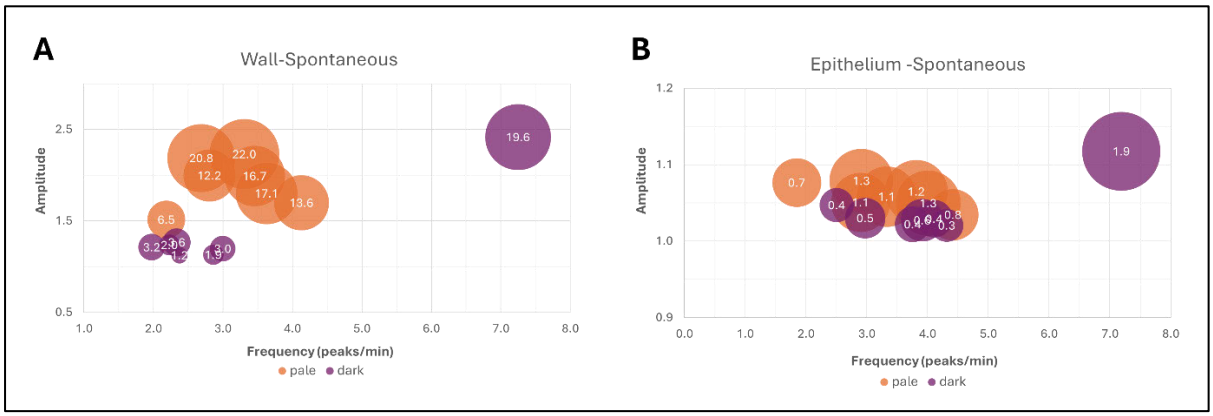


***Figure 42:*** *Spontaneous contractions of rat seminiferous tubules of different spermatogenic stages are different with regard to their frequency, amplitude and movement score along the wall and adjacent germinal epithelium.*
The newly developed merged FIJI code detects more vigorous contractions in the **A)** tubular wall and **B)** germinal epithelium (GE) of pale seminiferous tubules (STs) after spermiation (orange bubbles) than in dark STs before spermiation (purple bubbles) of the same animals. The axis of **B)** was stretched in order to highlight the difference in the amplitude of both cohorts. Pale and dark STs from male rats (n=7) were live recorded as image stacks capturing one frame per sec for a recording period of 5 min. The regions of interest (ROI) along the **A)** wall or the **B)** adjacent GE were selected for a height of 20 and width of 50 pixels each. For each recording the mean of the frequency, amplitude and movement score of all ROIs was calculated and depicted as a bubble plot in EXCEL. Each bubble represents the results for one animal while the positioning of the bubble with regard to the x-axis reflects the average frequency, the positioning with regard to the y-axis represents the average amplitude and the bubble size visualizes the average movement score.

### 4.2.8 Nitric oxide dampens the spontaneous contractions of seminiferous tubules before and after spermiation

In the pale cohort the largest shift of the spontaneous population upon NO treatment (**Figure 43**) was observed along the wall. This shift seems to be induced by an almost equal reduction in amplitude as well as in the frequency by approximately 0.5 -fold (**Figure 43 A, D, G**). This resulted in much smaller bubbles in the tubular wall after NO administration (**Figure 43 G**). In the GE and the inner luminal section no shift of the average spontaneous amplitude was observed. It is a reduction in the frequency of the spontaneous contractions that seems to cause a slight shift of the NO-treated orange population to the left side of the x-axis and a decrease in the movement score. In general, NO seems to have a marginal effect on the frequency of the spontaneous contractions but induces a notable dampening of the amplitude in the tubular wall. In the adjacent epithelium (**Figure 43 B, E, H)** and lumen (**Figure C, F, I**), however, NO induced a decrease in the spontaneous contraction frequency. Hence, this decrease seems to contribute more to a smaller movement score than the amplitude, which is visualized by the shrinking of the orange bubbles in comparison to the corresponding blue bubbles (**Figure 43 H, I**). In summary the largest effect upon NO treatment in STs after spermiation was recorded in the tubular wall.

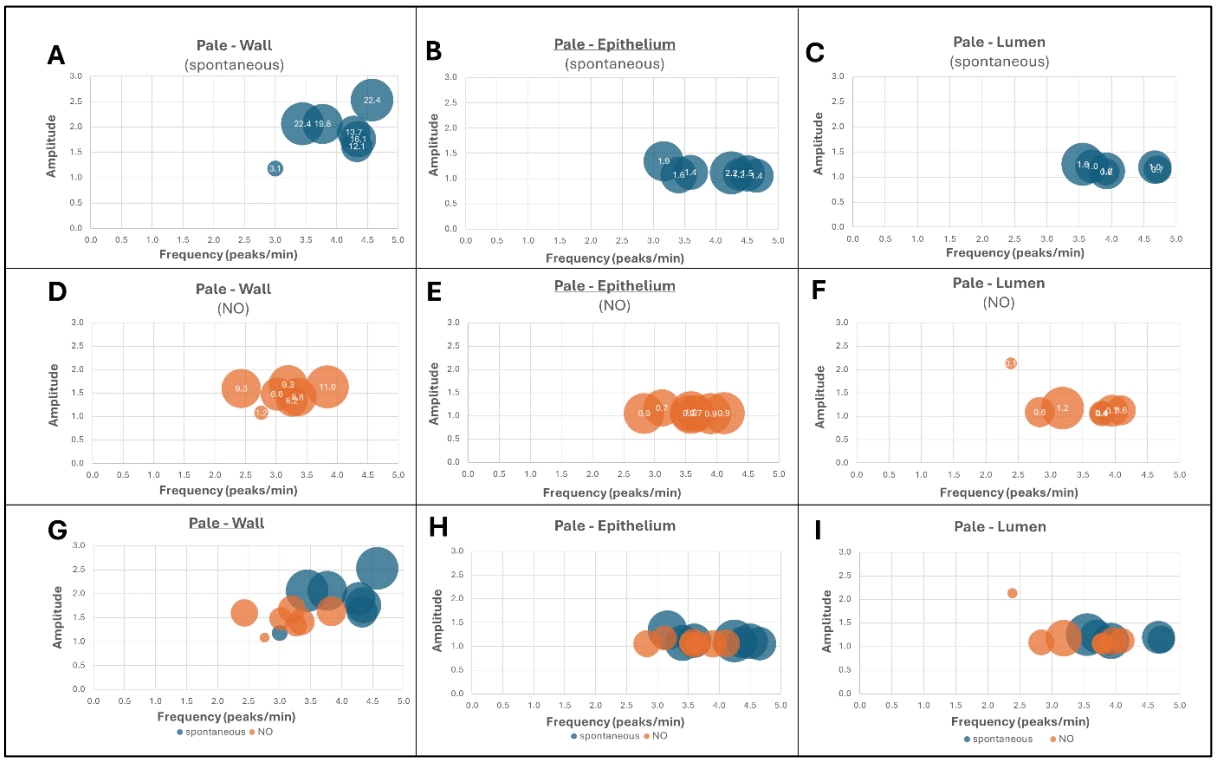


***Figure 43:*** Nitric oxide induced reduction in spontaneous movement of rat seminiferous tubules after spermiation with regard to their frequency, amplitude and movement score along the wall, germinal epithelium and lumen.

The merged FIJI analysis detects a reduction of the spontaneous contractions (blue bubbles) upon the treatment with the nitric oxide (NO) donor NONOate (10µM) (orange bubbles) in **A, D, G)** the tubular wall, **B, E. H)** the adjacent germinal epithelium (GE) and **C, F, I)** the inner lumen. Pale seminiferous tubules (STs) from male rats (n=7) were live recorded as image stacks capturing one frame per sec for a recording period of 5 min per treatment section. The regions of interest (ROIs) along the wall, GE and lumen were selected for a height of 20 and width of 50 pixels each. For each recording the average frequency, amplitude and movement score of all ROIs was calculated and depicted as a bubble plot in EXCEL. Each bubble represents the results for one animal while the positioning of the bubble with regard to the x-axis reflects the average frequency, the positioning with regard to the y-axis represents the average amplitude and the bubble size a visualizes the average movement score.

Similar to the pale tubules, already before the release of the sperm cells into the lumen a reduction of the spontaneous movement intensity was detected upon NO treatment in the dark tubular stage (**Figure 44**). This could be detected in the tubular wall (**Figure 44 A, C, E**) as well as in the adjacent GE (**Figure 44 B, D, F**). As briefly explained in the previous chapter **3.2.4.3**, the movement in the dark luminal section cannot be evaluated properly due to undersaturation of the pixel contrast. The dark STs, like their pale counterparts showed a decrease in the amplitude of their spontaneous contractions along the wall by approximately 0.5. However, no such decrease was detectable in their GE (**Figure 44 F**) and the amplitude upon NO administration remained stable. In the wall the frequency dropped by 1.0 values in average upon NO treatment while in the epithelium the frequency remained the same.

As for the pale tubules, in case of the STs right after spermiation the NO effect was predominantly observed along the wall (**Figure 44 E**), while its impact on the spontaneous movement in the epithelial layer (**Figure 44 F**) was marginal. This is highlighted by a larger decrease in the bubble

size upon NO treatment in the wall than in the GE. In summary, it seems that in the dark spermatogenic stage the frequency seems to have a higher contribution to the tissue movement than in the pale tubules. This matches the observations from the live recordings in which the average amplitude of the superficial wall contractions appears to be quite small, but at the same time the frequency is quite high.

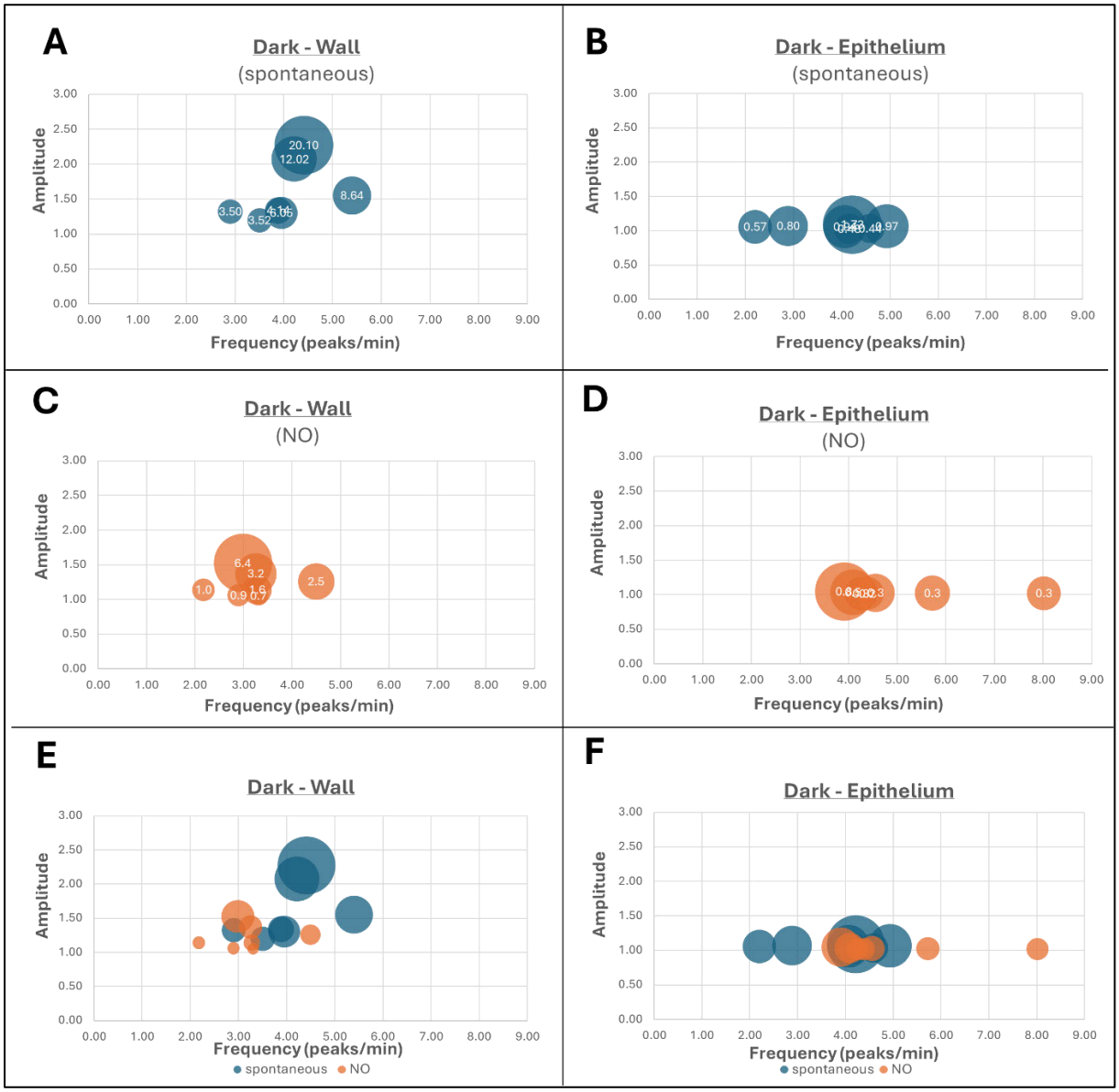


***Figure 44:*** *Nitric oxide induced reduction in spontaneous movement of rat seminiferous tubules before spermiation with regard to their frequency, amplitude and movement score along the wall and germinal epithelium.*
The merged FIJI analysis detects a reduction of the spontaneous contractions (blue bubbles) upon the treatment with the nitric oxide (NO) donor NONOate (10µM) (orange bubbles) in **A, C, E)** the tubular wall and **B, D, F)** the adjacent germinal epithelium (GE). Dark seminiferous tubules (STs) from male rats (n=7) were live recorded as image stacks capturing one frame per sec for a recording period of 5 min per treatment. The regions of interest (ROIs) along the wall and GE were selected for a height of 20 and width of 50 pixels each. For each recording the mean of the frequency, amplitude and movement score of all ROIs was calculated and depicted as a bubble plot in EXCEL. Each bubble represents the results for one animal while the positioning of the bubble with regard to the x-axis reflects the average frequency, the positioning with regard to the y-axis represents the average amplitude and the bubble size visualizes the average movement score.

### 4.2.9 Noradrenaline has relaxing effect on smooth muscle contraction in rat seminiferous tubules is unexpected

Considering the effect that NA generally exerts in smooth muscle (chapter **1.5.1.4**), the outcome of the imaging analyses after NA treatment was surprising. In both, dark (**Figure 46**) and pale STs (**Figure 45**) before and after sperm release from the GE into the tubular lumen, NA reduced the spontaneous contractility. The following results which were generated using the merged FIJI code analysis are in alignment with earlier findings when applying the movement score (chapter **4.2.3**) or frequency analysis only (chapter **4.2.6**).

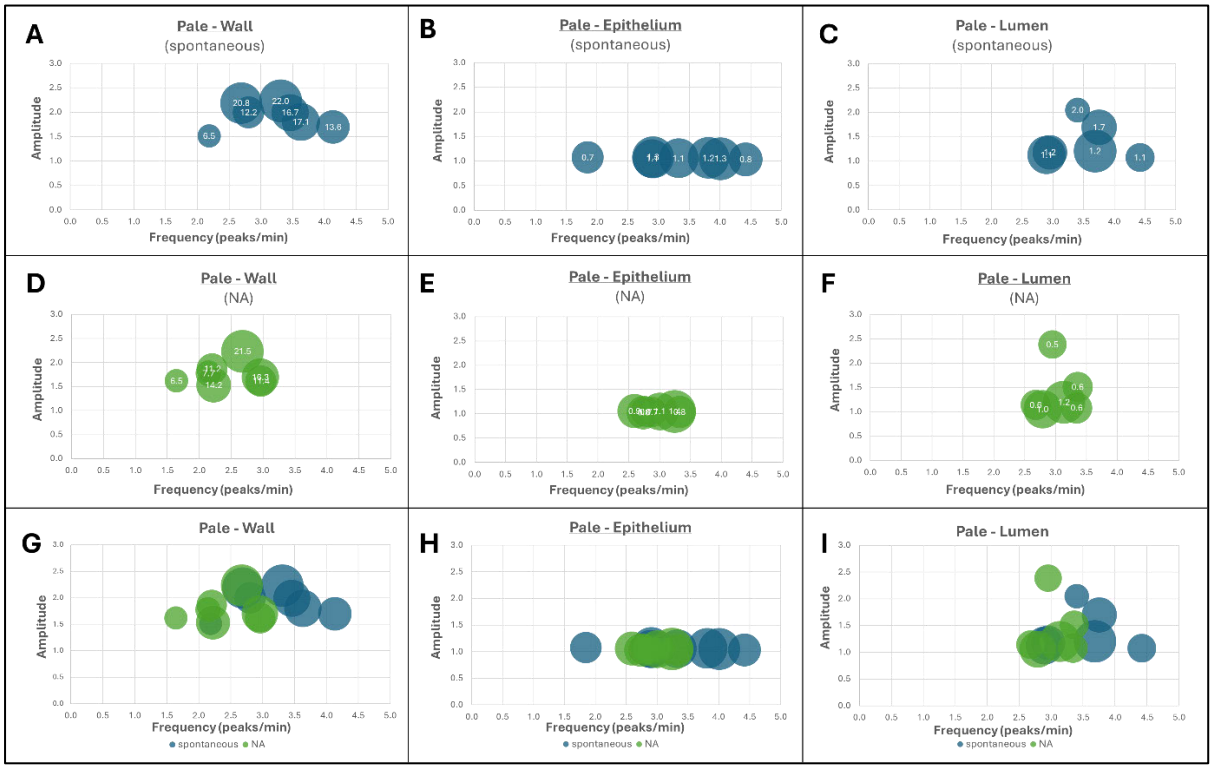


***Figure 45:*** *Noradrenaline dampens the spontaneous contractions of rat seminiferous tubules before spermiation with regard to their frequency, amplitude and movement score along the wall, germinal epithelium and lumen.*
The merged FIJI analysis detects a reduction of the spontaneous contractions (blue bubbles) upon the treatment with Noradrenaline (NA) (10µM) (green bubbles) in **A, D, G)** the tubular wall, **B, E, H)** the adjacent germinal epithelium (GE) and **C, F, I)** the inner lumen. Pale seminiferous tubules (STs) from male rats (n=7) were live recorded as image stacks capturing one frame per sec for a recording period of 5 min per treatment. The regions of interest (ROIs) along the wall and GE were selected for a height of 20 and width of 50 pixels each. For each recording the mean of the frequency, amplitude and movement score of all ROIs was calculated and depicted as a bubble plot in EXCEL. Each bubble represents the results for one animal while the positioning of the bubble with regard to the x-axis reflects the average frequency, the positioning with regard to the y-axis represents the average amplitude and the bubble size visualizes the average movement score.

In STs of the pale spermatogenic stage regardless of the analysed section, wall (**Figure 45 A, D, G**), germinal epithelium (**Figure 45 B, E, H**) or lumen (**Figure 45 C, F, I**), NA elicits a marginal effect and the bubble size of the untreated (blue bubbles) and NA-treated population (green bubbles) remains roughly the same. In all the different sections of the analysed tissue NA induced a shift

to the left in with regard to the y-axis, hence, decreases the frequency of the tissue contractions but seems to have no effect on the amplitude of the spontaneous contractions.

In case of the ST cohort before the spermiation (**Figure 46**) even seems to have very little to no effect on the spontaneous contraction pattern, neither along the tubular wall (**Figure 46 A, C, E**) nor within the adjacent GE (**Figure 46 B, D, E**). The localization of the bubble cohorts as well as the size of the bubbles seems to remain unimpaired by NA treatment.

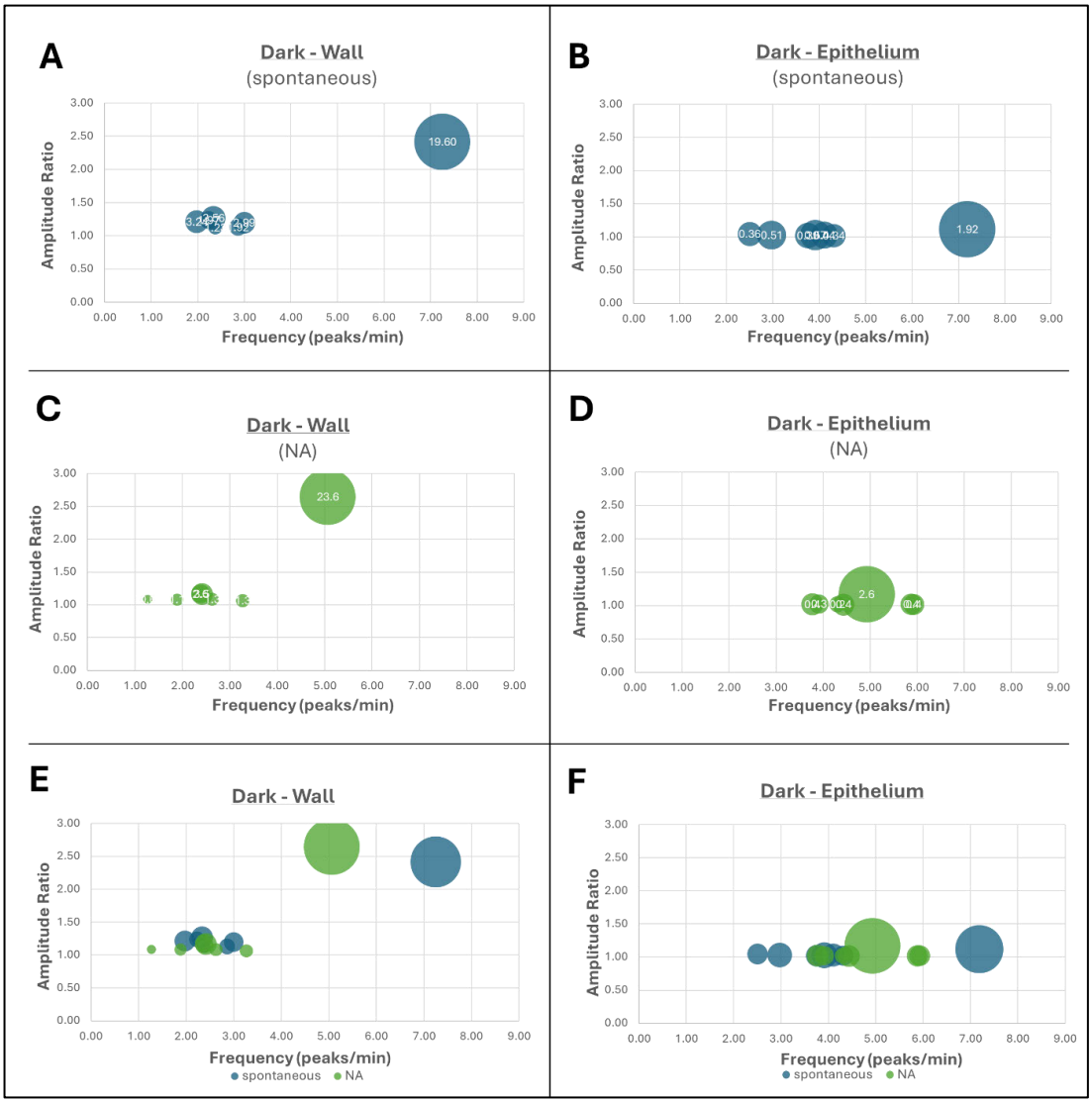


***Figure 46**: Noradrenaline surprisingly induced reduction in spontaneous contractions of rat seminiferous tubules after spermiation with regard to their frequency, amplitude and movement score along the wall and germinal epithelium.*
The merged FIJI analysis detects a reduction of the spontaneous contractions (blue bubbles) upon the treatment with Noradrenaline (NA) (10µM) (green bubbles) in **A, C, E)** the tubular wall, **B, D, F)** and the adjacent germinal epithelium (GE). Dark seminiferous tubules (STs) from male rats (n=7) were live recorded as image stacks capturing one frame per sec for a recording period of 5 min per treatment. The regions of interest (ROIs) along the wall and GE were selected for a height of 20 and width of 50 pixels each. For each recording the mean of the frequency, amplitude and movement score of all ROIs was calculated and depicted as a bubble plot in EXCEL. Each bubble represents the results for one animal while the positioning of the bubble with regard to the x-axis reflects the average frequency, the positioning with regard to the y-axis represents the average amplitude and the bubble size visualizes the average movement score.

To summarize these final experiments, it was surprising to see a reduction in the movement of both, dark and pale, tubule stages. Nevertheless, it was reassuring that the newly developed merged analysis detected and displayed the same NA-induced changes as the previous movement score code (**Figure 41**). In both tubules stages it seemed as if NA had a greater impact on the frequency than on the amplitude. Potential explanations for the dampening effect of NA on the spontaneous tubule contractions will be discussed in the chapter **5.2.5**.

# 5 Discussion

## 5.1 Vasculature

It is widely accepted that vascular SMCs undergo phenotypic transitions not only upon disease but also as a result of prolonged culturing (Chamley-Campbell et al., 1979; Frismantiene et al., 2018; Huber & Badylak, 2012; Worth et al., 2001). Basic knowledge regarding vascular signalling pathways was previously established on the basis of *in vitro* culture (Li et al., 2012; Pugsley & Tabrizchi, 2000; Qiu et al., 2014) often generated from aorta. Furthermore, the establishment of new therapeutics for cardiovascular disease still requires cell culture for drug testing (Karbassi et al., 2020; Rameshrad et al., 2016). However, the results obtained for chapter **4.1** of this thesis are indicative of dramatic changes upon extraction and culturing of these cells that seem mostly independent of biological sex (see results, **Figure 32**).

The subsequent discussion intends to question the suitability of aortic vascular SMC culture for the study of the cGMP signalling cascade, while exploring advantages and disadvantages of cell culture. Additionally, it aims to question the applied methods and to provide promising future directions for the research of cardiovascular diseases.

### 5.1.1 Primary aortic smooth muscle cells – Prospects of a cell culture model

Due to its size and thickness of the SMC layer, the aorta is a convenient source for harvesting primary vascular SMCs. Their extraction, however, destructs the integrity of the cell association. Furthermore, it terminates the constant exposure to fluctuating mechanical cues, e.g., changes in the blood pressure, and in the concentrations of molecules transported via the bloodstream, (e.g. oxygen, nutrients, hormonal factors). In a nutshell it can be said that culture changes everything. Therefore, a phenotypic adaptation of the extracted cells is crucial for their survival in cell culture (Liu et al., 2015).

Besides that, conclusions that are drawn on basis of aortic SMC culture should not be generalized for the entirety of vascular SMCs. Vascular SMCs of different vessel types (Tucker et al., 2024) show heterogeneous characteristics. For instance, as outlined in chapter **1.1** of the introduction, SMCs can be distinguished according to their electrophysiological coupling into multi- and single-unit type SMCs (Hafen & Burns, 2023). While vascular SMCs in smaller resistance vessels belong to the single-unit type (Pape et al., 2018; Pogoda et al., 2019), the smooth muscle of large arteries like the aorta belongs to the multi-unit type. Aortic SMCs rarely possesses gap junctions

and have the capacity to (re)act independently upon electrophysiological stimulation. This allows more precise fine tuning of the vessel diameter.

The length of the aorta additionally suggests that the genetic fingerprint of SMCs from different aortic segments vary (G. Liu et al., 2023; Yu et al., 2022). It was found that SMCs from different aortic areas, especially the ascending versus the descending sections, have different embryogenic origins (Donadon & Santoro, 2021; Roostalu & Wong, 2018). The results shown in this thesis, were obtained from a mixture of SMCs extracted from the aortic segment over a length from the heart until the abdominal bifurcation (see chapter **3.2.1.1**).

Arteries additionally are distinguished according to their layered structure (see chapter **1.3.1**) and a researcher recently started to address a proper distinction of elastic and muscular arteries regarding their cellular features (Murtada et al., 2021).

Lastly, it is important to mention that the phenotypic transition (discussed in the following section **5.1.1.2**) upon environmental or culture induced changes can be observed in arteries and in veins alike (Guo et al., 2022; Zhang et al., 2022), but because the arterial part of the vascular system is considered the "executing" vessel system substantially less attention has been given to the venous system, even though it houses ~ 70 % of a human's blood volume (Vekilov & Grande-Allen, 2018).

#### *5.1.1.1 Challenges in working with cultured primary vascular smooth muscle cells*

As briefly described (see chapter **1.3**, **Figure 11**) and visualized by histological staining (see chapter **4.1.1.1**, **Figure 26**) the aortic SMCs are tightly packed in between a dense network of elastic fibres. To dissolve this grid like cage of matrix proteins around the SMCs, most isolation protocols entail a digestion with enzymes such as collagenase (Chi et al., 2017; Rosàs-Canyelles et al., 2018; Sun et al., 2021). This approach usually yields a satisfactory number of SMCs but the mechanical and enzymatic singularization (method described in detail in chapter **3.2.2.1**) is harmful to the cells. The entire procedure is comparable to tissue damage due to vessel injury, disease or aging (Ahmed et al., 2024) and is known that naturally occurring enzymes such as collagenase affect vascular SMCs and induce proliferation and migration (Chi et al., 2017).

In general, tissue restoration depends on stem cell differentiation into cell lineages essential for the recovery and proliferation of non-specialized cells. While the arterial response to injury involves multiple cell types, previous research uncovered medial SMCs to play a particularly important role in this process (Roostalu & Wong, 2018). Their importance becomes evident in cases of arterial injuries when SMCs are absent, and adventitial cells migrate to the lesion and transdifferentiate into quickly proliferating synthetic SMCs. This process might in some cases

recapitulate developmental mechanisms during late embryogenesis (Roostalu et al., 2018; Roostalu & Wong, 2018).

#### *5.1.1.2 Phenotypic transition of cultured vascular smooth muscle cells leading to misinterpretation of physiological circumstances*

Another challenge, following the isolation of primary vascular SMCs, is the validation of the SMC identity. Because vascular smooth muscle already is a highly heterogenic tissue composed of different SMC subtypes (Frismantiene et al., 2018), a mosaic of different SMC phenotypes within primary culture retrieved from aortic media can be expected. However, the general impression of the cells in culture is a flattened morphology, an increased cell volume, and a decreased expression in myofilament and structural proteins (Worth et al., 2001). Their contractility seems to decline whilst proliferation, migration and ECM production take over. Furthermore, the characterization on basis of "specific" markers is difficult because SMCs share the expression of most marker proteins with other cell types of the same embryogenic origin (Muhl et al., 2020). SMA and calponin for a long time were designated as smooth muscle specific cytoskeletal protein markers that usually indicate a contractile ("healthy") and further differentiated SMC phenotype (el-Mezgueldi, 1996; Winder & Walsh, 1993). However, SMA is expressed in nearly all cells of the mesenchymal origin (Sung et al., 2014) including fibroblasts, myofibroblasts, SMCs and endothelial cells. In the primary cell culture obtained from rat aortic *tunica media* it was interesting to observe that all cells showed the characteristic filamentous staining pattern for SMA but only ~ 60% seemed to express calponin (**Figure 27 D**). Since both markers were found to be expressed quite densely at an equal level in the intact tissue of origin (**Figure 27 A, B**), this could be a first sign of a transition towards a less differentiated or rather synthetic SMC phenotype (Bennett et al., 2016; Shi et al., 2020). This transition seems to have a more severe effect on the expression of calponin than on SMA, at least in the early culturing stages.

The intermediate filament protein vimentin is frequently used for the distinction of (myo-) fibroblasts (Li & Kuemmerle, 2020; Tarbit et al., 2019) and, like SMA, was found to be expressed in all mesenchymal cells (Ostrowska-Podhorodecka & McCulloch, 2021). The azan staining of the intact aortic wall before (**Figure 26 A**) and after the removal (**Figure 26 B**) of the connective tissue layer (*tunica adventitia*) suggests a successful removal of the naturally occurring fibroblasts in the aortic wall (Majesky et al., 2012). However, in the extracted primary culture vimentin, a structural protein expressed by cells of the mesenchymal origin and formerly considered a marker for fibroblasts, was found to be expressed by the majority of the cells (**Figure 27 E, G**). In addition to that the immunofluorescent staining revealed the culture-induced reduction of the calponin expression, this could be another evidence of a switch towards a synthetic cell type with

a fibroblast-like character (Jia et al., 2024; Majesky, 2007). Vimentin is involved in matrix development and matrix adhesion, thus the increase in its expression seems a plausible response to culturing since SMCs in culture and in diseased arteries are known to increase ECM production (Chamley-Campbell et al., 1979). Under normal conditions SMCs in healthy vessels remain in a non-proliferative stage (Bennett et al., 2016). As a response to vessel injury and disease vascular SMCs are known to increase their proliferation drastically to close leaks in the vessel wall as quickly as possible. Hence, a quick turn-over and increase in proliferation are major traits of vessel pathology (Lutgens et al., 1999; Moon et al., 2003). Therefore, it was not surprising to detect the proliferation marker Ki67 in most of the cultured aortic cells (**Figure 27 H**).

A quite intriguing observation, however, was to find the expression of the stem cell marker nestin (Klein et al., 2014) in the *in vitro* cell culture (**Figure 27 H**) and thereby to confirm an earlier finding by Tang and colleagues (Tang et al., 2012). To determine whether nestin expression is triggered through extraction and culturing or is an innate feature of aortic SMCs, immunostaining of intact aortic tissue is a future direction of the research of the Middendorff lab. In primary culture it was surprising to see that the cells with the strongest nestin signal seemed to be cells that were not undergoing proliferation simultaneously, as they were found to be negative for Ki67 (**Figure 27 H**). However, nestin expression in cell culture may have different causes. The most obvious is to assume that a specific subtype of the cultured SMCs possess stem cell potential. In a disease context this seems reasonable, because depending on the acute requirements upon vessel injury mural cells are known to contribute to vascular healing (Armulik et al., 2011). Another explanation could be that this subclass of cells, has pericyte-like features (Roostalu & Wong, 2018; Volz et al., 2015) or that these cells are in fact pericytes, which are already known to have stem cell potential (Tang et al., 2012). Even if the latter is the case the characterization of the pericytes is difficult. Pericytes are actin – and myosin-positive cells in between the endothelial and muscular layer of vessels (Donadon & Santoro, 2021; Volz et al., 2015). They share a similar origin with SMCs in most organs and therefore fundamental characteristics of both lineages overlap and make it even harder to distinguish these two cell types. Knowing that pericytes fulfil slightly different functions than SMCs within vessels (e.g., the establishment and maintenance of the microenvironment for endothelial cells (Alarcon-Martinez et al., 2021; Donadon & Santoro, 2021)), the verification of specific marker proteins for both cell types could be valuable for future studies. Currently, platelet-derived growth factor receptor beta is under investigation (Donadon & Santoro, 2021) as a pericyte marker.

The characterization of isolated and cultured primary vascular SMCs using classical “specific” markers is difficult and may lead to misinterpretation of the cells’ origin and phenotype. Future

studies that monitor the transition of SMCs from isolation over a certain culturing period would be necessary to estimate the time for how long they maintain this character and reflect their counterparts in tissue most reliably. More in depth studies on suitable markers for the distinction between different cells of the vascular system, and SMC phenotypes specifically, are needed.

#### *5.1.1.3 Primary vascular smooth muscle cells culture - future model to study arterial disease and embryonic vascular development*

As mentioned earlier, cultured vascular SMCs share characteristics with those in injured or diseased blood vessels (Roostalu et al., 2018). A hallmark of lesion-prone disease, such as arterial aneurysms or atherosclerosis (Allahverdian et al., 2018; Bennett et al., 2016), is an increase in SMC proliferation which was also found in cell culture (Chamley et al., 1974). Under disease conditions arterial SMCs accelerate the production of ECM proteins, such as collagen (Jia et al., 2024) and migrate to the lesion or site of fibrosis. These alterations not only highlight the importance of SMCs for the maintenance of arteries but are similar to changes observed in culture. In many ways the response to arterial injury and the subsequent regeneration recapitulates embryonic pathways of vessel developmental pathways (Roostalu et al., 2018; Roostalu & Wong, 2018). Considering the primary cell extraction processes as a simulation of tissue injury, it is plausible that primary vascular SMC culture could serve as an *in vitro* model to study embryonic arterial development.

In summary, vascular SMC *in vitro* culture holds enormous potential for the identification of new biomarkers and the investigation of vascular disease and arterial development. For investigation of a healthy vascular context however, *in vivo* set ups or non-invasive cell tracking methods should be considered that may reflect the physiological circumstances within an intact artery more comparably (Lehners et al., 2018).

### 5.1.2 Hypotheses generated from cultured aortic SMCs

#### *5.1.2.1 Relevance of reliable reference genes for basic research is underestimated*

When performed accurately, real-time PCR (qPCR) is considered one of the most reliable methods for gene expression measurement (Kozera & Rapacz, 2013) and is often used to verify data obtained by other techniques (further advantages of qPCR to be discussed in chapter **5.1.3.2**). The most common way to analyse and display qPCR data is in relation to a predefined calibrator gene (Kozera & Rapacz, 2013; Pfaffl, 2001). This normalization is mainly there to correct for possible intra- and interkinetic variations of the qPCR reaction and differences between the compared samples caused for instance by sample preparation and processing.

To serve as a reliable calibrator, RGs must comply with certain requirements (for iteration of these requirements see introduction chapter **1.4.1.3**). Basic metabolism genes (aka. housekeeping genes, HKGs) were found to fulfil these criteria most frequently (Bustin et al., 2005). In former times this led to the belief that HKGs automatically are characterized by a stable expression regardless of the experimental conditions and sample origins. In most studies, that involve qPCR researchers chose the easiest strategy of using RGs that originally have been tested for similar experimental setups. However, what seems to work perfectly fine in one study does not guarantee functionality in another. Thus, individual and complex approaches for each experiment and careful validation of selected RGs is indispensable. It should be mentioned that most gene expression studies attempt the comparison of genes between cohorts within the same experimental condition or across a cohort with less heterogeneous samples, for instance comparing expression in tissue samples or cultured cells only. Thus, one would not usually expect such a drastic variation in the expression of the RG. However, the identification of a suitable RG for this study required the expression to be unimpaired by the sex of the study individuals and more importantly, between the *in vivo* and *in vitro* conditions of the aortic SMCs.

The isolation and exposure of primary vascular SMCs to culturing conditions requires quick and efficient adaption and since *in vitro* circumstances differ in every aspect from the physiological status, a drastic change in expression of numerous genes can be expected. Hence, it was not surprising to reveal a marked increase in the expression of the 'classical' RGs Actb and Gapdh (see **Figure 28**) upon isolation and culturing.

Gapdh used to be the most used RGs (Chapman & Waldenström, 2015; Suzuki et al., 2000) even though earlier studies already found it unsuitable for the comparison of tissue versus cultured cells (Oliveira et al., 1999). Latest examination running RG validation tools like NormFinder or BestKeeper, however, declared Gapdh as one of the most unstable RGs circulating (Taki et al., 2014) and the data obtained for this thesis supports this estimation. In fact, the spread of the absolute Ct values of the intact media samples was almost as big as the difference between cell culture and tissue (see **Figure 28**). Therefore, not only the suitability of both, Actb and Gapdh, for the comparison between culture and tissue, but also for the comparison between tissue samples of different animals seems questionable depending on the GOI under observation.

Because the difference in Actb and Gapdh expression even exceeded the differences in the GOI expression, both Actb and Gapdh were found unsuitable for the comparison of tissue versus cells. Something that should be considered as a potential booster of the drastic change in gene expression upon culturing is the shift towards a more proliferative SMC phenotype. Furthermore, this shift may be fuelled by the addition of 10% FBS to the cell culture medium, a serum

concentration that is considered normal in cell culture settings, where this additive ensures longevity and continuous proliferation. One could therefore consider utilizing Gapdh and Actb as a potential marker for this synthetic vascular SMC phenotype.

However, when comparing the tissue or cell cohort between the two sexes (see **Suppl. Figure 28.1**) both genes were found to at least be suitable for the comparison of different tissue samples from both male and female rats.

To give an impression of the impact of the stability of the RG expression the **Suppl. Figure 32.1** visualises the relative gene expression results of the male cohort when normalization is conducted to Gapdh instead of U2. The first notable difference in comparison to **Figure 29** is that it seems that in SMC culture all investigated genes are downregulated in their expression when comparing to the corresponding intact tissue of origin (**Suppl. Figure 32.1 A & B**). Regarding the individual comparison for each gene between tissue and cells (**Suppl. Figure 32.1 C**) the normalization to Gapdh results in a significant difference between tissue and cells expression of Gc-a which in the case of relative expression analysis to U2 was the only gene to remain at a physiological level after the cell extraction (**Figure 32 E**). Thus, normalization to an unsuitable RG can potentially lead to misinterpretation of a signalling pathway under investigation or in case of this thesis to a misjudgement of the impact of cell culture.

For the intended comparisons of expression levels previous studies served as a starting point for initial RG selection (see **Table 15**). The application of RG validation tools would have undeniably been less work intensive and time consuming than a literature research. It should be mentioned though that different validation tools come with specific advantages and disadvantages and often result in differing rankings for RG stability. Current research is therefore trying to combine the advantages of multiple validation software (Taki et al., 2014). Besides increasing efforts to optimize automized RG screening, the awareness of the importance of RG validation should increase.

To increase the chances of finding a suitable RG, genes involved in a broad variety of cellular processes were chosen for initial tests. Most candidates showed significant differences and because most of them are designated as HKGs (which are essential for cell survival) (Taki et al., 2014), this could be an indication of the extent of expressional changes in cultured vascular SMCs.

A group of genes that was characterized by the most stable expression was a group of ribonucleoproteins, the U-snRNPs (uridylic- rich small nuclear RNAs/ribonucleoproteins) also referred to as “snurps” (briefly mentioned in chapter **1.4.1**). Snurps are constitutively expressed, and their dysregulation is connected to several pathological stages (Vazquez-Arango & O'Reilly,

2018), which makes them promising RG candidates also for future expression studies. They play a pivotal role for the processing of pre-mRNAs as they target introns for excision. The majority of introns (~99%) are processed by the U2-type spliceosomes which consist of the U1, U2, U4, U5 and U6 snRNAs. This could be an explanation why ultimately, U2-expression was found to be the one unimpaired by the experimental conditions (chapter **4.1.2.4, Figures 29 & 30**). Surprisingly, U2 was even more stable than U5A which could mean that either the relevance or the frequency of the U2 snRNA is higher within the spliceosome. Additionally, this supports that a stable expression cannot even be expected from genes of the same family.

#### *5.1.2.2 Culture-induced changes in expression and function of cGMP-signalling components reveal promising directions for vascular research*

The phenomenon of culture induced changes in SMC relaxing signalling pathways has already been investigated in the early 90s. In a study performed by Suga and colleagues (Suga, Nakao, Mukoyama, et al., 1992) the researchers' aim was similar to the study question of the first thesis chapter. The researchers chose the same *in vitro* model (primary aortic rat cells), and an RNA based technique to support their hypothesis. The main realizations of Suga's publication support the findings of the present study.

Using Northern blot technique Suga and colleagues found Gc-b expression to increase upon culturing while Gc-a expression was hardly detectable in cultured rat aortic SMCs. Similarly to the present study, they found the level of NPRC mRNA to be augmented drastically upon culturing. In addition, they detected a change in the expression of actin variants (including Actb) and already suggested a change in the cells' phenotype to be the underlying cause.

Northern blotting, in contrast to qPCR, has a very low sensitivity, is labour intense and requires a very high quality of RNA (Yang et al., 2022). Because the classic protocols include extensive time windows for RNA handling the method unfortunately is quite prone to RNA degradation and contamination. It is obvious from the absolute Ct values of the qPCR measurements that the entire NP/cGMP signalling pathway is not very highly expressed. Therefore, RNA degradation due to contaminations of the northern blot samples could decrease the number of nucleic acids below the actual detection limit of the northern blot. This could potentially explain the missing Gc-a bands in the cell samples. Besides posttranslational modifications, RNA sample contaminations are most likely also the reason for poor resolution of the detected RNA-bands in Suga's publication.

An enormous advantage of the experimental design of the present study (**Figure 13**) is the possibility to directly compare the intact tissue and the primary cells retrieved from the exact same vessel of the exact same animal. In Suga's case, however, it is not described if the samples

from the cells and tissue were harvested from the same animals, and since northern blot requires a high concentration of the RNAs this is may not be the case. With regard to the direct comparison, it should also be highlighted that a valid quantification and comparison of changes between different samples can only be performed when the samples are on the same blotting membrane (Streit et al., 2009; Yang et al., 2022). Minor differences in the contrast of the membrane and thin lines between the columns suggest that the samples were not blotted on the same membrane (Figures 3 and 4 in (Suga, Nakao, Kishimoto, et al., 1992)).

At this stage of the discussion a short recap of the most relevant results obtained from the comparison in expression between the intact aortic smooth muscle layer and the retrieved cultured SMCs seems appropriate (see **Figures 31, 32 A** in the results section **4.1.3**):

**1)** The ratio between Gc-a and Gc-b expression is the opposite in tissue compared to the cultured cells. This is because Gc-b expression increases significantly, while Gc-a expression remains at the same level after isolation and culturing of the cells. In other words, it could be said that Gc-a seems to be the only gene investigated that remains at physiological levels in cultured vascular SMCs. The culture- induced dominance of the GC-B over the GC-A receptor can be observed at the functional level. After a longer period of culturing, vascular SMCs release more CNP- than ANP- induced cGMP.

**2)** The expression of sGC, as a key player in NO-related cGMP production, increases significantly upon culturing.

**3)** The most drastic increase in expression was found to be the one of the Np clearing receptor Nprc, which was barely expressed in the intact tissue but showed the highest expression level of all receptors investigated.

The three major observations will be discussed in the following sections.

#### *5.1.2.3 CNP/GC-B axis is more relevant in context of vascular disease than ANP/GC-A axis*

In comparison to the results by Suga (Suga, Nakao, Mukoyama, et al., 1992) it was interesting to see that the expression level of Gc-a seems to remain at physiological level throughout the process of isolation and culturing. This made the search for an appropriate RG extremely difficult, since it required the RG used for the normalization of the Ct values to be even more stable than Gc-a. Because of its stability between cells and tissue (see **Figure 32 B**), as well as between the different sexes (see **Figure 34 C, D**) Gc-a should be considered a promising RG candidate for future gene expression studies with primary aortic SMCs.

A more relevant observation regarding the specific receptors for ANP, BNP and CNP, however, is the increase in Gc-b expression and enzyme-function. GC-A and -B are known to be quite similar protein receptors when it comes to their shape, mechanism of activation and action (Potter,

2011a). Hence, it is surprising that GC-B but not GC-A changed under the experimental *in vitro* conditions. It seems reasonable to assume that the increase in GC-B is not only a coping mechanism in adapting to the changing SMC environment, but also that the CNP/GC-B axis could be more relevant in the context of vessel injury (Lehners et al., 2025).

ANP and BNP have a higher average plasma concentration than CNP. BNP, due to its lower binding affinity of NPRC and higher resistance to NEP (Ozaki et al., 1999; Suga, Nakao, Hosoda, et al., 1992; Watanabe et al., 1997), has the longest half-life and is therefore a well-established clinical marker for heart failure (Gaggin & Januzzi, 2013; Nishikimi & Nakagawa, 2022).

Under the name of vosoritide, CNP is actually the first NP based therapeutic with an approval for application in humans (Duggan, 2021). However, in comparison to ANP and BNP its therapeutic potential in the field of vascular disease still is underestimated. A recent review by Dickinson and colleagues provides detailed insights on the status quo in CNP-targeted research and highlights the importance of CNP, the underdog among the NPs, for the cardiovascular system and beyond (Dickinson et al., 2024). Furthermore, recent single-cell analysis studies share the impression that the CNP/GC-B/cGMP axis is a promising target, in the context of vascular disease and vessel injury (Lehners et al., 2025).

#### *5.1.2.4 NO-sGC-cGMP cascade indicates reproducibility of SMC phenotype related changes*

The eNOS-derived NO activation of sGC used to be negotiated as one of the most important regulatory systems in the human body (Kraehling & Sessa, 2017). As a second very important source of cGMP production sGC was therefore included in the expression analysis even though it has already been shown by earlier studies that sGC expression is altered in cultured vascular SMCs (Browner et al., 2004). The NO-sGC-cGMP pathway is known to be perturbed in multiple cardiovascular disease states where vasculature shows a significant decrease in the bioavailability of NO (Kraehling & Sessa, 2017). This has two potential underlying causes. Either a reduced NO production by the endothelium or, the cause more relevant to this study, an increased degradation of NO- induced cGMP production due to an increased expression of cGMP-degrading PDEs (Förstermann & Sessa, 2012). It would therefore be of interest to include the cGMP-degrading PDEs for subsequent gene expression studies using aortic SMCs. Considering their widespread use for the medical intervention in the cardiovascular field and knowing about their abundance and relevance in the vascular smooth muscle (see chapter **1.2.2.3**) it was surprising to see that there is hardly any literature to date that addresses the problem of culture-induced changes in PDE expression. Additionally, it would have been interesting to investigate sex-dependent differences in PDE expression. Wang and colleagues, for instance, found the PDE 1, 3, and 5 mRNA levels in microvascular endothelial cells and SMCs of vessels

that supply skeletal muscles to be sex- and age-dependent (Wang et al., 2010; Wang et al., 2021). Furthermore, it would have been of interest to correlate their gene expression with their contribution to the regulation of the cGMP levels measured using ELISA (see chapter **3.2.3.2**).

Similar to the qPCR data for the present study, Browner and colleagues, found sGC expression to increase in passaged rat aortic SMCs (Browner et al., 2004). Their study relied entirely on *in vitro* data, but no physiological level of sGC in intact vascular tissue was determined. In contrast, the present study elaborates the severity of the increase from the sGC tissue (Breitenstein et al., 2017) level upon culture (**Figure 32 E**) on basis of the direct comparison between intact media and the corresponding cultured cells. Nevertheless, it is reassuring to see that these culture-induced changes seem reproducible with varying study protocols of different research groups.

Again, it can be hypothesized that the increase in sGC expression is a compensatory mechanism to counteract the lack in NO (responsiveness) and to allow cell proliferation, growth and survival in culture and in cardiovascular pathology. The relevance of this cascade for therapeutic research becomes apparent through the numerous sGC stimulators and activators (Breitenstein et al., 2017).

#### *5.1.2.5 Drastic increase in Nprc expression upon cell culture suggests a physiological role beyond the clearance of natriuretic peptides*

NPRC is the most represented NPR in the human body (Fuller et al., 1988). It can be found in endocrine glands, the kidneys, lungs and most importantly in the endothelium. In the present study, NPRC showed the most drastic increase in its expression level upon isolation and culturing of the aortic SMCs. From being barely expressed in intact *tunica media*, NPRC turns out to be the NP receptor with the highest expression level in cell culture (**Figure 32 A**). This phenomenon has already been described in former *in vitro* investigations (Suga, Nakao, Mukoyama, et al., 1992).

In a study by Li and colleagues the researchers induced an increase in NPRC by knocking out GC-A in cultured A10 cells (a cell line from embryonic rat thoracic aorta) (Li et al., 2012; Rao et al., 1997) using an siRNA transfection approach. However, since in the experiments of this thesis no significant change in Gc-a expression was detected (**Figures 32 A, B**) but still a tremendous increase in Nprc expression was visible in culture, it is questionable whether a drop in Gc-a expression is an actual reason for the NPRC alteration *in vitro*. When performing an explorative correlation analysis between the relative gene expression of Gc-a and Nprc of the cultured SMCs (**Suppl. Figure 31.1**), the Spearman coefficient (rs) is calculated in between 0 to 1, which means that a positive correlation of both genes is possible but not certain. If this would be confirmed in following studies this would speak against the conclusion drawn by Li's group but does not mean

that a significant decrease in Gc-a expression could not result in an even more enhanced NPRC increase.

It is highly likely that the sudden increase in Nprc expression indicates or even promotes the transition of vascular SMCs towards another phenotype. Nprc signalling was found to be coupled to adenylyl cyclase inhibition and PLCβ activation (Anand-Srivastava et al., 1990) which both play an essential role for Ca2+-dependent SMC contractility (see **Figure 3**). An increase in NPRC could therefore indicate the cellular transition towards a more synthetic non-contractile (see **Figure 2**) or even towards a diseased phenotype, since NPRC was found to promote artherogenesis (Cheng et al., 2023).

Furthermore, there is considerable recent evidence that the NPRC possess capacities far beyond the clearance of NPs (Dickinson et al., 2024). For instance, it was found that the proangiogenic capacity of CNP is NPRC but not GC-B mediated (Bubb et al., 2019). This not only highlights the relevance of the CNP/GC-B axis (as discussed in the previous chapter 5.1.2.3) but also shows that the influence of NPRC on the NP-system (Matsukawa et al., 1999) should most definitely not be underestimated.

Thus, future studies to explore the therapeutic potential of NPRC are needed and may unveil NPRC as a reliable biomarker for certain pathological stages in cardiovascular disease.

### 5.1.3 Advantages and limitations of applied methods to investigate culture-induced changes of the natriuretic peptide receptors

The following section elaborates the eligibility and reliability of the methods chosen to achieve the aims of the vascular chapter in this thesis (see chapter **2.1**). Hence, the advantages and limitations of the techniques RT-qPCR and cGMP-specific ELISA will be discussed. It should be mentioned again that this study benefits from its sophisticated experimental design that allows direct comparison of gene expression levels from intact tissue and corresponding isolated cells as well as receptor function of the exact same cells from the same aorta for each experiment. This again highlights the convenient size of the aorta and the thickness of the tunica media which allows a decent harvest of primary SMCs (as mentioned in chapter **5.1.1** above).

A big accomplishment, and advantage over previous studies (Suga, Nakao, Mukoyama, et al., 1992), was the identification of U2 as an eligible RG for the direct comparison of *in vivo* and *in vitro* expression which again highlights the importance of constant RG re-evaluation and validation, as well as the improvement of appropriate software to facilitate this process (as already discussed in chapter **5.1.2.1** above).

#### *5.1.3.1 RT-qPCR- Advantages and limitations*

Even though RT-qPCR has been around for a while now it is still the commonly preferred technique for gene expression measurement. The technique is valued for its accuracy and reliability which is why it often serves to validate data obtained using other methods (Kozera & Rapacz, 2013). It is characterized by a high sensitivity, precision and speed of the detection at real time (Gachon et al., 2004). In cases where the amount of mRNA copies of a gene is very low, RT-qPCR often remains the last option for a reliable detection of any gene expression. This is to the advantage of this study, because initial tests for this thesis already indicated that a few key players in the cGMP signalling cascade seem to show a rather low expression rate (Lehners et al., 2025).

Although RT-qPCR is a standard in most molecular biology labs, its application and evaluation is not trivial. Most research groups have their own protocols for sample preparation and processing, which makes the comparison between different studies almost impossible (Bustin et al., 2005). In addition, it is extremely important to keep in mind that the level of gene expression does not directly translate to the amount of protein, due to post-translational modifications. In the case of NPRs GC-A and -B these are for instance phosphorylation (Potter, 2005, 2011a) and glycosylation (Müller et al., 2002). Gene expression data should therefore ideally be represented in combination with protein or other functional data.

#### *5.1.3.2 cGMP-ELISA – Advantages and limitations*

In the past, the team of Prof. Middendorff was hired to test commercially available NPR-antibodies for their specificity and application for diagnostic purposes. Back then (almost 20 years ago) a wide range of NPR receptor antibodies was already available, but only few were found to be specific enough to allow a reliable evaluation of the GCs' protein status. One explanation could be that both transmembrane receptors are expressed at a presumably low level in the SMCs (Lehners et al., 2025).

Nevertheless, the biggest issue remaining is that the antibodies for GC-A show a notable cross-reactivity with the GC-B antigen, which makes the simultaneous detection of the ANP and CNP-specific receptors in the same sample difficult. In addition, reliable antibodies for the NP clearing receptor are still scarce.

Hence, the cGMP-ELISA (see chapter **3.2.3.2, Figure 20**) was chosen to evaluate the amount of intracellular cGMP release upon activation of GC-A and -B by NP treatment. This competitive ELISA is highly specific for cGMP and detects even smallest concentrations within a pmol-range. Therefore, this assay was suitable for not only cell-based experimental approaches but also enabled the detection of cGMP released from the intact *tunica media* samples. A disadvantage

here was, however, that it required a lot of tissue to reach a detectable range of cGMP and thus, permitted to focus on specific aortic sections. The cell-based approach allowed the measurement of ANP and CNP-induced cGMP in the cells of the same animals analysed in the gene expression part of this study.

Nevertheless, there are a few limitations that should be taken into consideration when interpreting the cGMP levels. Firstly, the cGMP levels measured by ELISA do not directly equate to the amount of GC-A and GC-B protein of the samples. They should at most be seen as an indirect indicator of the receptor activation upon the treatment with the respective ligand (ANP or CNP, respectively). Indirect because the intracellular cGMP release not only depends on the amount of protein but also on the phosphorylation status of intracellular STRs of the NP receptors (see chapter **1.2.2.3, Figure 9**).

Secondly, there are additional proteins involved in the fine tuning of the cGMP level that are not sufficiently or at all blocked during the execution of the assay. These include NEP and NPRC, which both degrade NPs, as well as the cGMP degrading PDE 9, which is not targeted by the applied PDE inhibitor IBMX (Gupta et al., 2020).

Thirdly, due to the compact structure and thickness of the aortic *tunica media* it is impossible to estimate how many SMCs are exposed to the externally applied NPs or how much of the intracellular cGMP is released into the medium surrounding the tissue. This is of relevance especially for the measurements of cGMP release from the intact vessel tissue.

While all these individual points mentioned would require mindful optimization of the assay performed, it is worth considering other methods for future studies. In the past the Middendorff lab performed UV-induced affinity crosslinking to assess differences in the size of the GCs due to post-translational modifications (Müller et al., 2002). In principle this method works like standard SDS-PAGE, but in comparison to a classic WB, proteins are detected through binding of radiolabelled analogues of their respective ligands rather than an antibody-antigen-reaction. In the case of the NPRs iodinated ANP, CNP and cANF. The latter is an artificial variant of ANP that carries a ring-deletion and binds NPRC selectively (Almeida et al., 2014). While the downside of this method is the handling of radioactive materials, UV-crosslinking outranks WB for protein analysis when it comes to the specificity of NPR detection. Hence, UV-crosslinking circumvents the remaining lack in highly specific antibodies for GC-A, GC-B and NPRC and could potentially add valuable results in future studies.

### 5.1.4 Influence of sex differences on the cGMP system in vascular smooth muscle

Sex-differences are a hot topic of current research, and the influence of sex hormones is, besides the cell type under investigation and the influence of cGMP on their contraction, another conduit between the cardiovascular and the reproductive chapter of this thesis. While SMCs play multiple roles in both systems, key players of cGMP related signalling pathways are either known to be under hormonal regulation or involved in reproductive processes. To give a brief example, the CNP/GC-B axis is relevant for mammalian oocyte meiosis (Jaffe & Egbert, 2017) and CNP was detectable in seminal fluid of male swine (Chrisman et al., 1993).

#### *5.1.4.1 Persistent lack in female-focused studies*

Over the last decade the underrepresentation of female study subjects has gained attention (Baylis, 2010; Kim et al., 2010; Wong et al., 2013). Traditionally, novel therapeutics were predominantly tailored to the male sex, even though it is known that sex-differences are detectable in the manifestation (Hirakawa et al., 2007; Legato, 2004) and prevalence of cardiac disease. These differences interestingly often imply a hormonal protection in favour of females (Campos et al., 2014; Gardner et al., 2008). Ambiguous study results caused by unpredictable hormonal fluctuations in female cohorts often served as a potentially unjustified reason for this persistent sex-bias. However, the fact that therefore half of the population worldwide may experience insufficient or incorrect treatment should be more than reason to increase a focus on female-centred studies.

The initial inspiration to consider both sexes for this thesis arose from a recent publication by the Potter group (Wagner et al., 2022). In this study they used a CRISPR mouse model which upon sensitization of GC-A through ANP treatment is characterized by an irreversible phosphorylation of the cell internal STRs (see introduction chapter **1.2.2.3, Figure 9**). In other words, no desensitization of the GC-A occurs upon its maximum activation. In cGMP measurements of cardiac protein from male and female WT and the GC-A overactive mice (henceforth referred to as mutant) ((Wagner et al., 2022); Figure 2A), it was interesting to see that the male mutant barely reached a cGMP level as high as the female WT. Besides a sex-dependent difference in the amount of GC-A protein, which according to Wagner's publication (Figure 2C) did not seem to be the case, a higher basic level of phosphorylation of the STRs of the GC-A receptors in females could be a plausible explanation.

In accordance with the results of the present thesis (see gene expression results **Figure 32**), the female measurements showed a larger spread than the male data points, most likely because of

hormonal fluctuations. However, Potter's study did not include the determination of the estrus cycle stage in their female mice, and the observation was not further addressed.

Regarding the NP/cGMP cascade, it is remarkable that most studies focusing on the biological sex thus far are limited to the heart and rarely include the adjacent vasculature (Wagner et al., 2022; Wong et al., 2013). Especially, studies comparing singularized cells to their tissue of origin lack sex-dependent insights. This highlights the relevance of the knowledge gained in this thesis and points out possible directions for the scientific focus in the future.

#### *5.1.4.2 Impact of sex hormones on vascular NP/cGMP signalling and underestimating of the female estrus cycle*

In a 2013 study (Wong et al., 2013), researchers observed sex-difference in the cardiac expression of the NP (ANP, BNP) and NO system (NOS). Based on their findings, they proposed that cGMP production in males predominantly occurs through the NP system while the female physiology seems favour the NO axis.

In Wong's study, the levels of Gc-a and sGC in intact aortic tissue (see results **Figure 32 G**) only showed a trend towards a higher expression, in females and no significant difference between both sexes. Sex-differences in Gc-a and sGC expression therefore remain to be further investigated in the future.

As shown in earlier studies (Jankowski et al., 2005) and confirmed by Wong's work (Wong et al., 2013), cGMP production is influenced by ovarian hormones. Wong found differences in the cardiac expression of NO system-related genes between the proestrus and estrus stages of female rats. This additional layer of hormonal regulation of the cGMP system may serve as explanation for the higher spread in female expression levels. Hence, the determination of the cyclic stages in follow up studies would be essential (Cora et al., 2015). The dependence of the NP system on the cyclic stages and its sensitivity to hormonal treatment in the rat ovary is, however, already confirmed (Jankowski et al., 1997; Noubani et al., 2000; Reis et al., 1997).

#### *5.1.4.3 Loss of sexual identity in vascular smooth muscle cells in culture*

Former studies aimed to reveal a sex-dimorphism between vascular SMCs used in cell culture (Loukotová et al., 1998). In view of the comparison of aortic tissue and cells, the question that consequently arises is to what extent hormonal influences are retained when the vascular SMCs are isolated and cultured. A logical assumption would be that the absence of the reproductive organs and, - in the case of females the missing fluctuation of the sexual hormones, may eventually lead to an equalization of the cGMP system in cells of both sexes. Persisting differences between male and female culture on the other side would suggest that the cells maintain a "sex-memory" (Malorni et al., 2008).

Malorni and colleagues isolated and cultured aortic vascular SMCs from male and female rats to assess their susceptibility to oxidative stress. In early passages they found a sex-difference in the ratio between the estrogen receptors ERα and ERβ which seemed to be correlated with the cells' response to UV-radiation. While the male SMCs seemed more susceptible to radiation induced stress and were found to be more apoptotic-prone, female cells tend to fall into a mitotic arrest, also known as senescence. They hypothesized that freshly isolated vascular SMCs are capable of conserving a sex-memory in early passages (Malorni et al., 2008). Additionally, the researchers claimed that the sex-dimorphism in the ratio of the estrogen receptor expression vanished over longer periods of culturing.

Unfortunately, the gene expression profile observed in this study (**Figure 32 G, H**) did not show any significant differences between male and female rats and with the lack of significant sex-related differences already at tissue level, the data does unfortunately not allow any conclusions to be made in terms of the preservation of a sex memory in the extracted primary cells. It is interesting to see though that even in cell culture, SMCs of female origin seem to display a larger spread in their gene expression levels for all GOIs. The determination of the cycle stages and hormone levels of female study subject at the time of the organ harvest could therefore be a relevant addition for future studies. In this regard it would also be beneficial to include sex-hormone receptors into the gene expression study.

#### *5.1.4.4 Sex-differences beyond gene translation*

In contrast to the gene expression results, the determination of the enzyme activity of GC-A and GC-B by cGMP ELISA (chapter **3.2.3.2**) upon ANP and CNP treatment revealed minor differences between both sexes. After the treatment of one half of the intact aortic *tunica media* with ANP and of the other with CNP, the pairwise analysis showed a significant difference between the ANP- and CNP-induced cGMP production in the male but not in the female study group (see **Figure 33 B, C**). However, when comparing ANP-induced cGMP levels between male and female rats using an unpaired analysis, no significant difference was visible (see **Figure 33 E**). Comparable results were found for the CNP effects (see **Figure 33 F**). The significance in the pairwise analysis might be due to the large spread of the ANP-induced cGMP effects. The reasons for this spread in intact tissues, however, are not yet understood. A difference in the size of the animals and thus a difference in the amount of tissue used for the analysis was accounted for, since the cGMP level was normalized to the tissue weight.

Similar significant effects were found in the cultured SMCs when comparing sex-specific ANP- and CNP-induced cGMP production using pairwise comparison (see **Figure 34 B, C**), in contrast to ANP- or CNP-effects separately with non-pairwise analysis (see **Figure 34 E, F**). In the SMCs of

passage 1 (P1), ANP treatment induced higher cGMP levels than CNP (see **Figure 34 A**). This was the inverse to the mRNA expression of the ANP and CNP receptors in the SMCs of the same passage and from the same animals, i.e., Gc-b significantly exceeded Gc-a expression (see **Figure 31 B**). In the following passage (P2), however, the CNP-induced cGMP production of the cultured cells began to exceed the ANP-induced cGMP production. Even though this effect was readily visible in graphs (**Figure 35**), it did not reach statistical significance when performing pairwise comparisons. This might reflect that the typical Gc-a and Gc-b pattern at the mRNA level (Gc-b mRNA > Gc-a mRNA) in cell culture has now been translated to the protein level (GC-B > GC-A) visible by the receptors' cGMP production. Future experiments to characterize the exact timeline of the expressional switch and the subsequent adaptation at the protein level could help to define a time window during which the cells reflect the NPR status at the protein level and could therefore be of use for functional studies on GC-A and GC-B receptor interactions.

### 5.1.5 Outlook – Vasculature

The data in this thesis clearly demonstrates the significant changes in vascular SMCs due to phenotypic alterations induced by cell culture that have not been observed in early studies (Suga, Nakao, Kishimoto, et al., 1992; Worth et al., 2001). Future research that includes *in vitro* data only therefore must be verified in terms of relatability to the *in vivo* case. Nevertheless, vascular SMC culture has enormous potential as a future *in vitro* model for vascular disease (chapter **5.1.1.3**).

Both, the comparison of SMC culture with healthy intact tissue or tissue affected by a certain disease highlight the demand for appropriate RGs. Therefore, it would be essential to standardize the requirements for reliable RGs and to continuously improve databanks and searching tools that facilitate the identification process of RGs depending on the individual research question (Xie et al., 2023).

If cell culture would be confirmed as a way to mimic pathophysiological mechanisms, *in vitro* culture using isolated primary vascular SMCs could help to identify and develop pioneering therapeutical approaches. Having said that and considering the results of this work, it is surprising that NPs, CNP in particular, as potential treatment options for certain types of cardiovascular disease are still being largely neglected.

Another aspect that should continue to be eagerly investigated, especially for the development of more patient-specific therapies, is the influence of sexual hormones on the smooth muscle relaxing signalling pathways. The larger spread of the female data in the present study suggests that future studies should definitely investigate the influence of different oestrus cyclic stages and life phases of women in particular.

## 5.2 Male reproductive tract

An initial step in the testing of men for infertility or sterility is a seminogram (Gatimel et al., 2017). A seminogram includes the microscopic assessment of sperm count, shape and sperm motility (Waberski et al., 2022) and ranks the results according to normed standards (Chawre et al., 2024). The application of live imaging for diagnostic purposes therefore is routinely used by andrologists. Often, however, other factors besides sperm vitality contributes towards a man's inability to procreate. In most of these cases the malfunction of SMCs is involved. This can for instance interfere with the capability to maintain an erection (Chen & Jiang, 2018), with an unimpaired performance of the accessory glands (Exintaris et al., 2006; Thorpe & Neal, 2003) or with the frequent transport of semen through small canals in the testis and adjacent epididymis (Elfgen et al., 2018; Müller et al., 2011; Robaire & Hinton, 2015; Stadler et al., 2021). The subsequent sections will discuss the steps taken to develop and improve an imaging analysis specifically tailored to the evaluation of ST contractions in rats. In the subsequent chapter, advantages and disadvantages of said technique and the animal model chosen will be discussed and main results, as well as reasons for unexpected findings, will be evaluated.

### 5.2.1 The transferability from rat to human is limited - Advantages and disadvantages of the animal model

Results from this chapter reiterated the notion that data obtained in *in vitro* settings should be handled with caution and why the application of cell culture lately is accompanied by more scepticism than *in vivo* studies.

Rodents, as small, quickly procreating mammals, are the preferred animal model in research (Meek et al., 2017). However, even though their physiology is closer to humans there are undeniable differences which should be considered when extrapolating from animal studies. Some of these, in relation to their reproductive tract, were briefly explained in the introductory chapters **1.5.1.1** and **1.5.1.2**.

Spermatogenesis and sperm production in rodents are a lot faster than in humans. Rats and mice mature, mate and procreate more frequently. Therefore, it is reasonable that the intensity of the spontaneous wall contractions in the rat STs is a lot more vigorous than it is in humans, to ensure a steady flow of semen through the testis. It is fascinating to consider that these notable forces in rodents are accomplished by a single layer of peritubular SMCs (**Figure 15 B**) (Ellis et al., 1981), while in the human case the SMCs of the STs is multilayered. A second reason why more intense contractions might be necessary in rodents is that their sperm acrosomes, the head-part of the

sperm, are hook-shaped (Lin et al., 2013; Tourmente et al., 2016), hence more forceful contractions could be beneficial to release the spermatozoa from the GE. This leads directly to another very important difference between rats and male humans, which is the arrangement of spermatogenic stages of the GE in sections following one after another, whereas in human STs the stages are arranged in a spiral shaped manner (**Figure 17**) (Chaturvedi & Johnson, 1993).

This anatomical feature is a major advantage to investigate the contractile behaviour in relation to spermatogenesis and to test the hypothesis whether the distinct morphology of the smooth muscle and the GE in each stage has an impact on the transfer of the superficial contractions from the outer wall towards the tubular lumen.

### 5.2.2 Advantages and disadvantages of the live imaging approach

The selection of specific spermatogenic stages based on their appearance in brightfield microscopy (Parvinen & Vanha-Perttula, 1972) is convenient and the size of the rat organs makes the handling of the fragile testicular tissue manageable. Another advantage of the *ex vivo* procedure is that the STs remain intact and stay vital under life-sustaining measures. The live imaging setup (**Figure 22**) allows for the maintenance of a physiological temperature, which in the case of the testis in rats is slightly below body temperature, and the supply of nutrients at a constant flow rate (Mietens et al., 2014). Furthermore, the treatment of isolated STs with different substances is facilitated and the setup allows for consecutive treatments over a longer period of time. However, it should be noted that the dissection of the singularized tubules damages the tissue, where a few physiological circumstances that have an impact on the motility of the tissue are not sustained. For instance, the absence of interstitial Leydig cells (Müller et al., 2011) as the predominant source of testosterone is known to affect SMC contractility and replication (Gur et al., 2020; Jia et al., 2024). Or the removal of the testicular capsule, the *tunica albuginea*, which keeps the STs tightly packed together and provides structural support for the testis (Schmidt et al., 2023). This could lower the resistance that is posed on the STs externally and might decrease the range of their spontaneous contractions. Lastly, the STs are unnaturally stretched out for the *ex vivo* imaging approach, while a curvature of the semen canals usually would slow down the flow rate of the seminal fluid through the lumen.

### 5.2.3 Advantages and disadvantages of the FIJI analysis in comparison to previous methods

The most obvious advantage of the newly developed FIJI analysis is the simultaneous detection and less subjective evaluation of tissue movements in the entire section in focus. Thus far,

approaches, like the kymographs or Fourier analysis (**Figure 18**) were limited to single tissue sections followed over the period of the recording. In case of the kymographs for instance, the selection for the reslice position and counting of the peaks largely depended on the perception of the individual that performed the analysis. The novel semiautomated FIJI code analyses the original recordings faster and with more precision and ensures the exact same evaluation settings (amplitude threshold for peak detection, normalization for contrast fluctuations etc.) for an entire cohort of recordings.

From an analytical perspective, Fourier analysis (Byrne et al., 2013) remains the most sophisticated way to unravel the mechanics of ST contractions, because the resolution of the frequency and amplitude patterns of these superficial contractions can be very detailed. Nevertheless, Fourier is complex and requires high mathematical skill. In addition, the outcome for this specific analysis is intellectually challenging, hard to interpret and therefore harder to grasp for people outside of this specific field in research.

The latest stage of the FIJI movement analysis entails a separate read out for the overall movement intensity, scored mainly based on pixel intensity fluctuation, frequency and the amplitude. The code was specifically tailored to answer research questions for this part of the study and therefore also the readout is condensed to the most relevant results. The display as bubble plots makes the data more accessible than the previous display as cumulative frequency curves. In the early developmental stages of the FIJI plugin these cumulative curves often showed a statistically significant difference between the compared cohorts (spermatogenic stage, e.g., **Figure 36** or substance treatment, e.g., **Figure 38**) even though for a large part they seemed to overlap which made it difficult to conclude that this difference is of physiological relevance. But at that stage it was still the case that the majority of pixels analysed showed minimal to no movement and thus contributed to the overlap of the curves. In the final stage of the FIJI code the evaluation only focused on areas within the tissue that previously showed a large movement score and thus reduced the amount of interference from pixels that did not move. In addition, the visualization as bubble plots made potentially physiological differences more recognisable and furthermore allowed one an estimate of the contribution of the frequency and amplitude to the difference in the movement patterns between the spermatogenic stages or different treatments.

A downside of this analysis is that the coding aspects and adaptation of the FIJI interface require specific skillsets. Another disadvantage is that the decimation of the originally recorded live imaging sequences may result in blurring of the data and therefore could cause the loss of potentially meaningful observations. This already flagged another drawback of the Fiji analysis

tool, which is that the inputs and the outputs for the analysis requires a large RAM and storage capacity.

Lastly, it should be noted that the evaluation of tissue contractions based on contrast fluctuations allows for a very precise resolution of movement because the technology is able to detect and distinguish between numerous shades on the grey scale. At the same time the contrast detection faces limitations, especially on the very bright or very dark end of the grey spectrum. The latter is the reason why no luminal movement could be in the dark tubules. To answer the question whether the spontaneous or pharmacologically induced contractions of the tubular wall trigger luminal transport of the sperm during spermiation it would be necessary to adjust the illumination of the lumen for the sake of the proper detection of the wall, which as the location of the PTCs was the main region of interest in this thesis.

Nevertheless, it is a promising tool that holds enormous potential to assist with the diagnosis of SMC related disease in the reproductive tract and beyond in the near future.

### 5.2.4 Spermatogenesis impacts spontaneous contractile behaviour of seminiferous tubules

At every stage of the code development for the unified analysis of the contraction amplitude, frequency and movement intensity, a significant difference between the spermatogenic stages dark (before spermiation) and pale (after spermiation) was detectable. The original movement score analysis (Stadler et al., 2021) detected more vigorous contractions in the pale tubules (**Figure 36**). The frequency analysis showed a different distribution of ROIs with different contraction frequencies (**Figure 39**). Overall, it seemed that the dark STs had a slightly higher number of ROIs with a very high frequency. This, however, shows that the amplitude is more important for the calculation of the general movement intensity, which is ranked according to the movement score. Lastly, the unified analysis for the spontaneous contractions revealed a notable shift towards a higher frequency, amplitude and movement intensity for the pale cohort (**Figure 42**).

These results show indisputably a correlation between spermatogenesis and the contraction performance of the STs. It could be hypothesized that the rhythm of the spontaneous ST contractions is coordinated with the timing of the spermatogenesis. This, however, would mean that there must be certain triggers of the peritubular SMCs to adjust their contractions accordingly. One signalling mechanism that seems reasonable is the activation of stretch-induced baroreceptors in the outer tubular layer that respond to the change in pressure depending on the filling status of the tubular lumen. Another reason of a mechanical nature

related to the filling status could just simply be that the tighter tubular lumen is filled with sperm the more it limits the actual contraction range. An analogy for that could be a water hose that is held shut in from with the tap fully turned on and the movement of the hose when the spout is suddenly opened.

In addition, there could be signalling molecules secreted by the spermatogonia/spermatozoa (Kaupp & Strünker, 2017) to signal either the decrease or increase in spontaneous contractions to the PTCs. Similar to the regulation of the blood pressure in the aorta (Togashi et al., 1992; Umans & Levi, 1995) this could either regulate the flow rate of the seminal fluid or could facilitate the sperm cell release from the GE and their passage of the blood-testis-barrier that protects the sperm cells during their maturation (**Figures 15 & 16**) (Wanjari & Gopalakrishnan, 2024).

The signalling molecules and respective receptors involved remain to be investigated more specifically. A first step in mimicking the fine tuning of the sperm transport in the STs was the targeted treatment of dark and pale tubules with SMC relaxing and contracting stimulants that will be discussed in the following section.

### 5.2.5 Smooth muscle relaxing and contracting stimulants affect spontaneous contractions of seminiferous tubules depending on their spermatogenic stage

The rationale behind the treatment with an NO donor was to facilitate the flow of the seminal fluid through the tubular lumen passively, by relaxation of the SMCs and therefore dilation of potentially the whole tubule.

The final, as well as the intermediate, stages of the FIJI unified movement analysis detected a reduction in the spontaneous movement (**Figures 37, 40 & 43**), regardless of the spermatogenic stage of the ST. The difference between the relative movement score results, based on the comparison of the spontaneous versus the NO-induced movement scores, was not found to be statistically significant between the two spermatogenic stages (**Figure 37 E**). It could therefore be hypothesized that the NO treatment induces an equipotent smooth muscle relaxation on dark and pale rat STs.

According to the unified results the biggest change in the spontaneous contraction pattern due to the NO treatment was achieved in the ST wall (**Figure 43**). This again was expected since the cells expressing the NO receptor sGC are located in the outer layer of the tubules.

Even though the NO effect was as expected the question as to where NO under normal circumstances would be released remains. As a gaseous signalling molecule (Garcia & Stein, 2006), NO diffuses through multiple cell layers and even beyond the blood-testis-barrier (Hau et

al., 2023). Therefore, different sources of NO, like for instance the spermatogonia or spermatozoa, the vascular cells of smaller vessels near the tubules or the Leydig cells in the interstitial compartment of the testis are possible. Potential future experiments to clarify this could include the detection of the NOS enzymes in testicular tubules of different spermatogenic stages at the level of gene and protein expression. In previous studies, NOS were detectable at the level of gene expression in Sertoli and Leydig cells, as well as in human and rat spermatids (Staicu et al., 2019: Wang et al., 2014). iNOS is known to be of particular interest in inflammatory circumstances (O'Bryan et al., 2000). Singh and Lal demonstrated a "[...] reproductive-stage dependent, cell specific existence [...]" of iNOS and nNOS in testis of the catfish (Singh & Lal 2017). However, until now, little is known about the expressional landscape of the different NOS in different spermatogenic stages in rodents and humans.

In addition, it is important to address the cGMP degradation, downstream of the NO production and binding to sGC, that is mainly performed by cGMP specific PDEs (see chapter **1.2.2.3**). It was found that pharmacological treatment with NO interfered with the expression of PDEs in pulmonary arteries (Busch et al., 2010). If the same is the case in the testis and especially in different spermatogenic stages of the STs remains to be investigated.

The treatment with NA surprisingly showed the exact opposite effect of the expected outcome. NA, which is known to induce SMC contractions (chapters **1.2.1**, **1.5.1.4**), in earlier studies by the Middendorff lab served as a vitality control for tissues of the male reproductive tract (Stadler et al., 2021; Weiser et al., 2020). However, it was very surprising to see that NA induced a very minor response in the testicular tissue, and if at all seemed to decrease the tissue contractility rather than to increase it. Running the unified movement analysis, the code detected a shift of the spontaneous cohort towards a lower frequency and amplitude, which resulted, in both the dark (**Figure 46**) and the pale cohort (**Figure 45**), in a reduction of the average bubble size. These unexpected findings matched the earlier results of the movements score (**Figure 38**) and frequency only analyses (**Figure 41**). Reasons for the contraction dampening effect of NA remain to be investigated, but an initial step should be to assess the abundance of different adrenergic receptors in the PTCs of STs in different spermatogenic stages (Mazumder et al., 1985). Early studies confirmed the localization and activity of beta-adrenergic receptors in interstitial and Sertoli cells which upon activation could potentially induce an opposing effect in the testicular than the related alpha-adrenoceptors (Eikvar et al. 1993; Poyet & Labrie, 1987). This explanation seems to be the most reasonable considering that the beta 2-adrenergic subtype was found to be the most prominent in rat testis with the highest density detected in interstitial cells while some was found in the STs (Tolszczuk et al., 1988).

Another reason could be the NA concentration used for the contraction studies which, similar to the NO donor treatment (Dutta & Sengupta, 2022), is a lot higher than physiological levels under normal circumstances and could potentially be harmful for the tissue. In subsequent studies it thus would be essential to perform a dose-response curve and ideally to lower the concentration of NA to a more physiological level. Furthermore, the lack of a tissue response could also mean that the tissue is already dying but in experiments, using the same imaging set up with reproductive tissue samples overnight, the tissue in most cases remained responsive to substances such as NA and potassium chloride until the next day (data not shown). Lastly, it is plausible that the response of the tissue to NA is a unique and quick cramp-like shrinking of the tissue. In this case the FJI code analysis, which is more intent for continuous movements with a specific amplitude and frequency, would not detect a significant change in the contractility of the tissue. To induce a contractile response in future studies the treatment with other substances such as potassium chloride or ideally with agonists that are selective for alpha-adrenergic receptors such as phenylephrine or methoxamine should be considered to avoid co-stimulation of beta-adrenergic receptors.

### 5.2.6 Outlook – Reproductive tract

The application of the newly developed FIJI-based live imaging analysis for the detection of smooth muscle-related male reproductive disease holds enormous potential for future diagnosis and andrology. Therefore, the development of a fully automated operation system that is simple to navigate would be necessary. Furthermore, the immediate adaptation of the analysis to different tissues (e.g., prostate, epididymis, vas deferens) that are being investigated could be pursued. To achieve this, the inclusion of generative AI for automated analysis is a possibility. However, this would depend on adequate training of the AI that would require the recording of healthy tissue samples. This reveals a fundamental problem in basic research which is generally the lack of healthy donor tissue, since in very rare cases young men without specific reason would give their consent for the retrieval of a biopsy. To circumvent this problem, the development of an *in vivo* live imaging approach that no longer requires the dissection of the tissue from the body would be pioneering.

Regarding the testis, it would be interesting to focus on different areas of the testis such as the *rete testis* at the transition zone to the adjacent epididymis and to see whether the localization of the STs within the testicular capsule has an influence on the contractile behaviour and to see how they would respond to the treatments with different substances.

With regard to the singularized STs, a more precise resolution for the transition of the contraction or relaxation from the ST wall towards the inner lumen could add knowledge to the general understanding of testicular tissue contractions and identify most relevant cellular components.

The combination of the live imaging procedure with fluorescence staining of specific cell types (e.g., different stages of the gametes, Sertoli cells, or the PTCs) could facilitate the visualization of the passage of spermatogonia over the BTB and the tracking of the developing sperm cells while they move through the GE towards the lumen. In both cases it is thinkable that the wall contractions facilitate these processes.

In addition, the application of genetically modified mice that allow the live tracking of cGMP flux *in vivo* (Thunemann et al., 2013) and to follow transcellular signalling could be helpful. An additional advantage of the latter would also be that the relaxing and contracting capacity of different substances could be assessed. Referring to the first chapter of this thesis the NPs could be promising group to look at, especially CNP (Chrisman et al., 1993; Dickinson et al., 2024).

# Supplements

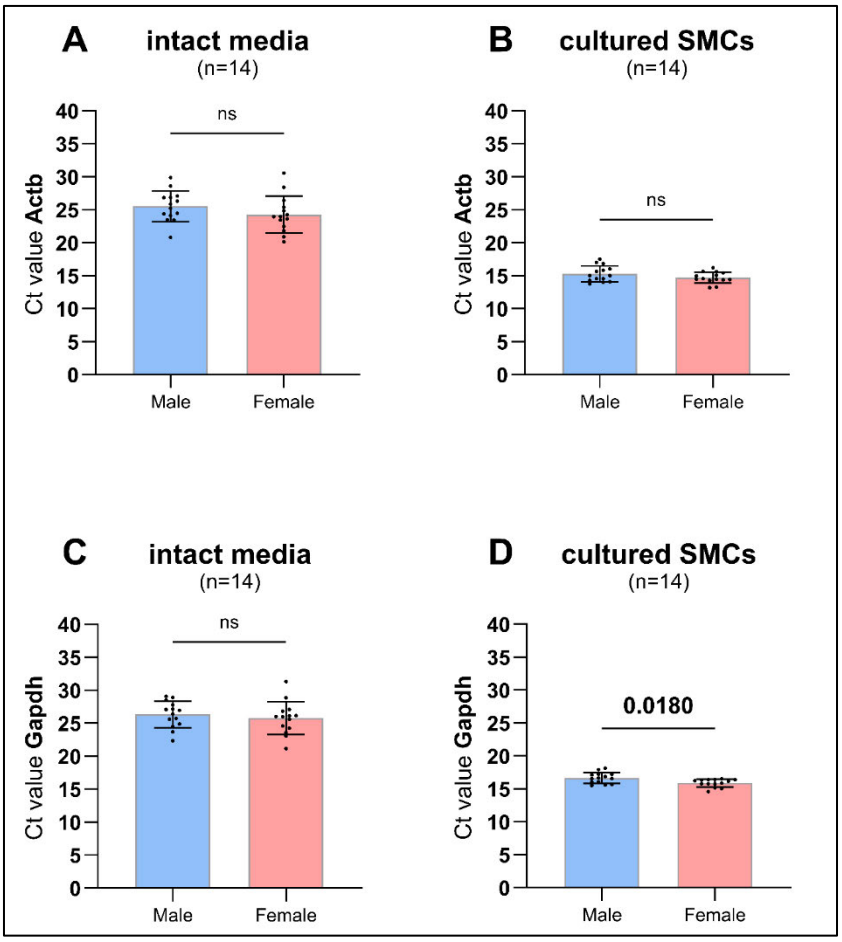


***Supp. 28.1**: Sex-dependent comparison of classical reference gene expression in intact media and corresponding cultured smooth muscle cells of male and female rat aortae.*

Comparison of the absolute cycle threshold (Ct) values of **A, B)** beta-actin (Actb) and **C, D)** glyceraldehyde-3-phosphate-dehydrogenase (Gapdh) in **A, C)** intact aortic tunica media and **B, D)** cultured smooth muscle cells (SMCs). Ct values of male (blue bars, n=14) and female (pink bars, n=14) rats. The comparison according unpaired, non-parametric Mann Whitney test only revealed the difference between male and female expression to be non-significant(ns). Only between the expression of Gapdh in cultured SMCs a significant difference was detectable (p=0.018). Whiskers indicate ± SD.

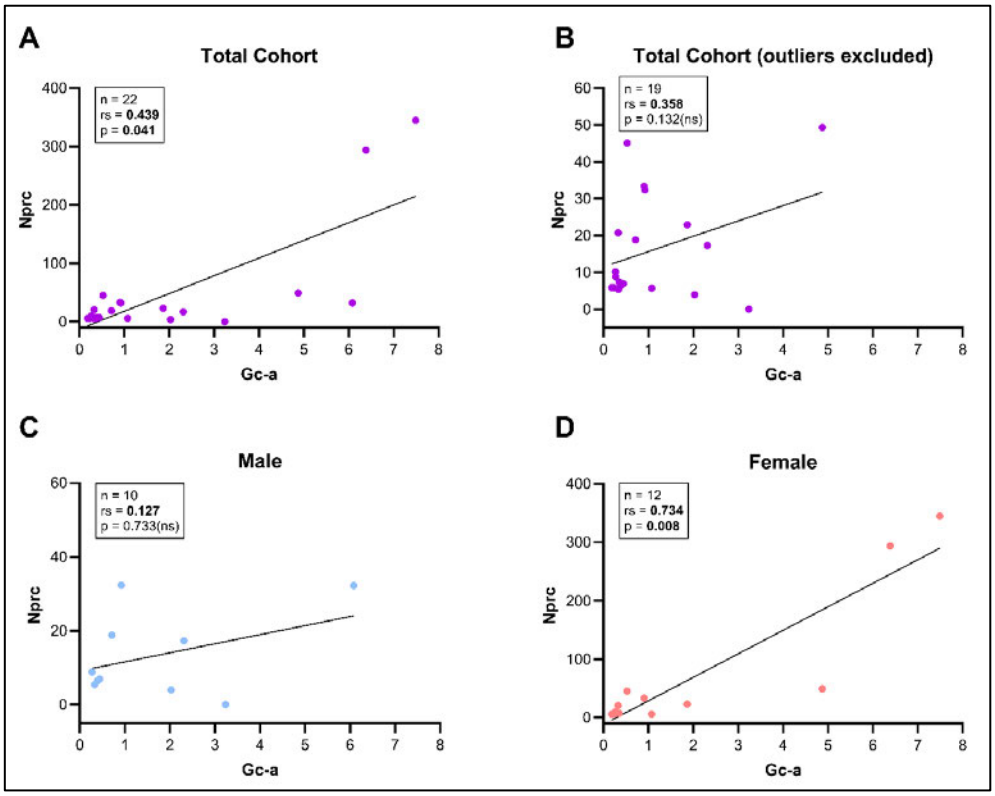


***Supp. 31.1**: Potential positive correlation of relative gene expression levels of Gc-a and Nprc in rat aortic smooth muscle cells.*

Guanylyl cyclase A (Gc-a), Natriuretic peptide clearance receptor (Nprc). Spearman correlation (two-tailed, non-parametric) was performed for **A)** the entire study cohort, **B)** the entire cohort after removal of outliers identified by ROUT test, **C)** male and **D)** female rats only. Spearman coefficients (rs), n-number and p-value are indicated in the upper left corner of each graph.

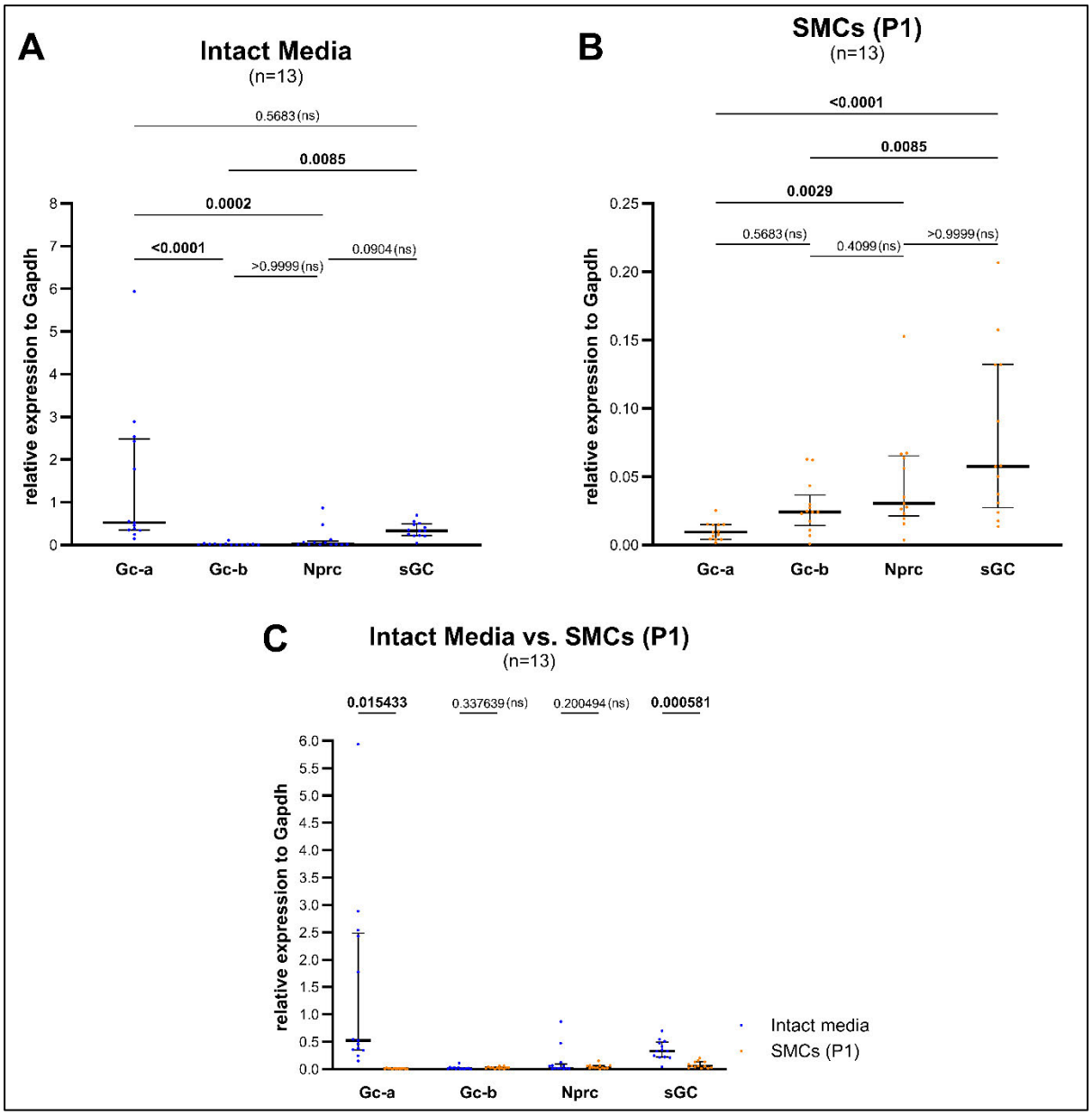


***Supp. 32.1**: Comparison of relative gene expression levels of the natriuretic peptide (NP)/cyclic guanosine monophosphate (cGMP) pathway components in the intact media and corresponding cultured smooth muscle cells (SMCs) of male rat aortae.*

The expression levels of guanylyl cyclase A (*Gc-a*) and -B (*Gc-b*), natriuretic peptide clearance receptor (*Nprc*), and soluble guanylyl cyclase (*sGC*) in the intact media (blue dots) and corresponding cultured aortic SMCs (orange dots) of the first culture passage after extraction (P1) were normalized to Glyceraldehyde-3-phosphate dehydrogenase (Gapdh) according to the ΔCt method for relative gene expression analysis. Differences in relative gene expression levels in **A)** intact tissue and **B)** SMCs were analysed by non-parametric Friedman test with Dunn's correction for multiple comparisons of paired values. Beware of different scaling of the y-axes. **C)** Differences in the expression of the genes studied in the intact media and the corresponding SMCs of the same male rats (n=13) were analysed by non-parametric multiple paired t-test. The median is indicated by a thick line while whiskers indicate the interquartile range. Numeric *p*-values are given for each comparison while significant differences are highlighted in bold and non-significant values are indicated with (ns).

# Summary

Numerous therapeutics target the relaxation of smooth muscle. A signalling molecule that plays a decisive role in this process is cyclic guanosine monophosphate (cGMP). Most knowledge about the cGMP signalling system has been generated based on cell culture. Lately, conclusions regarding smooth muscle physiology based purely on *in vitro* data have been highly debated.

Especially for vascular smooth muscle cells, which are characterized by high plasticity, drastic changes under cell culturing condition have been shown, by which the cGMP system, among others, seems to be strongly affected. Since the culture-induced modification of the cell genotype involves various reference genes, the comparison between *in vivo* and *in vitro* is often found to be difficult.

The aim of this work was therefore to find a reference gene that allows the direct comparison of aortic smooth muscle cells in the intact vessels versus culture at the gene expression level, and ideally enable the characterization of sex-dependent differences.

Subsequently, the reference gene U2 was then used to compare the expression of the natriuretic peptide receptors (GC-A, GC-B, NPRC) and the receptor for nitric oxide (sGC) in intact tissue versus cell culture and four receptors which are known to significantly regulate the intracellular cGMP level were investigated.

The comparison showed a drastic change in the expression profile of the aortic cells in culture. With the exception of Gc-a, which maintained a stable expression level, the expression of all receptors increased dramatically in cell culture. It can be suggested that this difference probably leads to a disturbance of cellular cGMP homeostasis due to a shift in the ratio of the receptors to each other. Since antibodies, especially for the natriuretic peptide receptors, still do not allow satisfactory detection, the gene expression data were confirmed at the functional level using cGMP ELISA.

No significant differences between the two sexes could be detected besides a higher fluctuation range of the data points in females. This could suggest a cycle-related regulation of the cGMP system.

The second part of this thesis focused on smooth muscle cells in the male reproductive tract. Contrary to the vascular chapter of this work, only intact tissue was used for the investigations.

In the testis, smooth muscle cells surround the germinal epithelium of the seminiferous tubules in which the sperm are produced. Here the smooth muscle cells play an important role in transporting the seminal fluid and the spermatozoa it contains through the tubular lumen towards the epididymis. To ensure this directed transport, the superficial muscle layer of the testicular tubules contracts. A hypothesis based on preliminary results of this work suggests that the intensity of contraction is precisely coordinated with the spermatogenesis in a timely manner.

The aim of the second chapter of this thesis was therefore to establish a method to detect spontaneous contractions and their alteration by relaxing and contracting substances and to evaluate these with regard to different stages of spermatogenesis.

Using a previously tested method for live recording, seminiferous tubules of the rat were recorded before and after spermiation. For the evaluation, an analysis tool was adapted, that had previously been used in parasitology and involves the imaging tool FIJI.

Using this tool, tissue contractions could be differentiated in terms of their general intensity, amplitude and frequency.

It was shown that the seminiferous tubules before and after spermiation differ drastically with regard to their spontaneous contraction behaviour. Further experiments also showed that these contractions could be attenuated to the same extent by treatment with nitric oxide and, interestingly, also by noradrenaline.

The extent to which treatment with relaxing (nitric oxide) and contracting (noradrenaline) stimulants influences the different parameters of the contractions (intensity, amplitude, frequency) requires further investigation in order to develop the FIJI-based analysis method for pharmacological/diagnostic purposes in the future.

# Zusammenfassung

Die Regulation glattmuskulärer Relaxation wird vielseitig therapeutisch eingesetzt. Ein Signalmolekül dem dabei eine entscheidende Rolle zukommt ist zyklisches Guanosinmonophosphat (cGMP). Ein Großteil des bisherigen Wissens über das cGMP Signalsystem wurde basierend auf Zellkultur generiert. Seit geraumer Zeit werden Schlussfolgerungen bezüglich glattmuskulärer Physiologie, die rein auf *in vitro* Daten beruhen, jedoch stark debattiert.

Insbesondere für glattmuskuläre Zellen des Gefäßsystems, die durch eine hohe Plastizität ausgezeichnet sind, zeigten sich drastische Veränderungen durch Kulturbedingungen von denen unter Anderem auch das cGMP System stark betroffen scheint. Da die kulturinduzierte Modifizierung des Zellgenotyps diverse Referenzgene einschliesst, ist einen direkter Vergleich zwischen *in vivo* und *in vitro* oft schwierig.

Ziel dieser Arbeit war es daher zunächst ein Referenzgen zu finden welches die direkte Gegenüberstellung von glattmuskulären Aortenzellen im intakten Gefäß und Zellkultur auf Genexpressionsniveau erlaubt. Dabei sollte idealerweise auch der Vergleich der beiden Geschlechter ermöglicht werden. Anschließend wurde dieses Referenzgen (U2) dann für den Expressionsvergleich der Natriuretischen Peptidrezeptoren (GC-A, GC-B, NPRC), sowie des Rezeptors für Stickstoffmonooxid (sGC) im intakten Gewebe versus in Kultur angewendet. Diese vier Rezeptoren regulieren maßgeblich das intrazelluläre cGMP Level.

Bei dem Vergleich zeigte sich eine drastische Veränderung des Expressionsprofils der Aortenzellen in Kultur. Mit Ausnahme von Gc-a, welches ein stabiles Expressionsniveau zwischen bewahrte, stieg die Expression aller Rezeptoren in Zellkultur drastisch an. Es ist anzunehmen das dieser Unterschied vermutlich dazu führt, dass die zelluläre cGMP Homöostase gestört wird da sich die Ratio der Rezeptoren untereinander verschiebt.

Da Antikörper, insbesondere für die Natriuretischen Peptidrezeptoren, weiterhin keine zufriedenstellende Detektion ermöglichen, wurden die Genxpressionsdaten schlussendlich auf funktioneller Ebene mittels cGMP ELISA bestätigt.

Im Vergleich der beiden Geschlechter zueinander zeigten sich keine signifikanten Unterschiede. Lediglich eine höhere Schwankungbreite der Datenpunkte bei den Weibchen konnte beobachtet werden, was eine zyklusbedingte Regulation des cGMP Systems vermuten lässt.

Im zweiten Teil dieser Arbeit waren die glattmuskulären Zellen im männlichen Reproduktionstrakt im Fokus. Dabei wurde, entgegen des vaskulären Kapitels dieser Arbeit, ausschließlich intaktes Gewebe für die Untersuchungen verwendet.

Im Hoden ummanteln glattmuskuläre Zellen das Keimepithel der *tubuli seminiferi* in dem die Spermien gebildet werden. Hier sind die Muskelzellen maßgeblich daran beteiligt die Samenflüssigkeit samt der darin enthaltenen Spermatozoen durch das tubuläre Lumen gen Nebenhoden zu befördern. Um diesen gerichteten Transport zu gewährleisten kontrahieren die Muskelzellen in den Außenrändern der Hodenkanälchen. Eine Hypothese die auf Grundlage vorläufiger Ergebnisse dieser Arbeit enstand, suggeriert eine genaue Abstimmung der Kontraktionsintensität auf den zeitlichen Verlauf der Spermatogenese.

Ziel des zweiten Kapitels dieser Arbeit war es daher ein Verfahren zu etablieren um die spontanen Kontraktionen und deren Veränderung durch relaxierende (Stickstoffmonooxid) und kontrahierende (Noradrenalin) Substanzen zu detektieren und diese in Abhängigkeit verschiedener Spermatogenesestadien auszuwerten.

Mit einer bereits erprobten Methode zur Liveaufnahme wurden *tubulii seminiferi* der Ratte vor und nach Spermiatio gefilmt. Für die Auswertung wurde auf eine Analysetechnik zurückgegriffen die ursprünglich in der Parasitologie zur Anwendung kam und auf dem Imaging Tool FIJI beruht.

Mittels der vorerst final etablierten Analyse, können nun die Gewebekontraktionen hinsichtlich ihrer allgemeinen Intensität, ihrer Amplitude und ihrer Frequenz aufgeschlüsselt werden. Es zeigte sich, dass die *tubuli seminiferi* vor und nach Spermiatio sich drastisch im Hinblick auf ihr spontanes Kontraktionsverhalten unterscheiden. In nachfolgenden Experimenten konnte zudem noch gezeigt werden, dass diese spontanen Kontraktionen durch die Behandlung mit Sticksoffmonooxid und interessanterweise auch durch Noradrenalin im gleichen Ausmaß abgeschwächt werden.

Inwieweit die Behandlung mit relaxierenden und kontrahierenden Substanzen Einfluss auf die unterschiedlichen Parameter der Kontraktionen (Intensität, Amplitude, Frequenz) nimmt, bedarf weiterer Untersuchungen, um die FIJI-basierte Analysemethode zukünftig auch für pharmakologische/diagnostische Zwecke auf den Weg zu bringen.

# Declaration of Independence

I herewith declare that I have completed this doctoral thesis single-handedly without any unauthorized help of a second party and only with the assistance acknowledged therein. I have appropriately acknowledged and cited all text passages that are derived verbatim from or are based on the content of published work of others, and all information relating to verbal communications. I consent to the use of an anti-plagiarism software to check my thesis. I have abided by the principles of good scientific practise laid down in the charter of the JLU Giessen „Satzung der Justus-Liebig-Universität Gießen zur Sicherung guter wissenschaftlicher Praxis“in carrying out the investigations described in the dissertation.

◊

Ich erkläre hiermit, dass ich die vorgelegte Dissertation selbstständig und ohne unerlaubte fremde Hilfe und nur mit den Hilfen angefertigt habe, die ich in der Dissertation angegeben habe. Alle Textstellen, die wörtlich oder sinngemäß aus veröffentlichten Schriften entnommen sind, und alle Angaben, die auf mündlichen Auskünften beruhen, sind als solche kenntlich gemacht. Ich stimme einer evtl. Überprüfung meiner Dissertation durch eine Antiplagiats-Software zu. Bei den von mir durchgeführten und in der Dissertation erwähnten Untersuchungen habe ich die Grundsätze guter wissenschaftlicher Praxis, wie sie in der „Satzung der Justus-Liebig-Universität Gießen zur Sicherung guter wissenschaftlicher Praxis“ niedergelegt sind, eingehalten.

Christine A. Rager



I certify that I have made all reasonable efforts to secure copyright permissions for third-party content included in this thesis and have not knowingly added copyright content to my work without the owner’s permission.

# Acknowledgements

Before I begin to express my gratitude, I would like to start with a disclaimer. The journey of my PhD was accompanied by a lot of amazing human beings and even though the subsequent section seems very long the fear of missing out on so many people remains. Hence, I would like to apologies in advance to everyone who I may have forgotten.

I would like to express my dearest appreciation for my supervisors and thank them for their restless support and advise.

I thank **Ralf Middendorff** for his critical thinking, his attention to detail and his astonishing wisdom. I see Ralf as one of the most intelligent people I have ever met, and I am extremely thankful for the time I spent as part of his lab.

I thank **Betty Exintaris** for showing me the importance of creating and maintaining a professional social network. I thank Betty for the opportunity to collect plenty of teaching experience and the impact she had on the shaping of my future career in academic education.

I thank **Andrea Mietens** for acting as my co-supervisor even though she never fully agreed to this role. I thank Andrea for her skill to think out of the box and for her valuable opinions that improved both of our publications.

I thank **Michael R. Whittaker** for acting as my co-supervisor and his kind and funny spirit. During the time I spend at MIPS I cannot remember one day that Mikey was in a bad mood, and it is truly inspiring to work surrounded by people like him who simply enjoy what they are doing.

I thank **Andreas Meinhardt** and **Katherine Loveland** for seeing the potential in every single IRTG student, including myself, and for making their exchange between Monash and the JLU such an outstanding experience.

A big thank you goes to the administration personnel at the Institute of Anatomy of the JLU and at the Faculty of Translational Sciences at Monash. Without their support I would have barely managed to stay on top of all the requirements for my degree. Thank you to **Pia Jürgens**, **Eva Wewel**, **Rose Kiarie**, **Danielle Popescu** and **Ashna Nimbalkar** for being such organising talents and simply superheroes.

Thank you to **Joohyung Lee**, **Erik Maronde** and **Rebecca Ritchie** for taking on the responsibilities that came with being my milestone panel. I would like to highlight the role of Rebecca whose team provided me with so much advice and technical support.

Thank you to **Ivan Manzini**, my supervisor for the Dr.rer.nat at the natural sciences faculty of the JLU, and to **Katrin Richter** for the suggestion to approach Ivan in the first place.

Thank you to **Ann-Cathrine Gronau** who initiated my contact with Ralf Middendorff and who recently received her doctorate. I am very proud of you, Aki!

Thank you to **Sabine Tasch**. Without Sabine, I would have just simply been lost. I thank her for every single advice she gave me in- and outside of the wet lab and admire her for being a powerhouse of a women. Every researcher would be grateful to have such an experienced technician on board, and I cannot thank her enough!

A gigantic THANK YOU goes to **Cameron Nowell** who besides all his duties as the Head of the Imaging Facility at MIPS gave so much of his precious time to establish the FIJI evaluation tailored specifically to my project. Thank you so much, Cam!

I would like to highlight the efforts of **Tobias Klöpper** in particular. Tobi accompanied my PhD journey as MD student under my supervision. Without his support, resilience and precious insight on the theory and methodology of our shared project my thesis and publications would have never reached their final quality.

I thank **Beatrix Bester**, **Magdalena Kuchta** at the JLU and **Bilal Mahboob** and **Katayoun Nazemi** at MIPS for being in my life as colleagues and friends. For making work endurable and lunch breaks awesome!

I am extremely grateful for my supervisor in education **Nilushi Karunaratne**. Nel is such a caring and supportive character, and it has been and still is a true pleasure to work with her.

Thanks also to my teaching family and all the enlightening and wonderful moments we have shared together as part of the education crew at MIPS. A special thank you goes out to **Rita Wardan**, **Alex Parker** and **Zoe Porter**. You are all amazing!

A big thank you to the teams of **Wolfgang Kummer**, **Martin Diener** and **Andreas Böning** at the JLU for the support with expertise, facilities and experimental animals.

Lastly, I would like to thank my family and friends. I consider myself very lucky to be surrounded by so many inspiring, kind and supportive characters.

I would like to highlight the role of my housemates **Tugce**, **Alper**, **Joven** and **Ami** who are doing an amazing job in replacing my family so far from home. I love you very much!

Middendorff Lab, June 2024 Giessen

Quinn/Whittaker Lab,
October 2024 Melbourne

# References


Ahmed, B., Rahman, A. A., Lee, S., & Malhotra, R. (2024). The Implications of Aging on Vascular Health. *Int J Mol Sci*, *25*(20). https://doi.org/10.3390/ijms252011188

Al-Lamki, R. S., Bradley, J. R., & Pober, J. S. (2017). Human Organ Culture: Updating the Approach to Bridge the Gap from In Vitro to In Vivo in Inflammation, Cancer, and Stem Cell Biology. *Front Med (Lausanne)*, *4*, 148. https://doi.org/10.3389/fmed.2017.00148

Alarcon-Martinez, L., Yemisci, M., & Dalkara, T. (2021). Pericyte morphology and function. *Histol Histopathol*, *36*(6), 633-643. https://doi.org/10.14670/hh-18-314

Allahverdian, S., Chaabane, C., Boukais, K., Francis, G. A., & Bochaton-Piallat, M. L. (2018). Smooth muscle cell fate and plasticity in atherosclerosis. *Cardiovasc Res*, *114*(4), 540-550. https://doi.org/10.1093/cvr/cvy022

Almeida, S. A., Cardoso, C. C., Orellano, L. A., Reis, A. M., Barcelos, L. S., & Andrade, S. P. (2014). Natriuretic peptide clearance receptor ligand (C-ANP4-23 ) attenuates angiogenesis in a murine sponge implant model. *Clin Exp Pharmacol Physiol*, *41*(9), 691-697. https://doi.org/10.1111/1440-1681.12251

Alwaal, A., Breyer, B. N., & Lue, T. F. (2015). Normal male sexual function: emphasis on orgasm and ejaculation. *Fertil Steril*, *104*(5), 1051-1060. https://doi.org/10.1016/j.fertnstert.2015.08.033

Anand-Srivastava, M. B., Sairam, M. R., & Cantin, M. (1990). Ring-deleted analogs of atrial natriuretic factor inhibit adenylate cyclase/cAMP system. Possible coupling of clearance atrial natriuretic factor receptors to adenylate cyclase/cAMP signal transduction system. *J Biol Chem*, *265*(15), 8566-8572.

Andreeva, E. R., Pugach, I. M., & Orekhov, A. N. (1997). Subendothelial smooth muscle cells of human aorta express macrophage antigen in situ and in vitro. *Atherosclerosis*, *135*(1), 19-27. https://doi.org/10.1016/s0021-9150(97)00136-6

Armulik, A., Genové, G., & Betsholtz, C. (2011). Pericytes: developmental, physiological, and pathological perspectives, problems, and promises. *Dev Cell*, *21*(2), 193-215. https://doi.org/10.1016/j.devcel.2011.07.001

Asunción-Alvarez, D., Palacios, J., Ybañez-Julca, R. O., Rodriguez-Silva, C. N., Nwokocha, C., Cifuentes, F., & Greensmith, D. J. (2024). Calcium signaling in endothelial and vascular smooth muscle cells: sex differences and the influence of estrogens and androgens. *Am J Physiol Heart Circ Physiol*, *326*(4), H950-h970. https://doi.org/10.1152/ajpheart.00600.2023

Balbach, M., Ghanem, L., Violante, S., Kyaw, A., Romarowski, A., Cross, J. R., Visconti, P. E., Levin, L. R., & Buck, J. (2023). Capacitation induces changes in metabolic pathways supporting motility of epididymal and ejaculated sperm. *Front Cell Dev Biol*, *11*, 1160154. https://doi.org/10.3389/fcell.2023.1160154

Banihani, S. A., & Shatnawi, R. M. (2020). Aspirin decreases human sperm motility and vitality, chelates seminal calcium, but insignificantly reduces seminal nitric oxide production. *Andrologia*, *52*(10), e13776. https://doi.org/10.1111/and.13776

Barchiesi, F., Jackson, E. K., Gillespie, D. G., Zacharia, L. C., Fingerle, J., & Dubey, R. K. (2002). Methoxyestradiols mediate estradiol-induced antimitogenesis in human aortic SMCs. *Hypertension*, *39*(4), 874-879. https://doi.org/10.1161/01.hyp.0000013863.25970.ba

Baylis, F. (2010). Pregnant women deserve better. *Nature*, *465*(7299), 689-690. https://doi.org/10.1038/465689a

Becker, S. M., & Kuznetsov, A. V. (2013). *Transport in Biological Media*. Elsevier Inc. https://doi.org/https://doi.org/10.1016/C2011-0-05837-4

Belz, G. G. (1995). Elastic properties and Windkessel function of the human aorta. *Cardiovasc Drugs Ther*, *9*(1), 73-83. https://doi.org/10.1007/bf00877747

Benak, D., Sotakova-Kasparova, D., Neckar, J., Kolar, F., & Hlavackova, M. (2019). Selection of optimal reference genes for gene expression studies in chronically hypoxic rat heart. *Mol Cell Biochem*, *461*(1-2), 15-22. https://doi.org/10.1007/s11010-019-03584-x

Benjamin, E. J., Virani, S. S., Callaway, C. W., Chamberlain, A. M., Chang, A. R., Cheng, S., Chiuve, S. E., Cushman, M., Delling, F. N., Deo, R., de Ferranti, S. D., Ferguson, J. F., Fornage, M., Gillespie, C., Isasi, C. R., Jiménez, M. C., Jordan, L. C., Judd, S. E., Lackland, D.,...Muntner, P. (2018). Heart Disease and Stroke Statistics-2018 Update: A Report From the American Heart Association. *Circulation*, *137*(12), e67-e492. https://doi.org/10.1161/cir.0000000000000558

Bennett, M. R., Sinha, S., & Owens, G. K. (2016). Vascular Smooth Muscle Cells in Atherosclerosis. *Circ Res*, *118*(4), 692-702. https://doi.org/10.1161/circresaha.115.306361

Borysenko, M., & Beringer, T. (1984). *Functional histology*. Little, Brown and Company.

Bozkurt, B., Nair, A. P., Misra, A., Scott, C. Z., Mahar, J. H., & Fedson, S. (2023). Neprilysin Inhibitors in Heart Failure: The Science, Mechanism of Action, Clinical Studies, and Unanswered Questions. *JACC Basic Transl Sci*, *8*(1), 88-105. https://doi.org/10.1016/j.jacbts.2022.05.010

Breitenstein, S., Roessig, L., Sandner, P., & Lewis, K. S. (2017). Novel sGC Stimulators and sGC Activators for the Treatment of Heart Failure. *Handb Exp Pharmacol*, *243*, 225-247. https://doi.org/10.1007/164_2016_100

Browner, N. C., Dey, N. B., Bloch, K. D., & Lincoln, T. M. (2004). Regulation of cGMP-dependent protein kinase expression by soluble guanylyl cyclase in vascular smooth muscle cells. *J Biol Chem*, *279*(45), 46631-46636. https://doi.org/10.1074/jbc.M408518200

Bubb, K. J., Aubdool, A. A., Moyes, A. J., Lewis, S., Drayton, J. P., Tang, O., Mehta, V., Zachary, I. C., Abraham, D. J., Tsui, J., & Hobbs, A. J. (2019). Endothelial C-Type Natriuretic Peptide Is a Critical Regulator of Angiogenesis and Vascular Remodeling. *Circulation*, *139*(13), 1612-1628. https://doi.org/10.1161/circulationaha.118.036344

Burnett, A. L., & Musicki, B. (2005). The nitric oxide signaling pathway in the penis. *Curr Pharm Des*, *11*(31), 3987-3994. https://doi.org/10.2174/138161205774913381

Busch, C. J., Graveline, A. R., Jiramongkolchai, K., Liu, H., Sanchez, L. S., & Bloch, K. D. (2010). Phosphodiesterase 3A expression is modulated by nitric oxide in rat pulmonary artery smooth muscle cells. *J Physiol Pharmacol*, 61(6), 663-669.

Bustin, S. A., Benes, V., Nolan, T., & Pfaffl, M. W. (2005). Quantitative real-time RT-PCR--a perspective. *J Mol Endocrinol*, *34*(3), 597-601. https://doi.org/10.1677/jme.1.01755

Byrne, M. D., Klausner, A. P., Speich, J. E., Southern, J. B., Habibi, J. R., & Ratz, P. H. (2013). Fourier transform analysis of rabbit detrusor autonomous contractions reveals length dependent increases in tone and slow wave development at long lengths. *J Urol*, *190*(1), 334-340. https://doi.org/10.1016/j.juro.2013.02.071

Caine, M., Raz, S., & Zeigler, M. (1975). Adrenergic and cholinergic receptors in the human prostate, prostatic capsule and bladder neck. *Br J Urol*, *47*(2), 193-202. https://doi.org/10.1111/j.1464-410x.1975.tb03947.x

Campos, C., Sartorio, C. L., Casali, K. R., Fernandes, R. O., Llesuy, S., da Rosa Araujo, A. S., Belló-Klein, A., & Rigatto, K. V. (2014). Low-dose estrogen is as effective as high-dose treatment in rats with postmenopausal hypertension. *J Cardiovasc Pharmacol*, *63*(2), 144-151. https://doi.org/10.1097/fjc.0000000000000034

Capettini, L. S., Cortes, S. F., & Lemos, V. S. (2010). Relative contribution of eNOS and nNOS to endothelium-dependent vasodilation in the mouse aorta. *Eur J Pharmacol*, *643*(2-3), 260-266. https://doi.org/10.1016/j.ejphar.2010.06.066

Carbone, D. J., Jr., & Hodges, S. (2003). Medical therapy for benign prostatic hyperplasia: sexual dysfunction and impact on quality of life. *Int J Impot Res*, *15*(4), 299-306. https://doi.org/10.1038/sj.ijir.3901017

Carvajal, J. A., Germain, A. M., Huidobro-Toro, J. P., & Weiner, C. P. (2000). Molecular mechanism of cGMP-mediated smooth muscle relaxation. *J Cell Physiol*, *184*(3), 409-420. https://doi.org/10.1002/1097-4652(200009)184:3<409::Aid-jcp16>3.0.Co;2-k

Cesarini, V., Pisano, C., Rossi, G., Balistreri, C. R., Botti, F., Antonelli, G., Ruvolo, G., Jannini, E. A., & Dolci, S. (2019). Regulation of PDE5 expression in human aorta and thoracic aortic aneurysms. *Sci Rep, 9(1)*, 12206. https://doi.org/10.1038/s41598-019-48432-6

Chamley-Campbell, J., Campbell, G. R., & Ross, R. (1979). The smooth muscle cell in culture. *Physiol Rev*, *59*(1), 1-61. https://doi.org/10.1152/physrev.1979.59.1.1

Chamley, J. H., Campbell, G. R., & Burnstock, G. (1974). Dedifferentiation, redifferentiation and bundle formation of smooth muscle cells in tissue culture: the influence of cell number and nerve fibres. *J Embryol Exp Morphol*, *32*(2), 297-323.

Chapman, J. R., & Waldenström, J. (2015). With Reference to Reference Genes: A Systematic Review of Endogenous Controls in Gene Expression Studies. *PLoS One*, *10*(11), e0141853. https://doi.org/10.1371/journal.pone.0141853

Chaturvedi, P. K., & Johnson, L. (1993). Architectural arrangement of stages of the spermatogenic cycle within human seminiferous tubules is related to efficiency of spermatogenesis. *Cell Tissue Res*, *273*(1), 65-70. https://doi.org/10.1007/bf00304612

Chawre, S., Khatib, M. N., Rawekar, A., Mahajan, S., Jadhav, R., & More, A. (2024). A Review of Semen Analysis: Updates From the WHO Sixth Edition Manual and Advances in Male Fertility Assessment. *Cureus*, *16*(6), e63485. https://doi.org/10.7759/cureus.63485

Chen, J. G., & Jiang, R. (2018). [Contraction mechanism of smooth muscle cells and its relationship with penile erection]. *Zhonghua Nan Ke Xue*, *24*(2), 172-175.

Cheng, C., Zhang, J., Li, X., Xue, F., Cao, L., Meng, L., Sui, W., Zhang, M., Zhao, Y., Xi, B., Yu, X., Xu, F., Yang, J., Zhang, Y., & Zhang, C. (2023). NPRC deletion mitigated atherosclerosis by inhibiting oxidative stress, inflammation and apoptosis in ApoE knockout mice. *Signal Transduct Target Ther*, *8*(1), 290. https://doi.org/10.1038/s41392-023-01560-y

Chi, J., Meng, L., Pan, S., Lin, H., Zhai, X., Liu, L., Zhou, C., Jiang, C., & Guo, H. (2017). Primary Culture of Rat Aortic Vascular Smooth Muscle Cells: A New Method. *Med Sci Monit*, *23*, 4014-4020. https://doi.org/10.12659/msm.902816

Chrisman, T. D., Schulz, S., Potter, L. R., & Garbers, D. L. (1993). Seminal plasma factors that cause large elevations in cellular cyclic GMP are C-type natriuretic peptides. *J Biol Chem*, *268*(5), 3698-3703.

Christ, G. J., & Andersson, K. E. (2007). Rho-kinase and effects of Rho-kinase inhibition on the lower urinary tract. *Neurourol Urodyn*, *26*(6 Suppl), 948-954. https://doi.org/10.1002/nau.20475

Chu, W. K., & Raeside, D. E. (1978). Fourier analysis of the echocardiogram. *Phys Med Biol*, *23*(1), 100-105. https://doi.org/10.1088/0031-9155/23/1/009

Chun, T. H., Itoh, H., Ogawa, Y., Tamura, N., Takaya, K., Igaki, T., Yamashita, J., Doi, K., Inoue, M., Masatsugu, K., Korenaga, R., Ando, J., & Nakao, K. (1997). Shear stress augments expression of C-type natriuretic peptide and adrenomedullin. *Hypertension*, *29*(6), 1296-1302. https://doi.org/10.1161/01.hyp.29.6.1296

Chusho, H., Tamura, N., Ogawa, Y., Yasoda, A., Suda, M., Miyazawa, T., Nakamura, K., Nakao, K., Kurihara, T., Komatsu, Y., Itoh, H., Tanaka, K., Saito, Y., Katsuki, M., & Nakao, K. (2001). Dwarfism and early death in mice lacking C-type natriuretic peptide. *Proc Natl Acad Sci U S A*, *98*(7), 4016-4021. https://doi.org/10.1073/pnas.071389098

Clermont, Y. (1958). Contractile elements in the limiting membrane of the seminiferous tubules of the rat. *Exp Cell Res*, *15*(2), 438-440. https://doi.org/10.1016/0014-4827(58)90052-1

Collins, P., Rosano, G. M., Sarrel, P. M., Ulrich, L., Adamopoulos, S., Beale, C. M., McNeill, J. G., & Poole-Wilson, P. A. (1995). 17 beta-Estradiol attenuates acetylcholine-induced coronary arterial constriction in women but not men with coronary heart disease. *Circulation*, *92*(1), 24-30. https://doi.org/10.1161/01.cir.92.1.24

Conti, M., Nemoz, G., Sette, C., & Vicini, E. (1995). Recent progress in understanding the hormonal regulation of phosphodiesterases. *Endocr Rev*, *16*(3), 370-389. https://doi.org/10.1210/edrv-16-3-370

Cora, M. C., Kooistra, L., & Travlos, G. (2015). Vaginal Cytology of the Laboratory Rat and Mouse: Review and Criteria for the Staging of the Estrous Cycle Using Stained Vaginal Smears. *Toxicol Pathol*, *43*(6), 776-793. https://doi.org/10.1177/0192623315570339

Crews, J. K., & Khalil, R. A. (1999). Gender-specific inhibition of Ca2+ entry mechanisms of arterial vasoconstriction by sex hormones. *Clin Exp Pharmacol Physiol*, *26*(9), 707-715. https://doi.org/10.1046/j.1440-1681.1999.03110.x

Czerny, M., Grabenwöger, M., Berger, T., Aboyans, V., Della Corte, A., Chen, E. P., Desai, N. D., Dumfarth, J., Elefteriades, J. A., Etz, C. D., Kim, K. M., Kreibich, M., Lescan, M., Di Marco, L., Martens, A., Mestres, C. A., Milojevic, M., Nienaber, C. A., Piffaretti, G.,...Hughes, G. C. (2024). EACTS/STS Guidelines for Diagnosing and Treating Acute and Chronic Syndromes of the Aortic Organ. *The Annals of Thoracic Surgery*, *118*(1), 5-115. https://doi.org/https://doi.org/10.1016/j.athoracsur.2024.01.021

Davies, K. P. (2015). Development and therapeutic applications of nitric oxide releasing materials to treat erectile dysfunction. *Future Sci OA*, *1*(1). https://doi.org/10.4155/fso.15.53

Davis, M. J., & Hill, M. A. (1999). Signaling mechanisms underlying the vascular myogenic response. *Physiol Rev*, *79*(2), 387-423. https://doi.org/10.1152/physrev.1999.79.2.387

de Bold, A. J., Borenstein, H. B., Veress, A. T., & Sonnenberg, H. (1981). A rapid and potent natriuretic response to intravenous injection of atrial myocardial extract in rats. *Life Sci*, *28*(1), 89-94. https://doi.org/10.1016/0024-3205(81)90370-2

de Bold, A. J., de Bold, M. L., & Sarda, I. R. (1986). Functional-morphological studies on in vitro cardionatrin release. *J Hypertens Suppl*, *4*(2), S3-7.

de Souza, I. L. L., Ferreira, E. D. S., Vasconcelos, L. H. C., Cavalcante, F. A., & da Silva, B. A. (2022). Erectile Dysfunction: Key Role of Cavernous Smooth Muscle Cells. *Front Pharmacol*, *13*, 895044. https://doi.org/10.3389/fphar.2022.895044

Dehaini, H., Fardoun, M., Abou-Saleh, H., El-Yazbi, A., Eid, A. A., & Eid, A. H. (2018). Estrogen in vascular smooth muscle cells: A friend or a foe? *Vascul Pharmacol*, *111*, 15-21. https://doi.org/10.1016/j.vph.2018.09.001

Denecke, S., Nowell, C. J., Fournier-Level, A., Perry, T., & Batterham, P. (2015). The Wiggle Index: An Open Source Bioassay to Assess Sub-Lethal Insecticide Response in Drosophila melanogaster. *PLoS One*, *10*(12), e0145051. https://doi.org/10.1371/journal.pone.0145051

Dickinson, Y. A., Moyes, A. J., & Hobbs, A. J. (2024). C-type natriuretic peptide (CNP): The cardiovascular system and beyond. *Pharmacol Ther*, *262*, 108708. https://doi.org/10.1016/j.pharmthera.2024.108708

Dimmeler, S., & Zeiher, A. M. (1999). Nitric oxide-an endothelial cell survival factor. *Cell Death Differ*, *6*(10), 964-968. https://doi.org/10.1038/sj.cdd.4400581

Dinardo, C. L., Venturini, G., Zhou, E. H., Watanabe, I. S., Campos, L. C., Dariolli, R., da Motta-Leal-Filho, J. M., Carvalho, V. M., Cardozo, K. H., Krieger, J. E., Alencar, A. M., & Pereira, A. C. (2014). Variation of mechanical properties and quantitative proteomics of VSMC along the arterial tree. *Am J Physiol Heart Circ Physiol*, *306*(4), H505-516. https://doi.org/10.1152/ajpheart.00655.2013

Donadon, M., & Santoro, M. M. (2021). The origin and mechanisms of smooth muscle cell development in vertebrates. *Development*, *148*(7). https://doi.org/10.1242/dev.197384

Dornas, W. C., & Silva, M. E. (2011). Animal models for the study of arterial hypertension. *J Biosci*, *36*(4), 731-737. https://doi.org/10.1007/s12038-011-9097-y

Dubey, R. K., Gillespie, D. G., Imthurn, B., Rosselli, M., Jackson, E. K., & Keller, P. J. (1999). Phytoestrogens inhibit growth and MAP kinase activity in human aortic smooth muscle cells. *Hypertension*, *33*(1 Pt 2), 177-182. https://doi.org/10.1161/01.hyp.33.1.177

Duda, D. G., Fukumura, D., & Jain, R. K. (2004). Role of eNOS in neovascularization: NO for endothelial progenitor cells. *Trends Mol Med*, *10*(4), 143-145. https://doi.org/10.1016/j.molmed.2004.02.001

Duggan, S. (2021). Vosoritide: First Approval. *Drugs*, *81*(17), 2057-2062. https://doi.org/10.1007/s40265-021-01623-w

Dutta, S., & Sengupta, P. (2022). The Role of Nitric Oxide on Male and Female Reproduction. *Malays J Med Sci*, *29*(2), 18-30. https://doi.org/10.21315/mjms2022.29.2.3

Edwards, B. S., Zimmerman, R. S., Schwab, T. R., Heublein, D. M., & Burnett, J. C., Jr. (1988). Atrial stretch, not pressure, is the principal determinant controlling the acute release of atrial natriuretic factor. *Circ Res*, *62*(2), 191-195. https://doi.org/10.1161/01.res.62.2.191

Ehret, G. B., Munroe, P. B., Rice, K. M., Bochud, M., Johnson, A. D., Chasman, D. I., Smith, A. V., Tobin, M. D., Verwoert, G. C., Hwang, S. J., Pihur, V., Vollenweider, P., O'Reilly, P. F., Amin, N., Bragg-Gresham, J. L., Teumer, A., Glazer, N. L., Launer, L., Zhao, J. H.,...Johnson, T. (2011). Genetic variants in novel pathways influence blood pressure and cardiovascular disease risk. *Nature*, *478*(7367), 103-109. https://doi.org/10.1038/nature10405

Eikvar, L., Bjørnerheim, R., Attramadal, H., & Hansson, V. (1993). Beta-adrenoceptor mediated responses and subtypes of beta-adrenoceptors in cultured rat Sertoli cells. *J Steroid Biochem Mol Biol*, 44(1), 85-91. https://doi.org/10.1016/0960-0760(93)90155-p

el-Mezgueldi, M. (1996). Calponin. *Int J Biochem Cell Biol*, *28*(11), 1185-1189. https://doi.org/10.1016/s1357-2725(96)00085-4

El Mourabit, H., Loeuillard, E., Lemoinne, S., Cadoret, A., & Housset, C. (2016). Culture Model of Rat Portal Myofibroblasts. *Front Physiol*, *7*, 120. https://doi.org/10.3389/fphys.2016.00120

Elfgen, V., Mietens, A., Mewe, M., Hau, T., & Middendorff, R. (2018). Contractility of the epididymal duct: function, regulation and potential drug effects. *Reproduction*, *156*(4), R125-r141. https://doi.org/10.1530/rep-17-0754

Ellis, L. C., Groesbeck, M. D., Farr, C. H., & Tesi, R. J. (1981). Contractility of seminiferous tubules as related to sperm transport in the male. *Arch Androl*, *6*(4), 283-294. https://doi.org/10.3109/01485018108987539

Emdin, C. A., Khera, A. V., Klarin, D., Natarajan, P., Zekavat, S. M., Nomura, A., Haas, M., Aragam, K., Ardissino, D., Wilson, J. G., Schunkert, H., McPherson, R., Watkins, H., Elosua, R., Bown, M. J., Samani, N. J., Baber, U., Erdmann, J., Gormley, P.,...Kathiresan, S. (2018). Phenotypic Consequences of a Genetic Predisposition to Enhanced Nitric Oxide Signaling. *Circulation*, *137*(3), 222-232. https://doi.org/10.1161/circulationaha.117.028021

Exintaris, B., Nguyen, D. T., Dey, A., & Lang, R. J. (2006). Spontaneous electrical activity in the prostate gland. *Auton Neurosci*, *126-127*, 371-379. https://doi.org/10.1016/j.autneu.2006.02.019

Faibish, D., Suzuki, M., & Bartlett, J. D. (2016). Appropriate real-time PCR reference genes for fluoride treatment studies performed in vitro or in vivo. *Arch Oral Biol*, *62*, 33-42. https://doi.org/10.1016/j.archoralbio.2015.11.004

Figueiredo, A. F. A., Hess, R. A., Batlouni, S. R., Wnuk, N. T., Tavares, A. O., Abarikwu, S. O., Costa, G. M. J., & França, L. R. (2021). Insights into differentiation and function of the transition region between the seminiferous tubule and rete testis. *Differentiation*, *120*, 36-47. https://doi.org/10.1016/j.diff.2021.06.002

Fleck, D., Kenzler, L., Mundt, N., Strauch, M., Uesaka, N., Moosmann, R., Bruentgens, F., Missel, A., Mayerhofer, A., Merhof, D., Spehr, J., & Spehr, M. (2021). ATP activation of peritubular cells drives testicular sperm transport. *Elife*, *10*. https://doi.org/10.7554/eLife.62885

Fleige, S., & Pfaffl, M. W. (2006). RNA integrity and the effect on the real-time qRT-PCR performance. *Mol Aspects Med*, *27*(2-3), 126-139. https://doi.org/10.1016/j.mam.2005.12.003

Fleming, I., & Busse, R. (1999). NO: the primary EDRF. *J Mol Cell Cardiol*, *31*(1), 5-14. https://doi.org/10.1006/jmcc.1998.0839

Förstermann, U., Closs, E. I., Pollock, J. S., Nakane, M., Schwarz, P., Gath, I., & Kleinert, H. (1994). Nitric oxide synthase isozymes. Characterization, purification, molecular cloning, and functions. *Hypertension*, *23*(6 Pt 2), 1121-1131. https://doi.org/10.1161/01.hyp.23.6.1121

Förstermann, U., & Sessa, W. C. (2012). Nitric oxide synthases: regulation and function. *Eur Heart J*, *33*(7), 829-837, 837a-837d. https://doi.org/10.1093/eurheartj/ehr304

Forte, P., Kneale, B. J., Milne, E., Chowienczyk, P. J., Johnston, A., Benjamin, N., & Ritter, J. M. (1998). Evidence for a difference in nitric oxide biosynthesis between healthy women and men. *Hypertension*, *32*(4), 730-734. https://doi.org/10.1161/01.hyp.32.4.730

Foster, D. C., Wedel, B. J., Robinson, S. W., & Garbers, D. L. (1999). Mechanisms of regulation and functions of guanylyl cyclases. *Rev Physiol Biochem Pharmacol*, *135*, 1-39. https://doi.org/10.1007/BFb0033668

França, L. R., Hess, R. A., Dufour, J. M., Hofmann, M. C., & Griswold, M. D. (2016). The Sertoli cell: one hundred fifty years of beauty and plasticity. *Andrology*, *4*(2), 189-212. https://doi.org/10.1111/andr.12165

Francis, S. H., Corbin, J. D., & Bischoff, E. (2009). Cyclic GMP-hydrolyzing phosphodiesterases. *Handb Exp Pharmacol*(191), 367-408. https://doi.org/10.1007/978-3-540-68964-5_16

Friebe, A., Sandner, P., & Schmidtko, A. (2017). Meeting report of the 8(th) International Conference on cGMP "cGMP: generators, effectors, and therapeutic implications" at Bamberg, Germany, from June 23 to 25, 2017. *Naunyn Schmiedebergs Arch Pharmacol*, *390*(12), 1177-1188. https://doi.org/10.1007/s00210-017-1429-5

Frismantiene, A., Philippova, M., Erne, P., & Resink, T. J. (2018). Smooth muscle cell-driven vascular diseases and molecular mechanisms of VSMC plasticity. *Cell Signal*, *52*, 48-64. https://doi.org/10.1016/j.cellsig.2018.08.019

Fuller, F., Porter, J. G., Arfsten, A. E., Miller, J., Schilling, J. W., Scarborough, R. M., Lewicki, J. A., & Schenk, D. B. (1988). Atrial natriuretic peptide clearance receptor. Complete sequence and functional expression of cDNA clones. *J Biol Chem*, *263*(19), 9395-9401.

Furchgott, R. F., & Zawadzki, J. V. (1980). The obligatory role of endothelial cells in the relaxation of arterial smooth muscle by acetylcholine. *Nature*, *288*(5789), 373-376. https://doi.org/10.1038/288373a0

Gachon, C., Mingam, A., & Charrier, B. (2004). Real-time PCR: what relevance to plant studies? *J Exp Bot*, *55*(402), 1445-1454. https://doi.org/10.1093/jxb/erh181

Gaggin, H. K., & Januzzi, J. L., Jr. (2013). Biomarkers and diagnostics in heart failure. *Biochim Biophys Acta*, *1832*(12), 2442-2450. https://doi.org/10.1016/j.bbadis.2012.12.014

Garcia, X., & Stein, F. (2006). Nitric oxide. *Semin Pediatr Infect Dis*, *17*(2), 55-57. https://doi.org/10.1053/j.spid.2006.04.002

Gardner, J. D., Brower, G. L., Voloshenyuk, T. G., & Janicki, J. S. (2008). Cardioprotection in female rats subjected to chronic volume overload: synergistic interaction of estrogen and phytoestrogens. *Am J Physiol Heart Circ Physiol*, *294*(1), H198-204. https://doi.org/10.1152/ajpheart.00281.2007

Gatimel, N., Moreau, J., Parinaud, J., & Léandri, R. D. (2017). Sperm morphology: assessment, pathophysiology, clinical relevance, and state of the art in 2017. *Andrology*, *5*(5), 845-862. https://doi.org/10.1111/andr.12389

Gilbert, S. F. (2000). *Developmental Biology-Spermatogenesis* (6 ed.). Sinauer Associates.

Gong, B., Ma, M., Xie, W., Yang, X., Huang, Y., Sun, T., Luo, Y., & Huang, J. (2017). Direct comparison of tadalafil with sildenafil for the treatment of erectile dysfunction: a systematic review and meta-analysis. *Int Urol Nephrol*, *49*(10), 1731-1740. https://doi.org/10.1007/s11255-017-1644-5

Goshi, E., Zhou, G., & He, Q. (2019). Nitric oxide detection methods in vitro and in vivo. *Med Gas Res*, *9*(4), 192-207. https://doi.org/10.4103/2045-9912.273957

Guo, Z., Zhang, W., Li, X., Wang, T., Yang, X., & Fan, L. (2022). Biomechanical stretch-induced CLOCK upregulation in venous smooth muscle cells promotes phenotypic and functional transformation. *Vascul Pharmacol*, *146*, 107097. https://doi.org/10.1016/j.vph.2022.107097

Gupta, A., Pandey, A. N., Sharma, A., Tiwari, M., Yadav, P. K., Yadav, A. K., Pandey, A. K., Shrivastav, T. G., & Chaube, S. K. (2020). Cyclic nucleotide phosphodiesterase inhibitors: possible therapeutic drugs for female fertility regulation. *Eur J Pharmacol*, *883*, 173293. https://doi.org/10.1016/j.ejphar.2020.173293

Gur, S., Alzweri, L., Yilmaz-Oral, D., Kaya-Sezginer, E., Abdel-Mageed, A. B., Dick, B., Sikka, S. C., Volkan Oztekin, C., & Hellstrom, W. J. G. (2020). Testosterone positively regulates functional responses and nitric oxide expression in the isolated human corpus cavernosum. *Andrology*, *8*(6), 1824-1833. https://doi.org/10.1111/andr.12866

Hafen, B. B., & Burns, B. (2023). Physiology, Smooth Muscle. In *StatPearls*. StatPearls Publishing.

Hafen, B. B., Shook, M., & Burns, B. (2023). Anatomy, Smooth Muscle. In *StatPearls*. StatPearls Publishing

Copyright © 2023, StatPearls Publishing LLC.

Halayko, A. J., Salari, H., Ma, X., & Stephens, N. L. (1996). Markers of airway smooth muscle cell phenotype. *Am J Physiol*, *270*(6 Pt 1), L1040-1051. https://doi.org/10.1152/ajplung.1996.270.6.L1040

Han, X., Zhang, S., Chen, Z., Adhikari, B. K., Zhang, Y., Zhang, J., Sun, J., & Wang, Y. (2020). Cardiac biomarkers of heart failure in chronic kidney disease. *Clin Chim Acta*, *510*, 298-310. https://doi.org/10.1016/j.cca.2020.07.040

Hau, R. K., Wright, S. H., & Cherrington, N. J. (2023). In Vitro and In Vivo Models for Drug Transport Across the Blood-Testis Barrier. *Drug Metab Dispos*, *51*(9), 1157-1168. https://doi.org/10.1124/dmd.123.001288

Heistad, D. D., Marcus, M. L., Larsen, G. E., & Armstrong, M. L. (1981). Role of vasa vasorum in nourishment of the aortic wall. *Am J Physiol*, *240*(5), H781-787. https://doi.org/10.1152/ajpheart.1981.240.5.H781

Herrero, M. B., de Lamirande, E., & Gagnon, C. (2003). Nitric oxide is a signaling molecule in spermatozoa. *Curr Pharm Des*, *9*(5), 419-425. https://doi.org/10.2174/1381612033391720

Hess, R. A., & Renato de Franca, L. (2008). Spermatogenesis and cycle of the seminiferous epithelium. *Adv Exp Med Biol*, *636*, 1-15. https://doi.org/10.1007/978-0-387-09597-4_1

Hirakawa, Y., Masuda, Y., Kuzuya, M., Iguchi, A., Kimata, T., & Uemura, K. (2007). Impact of gender on in-hospital mortality of patients with acute myocardial infarction undergoing percutaneous coronary intervention: an evaluation of the TAMIS-II data. *Intern Med*, *46*(7), 363-366. https://doi.org/10.2169/internalmedicine.46.6137

Hofmann, F. (2020). The cGMP system: components and function. *Biol Chem*, *401*(4), 447-469. https://doi.org/10.1515/hsz-2019-0386

Hong, F. F., Liang, X. Y., Liu, W., Lv, S., He, S. J., Kuang, H. B., & Yang, S. L. (2019). Roles of eNOS in atherosclerosis treatment. *Inflamm Res*, *68*(6), 429-441. https://doi.org/10.1007/s00011-019-01229-9

Hong, H., Sun, J., & Cai, W. (2009). Multimodality imaging of nitric oxide and nitric oxide synthases. *Free Radic Biol Med*, *47*(6), 684-698. https://doi.org/10.1016/j.freeradbiomed.2009.06.011

Hortells, L., Sosa, C., Millán, Á., & Sorribas, V. (2015). Critical Parameters of the In Vitro Method of Vascular Smooth Muscle Cell Calcification. *PLoS One*, *10*(11), e0141751. https://doi.org/10.1371/journal.pone.0141751

Hu, Y., Zhang, Z., Torsney, E., Afzal, A. R., Davison, F., Metzler, B., & Xu, Q. (2004). Abundant progenitor cells in the adventitia contribute to atherosclerosis of vein grafts in ApoE-deficient mice. *J Clin Invest*, *113*(9), 1258-1265. https://doi.org/10.1172/jci19628

Huang, P. L., Dawson, T. M., Bredt, D. S., Snyder, S. H., & Fishman, M. C. (1993). Targeted disruption of the neuronal nitric oxide synthase gene. *Cell*, *75*(7), 1273-1286. https://doi.org/10.1016/0092-8674(93)90615-w

Huber, A., & Badylak, S. F. (2012). Phenotypic changes in cultured smooth muscle cells: limitation or opportunity for tissue engineering of hollow organs? *J Tissue Eng Regen Med*, *6*(7), 505-511. https://doi.org/10.1002/term.451

Ibrahim, E., Lynne, C. M., & Brackett, N. L. (2016). Male fertility following spinal cord injury: an update. *Andrology*, *4*(1), 13-26. https://doi.org/10.1111/andr.12119

Ignarro, L. J., Bush, P. A., Buga, G. M., Wood, K. S., Fukuto, J. M., & Rajfer, J. (1990). Nitric oxide and cyclic GMP formation upon electrical field stimulation cause relaxation of corpus cavernosum smooth muscle. *Biochem Biophys Res Commun*, *170*(2), 843-850. https://doi.org/10.1016/0006-291x(90)92168-y

Ignarro, L. J., Byrns, R. E., Buga, G. M., Wood, K. S., & Chaudhuri, G. (1988). Pharmacological evidence that endothelium-derived relaxing factor is nitric oxide: use of pyrogallol and superoxide dismutase to study endothelium-dependent and nitric oxide-elicited vascular smooth muscle relaxation. *J Pharmacol Exp Ther*, *244*(1), 181-189.

Jacob, H. J. (2010). The rat: a model used in biomedical research. *Methods Mol Biol*, *597*, 1-11. https://doi.org/10.1007/978-1-60327-389-3_1

Jaffe, L. A., & Egbert, J. R. (2017). Regulation of Mammalian Oocyte Meiosis by Intercellular Communication Within the Ovarian Follicle. *Annu Rev Physiol*, *79*, 237-260. https://doi.org/10.1146/annurev-physiol-022516-034102

Jaminon, A., Reesink, K., Kroon, A., & Schurgers, L. (2019). The Role of Vascular Smooth Muscle Cells in Arterial Remodeling: Focus on Calcification-Related Processes. *Int J Mol Sci*, *20*(22). https://doi.org/10.3390/ijms20225694

Jankowski, M., Reis, A. M., Mukaddam-Daher, S., Dam, T. V., Farookhi, R., & Gutkowska, J. (1997). C-type natriuretic peptide and the guanylyl cyclase receptors in the rat ovary are modulated by the estrous cycle. *Biol Reprod*, *56*(1), 59-66. https://doi.org/10.1095/biolreprod56.1.59

Jankowski, M., Wang, D., Mukaddam-Daher, S., & Gutkowska, J. (2005). Pregnancy alters nitric oxide synthase and natriuretic peptide systems in the rat left ventricle. *J Endocrinol*, *184*(1), 209-217. https://doi.org/10.1677/joe.1.05702

Jensen, A. M. (2005). Potential roles for BMP and Pax genes in the development of iris smooth muscle. *Dev Dyn*, *232*(2), 385-392. https://doi.org/10.1002/dvdy.20224

Jensen, L. F., Bentzon, J. F., & Albarrán-Juárez, J. (2021). The Phenotypic Responses of Vascular Smooth Muscle Cells Exposed to Mechanical Cues. *Cells*, *10*(9). https://doi.org/10.3390/cells10092209

Jia, K., Luo, X., Yi, J., & Zhang, C. (2024). Hormonal influence: unraveling the impact of sex hormones on vascular smooth muscle cells. *Biol Res*, *57*(1), 61. https://doi.org/10.1186/s40659-024-00542-w

Jiang, X., Rowitch, D. H., Soriano, P., McMahon, A. P., & Sucov, H. M. (2000). Fate of the mammalian cardiac neural crest. *Development*, *127*(8), 1607-1616. https://doi.org/10.1242/dev.127.8.1607

Kangasniemi, M., Kaipia, A., Mali, P., Toppari, J., Huhtaniemi, I., & Parvinen, M. (1990). Modulation of basal and FSH-dependent cyclic AMP production in rat seminiferous tubules staged by an improved transillumination technique. *Anat Rec*, *227*(1), 62-76. https://doi.org/10.1002/ar.1092270108

Karbasion, N., Xu, Y., Snider, J. C., & Bersi, M. R. (2024). Primary Mouse Aortic Smooth Muscle Cells Exhibit Region- and Sex-Dependent Biological Responses In Vitro. *J Biomech Eng*, *146*(6). https://doi.org/10.1115/1.4064965

Karbassi, E., Fenix, A., Marchiano, S., Muraoka, N., Nakamura, K., Yang, X., & Murry, C. E. (2020). Cardiomyocyte maturation: advances in knowledge and implications for regenerative medicine. *Nat Rev Cardiol*, *17*(6), 341-359. https://doi.org/10.1038/s41569-019-0331-x

Kasamatsu, S., Tsutsuki, H., Ida, T., Sawa, T., Watanabe, Y., Akaike, T., & Ihara, H. (2022). Regulation of nitric oxide/reactive oxygen species redox signaling by nNOS splicing variants. *Nitric Oxide*, *120*, 44-52. https://doi.org/10.1016/j.niox.2022.01.004

Kaupp, U. B., & Strünker, T. (2017). Signaling in Sperm: More Different than Similar. *Trends Cell Biol*, *27*(2), 101-109. https://doi.org/10.1016/j.tcb.2016.10.002

Kerr, M. A., & Kenny, A. J. (1974). The purification and specificity of a neutral endopeptidase from rabbit kidney brush border. Biochem J, 137(3), 477-488. https://doi.org/10.1042/bj1370477

Khalil, R. A. (2005). Sex hormones as potential modulators of vascular function in hypertension. *Hypertension*, *46*(2), 249-254. https://doi.org/10.1161/01.HYP.0000172945.06681.a4

Kim, A. M., Tingen, C. M., & Woodruff, T. K. (2010). Sex bias in trials and treatment must end. *Nature*, *465*(7299), 688-689. https://doi.org/10.1038/465688a

Klein, D., Meissner, N., Kleff, V., Jastrow, H., Yamaguchi, M., Ergün, S., & Jendrossek, V. (2014). Nestin(+) tissue-resident multipotent stem cells contribute to tumor progression by differentiating into pericytes and smooth muscle cells resulting in blood vessel remodeling. *Front Oncol*, *4*, 169. https://doi.org/10.3389/fonc.2014.00169

Kleppisch, T. (2009). Phosphodiesterases in the central nervous system. *Handb Exp Pharmacol*(191), 71-92. https://doi.org/10.1007/978-3-540-68964-5_5

Kloss, S., Furneaux, H., & Mülsch, A. (2003). Post-transcriptional regulation of soluble guanylyl cyclase expression in rat aorta. *J Biol Chem*, *278*(4), 2377-2383. https://doi.org/10.1074/jbc.M206453200

Kobayashi, H., Kabuto, M., Ide, H., Hosotani, K., & Kubota, T. (1992). An artificial blood vessel with an endothelial-cell monolayer. *J Neurosurg*, *77*(3), 397-402. https://doi.org/10.3171/jns.1992.77.3.0397

Köhler, R., & Hoyer, J. (2007). Frontiers in Neuroscience

Role of TRPV4 in the Mechanotransduction of Shear Stress in Endothelial Cells. In W. B. Liedtke & S. Heller (Eds.), *TRP Ion Channel Function in Sensory Transduction and Cellular Signaling Cascades*. CRC Press/Taylor & Francis

Copyright © 2007, Taylor & Francis Group, LLC.

Kozera, B., & Rapacz, M. (2013). Reference genes in real-time PCR. *J Appl Genet*, *54*(4), 391-406. https://doi.org/10.1007/s13353-013-0173-x

Kraehling, J. R., & Sessa, W. C. (2017). Contemporary Approaches to Modulating the Nitric Oxide-cGMP Pathway in Cardiovascular Disease. *Circ Res*, *120*(7), 1174-1182. https://doi.org/10.1161/circresaha.117.303776

Krämer, A., Utans, U., Keller, W., & Lamond, A. (1990). Components involved in nuclear pre-mRNA splicing. *Mol Biol Rep*, 14(2-3), 199-200. https://doi.org/10.1007/bf00360472

Kraft, T., & Brenner, B. (2018). Muskulatur. Glatte Muskulatur. In *Pape, H.-C.; Kurtz, A.; Silbernagel S.; Physiologie* (8 ed.). Georg Thieme Verlag.

Krawutschke, C., Koesling, D., & Russwurm, M. (2015). Cyclic GMP in Vascular Relaxation: Export Is of Similar Importance as Degradation. *Arterioscler Thromb Vasc Biol*, *35*(9), 2011-2019. https://doi.org/10.1161/atvbaha.115.306133

Kuhn, M. (2004). Molecular physiology of natriuretic peptide signalling. *Basic Res Cardiol*, *99*(2), 76-82. https://doi.org/10.1007/s00395-004-0460-0

Kuhn, M. (2016). Molecular Physiology of Membrane Guanylyl Cyclase Receptors. *Physiol Rev*, *96*(2), 751-804. https://doi.org/10.1152/physrev.00022.2015

Kuwahara, K. (2021). The natriuretic peptide system in heart failure: Diagnostic and therapeutic implications. *Pharmacol Ther*, *227*, 107863. https://doi.org/10.1016/j.pharmthera.2021.107863

Lannoy, M., Slove, S., & Jacob, M. P. (2014). The function of elastic fibers in the arteries: beyond elasticity. *Pathol Biol (Paris)*, *62*(2), 79-83. https://doi.org/10.1016/j.patbio.2014.02.011

Leblond, C. P., & Clermont, Y. (1952). Definition of the stages of the cycle of the seminiferous epithelium in the rat. *Ann N Y Acad Sci*, *55*(4), 548-573. https://doi.org/10.1111/j.1749-6632.1952.tb26576.x

Legato, M. J. (2004). Gender-specific medicine: the view from Salzburg. *Gend Med*, *1*(2), 61-63. https://doi.org/10.1016/s1550-8579(04)80011-1

Lehners, M., Dobrowinski, H., Feil, S., & Feil, R. (2018). cGMP Signaling and Vascular Smooth Muscle Cell Plasticity. *J Cardiovasc Dev Dis*, *5*(2). https://doi.org/10.3390/jcdd5020020

Lehners, M., Schmidt, H., Zaldivia, M. T. K., Stehle, D., Krämer, M., Peter, A., Adler, J., Lukowski, R., Feil, S., & Feil, R. (2025). Single-cell analysis identifies the CNP/GC-B/cGMP axis as marker and regulator of modulated VSMCs in atherosclerosis. *Nat Commun*, *16*(1), 429. https://doi.org/10.1038/s41467-024-55687-9

Leineweber, K., Moosmang, S., & Paulson, D. (2017). Genetics of NO Deficiency. *Am J Cardiol*, *120*(8s), S80-s88. https://doi.org/10.1016/j.amjcard.2017.06.013

Leitman, D. C., Andresen, J. W., Kuno, T., Kamisaki, Y., Chang, J. K., & Murad, F. (1986). Identification of multiple binding sites for atrial natriuretic factor by affinity cross-linking in cultured endothelial cells. *J Biol Chem*, *261*(25), 11650-11655.

Leong, X. F., Ng, C. Y., & Jaarin, K. (2015). Animal Models in Cardiovascular Research: Hypertension and Atherosclerosis. *Biomed Res Int*, *2015*, 528757. https://doi.org/10.1155/2015/528757

Lerman, L. O., Kurtz, T. W., Touyz, R. M., Ellison, D. H., Chade, A. R., Crowley, S. D., Mattson, D. L., Mullins, J. J., Osborn, J., Eirin, A., Reckelhoff, J. F., Iadecola, C., & Coffman, T. M. (2019). Animal Models of Hypertension: A Scientific Statement From the American Heart Association. *Hypertension*, *73*(6), e87-e120. https://doi.org/10.1161/hyp.0000000000000090

Li, C., & Kuemmerle, J. F. (2020). The fate of myofibroblasts during the development of fibrosis in Crohn's disease. *J Dig Dis*, *21*(6), 326-331. https://doi.org/10.1111/1751-2980.12852

Li, K., & Brownley, A. (2010). Primer design for RT-PCR. *Methods Mol Biol*, *630*, 271-299. https://doi.org/10.1007/978-1-60761-629-0_18

Li, Y., Madiraju, P., & Anand-Srivastava, M. B. (2012). Knockdown of natriuretic peptide receptor-A enhances receptor C expression and signalling in vascular smooth muscle cells. *Cardiovasc Res*, *93*(2), 350-359. https://doi.org/10.1093/cvr/cvr319

Lin, Y. W., Hsu, T. H., & Yen, P. H. (2013). Mouse sperm acquire a new structure on the apical hook during epididymal maturation. *Asian J Androl*, *15*(4), 523-528. https://doi.org/10.1038/aja.2013.46

Lincoln, T. M., Wu, X., Sellak, H., Dey, N., & Choi, C. S. (2006). Regulation of vascular smooth muscle cell phenotype by cyclic GMP and cyclic GMP-dependent protein kinase. *Front Biosci*, *11*, 356-367. https://doi.org/10.2741/1803

Liu, D., Ceddia, R. P., Zhang, W., Shi, F., Fang, H., & Collins, S. (2023). Discovery of another mechanism for the inhibition of particulate guanylyl cyclases by the natriuretic peptide clearance receptor. *Proc Natl Acad Sci U S A*, *120*(28), e2307882120. https://doi.org/10.1073/pnas.2307882120

Liu, G., Li, J., Ming, Y., Xiang, B., Zhou, X., Chen, Y., Chen, N., Abudupataer, M., Zhu, S., Sun, X., Sun, Y., Lai, H., Feng, S., Wang, C., & Zhu, K. (2023). A hiPSC-derived lineage-specific vascular smooth muscle cell-on-a-chip identifies aortic heterogeneity across segments. *Lab Chip*, *23*(7), 1835-1851. https://doi.org/10.1039/d2lc01158a

Liu, R., Leslie, K. L., & Martin, K. A. (2015). Epigenetic regulation of smooth muscle cell plasticity. *Biochim Biophys Acta*, *1849*(4), 448-453. https://doi.org/10.1016/j.bbagrm.2014.06.004

Livak, K. J., & Schmittgen, T. D. (2001). Analysis of relative gene expression data using real-time quantitative PCR and the 2(-Delta Delta C(T)) Method. *Methods (San Diego, Calif.)*, *25*(4), 402-408. https://doi.org/10.1006/meth.2001.1262

Loukotová, J., Kunes, J., & Zicha, J. (1998). Cytosolic free calcium response to angiotensin II in aortic VSMC isolated from male and female SHR. *Physiol Res*, *47*(6), 507-510.

Lucas, K. A., Pitari, G. M., Kazerounian, S., Ruiz-Stewart, I., Park, J., Schulz, S., Chepenik, K. P., & Waldman, S. A. (2000). Guanylyl cyclases and signaling by cyclic GMP. *Pharmacol Rev*, *52*(3), 375-414.

Luetjens, C. M., Weinbauer, G. F., & Wistuba, J. (2005). Primate spermatogenesis: new insights into comparative testicular organisation, spermatogenic efficiency and endocrine control. *Biol Rev Camb Philos Soc*, *80*(3), 475-488. https://doi.org/10.1017/s1464793105006755

Lukowski, R., Rybalkin, S. D., Loga, F., Leiss, V., Beavo, J. A., & Hofmann, F. (2010). Cardiac hypertrophy is not amplified by deletion of cGMP-dependent protein kinase I in cardiomyocytes. *Proc Natl Acad Sci U S A*, *107*(12), 5646-5651. https://doi.org/10.1073/pnas.1001360107

Luo, Y., Zhu, Y., Basang, W., Wang, X., Li, C., & Zhou, X. (2021). Roles of Nitric Oxide in the Regulation of Reproduction: A Review. *Front Endocrinol (Lausanne)*, *12*, 752410. https://doi.org/10.3389/fendo.2021.752410

Lutgens, E., de Muinck, E. D., Kitslaar, P. J., Tordoir, J. H., Wellens, H. J., & Daemen, M. J. (1999). Biphasic pattern of cell turnover characterizes the progression from fatty streaks to ruptured human atherosclerotic plaques. *Cardiovasc Res*, *41*(2), 473-479. https://doi.org/10.1016/s0008-6363(98)00311-3

Maack, T., Suzuki, M., Almeida, F. A., Nussenzveig, D., Scarborough, R. M., McEnroe, G. A., & Lewicki, J. A. (1987). Physiological role of silent receptors of atrial natriuretic factor. *Science*, *238*(4827), 675-678. https://doi.org/10.1126/science.2823385

MacDonald, J. A., & Walsh, M. P. (2018). Regulation of Smooth Muscle Myosin Light Chain Phosphatase by Multisite Phosphorylation of the Myosin Targeting Subunit, MYPT1. *Cardiovasc Hematol Disord Drug Targets*, *18*(1), 4-13. https://doi.org/10.2174/1871529x18666180326120638

Madersbacher, S., Sampson, N., & Culig, Z. (2019). Pathophysiology of Benign Prostatic Hyperplasia and Benign Prostatic Enlargement: A Mini-Review. *Gerontology*, *65*(5), 458-464. https://doi.org/10.1159/000496289

Majack, R. A. (1987). Beta-type transforming growth factor specifies organizational behavior in vascular smooth muscle cell cultures. *J Cell Biol*, *105*(1), 465-471. https://doi.org/10.1083/jcb.105.1.465

Majesky, M. W. (2007). Developmental basis of vascular smooth muscle diversity. *Arterioscler Thromb Vasc Biol*, *27*(6), 1248-1258. https://doi.org/10.1161/atvbaha.107.141069

Majesky, M. W., Dong, X. R., Hoglund, V., Daum, G., & Mahoney, W. M., Jr. (2012). The adventitia: a progenitor cell niche for the vessel wall. *Cells Tissues Organs*, *195*(1-2), 73-81. https://doi.org/10.1159/000331413

Makuch, R., Birukov, K., Shirinsky, V., & Dabrowska, R. (1991). Functional interrelationship between calponin and caldesmon. *Biochem J*, *280 ( Pt 1)*(Pt 1), 33-38. https://doi.org/10.1042/bj2800033

Malorni, W., Straface, E., Matarrese, P., Ascione, B., Coinu, R., Canu, S., Galluzzo, P., Marino, M., & Franconi, F. (2008). Redox state and gender differences in vascular smooth muscle cells. *FEBS Lett*, *582*(5), 635-642. https://doi.org/10.1016/j.febslet.2008.01.034

Marten, N. W., Burke, E. J., Hayden, J. M., & Straus, D. S. (1994). Effect of amino acid limitation on the expression of 19 genes in rat hepatoma cells. *Faseb j*, *8*(8), 538-544. https://doi.org/10.1096/fasebj.8.8.8181673

Matsukawa, N., Grzesik, W. J., Takahashi, N., Pandey, K. N., Pang, S., Yamauchi, M., & Smithies, O. (1999). The natriuretic peptide clearance receptor locally modulates the physiological effects of the natriuretic peptide system. *Proc Natl Acad Sci U S A*, *96*(13), 7403-7408. https://doi.org/10.1073/pnas.96.13.7403

Maurice, D. H., Ke, H., Ahmad, F., Wang, Y., Chung, J., & Manganiello, V. C. (2014). Advances in targeting cyclic nucleotide phosphodiesterases. *Nat Rev Drug Discov*, *13*(4), 290-314. https://doi.org/10.1038/nrd4228

Mazumder, R., Das, T. K., & Biswas, N. M. (1985). Spermatogenesis of rat: effect of central norepinephrine synthesis inhibition by diethyldithiocarbamate. *Andrologia*, *17*(4), 400-405. https://doi.org/10.1111/j.1439-0272.1985.tb01029.x

McMahon, C. G., Abdo, C., Incrocci, L., Perelman, M., Rowland, D., Waldinger, M., & Xin, Z. C. (2004). Disorders of orgasm and ejaculation in men. *J Sex Med*, *1*(1), 58-65. https://doi.org/10.1111/j.1743-6109.2004.10109.x

Means, A. R., Bagchi, I. C., VanBerkum, M. F., & Kemp, B. E. (1991). Regulation of smooth muscle myosin light chain kinase by calmodulin. *Adv Exp Med Biol*, *304*, 11-24. https://doi.org/10.1007/978-1-4684-6003-2_3

Meek, S., Mashimo, T., & Burdon, T. (2017). From engineering to editing the rat genome. *Mamm Genome*, *28*(7-8), 302-314. https://doi.org/10.1007/s00335-017-9705-8

Mehats, C., Andersen, C. B., Filopanti, M., Jin, S. L., & Conti, M. (2002). Cyclic nucleotide phosphodiesterases and their role in endocrine cell signaling. *Trends Endocrinol Metab*, *13*(1), 29-35. https://doi.org/10.1016/s1043-2760(01)00523-9

Mendelsohn, M. E. (2002). Genomic and nongenomic effects of estrogen in the vasculature. *Am J Cardiol*, *90*(1a), 3f-6f. https://doi.org/10.1016/s0002-9149(02)02418-9

Méndez-Barbero, N., Gutiérrez-Muñoz, C., & Blanco-Colio, L. M. (2021). Cellular Crosstalk between Endothelial and Smooth Muscle Cells in Vascular Wall Remodeling. *Int J Mol Sci*, *22*(14). https://doi.org/10.3390/ijms22147284

Mewe, M., Wulfsen, I., Middendorff, R., & Bauer, C. K. (2007). Differential modulation of bovine epididymal activity by oxytocin and noradrenaline. *Reproduction*, *134*(3), 493-501. https://doi.org/10.1530/rep-07-0220

Michel, M. C. (2007). Alpha1-adrenoceptors and ejaculatory function. *Br J Pharmacol*, *152*(3), 289-290. https://doi.org/10.1038/sj.bjp.0707369

Middendorff, R., Davidoff, M. S., Behrends, S., Mewe, M., Miethens, A., & Müller, D. (2000). Multiple roles of the messenger molecule cGMP in testicular function. *Andrologia*, *32*(1), 55-59.

Mietens, A., Tasch, S., Stammler, A., Konrad, L., Feuerstacke, C., & Middendorff, R. (2014). Time-lapse imaging as a tool to investigate contractility of the epididymal duct--effects of cGMP signaling. *PLoS One*, *9*(3), e92603. https://doi.org/10.1371/journal.pone.0092603

Mills, T. M., Chitaley, K., & Lewis, R. W. (2001). Vasoconstrictors in erectile physiology. *Int J Impot Res*, *13 Suppl 5*, S29-34. https://doi.org/10.1038/sj.ijir.3900774

Misono, K. S., Grammer, R. T., Fukumi, H., & Inagami, T. (1984). Rat atrial natriuretic factor: isolation, structure and biological activities of four major peptides. *Biochem Biophys Res Commun*, *123*(2), 444-451. https://doi.org/10.1016/0006-291x(84)90250-x

Miyake, K., Yamamoto, M., & Mitsuya, H. (1986). Pharmacological and histological evidence for adrenergic innervation of the myoid cells in the rat seminiferous tubule. *Tohoku J Exp Med*, *149*(1), 79-87. https://doi.org/10.1620/tjem.149.79

Miyake, K., Yamamoto, M., Narita, H., Hashimoto, J., & Mitsuya, H. (1986). Evidence for contractility of the human seminiferous tubule confirmed by its response to noradrenaline and acetylcholine. *Fertil Steril*, *46*(4), 734-737. https://doi.org/10.1016/s0015-0282(16)49663-9

Mónica, F. Z., & De Nucci, G. (2019). Tadalafil for the treatment of benign prostatic hyperplasia. *Expert Opin Pharmacother*, *20*(8), 929-937. https://doi.org/10.1080/14656566.2019.1589452

Moon, S. K., Cha, B. Y., & Kim, C. H. (2003). In vitro cellular aging is associated with enhanced proliferative capacity, G1 cell cycle modulation, and matrix metalloproteinase-9 regulation in mouse aortic smooth muscle cells. *Arch Biochem Biophys*, *418*(1), 39-48. https://doi.org/10.1016/s0003-9861(03)00402-8

Morelli, A., Filippi, S., Zhang, X. H., Luconi, M., Vignozzi, L., Mancina, R., & Maggi, M. (2005). Peripheral regulatory mechanisms in erection. *Int J Androl*, *28 Suppl 2*, 23-27. https://doi.org/10.1111/j.1365-2605.2005.00550.x

Morrison, T. B., Weis, J. J., & Wittwer, C. T. (1998). Quantification of low-copy transcripts by continuous SYBR Green I monitoring during amplification. *Biotechniques*, *24*(6), 954-958, 960, 962.

Muhl, L., Genové, G., Leptidis, S., Liu, J., He, L., Mocci, G., Sun, Y., Gustafsson, S., Buyandelger, B., Chivukula, I. V., Segerstolpe, Å., Raschperger, E., Hansson, E. M., Björkegren, J. L. M., Peng, X. R., Vanlandewijck, M., Lendahl, U., & Betsholtz, C. (2020). Single-cell analysis uncovers fibroblast heterogeneity and criteria for fibroblast and mural cell identification and discrimination. *Nat Commun*, *11*(1), 3953. https://doi.org/10.1038/s41467-020-17740-1

Müller, D., Cortes-Dericks, L., Budnik, L. T., Brunswig-Spickenheier, B., Pancratius, M., Speth, R. C., Mukhopadhyay, A. K., & Middendorff, R. (2006). Homologous and lysophosphatidic acid-induced desensitization of the atrial natriuretic peptide receptor, guanylyl cyclase-A, in MA-10 leydig cells. *Endocrinology*, *147*(6), 2974-2985. https://doi.org/10.1210/en.2006-0092

Müller, D., Middendorff, R., Olcese, J., & Mukhopadhyay, A. K. (2002). Central nervous system-specific glycosylation of the type A natriuretic peptide receptor. *Endocrinology*, *143*(1), 23-29. https://doi.org/10.1210/endo.143.1.8597

Müller, D., Mukhopadhyay, A. K., Davidoff, M. S., & Middendorff, R. (2011). Cyclic GMP signaling in rat urinary bladder, prostate, and epididymis: tissue-specific changes with aging and in response to Leydig cell depletion. *Reproduction*, *142*(2), 333-343. https://doi.org/10.1530/rep-10-0517

Müller, D., Mukhopadhyay, A. K., Speth, R. C., Guidone, G., Potthast, R., Potter, L. R., & Middendorff, R. (2004). Spatiotemporal regulation of the two atrial natriuretic peptide receptors in testis. *Endocrinology*, *145*(3), 1392-1401. https://doi.org/10.1210/en.2003-0706

Mullis, K., Faloona, F., Scharf, S., Saiki, R., Horn, G., & Erlich, H. (1986). Specific enzymatic amplification of DNA in vitro: the polymerase chain reaction. *Cold Spring Harb Symp Quant Biol*, *51 Pt 1*, 263-273. https://doi.org/10.1101/sqb.1986.051.01.032

Murtada, S. I., Kawamura, Y., Weiss, D., & Humphrey, J. D. (2021). Differential biomechanical responses of elastic and muscular arteries to angiotensin II-induced hypertension. *J Biomech*, *119*, 110297. https://doi.org/10.1016/j.jbiomech.2021.110297

Nagase, M., Katafuchi, T., Hirose, S., & Fujita, T. (1997). Tissue distribution and localization of natriuretic peptide receptor subtypes in stroke-prone spontaneously hypertensive rats. *J Hypertens*, *15*(11), 1235-1243. https://doi.org/10.1097/00004872-199715110-00007

Nakagawa, Y., Nishikimi, T., & Kuwahara, K. (2019). Atrial and brain natriuretic peptides: Hormones secreted from the heart. *Peptides*, *111*, 18-25. https://doi.org/10.1016/j.peptides.2018.05.012

Narayan, P., & Lepor, H. (2001). Long-term, open-label, phase III multicenter study of tamsulosin in benign prostatic hyperplasia. *Urology*, *57*(3), 466-470. https://doi.org/10.1016/s0090-4295(00)01042-6

Nathan, C. F., & Hibbs, J. B., Jr. (1991). Role of nitric oxide synthesis in macrophage antimicrobial activity. *Curr Opin Immunol*, *3*(1), 65-70. https://doi.org/10.1016/0952-7915(91)90079-g

Nelson, R. J., Demas, G. E., Huang, P. L., Fishman, M. C., Dawson, V. L., Dawson, T. M., & Snyder, S. H. (1995). Behavioural abnormalities in male mice lacking neuronal nitric oxide synthase. *Nature*, *378*(6555), 383-386. https://doi.org/10.1038/378383a0

Nielsen, S. J., Gøtze, J. P., Jensen, H. L., & Rehfeld, J. F. (2008). ProCNP and CNP are expressed primarily in male genital organs. *Regul Pept*, *146*(1-3), 204-212. https://doi.org/10.1016/j.regpep.2007.09.022

Nielsen, S. J., Iversen, P., Rehfeld, J. F., Jensen, H. L., & Goetze, J. P. (2009). C-type natriuretic peptide in prostate cancer. *Apmis*, *117*(1), 60-67. https://doi.org/10.1111/j.1600-0463.2008.00016.x

Nishikimi, T., & Nakagawa, Y. (2022). B-Type Natriuretic Peptide (BNP) Revisited-Is BNP Still a Biomarker for Heart Failure in the Angiotensin Receptor/Neprilysin Inhibitor Era? *Biology (Basel)*, *11*(7). https://doi.org/10.3390/biology11071034

Noubani, A., Farookhi, R., & Gutkowska, J. (2000). B-type natriuretic peptide receptor expression and activity are hormonally regulated in rat ovarian cells. *Endocrinology*, *141*(2), 551-559. https://doi.org/10.1210/endo.141.2.7305

Nowell, C. (2021). *Tissue Contractility Measurement (Version 1)*. Monash University.

O'Bryan, M. K., Schlatt, S., Gerdprasert, O., Phillips, D. J., de Kretser, D. M., & Hedger, M. P. (2000). Inducible nitric oxide synthase in the rat testis: evidence for potential roles in both normal function and inflammation-mediated infertility. *Biol Reprod*, *63*(5), 1285-1293. https://doi.org/10.1095/biolreprod63.5.1285

O'Donnell, J., Zeppenfeld, D., McConnell, E., Pena, S., & Nedergaard, M. (2012). Norepinephrine: a neuromodulator that boosts the function of multiple cell types to optimize CNS performance. *Neurochem Res*, *37*(11), 2496-2512. https://doi.org/10.1007/s11064-012-0818-x

O'Donnell, L., Nicholls, P. K., O'Bryan, M. K., McLachlan, R. I., & Stanton, P. G. (2011). Spermiation: The process of sperm release. *Spermatogenesis*, *1*(1), 14-35. https://doi.org/10.4161/spmg.1.1.14525

Ojha, N., & Dhamoon, A. S. (2025). Myocardial Infarction. In *StatPearls*. StatPearls Publishing

Copyright © 2025, StatPearls Publishing LLC.

Oliveira, J. G., Prados, R. Z., Guedes, A. C., Ferreira, P. C., & Kroon, E. G. (1999). The housekeeping gene glyceraldehyde-3-phosphate dehydrogenase is inappropriate as internal control in comparative studies between skin tissue and cultured skin fibroblasts using Northern blot analysis. *Arch Dermatol Res*, 291(12), 659-661. https://doi.org/10.1007/s004030050471

Orshal, J. M., & Khalil, R. A. (2004). Gender, sex hormones, and vascular tone. Am J Physiol Regul Integr Comp Physiol, 286(2), R233-249. https://doi.org/10.1152/ajpregu.00338.2003

Ostrowska-Podhorodecka, Z., & McCulloch, C. A. (2021). Vimentin regulates the assembly and function of matrix adhesions. *Wound Repair Regen*, *29*(4), 602-612. https://doi.org/10.1111/wrr.12920

Owens, G. K. (1995). Regulation of differentiation of vascular smooth muscle cells. *Physiol Rev*, *75*(3), 487-517. https://doi.org/10.1152/physrev.1995.75.3.487

Owens, G. K., Kumar, M. S., & Wamhoff, B. R. (2004). Molecular regulation of vascular smooth muscle cell differentiation in development and disease. *Physiol Rev*, *84*(3), 767-801. https://doi.org/10.1152/physrev.00041.2003

Ozaki, J., Shimizu, H., Hashimoto, Y., Itoh, H., Nakao, K., & Inui, K. (1999). Enzymatic inactivation of major circulating forms of atrial and brain natriuretic peptides. *Eur J Pharmacol*, *370*(3), 307-312. https://doi.org/10.1016/s0014-2999(99)00115-6

Pape, H.-C., Kurtz, A., & Silbernagel, S. (2018). *Physiologie* (8 ed.). Georg Thieme Verlag.

Parvinen, M., & Vanha-Perttula, T. (1972). Identification and enzyme quantitation of the stages of the seminiferous epithelial wave in the rat. *Anat Rec*, *174*(4), 435-449. https://doi.org/10.1002/ar.1091740404

Pedroza, A. J., Tashima, Y., Shad, R., Cheng, P., Wirka, R., Churovich, S., Nakamura, K., Yokoyama, N., Cui, J. Z., Iosef, C., Hiesinger, W., Quertermous, T., & Fischbein, M. P. (2020). Single-Cell Transcriptomic Profiling of Vascular Smooth Muscle Cell Phenotype Modulation in Marfan Syndrome Aortic Aneurysm. *Arterioscler Thromb Vasc Biol*, *40*(9), 2195-2211. https://doi.org/10.1161/atvbaha.120.314670

Pfaffl, M. W. (2001). A new mathematical model for relative quantification in real-time RT-PCR. *Nucleic Acids Res*, *29*(9), e45. https://doi.org/10.1093/nar/29.9.e45

Pfeifer, A., Klatt, P., Massberg, S., Ny, L., Sausbier, M., Hirneiss, C., Wang, G. X., Korth, M., Aszódi, A., Andersson, K. E., Krombach, F., Mayerhofer, A., Ruth, P., Fässler, R., & Hofmann, F. (1998). Defective smooth muscle regulation in cGMP kinase I-deficient mice. *Embo j*, *17*(11), 3045-3051. https://doi.org/10.1093/emboj/17.11.3045

Phelps, C., Chess-Williams, R., & Moro, C. (2023). The role of intracellular calcium and Rho kinase pathways in G protein-coupled receptor-mediated contractions of urinary bladder urothelium and lamina propria. *Am J Physiol Cell Physiol*, *324*(3), C787-c797. https://doi.org/10.1152/ajpcell.00441.2022

Pogoda, K., Kameritsch, P., Mannell, H., & Pohl, U. (2019). Connexins in the control of vasomotor function. *Acta Physiol (Oxf)*, *225*(1), e13108. https://doi.org/10.1111/apha.13108

Pohl, U., Holtz, J., Busse, R., & Bassenge, E. (1986). Crucial role of endothelium in the vasodilator response to increased flow in vivo. *Hypertension*, *8*(1), 37-44. https://doi.org/10.1161/01.hyp.8.1.37

Porter, J. G., Arfsten, A., Fuller, F., Miller, J. A., Gregory, L. C., & Lewicki, J. A. (1990). Isolation and functional expression of the human atrial natriuretic peptide clearance receptor cDNA. *Biochem Biophys Res Commun*, *171*(2), 796-803. https://doi.org/10.1016/0006-291x(90)91216-f

Potter, L. R. (2005). Domain analysis of human transmembrane guanylyl cyclase receptors: implications for regulation. *Front Biosci*, *10*, 1205-1220. https://doi.org/10.2741/1613

Potter, L. R. (2011a). Guanylyl cyclase structure, function and regulation. *Cell Signal*, *23*(12), 1921-1926. https://doi.org/10.1016/j.cellsig.2011.09.001

Potter, L. R. (2011b). Natriuretic peptide metabolism, clearance and degradation. *Febs j*, *278*(11), 1808-1817. https://doi.org/10.1111/j.1742-4658.2011.08082.x

Potter, L. R., Abbey-Hosch, S., & Dickey, D. M. (2006). Natriuretic peptides, their receptors, and cyclic guanosine monophosphate-dependent signaling functions. *Endocr Rev*, *27*(1), 47-72. https://doi.org/10.1210/er.2005-0014

Potter, L. R., Yoder, A. R., Flora, D. R., Antos, L. K., & Dickey, D. M. (2009). Natriuretic peptides: their structures, receptors, physiologic functions and therapeutic applications. *Handb Exp Pharmacol*(191), 341-366. https://doi.org/10.1007/978-3-540-68964-5_15

Poyet, P., & Labrie, F. (1987). Characterization of beta-adrenergic receptors in dispersed rat testicular interstitial cells. *J Androl,* 8(1), 7-13. https://doi.org/10.1002/j.1939-4640.1987.tb02409.x

Pozzi, E., Cakir, O. O., & Muneer, A. (2021). The Role of Nitric oxide (NO) Donors in the Treatment of Male Infertility. *Curr Pharm Des*, *27*(24), 2784-2789. https://doi.org/10.2174/1381612826666201112144828

Preston, S., Jabbar, A., Nowell, C., Joachim, A., Ruttkowski, B., Baell, J., Cardno, T., Korhonen, P. K., Piedrafita, D., Ansell, B. R., Jex, A. R., Hofmann, A., & Gasser, R. B. (2015). Low cost whole-organism screening of compounds for anthelmintic activity. *Int J Parasitol*, *45*(5), 333-343. https://doi.org/10.1016/j.ijpara.2015.01.007

Preston, S., Jabbar, A., Nowell, C., Joachim, A., Ruttkowski, B., Cardno, T., Hofmann, A., & Gasser, R. B. (2016). Practical and low cost whole-organism motility assay: A step-by-step protocol. *Mol Cell Probes*, *30*(1), 13-17. https://doi.org/10.1016/j.mcp.2015.08.005

Pugsley, M. K., & Tabrizchi, R. (2000). The vascular system. An overview of structure and function. *J Pharmacol Toxicol Methods*, *44*(2), 333-340. https://doi.org/10.1016/s1056-8719(00)00125-8

Qiu, J., Zheng, Y., Hu, J., Liao, D., Gregersen, H., Deng, X., Fan, Y., & Wang, G. (2014). Biomechanical regulation of vascular smooth muscle cell functions: from in vitro to in vivo understanding. *J R Soc Interface*, *11*(90), 20130852. https://doi.org/10.1098/rsif.2013.0852

Rager, C., Klöpper, T., Pfeil, U., Tasch, S., Whittaker, M. R., Exintaris, B., Mietens, A., & Middendorff, R. (2023). Reference Gene U2 Enables Direct Comparison between Relative Gene Expression Levels of Vascular Smooth Muscle Cells in Tissue and Culture Using Real-Time Quantitative PCR. *Cells*, *12*(17), 2135. https://www.mdpi.com/2073-4409/12/17/2135

Rager, C., Klöpper, T., Tasch, S., Whittaker, M. R., Exintaris, B., Mietens, A., & Middendorff, R. (2025). The Influence of Cell Isolation and Culturing on Natriuretic Peptide Receptors in Aortic Vascular Smooth Muscle Cells. *Cells*, *14*(1). https://doi.org/10.3390/cells14010051

Rajfer, J., Aronson, W. J., Bush, P. A., Dorey, F. J., & Ignarro, L. J. (1992). Nitric oxide as a mediator of relaxation of the corpus cavernosum in response to nonadrenergic, noncholinergic neurotransmission. *N Engl J Med*, *326*(2), 90-94. https://doi.org/10.1056/nejm199201093260203

Ramaswamy, S., & Weinbauer, G. F. (2014). Endocrine control of spermatogenesis: Role of FSH and LH/testosterone. *Spermatogenesis*, *4*(2), e996025. https://doi.org/10.1080/21565562.2014.996025

Rameshrad, M., Babaei, H., Azarmi, Y., & Fouladi, D. F. (2016). Rat aorta as a pharmacological tool for in vitro and in vivo studies. *Life Sci*, *145*, 190-204. https://doi.org/10.1016/j.lfs.2015.12.043

Rao, R. S., Miano, J. M., Olson, E. N., & Seidel, C. L. (1997). The A10 cell line: a model for neonatal, neointimal, or differentiated vascular smooth muscle cells? *Cardiovasc Res*, *36*(1), 118-126. https://doi.org/10.1016/s0008-6363(97)00156-9

Rayment, I., Holden, H. M., Whittaker, M., Yohn, C. B., Lorenz, M., Holmes, K. C., & Milligan, R. A. (1993). Structure of the actin-myosin complex and its implications for muscle contraction. *Science*, *261*(5117), 58-65. https://doi.org/10.1126/science.8316858

Razavi, H. M., Hamilton, J. A., & Feng, Q. (2005). Modulation of apoptosis by nitric oxide: implications in myocardial ischemia and heart failure. *Pharmacol Ther*, *106*(2), 147-162. https://doi.org/10.1016/j.pharmthera.2004.11.006

Regitz-Zagrosek, V., & Kararigas, G. (2017). Mechanistic Pathways of Sex Differences in Cardiovascular Disease. *Physiol Rev*, *97*(1), 1-37. https://doi.org/10.1152/physrev.00021.2015

Reis, A. M., Jankowski, M., Mukaddam-Daher, S., Tremblay, J., Dam, T. V., & Gutkowska, J. (1997). Regulation of the natriuretic peptide system in rat uterus during the estrous cycle. *J Endocrinol*, *153*(3), 345-355. https://doi.org/10.1677/joe.0.1530345

Ribatti, D. (2009). William Harvey and the discovery of the circulation of the blood. *J Angiogenes Res*, *1*, 3. https://doi.org/10.1186/2040-2384-1-3

Robaire, B., & Hinton, B. T. (2015). *The Epididymis* (Vol. 4). Elsevier.

Robbins, R. A., & Grisham, M. B. (1997). Nitric oxide. *Int J Biochem Cell Biol*, *29*(6), 857-860. https://doi.org/10.1016/s1357-2725(96)00167-7

Rong, J. X., Shapiro, M., Trogan, E., & Fisher, E. A. (2003). Transdifferentiation of mouse aortic smooth muscle cells to a macrophage-like state after cholesterol loading. *Proc Natl Acad Sci U S A*, *100*(23), 13531-13536. https://doi.org/10.1073/pnas.1735526100

Roostalu, U., Aldeiri, B., Albertini, A., Humphreys, N., Simonsen-Jackson, M., Wong, J. K. F., & Cossu, G. (2018). Distinct Cellular Mechanisms Underlie Smooth Muscle Turnover in Vascular Development and Repair. *Circ Res*, *122*(2), 267-281. https://doi.org/10.1161/circresaha.117.312111

Roostalu, U., & Wong, J. K. (2018). Arterial smooth muscle dynamics in development and repair. *Dev Biol*, *435*(2), 109-121. https://doi.org/10.1016/j.ydbio.2018.01.018

Rosàs-Canyelles, E., Dai, T., Li, S., & Herr, A. E. (2018). Mouse-to-mouse variation in maturation heterogeneity of smooth muscle cells. *Lab Chip*, *18*(13), 1875-1883. https://doi.org/10.1039/c8lc00216a

Rossi, S. P., Walenta, L., Rey-Ares, V., Köhn, F. M., Schwarzer, J. U., Welter, H., Calandra, R. S., Frungieri, M. B., & Mayerhofer, A. (2018). Alpha 1 adrenergic receptor-mediated inflammatory responses in human testicular peritubular cells. *Mol Cell Endocrinol*, *474*, 1-9. https://doi.org/10.1016/j.mce.2018.01.027

Rotella, D. P. (2002). Phosphodiesterase 5 inhibitors: current status and potential applications. *Nat Rev Drug Discov*, *1*(9), 674-682. https://doi.org/10.1038/nrd893

Rubattu, S., Sciarretta, S., Morriello, A., Calvieri, C., Battistoni, A., & Volpe, M. (2010). NPR-C: a component of the natriuretic peptide family with implications in human diseases. *J Mol Med (Berl)*, *88*(9), 889-897. https://doi.org/10.1007/s00109-010-0641-2

Russell, L. D., Alger, L. E., & Nequin, L. G. (1987). Hormonal control of pubertal spermatogenesis. *Endocrinology, 120(4)*, 1615-1632. https://doi.org/10.1210/endo-120-4-1615

Rybalkin, S. D., Yan, C., Bornfeldt, K. E., & Beavo, J. A. (2003). Cyclic GMP phosphodiesterases and regulation of smooth muscle function. *Circ Res*, 93(4), 280-291. https://doi.org/10.1161/01.Res.0000087541.15600.2b

Saboor, F., Reckmann, A. N., Tomczyk, C. U., Peters, D. M., Weissmann, N., Kaschtanow, A., Schermuly, R. T., Michurina, T. V., Enikolopov, G., Müller, D., Mietens, A., & Middendorff, R. (2016). Nestin-expressing vascular wall cells drive development of pulmonary hypertension. *Eur Respir J*, *47*(3), 876-888. https://doi.org/10.1183/13993003.00574-2015

Salazar, J., Rojas-Quintero, J., Cano, C., Pérez, J. L., Ramírez, P., Carrasquero, R., Torres, W., Espinoza, C., Chacín-González, M., & Bermúdez, V. (2020). Neprilysin: A Potential Therapeutic Target of Arterial Hypertension? *Curr Cardiol Rev*, *16*(1), 25-35. https://doi.org/10.2174/1573403x15666190625160352

Sampilvanjil, A., Karasawa, T., Yamada, N., Komada, T., Higashi, T., Baatarjav, C., Watanabe, S., Kamata, R., Ohno, N., & Takahashi, M. (2020). Cigarette smoke extract induces ferroptosis in vascular smooth muscle cells. *Am J Physiol Heart Circ Physiol*, *318*(3), H508-h518. https://doi.org/10.1152/ajpheart.00559.2019

Sanbe, A., Tanaka, Y., Fujiwara, Y., Tsumura, H., Yamauchi, J., Cotecchia, S., Koike, K., Tsujimoto, G., & Tanoue, A. (2007). Alpha1-adrenoceptors are required for normal male sexual function. *Br J Pharmacol*, *152*(3), 332-340. https://doi.org/10.1038/sj.bjp.0707366

Sandner, P., Zimmer, D. P., Milne, G. T., Follmann, M., Hobbs, A., & Stasch, J. P. (2021). Soluble Guanylate Cyclase Stimulators and Activators. *Handb Exp Pharmacol*, *264*, 355-394. https://doi.org/10.1007/164_2018_197

Sarkar, R., Gordon, D., Stanley, J. C., & Webb, R. C. (1997). Cell cycle effects of nitric oxide on vascular smooth muscle cells. *Am J Physiol*, *272*(4 Pt 2), H1810-1818. https://doi.org/10.1152/ajpheart.1997.272.4.H1810

Sarzani, R., Dessì-Fulgheri, P., Paci, V. M., Espinosa, E., & Rappelli, A. (1996). Expression of natriuretic peptide receptors in human adipose and other tissues. *J Endocrinol Invest*, *19*(9), 581-585. https://doi.org/10.1007/bf03349021

Sasagawa, I., Ishigooka, M., Kubota, Y., Nakada, T., & Taniguchi, N. (1995). Effect of experimental cryptorchidism on alpha 1-adrenergic receptors of rat testis. *Arch Androl*, *35*(3), 213-218. https://doi.org/10.3109/01485019508987873

Schindelin, J., Arganda-Carreras, I., Frise, E., Kaynig, V., Longair, M., Pietzsch, T., Preibisch, S., Rueden, C., Saalfeld, S., Schmid, B., Tinevez, J. Y., White, D. J., Hartenstein, V., Eliceiri, K., Tomancak, P., & Cardona, A. (2012). Fiji: an open-source platform for biological-image analysis. *Nat Methods*, *9*(7), 676-682. https://doi.org/10.1038/nmeth.2019

Schmidt, J., Goode, D., Flannigan, R., & Mohammadi, H. (2023). A review of the experimental methods and results of testing the mechanical properties of Tunica Albuginea. *J Med Eng Technol*, *47*(4), 234-241. https://doi.org/10.1080/03091902.2023.2300829

Seeland, U., & Regitz-Zagrosek, V. (2012). Sex and gender differences in cardiovascular drug therapy. *Handb Exp Pharmacol*(214), 211-236. https://doi.org/10.1007/978-3-642-30726-3_11

Shi, J., Yang, Y., Cheng, A., Xu, G., & He, F. (2020). Metabolism of vascular smooth muscle cells in vascular diseases. *Am J Physiol Heart Circ Physiol*, *319*(3), H613-h631. https://doi.org/10.1152/ajpheart.00220.2020

Singh, V. K., & Lal, B. (2017). Pro-steroidogenic and pro-spermatogenic actions of nitric oxide (NO) on the catfish, Clarias batrachus: An in vivo study. *Gen Comp Endocrinol*, 242, 1-10. https://doi.org/10.1016/j.ygcen.2016.05.001

Somjen, D., Kohen, F., Jaffe, A., Amir-Zaltsman, Y., Knoll, E., & Stern, N. (1998). Effects of gonadal steroids and their antagonists on DNA synthesis in human vascular cells. Hypertension, 32(1), 39-45. https://doi.org/10.1161/01.hyp.32.1.39

Stadler, B., Nowell, C. J., Whittaker, M. R., Arnhold, S., Pilatz, A., Wagenlehner, F. M., Exintaris, B., & Middendorff, R. (2021). Physiological and pharmacological impact of oxytocin on epididymal propulsion during the ejaculatory process in rodents and men. *Faseb j*, *35*(6), e21639. https://doi.org/10.1096/fj.202100435R

Stadler, B., Whittaker, M. R., Exintaris, B., & Middendorff, R. (2020). Oxytocin in the Male Reproductive Tract; The Therapeutic Potential of Oxytocin-Agonists and-Antagonists. *Front Endocrinol (Lausanne)*, *11*, 565731. https://doi.org/10.3389/fendo.2020.565731

Staessen, J. A., Fagard, R., Thijs, L., & Amery, A. (1993). Fourier analysis of blood pressure profiles. *Am J Hypertens*, *6*(6 Pt 2), 184s-187s. https://doi.org/10.1093/ajh/6.6.184s

Staicu, F. D., Lopez-Úbeda, R., Romero-Aguirregomezcorta, J., Martínez-Soto, J. C., & Matás Parra, C. (2019). Regulation of boar sperm functionality by the nitric oxide synthase/nitric oxide system. *J Assist Reprod Genet*, *36*(8), 1721-1736. https://doi.org/10.1007/s10815-019-01526-6

Steinert, J. R., Chernova, T., & Forsythe, I. D. (2010). Nitric oxide signaling in brain function, dysfunction, and dementia. *Neuroscientist*, *16*(4), 435-452. https://doi.org/10.1177/1073858410366481

Steinmetz, M., Potthast, R., Sabrane, K., & Kuhn, M. (2004). Diverging vasorelaxing effects of C-type natriuretic peptide in renal resistance arteries and aortas of GC-A-deficient mice. *Regul Pept*, *119*(1-2), 31-37. https://doi.org/10.1016/j.regpep.2003.12.005

Streit, S., Michalski, C. W., Erkan, M., Kleeff, J., & Friess, H. (2009). Northern blot analysis for detection and quantification of RNA in pancreatic cancer cells and tissues. *Nat Protoc*, *4*(1), 37-43. https://doi.org/10.1038/nprot.2008.216

Strosberg, A. D. (1993). Structure, function, and regulation of adrenergic receptors. *Protein Sci*, *2*(8), 1198-1209. https://doi.org/10.1002/pro.5560020802

Sudoh, T., Kangawa, K., Minamino, N., & Matsuo, H. (1988). A new natriuretic peptide in porcine brain. *Nature*, *332*(6159), 78-81. https://doi.org/10.1038/332078a0

Sudoh, T., Minamino, N., Kangawa, K., & Matsuo, H. (1990). C-type natriuretic peptide (CNP): a new member of natriuretic peptide family identified in porcine brain. *Biochem Biophys Res Commun*, *168*(2), 863-870. https://doi.org/10.1016/0006-291x(90)92401-k

Suga, S., Nakao, K., Hosoda, K., Mukoyama, M., Ogawa, Y., Shirakami, G., Arai, H., Saito, Y., Kambayashi, Y., Inouye, K., & et al. (1992). Receptor selectivity of natriuretic peptide family, atrial natriuretic peptide, brain natriuretic peptide, and C-type natriuretic peptide. *Endocrinology*, *130*(1), 229-239. https://doi.org/10.1210/endo.130.1.1309330

Suga, S., Nakao, K., Kishimoto, I., Hosoda, K., Mukoyama, M., Arai, H., Shirakami, G., Ogawa, Y., Komatsu, Y., Nakagawa, O., & et al. (1992). Phenotype-related alteration in expression of natriuretic peptide receptors in aortic smooth muscle cells. *Circ Res*, *71*(1), 34-39. https://doi.org/10.1161/01.res.71.1.34

Suga, S., Nakao, K., Mukoyama, M., Arai, H., Hosoda, K., Ogawa, Y., & Imura, H. (1992). Characterization of natriuretic peptide receptors in cultured cells. *Hypertension*, *19*(6 Pt 2), 762-765. https://doi.org/10.1161/01.hyp.19.6.762

Sun, Y., Xu, H., Xu, X., Wang, H., Yuan, Y., An, Z., Xu, Z., & Wang, G. (2021). A novel method to obtain rat aortic media for primary culture of rat aortic smooth muscle cells. *In Vitro Cell Dev Biol Anim*, *57*(7), 726-734. https://doi.org/10.1007/s11626-021-00615-0

Sung, R., Lee, S. H., Ji, M., Han, J. H., Kang, M. H., Kim, J. H., Choi, J. W., Kim, Y. C., & Park, S. M. (2014). Epithelial-mesenchymal transition-related protein expression in biliary epithelial cells associated with hepatolithiasis. *J Gastroenterol Hepatol*, *29*(2), 395-402. https://doi.org/10.1111/jgh.12349

Surks, H. K. (2007). cGMP-dependent protein kinase I and smooth muscle relaxation: a tale of two isoforms. *Circ Res*, *101*(11), 1078-1080. https://doi.org/10.1161/circresaha.107.165779

Suvanto, O., & Kormano, M. (1970). The relation between in vitro contractions of the rat seminiferous tubules and the cyclic stage of the seminiferous epithelium. *J Reprod Fertil*, *21*(2), 227-232. https://doi.org/10.1530/jrf.0.0210227

Suzuki, T., Higgins, P. J., & Crawford, D. R. (2000). Control selection for RNA quantitation. *Biotechniques*, *29*(2), 332-337. https://doi.org/10.2144/00292rv02

Sweeney, H. L., & Hammers, D. W. (2018). Muscle Contraction. *Cold Spring Harb Perspect Biol*, *10*(2). https://doi.org/10.1101/cshperspect.a023200

Szpirer, C. (2020). Rat models of human diseases and related phenotypes: a systematic inventory of the causative genes. *J Biomed Sci*, *27*(1), 84. https://doi.org/10.1186/s12929-020-00673-8

Taki, F. A., Abdel-Rahman, A. A., & Zhang, B. (2014). A comprehensive approach to identify reliable reference gene candidates to investigate the link between alcoholism and endocrinology in Sprague-Dawley rats. *PLoS One*, *9*(5), e94311. https://doi.org/10.1371/journal.pone.0094311

Tang, Z., Wang, A., Yuan, F., Yan, Z., Liu, B., Chu, J. S., Helms, J. A., & Li, S. (2012). Differentiation of multipotent vascular stem cells contributes to vascular diseases. *Nat Commun*, *3*, 875. https://doi.org/10.1038/ncomms1867

Tarbit, E., Singh, I., Peart, J. N., & Rose'Meyer, R. B. (2019). Biomarkers for the identification of cardiac fibroblast and myofibroblast cells. *Heart Fail Rev*, *24*(1), 1-15. https://doi.org/10.1007/s10741-018-9720-1

Tawaragi, Y., Fuchimura, K., Tanaka, S., Minamino, N., Kangawa, K., & Matsuo, H. (1991). Gene and precursor structures of human C-type natriuretic peptide. *Biochem Biophys Res Commun*, *175*(2), 645-651. https://doi.org/10.1016/0006-291x(91)91614-i

Thompson, J., & Khalil, R. A. (2003). Gender differences in the regulation of vascular tone. *Clin Exp Pharmacol Physiol*, *30*(1-2), 1-15. https://doi.org/10.1046/j.1440-1681.2003.03790.x

Thong, A., Müller, D., Feuerstacke, C., Mietens, A., Stammler, A., & Middendorff, R. (2014). Neutral endopeptidase (CD10) is abundantly expressed in the epididymis and localized to a distinct population of epithelial cells--its relevance for CNP degradation. *Mol Cell Endocrinol*, *382*(1), 234-243. https://doi.org/10.1016/j.mce.2013.09.027

Thorneloe, K. S., & Nelson, M. T. (2005). Ion channels in smooth muscle: regulators of intracellular calcium and contractility. *Can J Physiol Pharmacol*, *83*(3), 215-242. https://doi.org/10.1139/y05-016

Thorpe, A., & Neal, D. (2003). Benign prostatic hyperplasia. *Lancet*, *361*(9366), 1359-1367. https://doi.org/10.1016/s0140-6736(03)13073-5

Thunemann, M., Fomin, N., Krawutschke, C., Russwurm, M., & Feil, R. (2013). Visualization of cGMP with cGi biosensors. *Methods Mol Biol*, *1020*, 89-120. https://doi.org/10.1007/978-1-62703-459-3_6

Tian, L., Chen, K., Cao, J., Han, Z., Wang, Y., Gao, L., Fan, Y., & Wang, C. (2017). Galectin-3 induces the phenotype transformation of human vascular smooth muscle cells via the canonical Wnt signaling. *Mol Med Rep*, *15*(6), 3840-3846. https://doi.org/10.3892/mmr.2017.6429

Togashi, H., Sakuma, I., Yoshioka, M., Kobayashi, T., Yasuda, H., Kitabatake, A., Saito, H., Gross, S. S., & Levi, R. (1992). A central nervous system action of nitric oxide in blood pressure regulation. *J Pharmacol Exp Ther*, *262*(1), 343-347.

Tolszczuk, M., Folléa, N., & Pelletier, G. (1988). Characterization and localization of beta-adrenergic receptors in control and cryptorchidized rat testis by in vitro autoradiography. *J Androl*, 9(3), 172-177. https://doi.org/10.1002/j.1939-4640.1988.tb01030.x

Torphy, T. J. (1998). Phosphodiesterase isozymes: molecular targets for novel antiasthma agents. *Am J Respir Crit Care Med*, *157*(2), 351-370. https://doi.org/10.1164/ajrccm.157.2.9708012

Torres, V. E., Cai, Y., Chen, X. I., Wu, G. Q., Geng, L., Cleghorn, K. A., Johnson, C. M., & Somlo, S. (2001). Vascular expression of polycystin-2. *J Am Soc Nephrol*, *12*(1), 1-9. https://doi.org/10.1681/asn.V1211

Tourmente, M., Zarka-Trigo, D., & Roldan, E. R. (2016). Is the hook of muroid rodent's sperm related to sperm train formation? *J Evol Biol*, *29*(6), 1168-1177. https://doi.org/10.1111/jeb.12857

Traish, A., Kim, N. N., Moreland, R. B., & Goldstein, I. (2000). Role of alpha adrenergic receptors in erectile function. *Int J Impot Res*, *12 Suppl 1*, S48-63.

Tucker, W. D., Arora, Y., & Mahajan, K. (2024). Anatomy, Blood Vessels. In *StatPearls*. StatPearls Publishing
Copyright © 2024, StatPearls Publishing LLC.

Tykocki, N. R., Boerman, E. M., & Jackson, W. F. (2017). Smooth Muscle Ion Channels and Regulation of Vascular Tone in Resistance Arteries and Arterioles. *Compr Physiol*, *7*(2), 485-581. https://doi.org/10.1002/cphy.c160011

Tymvios, C., Moore, C., Jones, S., Solomon, A., Sanz-Rosa, D., & Emerson, M. (2009). Platelet aggregation responses are critically regulated in vivo by endogenous nitric oxide but not by endothelial nitric oxide synthase. *Br J Pharmacol*, *158*(7), 1735-1742. https://doi.org/10.1111/j.1476-5381.2009.00408.x

U. S. National Institutes of Health, N. C. I. (2024). *Cross section of the testis*. Retrieved 13/08/2024 from https://training.seer.cancer.gov/

Umans, J. G., & Levi, R. (1995). Nitric oxide in the regulation of blood flow and arterial pressure. *Annu Rev Physiol*, *57*, 771-790. https://doi.org/10.1146/annurev.ph.57.030195.004011

van der Feltz, C., & Hoskins, A. A. (2019). Structural and functional modularity of the U2 snRNP in pre-mRNA splicing. *Crit Rev Biochem Mol Biol*, *54*(5), 443-465. https://doi.org/10.1080/10409238.2019.1691497

Vazquez-Arango, P., & O'Reilly, D. (2018). Variant snRNPs: New players within the spliceosome system. *RNA Biol*, *15*(1), 17-25. https://doi.org/10.1080/15476286.2017.1373238

Vekilov, D. P., & Grande-Allen, K. J. (2018). Mechanical Properties of Diseased Veins. *Methodist Debakey Cardiovasc J*, *14*(3), 182-187. https://doi.org/10.14797/mdcj-14-3-182

Vollmar, A. M., Gerbes, A. L., Nemer, M., & Schulz, R. (1993). Detection of C-type natriuretic peptide (CNP) transcript in the rat heart and immune organs. *Endocrinology*, *132*(4), 1872-1874. https://doi.org/10.1210/endo.132.4.8462485

Volz, K. S., Jacobs, A. H., Chen, H. I., Poduri, A., McKay, A. S., Riordan, D. P., Kofler, N., Kitajewski, J., Weissman, I., & Red-Horse, K. (2015). Pericytes are progenitors for coronary artery smooth muscle. *Elife*, *4*. https://doi.org/10.7554/eLife.10036

Waberski, D., Suarez, S. S., & Henning, H. (2022). Assessment of sperm motility in livestock: Perspectives based on sperm swimming conditions in vivo. *Anim Reprod Sci*, *246*, 106849. https://doi.org/10.1016/j.anireprosci.2021.106849

Wagner, B. M., Robinson, J. W., Healy, C. L., Gauthier, M., Dickey, D. M., Yee, S. P., Osborn, J. W., O'Connell, T. D., & Potter, L. R. (2022). Guanylyl cyclase-A phosphorylation decreases cardiac hypertrophy and improves systolic function in male, but not female, mice. *Faseb j*, *36*(1), e22069. https://doi.org/10.1096/fj.202100600RRR

Wang, J., Bingaman, S., & Huxley, V. H. (2010). Intrinsic sex-specific differences in microvascular endothelial cell phosphodiesterases. *Am J Physiol Heart Circ Physiol*, 298(4), H1146-1154. https://doi.org/10.1152/ajpheart.00252.2009

Wang, J., He, Q., Yan, X., Cai, Y., & Chen, J. (2014). Effect of exogenous nitric oxide on sperm motility in vitro. Biol Res, 47(1), 44. https://doi.org/10.1186/0717-6287-47-44

Wang, J., Kazmi, M. M., & Huxley, V. H. (2021). Microvascular Sex- and Age- Dependent Phosphodiesterase Expression. *Front Aging*, 2, 719698. https://doi.org/10.3389/fragi.2021.719698

Wanjari, U. R., & Gopalakrishnan, A. V. (2024). Blood-testis barrier: a review on regulators in maintaining cell junction integrity between Sertoli cells. *Cell Tissue Res*, *396*(2), 157-175. https://doi.org/10.1007/s00441-024-03894-7

Waqar, A., Jain, A., Joseph, C., Srivastava, K., Ochuba, O., Alkayyali, T., & Poudel, S. (2022). Cardioprotective Role of Estrogen in Takotsubo Cardiomyopathy. *Cureus*, *14*(3), e22845. https://doi.org/10.7759/cureus.22845

Watanabe, Y., Nakajima, K., Shimamori, Y., & Fujimoto, Y. (1997). Comparison of the hydrolysis of the three types of natriuretic peptides by human kidney neutral endopeptidase 24.11. *Biochem Mol Med*, *61*(1), 47-51. https://doi.org/10.1006/bmme.1997.2584

Webb, R. C. (2003). Smooth muscle contraction and relaxation. *Adv Physiol Educ*, *27*(1-4), 201-206. https://doi.org/10.1152/advan.00025.2003

Weis, W. I., & Kobilka, B. K. (2018). The Molecular Basis of G Protein-Coupled Receptor Activation. *Annu Rev Biochem*, *87*, 897-919. https://doi.org/10.1146/annurev-biochem-060614-033910

Weiser, D., Mietens, A., Stadler, B., Ježek, D., Schuler, G., & Middendorff, R. (2020). Contractions transport exfoliated epithelial cells through the neonatal epididymis. *Reproduction*, *160*(1), 109-116. https://doi.org/10.1530/rep-19-0617

Westerhof, N., Lankhaar, J. W., & Westerhof, B. E. (2009). The arterial Windkessel. *Med Biol Eng Comput*, *47*(2), 131-141. https://doi.org/10.1007/s11517-008-0359-2

Wilkinson, M. E., Charenton, C., & Nagai, K. (2020). RNA Splicing by the Spliceosome. *Annu Rev Biochem*, 89, 359-388. https://doi.org/10.1146/annurev-biochem-091719-064225

Will, C. L., & Lührmann, R. (2011). Spliceosome structure and function. *Cold Spring Harb Perspect Biol*, *3*(7). https://doi.org/10.1101/cshperspect.a003707

Winder, S. J., Allen, B. G., Clément-Chomienne, O., & Walsh, M. P. (1998). Regulation of smooth muscle actin-myosin interaction and force by calponin. *Acta Physiol Scand*, *164*(4), 415-426. https://doi.org/10.1111/j.1365-201x.1998.tb10697.x

Winder, S. J., & Walsh, M. P. (1993). Calponin: thin filament-linked regulation of smooth muscle contraction. *Cell Signal*, *5*(6), 677-686. https://doi.org/10.1016/0898-6568(93)90029-l

Wittmeier, P., & Hummel, S. (2022). Agarose gel electrophoresis to assess PCR product yield: comparison with spectrophotometry, fluorometry and qPCR. *Biotechniques*, *72*(4), 155-158. https://doi.org/10.2144/btn-2021-0094

Wolfsgruber, W., Feil, S., Brummer, S., Kuppinger, O., Hofmann, F., & Feil, R. (2003). A proatherogenic role for cGMP-dependent protein kinase in vascular smooth muscle cells. *Proc Natl Acad Sci U S A*, *100*(23), 13519-13524. https://doi.org/10.1073/pnas.1936024100

Wong, G. W., Laugerotte, A., & Wright, J. M. (2015). Blood pressure lowering efficacy of dual alpha and beta blockers for primary hypertension. *Cochrane Database Syst Rev*, *2015*(8), Cd007449. https://doi.org/10.1002/14651858.CD007449.pub2

Wong, P. G., Armstrong, D. W., Tse, M. Y., Brander, E. P., & Pang, S. C. (2013). Sex-specific differences in natriuretic peptide and nitric oxide synthase expression in ANP gene-disrupted mice. *Mol Cell Biochem*, *374*(1-2), 125-135. https://doi.org/10.1007/s11010-012-1511-8

Worth, N. F., Rolfe, B. E., Song, J., & Campbell, G. R. (2001). Vascular smooth muscle cell phenotypic modulation in culture is associated with reorganisation of contractile and cytoskeletal proteins. *Cell Motil Cytoskeleton*, *49*(3), 130-145. https://doi.org/10.1002/cm.1027

Wu, G., Sharina, I., & Martin, E. (2022). Soluble guanylyl cyclase: Molecular basis for ligand selectivity and action in vitro and in vivo. *Front Mol Biosci*, *9*, 1007768. https://doi.org/10.3389/fmolb.2022.1007768

Wunder, F., Woermann, A., Geerts, A., & Milde, M. (2013). Pharmacological characterization of receptor guanylyl cyclase reporter cell lines. *Eur J Pharmacol*, *698*(1-3), 131-136. https://doi.org/10.1016/j.ejphar.2012.11.009

Xie, F., Wang, J., & Zhang, B. (2023). RefFinder: a web-based tool for comprehensively analyzing and identifying reference genes. *Funct Integr Genomics*, *23*(2), 125. https://doi.org/10.1007/s10142-023-01055-7

Yang, T., Zhang, M., & Zhang, N. (2022). Modified Northern blot protocol for easy detection of mRNAs in total RNA using radiolabeled probes. *BMC Genomics*, *23*(1), 66. https://doi.org/10.1186/s12864-021-08275-w

Yetik-Anacak, G., & Catravas, J. D. (2006). Nitric oxide and the endothelium: history and impact on cardiovascular disease. *Vascul Pharmacol*, *45*(5), 268-276. https://doi.org/10.1016/j.vph.2006.08.002

Yeung, V. T., Ho, S. K., Nicholls, M. G., & Cockram, C. S. (1996). Binding of CNP-22 and CNP-53 to cultured mouse astrocytes and effects on cyclic GMP. *Peptides*, *17*(1), 101-106. https://doi.org/10.1016/0196-9781(95)02099-3

Yu, L., Zhang, J., Gao, A., Zhang, M., Wang, Z., Yu, F., Guo, X., Su, G., Zhang, Y., Zhang, M., & Zhang, C. (2022). An intersegmental single-cell profile reveals aortic heterogeneity and identifies a novel Malat1(+) vascular smooth muscle subtype involved in abdominal aortic aneurysm formation. *Signal Transduct Target Ther*, *7*(1), 125. https://doi.org/10.1038/s41392-022-00943-x

Yu, S., & McEniery, C. M. (2020). Central Versus Peripheral Artery Stiffening and Cardiovascular Risk. *Arterioscler Thromb Vasc Biol*, *40*(5), 1028-1033. https://doi.org/10.1161/atvbaha.120.313128

Zaneveld, L. J., De Jonge, C. J., Anderson, R. A., & Mack, S. R. (1991). Human sperm capacitation and the acrosome reaction. *Hum Reprod*, *6*(9), 1265-1274. https://doi.org/10.1093/oxfordjournals.humrep.a137524

Zengin, E., Chalajour, F., Gehling, U. M., Ito, W. D., Treede, H., Lauke, H., Weil, J., Reichenspurner, H., Kilic, N., & Ergün, S. (2006). Vascular wall resident progenitor cells: a source for postnatal vasculogenesis. Development, 133(8), 1543-1551. https://doi.org/10.1242/dev.02315

Zhang, D., Li, B., Xu, H., Li, J., Ma, C., Ge, W., Lu, C., & Cao, X. (2024). Identification of FBLL1 as a neuron-specific RNA 2'-O-methyltransferase mediating neuronal differentiation. *Proc Natl Acad Sci U S A*, 121(48), e2406961121. https://doi.org/10.1073/pnas.2406961121

Zhang, D., Shi, J., Liang, G., Liu, D., Zhang, J., Pan, S., Lu, Y., Wu, Q., Gong, C., & Guo, Y. (2022). miR-16-5p Is a Novel Mediator of Venous Smooth Muscle Phenotypic Switching. *J Cardiovasc Transl Res*, *15*(4), 876-889. https://doi.org/10.1007/s12265-022-10208-1

Zhao, A. Z., Yan, C., Sonnenburg, W. K., & Beavo, J. A. (1997). Recent advances in the study of Ca2+/CaM-activated phosphodiesterases: expression and physiological functions. Adv Second Messenger Phosphoprotein Res, 31, 237-251.

Zouhal, H., Jacob, C., Delamarche, P., & Gratas-Delamarche, A. (2008). Catecholamines and the effects of exercise, training and gender. *Sports Med*, *38*(5), 401-423. https://doi.org/10.2165/00007256-200838050-00004